Øivind Kåre Kjerstad

Dynamic Positioning of Marine Vessels in Ice

Thesis for the degree of Philosophiae Doctor

Trondheim, May 2016

Norwegian University of Science and Technology
Faculty of Engineering
Science and Technology
Department of MarineTechnology

NTNU
Norwegian University of
Science and Technology

NTNU
Norwegian University of Science and Technology

Thesis for the degree of Philosophiae Doctor

Faculty of Engineering
Science and Technology
Department of MarineTechnology

ISBN 978-82-326-1674-9 (printed version)
ISBN 978-82-326-1675-6 (electronic version)
ISSN 1503-8181

Doctoral theses at NTNU, 2016:168

Printed by Skipnes Kommunikasjon as

To my family

Abstract

This thesis is a collection of papers focusing on various aspects of dynamic positioning of marine vessels in ice. Most emphasis is put on the dynamic broken, or managed, sea-ice environment where pioneering operations have shown that conventional dynamic positioning systems are capable given light ice conditions. When the conditions toughen, or the ice drift direction changes quickly, these systems struggle and may fail. Yet, it is reported that manual control renders sufficient stationkeeping possible.

To understand the operational environment the vessel-ice interactions are studied using model scale experiments and numerical simulations. It is found that the multi-body interactions of the vessel-ice interaction contain complex processes that may introduce a significant and highly varying disturbance. To handle this it is concluded that the core control system must be reviewed with focus on increasing reactiveness to external perturbations together with an operation strategy complying with the ice dynamics.

Increasing reactiveness is approached in three ways; by extending conventional model based design methods to capture the ice dynamics, by introducing hybrid control theory to allow for instantaneous change of estimated variables, and finally, by incorporation of inertial measurements to form an acceleration feedforward in the control system. All are investigated theoretically and experimentally and show varying feasibility. For closed-loop experiments in managed ice, a framework using a state-of-the-art high fidelity numerical model is developed and applied.

Weather vaning coupled with the reactive algorithms is investigated for operating compliantly with the ice dynamics. It is advantageous as the optimal vessel heading is found through the vessel motion response, and not an explicit ice drift measurement. Finally, motivated by the oblique heading and ice load coupling a novel recursive thrust allocation algorithm for prioritization of selected degrees of freedom is proposed and investigated.

Acknowledgements

I would particularly like to thank Professor Roger Skjetne for believing in me to pursue a PhD, and for serving as my supervisor. He has given me complete freedom to pursue my own ideas, made it possible to attend key events that have shaped my research, and been very efficient and helpful in dealing with practical issues concerning financing and bureaucracy. Without his invaluable guidance, scientific excitement, quick response, and continued support this thesis would not be.

A big thank you is also in place for Professor Sveinung Løset for his involvement and enthusiasm for my research. His good leadership and vast field experience has been a big motivation and guidance. Together with Prof. Roger Skjetne he has made it possible to attend lectures, research cruises, and field trips that have been invaluable.

Many others have also contributed in various ways during the PhD, and the people in the following deserve particular recognition:

Arctic DP project affiliates: Ulrik Jørgensen, Ivan Metrikin, Joakim Haugen, Biao Su, Qin Zhang, Francesco Scibilia, Prof. Lars Imsland, Kenneth Eik, Arne Gürtner, Nils Albert Jenssen, Torbjørn Hals, Petter Stuberg, Prof. Morten Breivik, and Stian Ruud.

Friends and colleagues: Bo Zhao, Christoffer Thorvaldsen, Petter Norgren, Svenn Are T. Værnø, Andreas R. Dahl, Laxminarayan Thorat, Christoph Backi, Mauro Candeloro, Fredrik Dukan, Walter Caharija, Prof. Asgeir Sørensen, Torgeir Wahl, Wenjun Lu, Anton Kulepiskin, Marat Kashafutdinov, Andrei Tsarau, Aleksey Shestov, and Renat Yulmetov.

Master students: Håkon N. Skåtun, Anna Makrygiannis, Henrik E. Wold, Vegar Østhus, and Nam Dinh Tran.

Professional encounters: Prof. Andrew Teel and Prof. Thor I. Fossen.

Finally, I would like to thank my family. Especially my fiancée Birgitte M. Fjørtoft, son Elias, parents Einar and Anne Kristin Kjerstad, sisters Ingrid, Agnete, and Benedikte, and grandfather Kåre Kjerstad. We have always stood together in hard times, and you have been there for me with support, interested, and motivation during these years. Therefore, I dedicate this thesis to you as a token of my respect and deep gratitude.

Øivind Kåre Kjerstad
March 16. 2016

Preface

Exploring the Arctic has been the desire and destiny of adventurers and scientists for centuries, and history has repeatedly shown that understanding of the environment through experience, pragmatism, innovation, and good planning is a winning hand. When the Arctic DP project offered the possibility to not only research an interesting topic but also allow and encourage these principles through first hand experiences, I could not resist.

Initially, the challenge at hand was to figure out why automatic dynamic positioning of ships degrades when the ice environment toughens, and come up with countermeasures. Although this is a huge scope involving many interdisciplinary topics, the idea from the beginning was to investigate the control system algorithms. For open water, such can be designed purely theoretically using a set of assumptions with respect to the environment and a model of the vessel's dynamic behavior. The key to success is that these assumptions and models have foundation in reality. For stationkeeping operations in ice the insight on the processes and dynamics was not established. If a design is based on limited knowledge one might end up in a situation where the work has limited practical applications other than from an academic viewpoint. Therefore, to me, the research needed was twofold. First, I needed to develop a working understanding of the dynamics involved when a ship operates in ice, and secondly use this to propose enhancements to the control system.

Since my employment in 2010 I have participated in various activities providing some of the needed insight on challenges for dynamic positioning in ice. These activities deserve some attention in this section because they are not described in detail elsewhere. That is the nature of academic publishing being highly specific and focusing on a few aspects.

The first key experience was the experimental campaign DYnamic Positioning in ICe in 2011 and 2012. This was a joint industry and academic project

where free floating self-propelled model scale vessels were tested in the large ice basin at the Hamburg Ship Model Basin in Germany. This was great learning in experimental research and the use of model ice basins. However, foremost I got a fundamental understanding on ice behavior when in contact with floating structures and acknowledged the fact that the vessel and adjacent ice floes form large interconnected dynamic systems, which later was called ice floe contact networks. The discovery that the load is governed by these (amongst other phenomena) and not just the interaction process at the vessel-ice interface was an eye opener. The same type of interaction dynamics was also found when investigating the video material from another project; Construction and Intervention Vessel for Arctic Operations. This project looked into design of a construction and intervention vessel for Arctic operations, and tested it in the model ice tank at Aker Arctic in Finland.

The first real Arctic experience came in March 2012 during an Arctic offshore fieldwork course hosted by the University Center in Svalbard. Spending one week in the field gathering and testing ice core samples and logging ice properties in the Van Mijen fjord was truly valuable. Reading about this cannot compare to battling freezing and failing equipment, harsh and cold weather, wildlife, remoteness, and unforeseen events in addition to the scientific work. Analyzing the collected ice samples and data was a revelation of the great strength diversity of the ice material. It truly ranges from rock hard to slush.

In September 2012 I participated on the Oden Arctic Technology Research Cruise 2012 to the Fram-strait between Greenland and Svalbard. My main tasks were to gather ice samples and logging of ice properties, deploy environmental monitoring mooring buoys, and test a quadcopter drone. Although these activities gave additional insight to the Arctic research and operations challenges, it was being present at the icebreaker bridge for ten days, talking and listening to the crew and their experience, and looking at the ice behavior and onboard instruments put an extra perspective to the bigger picture. There is no substitute to the factual feeling of the abrupt motion of the icebreaker as it advances through heavy ice. Again, just prior to submitting this thesis I attended the Oden Arctic Technology Research Cruise 2015 which focused on ice management with two icebreakers, the Oden and the Frej. These expeditions were great motivation and inspiration where I was reassured of the fact that the low velocity interconnected ice floe contact networks seen in model scale also occur in full scale. Another key observation was the significant acceleration level in the ship, both

during transit, ice management, and low speed maneuvering.

Bearing these experiences in mind I came to the conclusion that, bluntly put, the Arctic environment can be categorized in three regimes with respect to ice and DP; open water, drifting sea ice, and landfast ice. All of these have their own challenges and characteristics, which will be touched upon in the introductory chapter of this thesis. I have chosen most emphasis on the second, investigating operations in drifting sea ice. There the stationkeeping vessel operates behind a fleet of icebreakers breaking up the natural ice to ease the environmental load. This method of operation has been developed through pioneering campaigns, and is the most likely future scenario for such operations. This environment hold the core set of challenges associated with operations in ice, which was the main reason for my choice.

As mentioned above, conventional motion control systems for marine vessels employ models in their design. Therefore, I set out to create one for the loads from managed sea ice on a stationkeeping vessel. In general these control design models are simplified approximations capturing the most fundamental processes as a function of variables that can either be measured or estimated in real time, or approximated offline. After spending considerable efforts I came to the conclusion that this was extremely challenging. The reason for this is that the key characteristic of the load that needs to be captured by the model is the rapid load variations. However, the mechanisms and variables governing this cannot be easily measured as they are rooted in the complex nature of the ice material, the interaction geometry within the ice floe contact networks, and other phenomena such as accumulation of ice floes and ambient ice pressure. No robust ice load model that captures the rapid variations in the load for control design could therefore be found. This had two major implications. The first is that alternative methods to a load model must be applied in the control design, and secondly that more complex numerical models incorporating each individual ice floe must be used for simulations. Although this was a blow to the model based design method, it is a great opportunity to study general methods for handling rapidly varying unmodeled and unmeasured external disturbances. This has applications outside the ice environment as there are open water scenarios where the precision of the positioning would greatly benefit from more reactive behavior.

In itself this thesis is not a guide on how to design a DP control system for ice. It is far from that. However, it gives some insight on the ice load dynamics in the low velocity regime and proposes a few promising solutions to designing a sufficiently reactive control system that is able to operate

compliantly with the environment. Overall this thesis has two main topics; the study of ice dynamics in the low velocity regime on a free-floating vessel, and control design for dynamic positioning to counter such environment. A significant component of the latter is the utilization of high fidelity numerical models to simulate the vessel ice interactions. Since ice tank time is very costly, far beyond my PhD research grant, numerical simulators were the only option to work with ice interactions on floating vessels. Luckily, a state-of-the-art model, developed within the KMB Arctic DP project by my colleague and good friend Ivan Metrikin, was available by the end of 2012, and from then on I was able to play with and test different concepts. Without access to this, and the collaboration around it, a lot of things would have been different.

All the proposed concepts are designed with ship shaped vessels in mind, but not restricted to this. Especially the application of inertial sensors together with a kinematic approach in the proposed acceleration feedforward control methods, and the use of hybrid systems control theory, which allows greater freedom to update the model estimates, seems promising. Both of these approaches have been tested in experiments. The use of inertial sensors was tested on the Norwegian University of Science and Technology (NTNU) owned research vessel Gunnerus outside Trondheim and later by Kristiansund. To measure the complete six degrees of freedom acceleration vector four high fidelity motion reference units were placed on specific locations in the hull. This experiment was an addition to a campaign by MARINTEK/NTNU where different maneuvers to investigate the dynamic vessel response were performed for evaluation of vessel performance and simulator accuracy. Seeing how this kind of work is performed first-hand was very educative and insightful.

The hybrid systems control theory was tested in closed loop at the MCLab at the Department of Marine Technology at NTNU on CyberShip3, a model scale, battery powered, self-propelled vessel. Hybrid systems theory is a new branch of modeling, at least from the marine vessels application, which allows more freedom in the control design. In a way it becomes more like computer programming, allowing for incorporation of discontinuous elements such as switching logic, discrete states, and timers. The great thing about it is that one may still analyze the mathematical properties of the closed loop system. Although the theoretical results were verified, showing an improvement in performance, I also learned a lot from the system implementation and experimental setup. It is truly fascinating seeing one's own idea and creation do what it was theoretically intended to do.

Stationkeeping in ice is a highly complicated feat and the control system is of critical importance (in more than one aspect). In many ways one may hope for the emergence of alternative energy sources, leaving the Arctic oil untouched. Nevertheless, if not, extraction of the resources must be done without harming the fragile Arctic environment. We have to know what we are undertaking, and we must be safe.

Abbreviations

ACEX	Arctic Coring Expedition
ADS	Arctic Drillship
CA	Control Application
CIVARCTIC	Construction and Intervention Vessel for Arctic Operations
CS3	CyberShip 3
DOF	Degrees of Freedom
DP	Dynamic Positioning
DYPIC	Dynamic Positioning in Ice
GNSS	Global Navigation Satellite System
H-time	Hazard Time
HSVA	Hamburg Ship Model Basin
IM	Ice Management
KMB	Competence project with user involvement
LTI	Linear Time Invariant
MC-Lab	Marine Cybernetics Laboratory

MCSim	Marine Cybernetics Simulator
NED	North East Down
NIT	Numerical Ice Tank
PD	Proportional Derivative
PID	Proportional Integral Derivative
ROV	Remote Operated Vehicle
RPM	Revolutions pr. Minute
SALM	Single Anchor Leg Mooring
SNAME	The Society of Naval Architects Marine Engineers
T-time	Total Time
TAMP	Thruster Assisted Position Mooring
UPS	Uninterruptible Power Supply
WOPC	Weather Optimal Positioning Control

Contents

Part I

Cold Frontiers and Dynamic Positioning

Chapter 1

Introduction

1.1 Background and Motivation

Ever since the first humans ventured towards the polar regions inhospitable environments it has been all about discovery, science, and economic opportunities. It is still. In the early days mapping and conquering new land, discovering sailing routes, hunting, and mining were driving factors. It required smartness and technological adaptation to meet the polar challenges, and those who were able stood out. For the early voyages finding the most appropriate route was often the main navigational objective. It was often not the shortest. The same tactics are still common in today's transit ice navigation (Kjerstad, 2011).

Over the last century the polar regions have been mapped, sailing routes discovered, hunting has been condemned and almost abandoned, and mining is in decline. However, new driving factors have emerged through promising hydrocarbon resource estimates (Gautier et al., 2009), peaking tourism numbers (Snyder, 2007), and scientific research cruises. These activities have different needs than their predecessors, and there is often a requirement for operation on a geo-fixed site. Thus, some form of stationkeeping system is needed. In polar regions, or not, this may be achieved by either:

- Mooring, where the ship is held in place by one or multiple anchors.
- Thruster assisted position mooring (TAMP), where a control system uses the ship's propulsion system to aid the mooring by for instance dampening motion, reducing tension, and/or seeking an optimal set-

point.

- Dynamic positioning (DP), where a control system uses the ship's propulsion to reach and maintain a slowly moving or fixed reference setpoint.

Although a handful of pioneering operations have been attempted, no operational standards are in place. Thus, it is fair to say that stationkeeping in ice is still in its infant years. Many of the operations are regarded as successful, although most, if not all, have encountered unforeseen challenges. Examples are ice intrusion during the open water season, ice accumulation on the vessel and in moonpools, tunnel thruster ice clogging, degraded or failing DP systems, ice re-freezing around the vessel, amongst others (Keinonen and Martin, 2012).

This thesis is a part of the KMB Arctic DP project (Skjetne et al., 2014), and focuses on ice dynamics and DP control system design. The latter is an integral system used in a variety of marine operations with both long and short term timeframe. In open water DP is usually considered to be a single vessel operation, but in ice the prevailing view is the opposite. Further context is therefore needed to understand how the operation relates to environment, and how this may be a perfect catalyst for researching new solutions to push the DP control system to the next level.

1.2 Thesis Outline Structure

The thesis is a collection of papers extended with additional material to unify the publications and discussion for readers not familiar with both research on ice interactions during marine operations, and control engineering. It consists of three parts:

- Part I presents the research objectives and summarizes the main contribution in context of the marine environment, the operation, and state-of-the-art and future outlook of DP control systems. It has four chapters and provides the background material before the research questions:
  - Chapter 1 provides a brief introduction and motivation.
  - Chapter 2 gives an overview of offshore operations in cold environments with focus on the marine environment, the operation

design philosophy, ice management (IM), and pioneering operations.

  - Chapter 3 presents an overview and future outlook of DP control systems with focus on algorithmic structure and functionality.
  - Chapter 4 presents the research objectives and summarizes the main contributions.

- Part II consist chapters 5 and 6 presenting a selected set of international peer-reviewed journal and conference publications produced during the period 2010-2016.
- Part III with Chapter 7 gives a summary of the work and closing remarks.

1.3 Readership

The primary readership for this thesis is scientists, engineers, and students familiar with one or more of the following:

- Design of stationkeeping control systems.
- Stationkeeping operations in ice-covered waters.
- Modeling and measurement of global loads on floating structures.

Chapter 2

Offshore Operations in Cold Environments

In order to understand the cold environment challenges for DP systems, it is of utmost importance to understand the conditions and operations and learn from previous experiences. Therefore, this chapter is devoted to present a basic overview of the environment, operation design philosophy, ice management, and pioneering operations.

2.1 The Marine Environment

Both polar regions contain large oceans, and ship operations are often confronted with challenges that are uncommon to other seas. These are related to low temperatures, ice features in the sea, icing on the ship and equipment, snow, and fog. With harsh wind, quickly forming low pressure storms, darkness, and remoteness it is truly a challenging environment.

Although many of the mentioned phenomena can cause problems during DP operations, the main diversifier is presence of ice. It is easy to think of ice as a continuous sheet of ice, or ice floes, with more or less uniform thickness that covers the ocean. However, it is not. Ice is a dynamic matter which due to physical environmental processes such as gravity waves, wind, current, atmospheric pressure, Coriolis, and temperature fluctuations may be broken up, compressed, mixed with ice and ice features from other regions, and refrozen on a large temporal and spatial scale. The sea ice may survive summers and harden over time as the brine drains from the ice material.

Figure 2.1: An example of the complex composition of drifting ice which includes large floes, rubble out of plane, ridges, and icebergs. The photo was taken during Oden Arctic Technology Cruise 2012 in the Fram strait.

This may create highly diversified ice fields as seen in Figure 2.1. To explain this, three crude categories of marine environments are used:

- Open water
- Drifting sea ice
- Landfast ice

Open water bears many similarities with open water in non-polar regions. However, two additional challenges may be of high importance. The first is sea-spray icing. This happens as waves interact with the vessel and sea-spray droplets form and freezes to the ship's superstructure. This can cause a number of challenges ranging from minor equipment failure to destabilizing and capsizing ships by increasing the metacentric height. Sea-spray icing must not be confused with atmospheric icing, which is the icing occurring irrespective of sea-spray due to droplets in the air. However, this can also be challenging if sensors and equipment become ice covered.

The second challenge in open water is glacial ice. Although large features

are obvious threats they can often be detected and monitored early. This makes risk evaluation easier. Smaller features pose an additional challenge as they can be hidden in complex weather scenarios until being at close range. Combined with wave motion excitation such can cause high impact loads and hull damage.

Drifting sea ice can be defined as ice features free from land, and potentially moving. It occurs in about 10% of the world ocean's surface, growing, melting, and drifting under the influence of solar, atmospheric, oceanic, and tidal forcing (Leppäranta, 2011). The main operational difference from open water is the physical interaction with ice. The implication severity depends on a wide range of variables, and some of the most important are believed to be:

- Ice cover composition
- Ice material properties
- Ambient ice pressure
- Ice drift characteristics
- Vessel hull characteristics and operational strategy

As ice is affected by the abovementioned environmental processes, it becomes a nonhomogeneous matter. It is composed of a variety of features which have been either mixed or frozen in, or formed over time. Although a rich classification exists (see e.g. (WMO, 2014)), the following generalizations are sufficient to discuss the ice cover with respect to DP operations:

- Ice floes: Ice from frozen sea water which may have been broken up a number of times by environmental processes. One ice floe may therefore contain features such as pressure ridges and iceberg remnants.
- Pressure ridges: Out of plane accumulation (and re-freezing) of ice fragments at the contact line between ice floes, formed by pressure. Often referred to as just ridges.
- Glacial ice: Fresh water ice which has broken away from a glacier or an ice shelf. Also known as icebergs or iceberg remnants.
- Rubble and brash: Fragments of ice caused by ice-ice interaction or the interaction with fixed or moving structures.

The ice cover composition also includes ice concentration, and floe size distribution. The former is the ratio of the area of ice features to the total

Figure 2.2: Left: Storing ice cores after compression tests. Right: Deploying multi-beam upward looking sonar. Both pictures are from Oden Arctic Technology Cruise 2012. Courtesy Øyvind Hagen and Statoil.

area of surface. This is shown to be of great importance to the load level experienced by a ship (Comfort et al., 1999). The latter is the statistical distribution of ice floe sizes in the operational area. This is also believed to be of major importance. For instance, small ice floes in low concentration will cause low loads as the ice will mostly be deflected. This interaction type will not be as prominent in large ice floes and high ice concentration, where more complex interactions including significant ice material failure processes and rafting will become more predominant.

Within the ice cover, each ice feature will have its own material properties that impact the load on a ship or structure. This is determined by factors such as geometry, temperature, age, salinity, porosity, crystallography, etc. Here it is often talked about first-, second-, and multi-year ice. The reason for this is that as the ice ages (if not melting completely in the summer season), the brine pockets drains and the material consolidates, making it harder. Harder ice requires more energy to break, and is thus tougher to operate in. Another aspect of operation in ice that is particularly important to floating structures is the lack of waves. Although some swell may occur, the ice cover effectively dampens the waves exponentially with distance to the ice edge (Frankenstein et al., 2001; Broström and Christensen, 2008).

Sea ice drift may be divided into two different processes. The first is the mean drift, which depends on large scale circulation patterns such as the Beaufort Gyre and the Transpolar Drift Stream. The second is variations

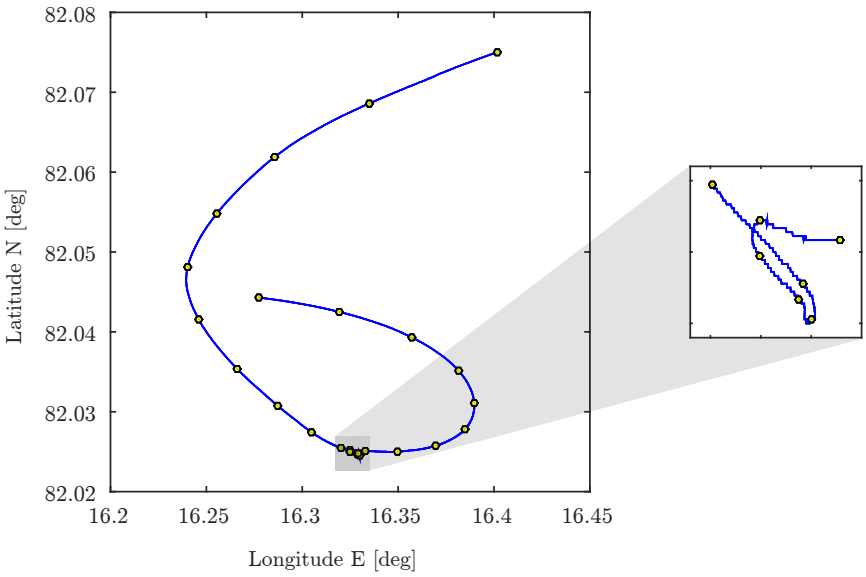

Figure 2.3: The ice drift from one ice drift tracker during the Oden Arctic Technology Cruise 2015. The points mark hour intervals.

due to processes such as tides, Coriolis, and wind. Together they create ice drift with great variation in both direction and velocity on a daily basis. Figure 2.3 shows an example of the variability. This is especially challenging for ship shaped vessels since ice drift which is not countered by the bow (or stern) may result in high loads. This problem does not arise for vessels that have a more circular shape. However, these will have a sustained higher load than ship shaped ones operated compliantly with the ice drift (given comparable deck size).

Ice pressure is another phenomena occurring in sea ice that is of high importance for ship operations. It is caused by large scale environmental forces acting from opposing directions on an ice field, and results in 10/10 ice concentration and sustained pressure between the ice floes. The phenomenon is known for forming ice ridges and rafted ice, and may cause significant damage and/or forcelift ships up on the ice.

The last category is landfast ice. This is when the ice cover is intact and fixed to land. Although operating in this environment without physically transforming it to one of the other two categories is unlikely, it may be possible. In that case there are two main challenges. The first is thermal expansion of the ice cover. It happens when the temperature changes and

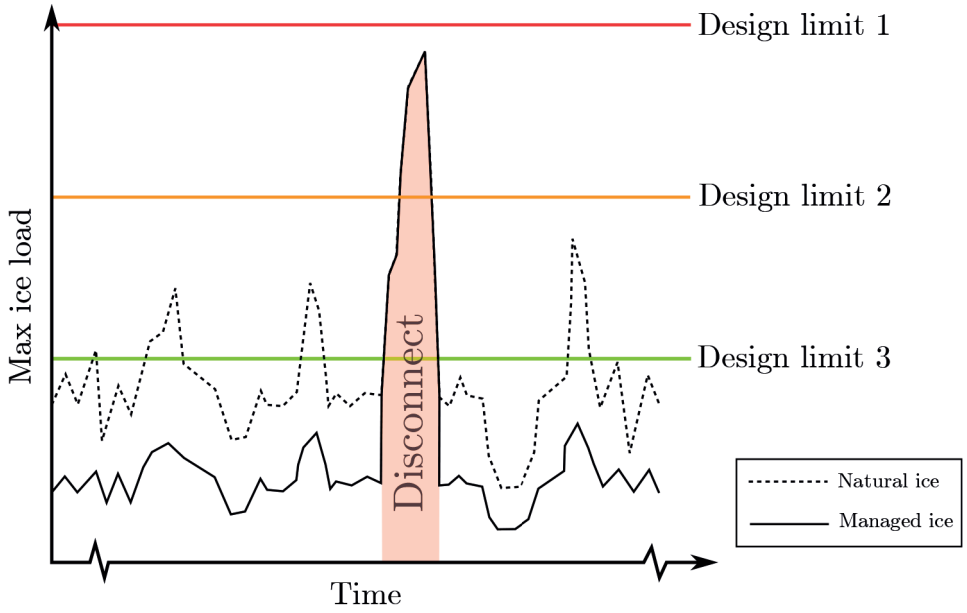

Figure 2.4: Illustration of the maximum ice load level with and without ice management, and the relation to structure design limits.

causes the spatial size of the ice sheet to contract or expand. From the vessel's point of view, it will experience moving ice. The severity depends on the size of the ice cover, the geometry of the land the ice is fixed to, the distance from the vessel to land, and the temperature fluctuation. The second challenge is that the ice cover around the vessel can re-freeze.

2.2 Operation Design Philosophy

For all long term geo-fixed marine campaigns in low temperature polar environments the operation design philosophy will question whether to use bottom-fixed or floating structures. The answer depends on a wide range of variables, both economical, risk, and environmental. One obvious factor is the water depth. If the area is too deep for conventional bottom-founded structures, then a floater must be used. In shallower waters, if a fixed structure is to be used, it must be designed to take all expected loads. This is shown as Design limit 1 in Figure 2.4. The problem is that it will often be unpractical and not economically viable due to the extreme strength that the structure will require. This especially applies in areas with potential

for both pressurized sea ice and abnormal ice features such as icebergs and consolidated multi-year ridges. A floating structure may often be an attractive alternative since it can disconnect and move out of harm's way. This option allows for a lower design limit (as illustrated by Design limit 2 in Figure 2.4). As disconnecting and evasive action takes time it requires identification of the high loads ahead in time so that the design limit is not exceeded. Therefore, floating structures with the ability to disconnect require surveillance, detection, monitoring, and forecasting systems to observe the ice conditions around the operational area. Another aspect of disconnections is that it may render the structure unable to do its main purpose for days or even weeks. This can have severe economic consequences, and should be avoided. Therefore, adding physical manipulation by a fleet of support vessels makes sense. By breaking up the incoming ice the overall load level will be reduced on the structure (Eik, 2010), and more control is gained with the ice condition. A side-effect of this is that the design limit can be lowered again (as illustrated by Design limit 3 in Figure 2.4).

The physical intervention in the ice cover and the surveillance, detection, monitoring, and forecasting is often called ice management (IM) or ice defense, and it has been clear since the earliest stationkeeping operations in ice that these actions are critical to ensure safety. In general it is risk control which purpose is to ensure continuation of the operation with a high degree of confidence, beyond the time it takes to terminate activities and evacuate safely. This is needed whenever there is a probability of either icebergs or sea ice intrusion. Eik (2010) defines IM as the sum of all activities where the objective is to reduce or avoid actions from any kind of ice features.

2.3 Ice Management

To implement IM a few key concepts are used:

- IM fleet; one or more support vessels working to avoid or lower ice loads on the protected vessel.
- Protected vessel; the stationkeeping structure performing the main objective of the operation.
- T-time, or total time; the time it takes to terminate the operations onboard the protected vessel and perform evasive action.
- H-time, or hazard time; the time it takes for a hazard to reach the

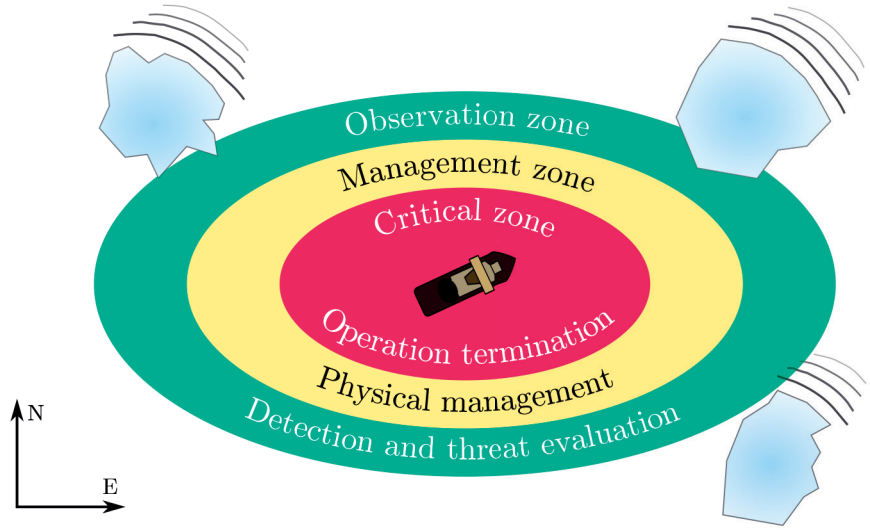

Figure 2.5: Example of division of the operation area in three zones. The figure is not in scale but for illustrative purposes only. Adapted from (Younan et al., 2012).

operation site.

The surveillance and physical intervention of IM cater for a natural division of the operation area into three circular overlapping sectors as seen in Figure 2.5 (Hamilton et al., 2011; Younan et al., 2012; Hamilton et al., 2014). In the outer observation zone only surveillance, detection, monitoring, and forecasting is performed. This relies on various intelligence sources shown in Table 2.1 (and compared in Table 2.2). In the middle management zone, physical intervention is carried out to remove hazards with trajectories that may enter the inner critical zone. If a hazard enters the critical zone, termination must be initiated. The actual spatial zone sizes depend on the ice drift, the T-time, and the IM fleet tactics.

The T-time is often dependent on the mode of termination. This may be either controlled or in emergency. As an example, controlled termination and evasive action when drilling with a pressurized riser can take 24 hours or more, but in an emergency scenario it can be achieved in much less (a few hours). The challenge with controlled termination is the time a hazard must be detected in advance. This requires a very precise surveillance, detection, monitoring, and forecasting system. If imprecise, it may initiate unnecessary terminations lowering the up-time of the struc-

Table 2.1: Sensor platform overview. Adapted from (Haugen et al., 2011).

	Platform				
Sensor type	Satellite	Aerial	Shipboard	Buoy	Underwater
Optical	✓	✓	✓		
Laser altimeter/scanner	✓	✓			✓
Radiometer	✓	✓	✓		
Synthetic aperture radar	✓	✓			
Marine radar			✓		
Scatterometer	✓	✓			
Radar altimeter	✓	✓			
Acoustic techniques			✓		✓
Meteorological suite		✓	✓	✓	
Oceanographic suite			✓		✓

ture (i.e. the time the structure is performing its main task), or fail to identify hazards leading to emergency termination or in the worst case hazard collision. The benefit of a controlled termination is that it enables for quick resume of operation. It does not require the same degree of inspection, maintenance, and replacements as after an emergency termination. The T-time will also be impacted by the stationkeeping system. A DP system, as opposed to moorings or thruster assisted moorings, will not have the mooring turret to disconnect. Table 2.3 shows an example of the relation between the T-time, H-time, and state of the operation from the moored Kulluk during its Beaufort Sea campaign in the 1980s.

Table 2.2: Sensor platform comparison. Adapted from (Haugen et al., 2011)

Platform	**Coverage**	**Spatial res.**	**Temp. res.**	**Cost per area**	**Suggested regions**
Satellite	Excellent	Interm.	Low	Interm.	Distant
Aerial	Very good	High	Interm.	Interm.	Distant to close
Shipboard	Low	Interm.	High	Low	Close
Buoys	High	Sparse	Interm.	High	Distant to interm.
Sub-sea	Good	Excellent	Interm.	Interm.	Close to interm.

Table 2.3: H-time: Time until the hazard reaches the stationkeeping vessel, T-time: The total time it takes to securely stop the operation and move off site. M-time: Move-off time. Courtesy of (Shell, 2011).

Alert Level	Time calculation	Status
Green	(H-time – T-time) is greater than 24 hours	Normal operations
Blue	(H-time – T-time) is greater than 12 hours and less than 24 hours	Initiate risk assessment. Validate secure times and move times.
Yellow	(H-time – T-time) is greater than 6 hours and less than 12 hours	Limited well operations in line with the critical operations and curtailment plan. Commence securing well.
Red	(H-time – M-time) is less than 6 hours	Well-securing operations completed. Commence anchor recovery operations.
Black	Drill site evacuated	Move drilling vessel to a safe location.

The physical intervention depends on the operation location and conditions. This is often referred to as IM fleet tactics, or just IM tactics. To discuss the different approaches Figure 2.6 is used. It shows the probability of sea ice through the year for an imagined Arctic operation site that is inside the polar ice cover in winter, but outside in summer. Thus, the site will contain all the common ice threats. In the summer season the scenario is open water, and glacial ice features and remnants of large ice ridges pose the main ice hazards. Although unlikely, there is also a risk of sea ice intrusion due to unfavorable weather and pressure processes in the ice cover higher north. For the large ice features the physical intervention tactic is towing hazards well off collision course. Here it is key to ensure that the towing does not set the hazard on a new collision course when the drift changes. When no hazards are present, the IM fleet may either be in standby, scouting, or performing other tasks that normally require open water. Examples of the latter are anchor handling, tugging, and supply.

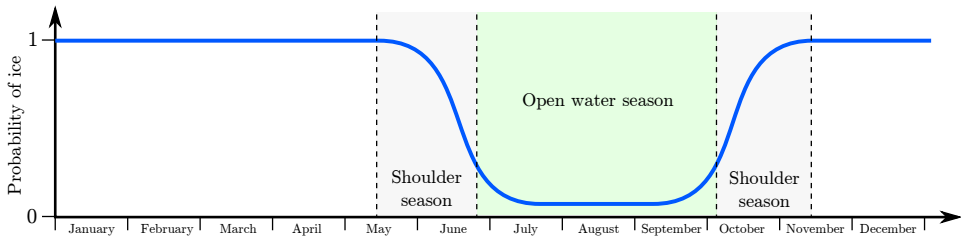

Figure 2.6: Illustration of the probability of ice on a fictive Arctic station-keeping operation site. Based on (Keinonen and Martin, 2012).

When significant sea ice is present (> 15-20% ice concentration), either in winter, the shoulder seasons, or during the odd ice intrusion in summer, the tactic shift from focus on individual ice features alone to also creating a channel of managed ice for the protected vessel to operate in. The idea behind this is that smaller floes will be deflected off the protected vessel and the amount of ice mass in direct or in-direct interaction with the vessel is reduced. Thus, lowering the loads compared to breaking unmanaged ice. Figure 2.7 illustrates the concept and shows some of the potential maneuvering patterns that may be applied by the IM fleet together with a satellite picture of an area which has been subject to physical IM for some time. Creating the channel when the ice drift loops may in many cases be a challenge alone as the IM fleet must be able to move according to the ice drift pattern in such a way that the center of the channel aligns with the operation point of the protected vessel. If not, the protected vessel may interact with unmanaged ice and have greater risk of position loss (Hamilton et al., 2011). The optimal size and composition of the IM fleet and its maneuvering tactics depend on may variables, but some important ones are ice concentration, ice thickness, drift dynamics, target managed ice floe sizes, and the various icebreaker capabilities.

Although IM is designed to counter many of the challenges on an operational fleet level, there is also a strong need for measures against low temperature challenges on the particular ships. This is referred to as winterization, which is designed to protect the vessels functions, systems, and equipment considered important to safety, provide suitable equipment and supplies, and implement procedures for safe operation and personnel welfare (DNV, 2013).

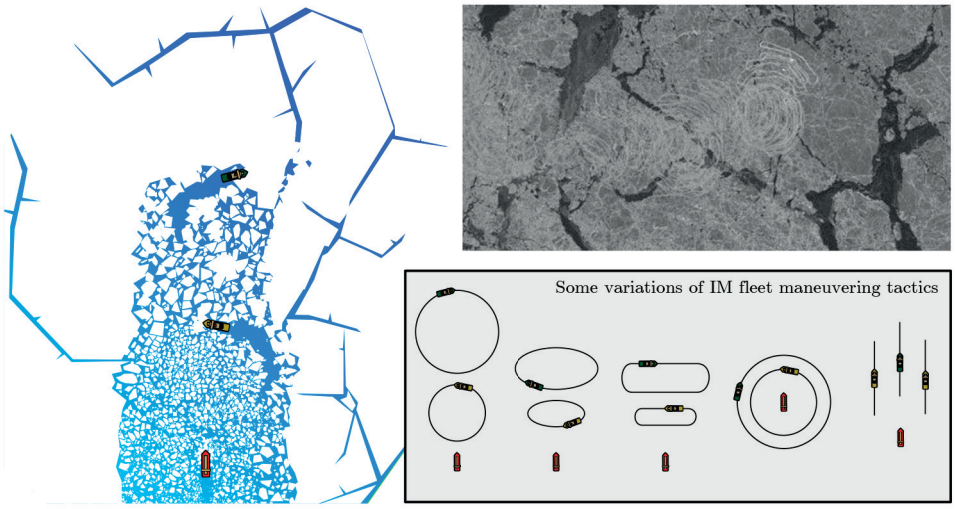

Figure 2.7: Left: Illustration of physical ice management in drifting sea ice. Upstream are two icebreakers performing physical IM to reduce the environmental load on the downstream protected vessel. Right bottom: Various IM fleet maneuvering tactics that may be employed. Right top: A radar satellite image from an IM operation during Oden Arctic Technology Cruise 2015. The drawings are adapted from (Haugen, 2014) and (Hamilton et al., 2011).

2.4 Pioneering Operations

In order to develop a DP control system that handles ice interactions, it is of utmost importance to gain insight from the few full scale operations that have been commenced (see Table 2.4). These can be separated by the method of stationkeeping: mooring or DP. Although mooring operations gives additional insight on the specific ice challenges and IM aspects, this section will focus on the DP operations to investigate the relation between operating in ice and the behavior of the control system. In the tree documented operations, two different vessels have been used, and all operated in drifting sea ice where various ice conditions was encountered.

The first claimed DP operation in drifting sea ice was performed outside Sakhalin in May-June 1999 (Keinonen et al., 2000). The Coflexip Stena Offshore Constructor, an ice classed vessel at the time, provided support for compression diving for construction, repair, and testing of a pipeline going from the Molikpaq platform to a single anchor leg mooring (SALM)

Table 2.4: Documented operations. Extended from (Aksnes, 2011).

Location	Stationkeeping method	Operation type	Timeframe
Beaufort Sea *(Canmar drillships)*	Mooring through waterline	Drilling	Long term, 1976 - late 1980's
Beaufort Sea *(Kulluk)*	Submerged mooring system	Drilling	Long term, 1983 - 1993
Grand Banks *(Terra Nova)*	Submerged turret mooring system	Hydrocarbon production	Long term, 2002 - present
Grand Banks *(White Rose)*	Submerged turret mooring system	Hydrocarbon production	Long term, 2005 - present
Pechora Sea	Loading tower	Offloading	Long term, 2000 - present
Offshore Sakhalin *(CSO Constructor)*	DP	Diving support	Short term, 1999
Arctic basin *(Vidar Viking)*	DP	Drilling	Short term, 2004
Greenland sea *(Vidar Viking)*	DP	Drilling	Short term, 2008

buoy using a conventional commercial DP system. To reduce the ice load on the Constructor, two icebreakers, Smit Sakhalin and Magaden worked upstream to break the incoming ice into smaller floes. The operation lasted six weeks and encountered different ice conditions. During this time the operation experienced 22% downtime due to severe ice.

Although the operation is labeled as a success, nothing is disclosed about positioning performance or operational limits. Thus, there are no indications of how accurately the DP control system was able to compensate the ice loads. However, it is reported that one of the most significant challenges was to determine the ice drift and set the heading towards it. Another noteworthy aspect is that the vessel was occasionally operated with an oblique angle to create an open lead to load or retrieve subsea equipment. This is interesting because it creates an asymmetrical loading scenario which is more challenging.

In the two remaining operations the Vidar Viking was used. This is a combined icebreaker and anchor handling tug supply vessel. During the Arctic Coring Expedition (ACEX) in August and September 2004 it was

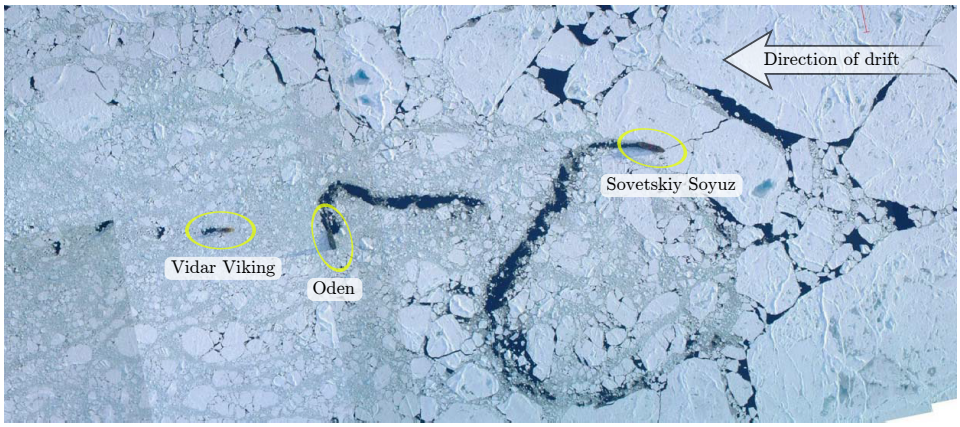

Figure 2.8: Picture of the Arctic Coring Expedition fleet taken form helicopter. Adapted from (Keinonen et al., 2006)

used to drill core samples in the Lomonosov ridge at about 88° N (Keinonen et al., 2006; Moran et al., 2006). It was accompanied by the icebreakers Sovetskiy Soyuz and Oden for similar physical ice management tasks similar to the 1999 Sakhalin operation. Figure 2.8 shows the IM fleet during the stationkeeping operation. Since this was deep within the Arctic pack ice, the fleet encountered severe ice conditions with a high percentage of thick multi-year ice. With respect to the angle of the drillstring, the DP operation had an allowable operational area which should not exceed 5% of the water depth. This gave a circle of operation of about 50 meters for the coring sites. The T-time of the operation was 4 hours. Both automatic and manual DP were tested, with the bow and the stern of the Vidar Viking heading into the ice drift. The only feasible mode of stationkeeping turned out to be manual control of the two stern propellers with the bow towards the ice drift. The tunnel thrusters were ineffective in the heavy ice. To counter the ice, a maneuvering-based operational strategy where the vessel moved up and drifted back along the ice drift direction within the operational area was used. The benefit of this was that it utilizes the inertia of the vessel to handle the ice features when moving upstream. Overall, the mission obtained a net up-time of exceeding 90 % of what was considered possible. During the operation two major drive-offs occurred, and at one instance it was interrupted due to insufficient icebreaking.

The last operation was east of Greenland in 2008. The fleet consisted of Vidar Viking as a drillship protected by the Oden (Rohlén, 2009). Figure 2.9 shows a picture from the operation. Not much is disclosed about the ice

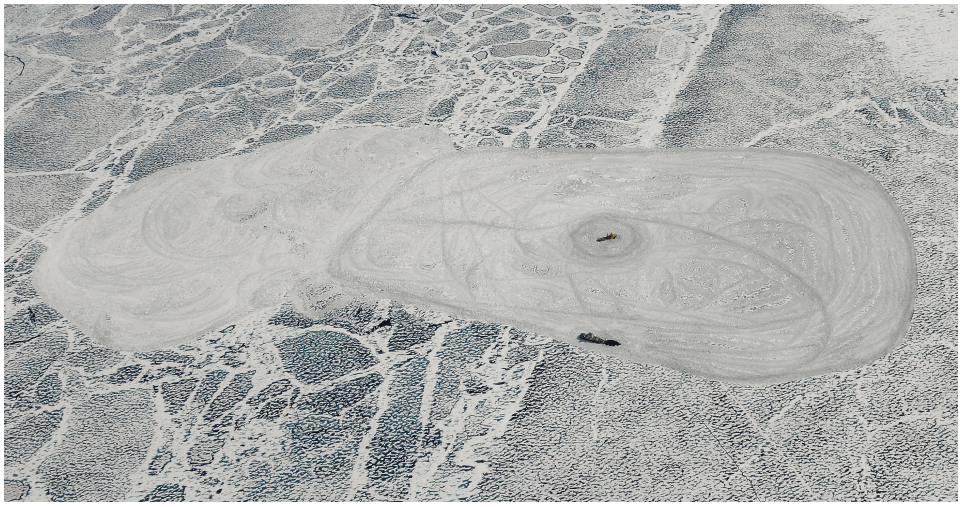

Figure 2.9: Picture taken from a helicopter during the 2008 operation with Vidar Viking and Oden. Notice the approach to IM as a result of very slow ice drift. Courtesy of Per Frejvall and Statoil.

conditions, other than that they were lighter than what was encountered during ACEX. It is reported that the automatic DP system was able to maintain position for long periods of time, in well managed ice. Also here the heading of the vessel against the ice drift is emphasized as an important factor. It was only challenged by large floes and propeller wash from Oden, when it got too close.

From these pioneering campaigns it seems clear that there is a window of opportunity where automatic DP will be feasible. However, the boundary of such will depend on variables such as the ice condition, vessel power, control system capability to handle the environment, and operation strategy. Special emphasis must be put on tracking the ice drift, which today is done manually by an operator. In regard to DP control system capability and reactivity, the ACEX indicates that there is a margin between what commercially open water systems can achieve and what is possible within the capability of the vessel. Thus, there is a margin of improvement.

Chapter 3

Dynamic Positioning Control Systems

As the publications presented in Part II goes into detail on specific aspects of the DP control system, a fundamental overview of its structure and content is presented here along with challenges in ice and an outlook for future developments.

3.1 Historical Background

In the early 1960s the geological sciences and the oil and gas industry wanted to investigate areas where conventional fixed or moored platform system could not go. Without any means of physical anchoring the idea of a system which enabled stationkeeping solely through thrusters was conceived (Breivik et al., 2015). In 1961 the coring vessel Eureka became the first with an electronic computer system to do this (Fay, 1989). This marks the start of the DP era, which as today applies the same principles; to automatically control the vessels planar motions and keep it within specified position limits with minimum fuel consumption and mechanical wear-and-tear (Balchen et al., 1980; Østby and Kvaal, 2015).

From the first pioneering systems using single-input single-output proportional-integral-derivative (PID) control the DP control algorithms have evolved to sophisticated nonlinear control methods incorporating and exploiting mathematical models of the environment (Strand, 1999; Skjetne, 2005; Sørensen, 2005, 2011). The models describe the dynamics of the vessel and provide

Table 3.1: A list of DP vendors for offshore ships as of October 2015. Keep in mind that he location of the headquarters do not always reflect the location of the DP research and development.

Company name	Product name	Headquarters
General Electric	SeaStream DP	United States
Imtech Marine	Dynamic Positioning and Tracking	Netherlands
Kongsberg Maritime	K-Pos DP	Norway
Marine Technologies	Bridge Mate DP	United States
Navis	NavDP	Finland
Norr Systems	P-Class DP	Singapore
Praxis Automation Technology	Mega-Guard DP	Netherlands
Rolls-Royce Marine	Icon DP	United Kingdom
Sirehna	Easy DP	France
Wärtsilä	Platinum DP	Finland

a relationship between the measurements, vessel states, and the thrusters' actuation. The algorithms take into account effects such as inertia, cross-couplings between the degrees of freedom (DOF), nonlinear damping and restoration, wave perturbations, and thruster loss effects (Sørensen et al., 1996). An in-depth description of state-of-the-art theory is found in (Fossen, 2011; Sørensen, 2012). For more insight, Breivik (2010); Breivik et al. (2015); Østby and Kvaal (2015) provides an overview of the historical DP development and puts it in context with early ship automation.

Today DP is a success story with more than 2000 vessels of various kinds (Sørensen, 2012). The number is assumed to grow as the technology gets more widespread. A number of robust commercial solutions are available on the open market, all handling different operational scenarios in the presence of wind, waves, and currents. Examples include sub-sea construction, pipe-laying, crew change, search and rescue, remote operated vehicle (ROV) support, anchor handling, diving support, drilling, virtual anchoring, low speed maneuvering etc. Most commercial solutions target larger ships such as cruise liners, mega-yachts, fishery, and various offshore oil and gas vessels, but some systems are made for smaller ships in the leisure market (see for instance (Volvo Penta, 2014)). A list of the most prominent DP vendors can

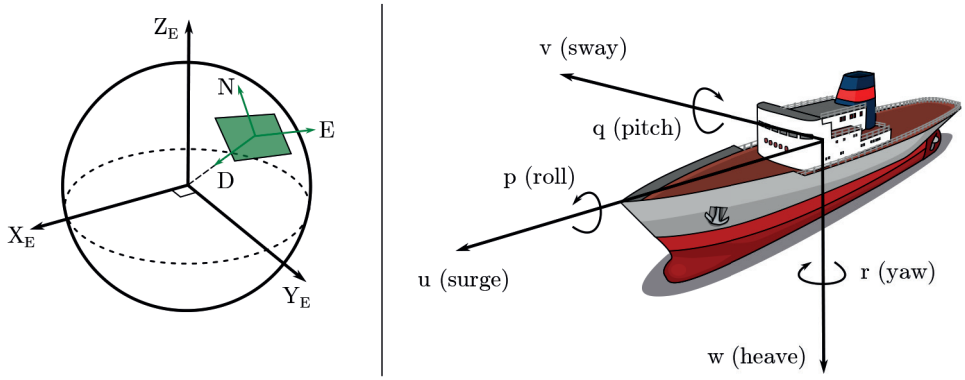

Figure 3.1: Two important reference frames for motion control of ships, the (NED) frame and the vessel body frame. Adopted from (Breivik, 2010).

be seen in Table 3.1. At first glance the solutions can look different, utilizing different hardware components, and offer somewhat varying functionality besides pure position and heading control. However, the structure of the control loop converting measurements to thruster output follow a strict model. An overview of this is given next.

3.2 Structure and Functionality

Before embarking on the structure of the feedback loop, some fundamental relations and concepts must be presented. The first is the reference frames, illustrated in Figure 3.1, where the kinematic and kinetic relations are described. The north-east-down (NED) frame is an Earth fixed tangent plane with the axes point according to the name. The positioning objective is defined in this frame, and it is considered to be inertial. Although this is a simplification the impact on the stationkeeping ability is negligible as it just adds to the external disturbance from waves, wind, current, and other modelling errors. The second frame is the body frame which is fixed to the vessel body according to (SNAME, 1950). The control output is defined in this frame. Traditionally, one, two, or all of the planar DOFs are controlled (surge, sway, and yaw), but for some vessels, such as semi-submersibles and cruise liners, roll and pitch damping may be included. In addition to the NED and body frames, each sensor has its own frame. It is fixed to the ship and therefore has a static relationship with the body frame. Thus, it is common to transform the sensor measurements from the individual sensor

frames to the body frame.

All modern DP control systems are comprised of hardware and software which act together to provide reliable stationkeeping. The necessary reliability is determined by the consequence of loss of stationkeeping capability. The larger the consequence, the more reliable the DP system should be (Sørensen, 2012). To achieve this the International Maritime Organization (1994) groups the control system into three equipment classes, also known as the DP classes. Class societies often use four classes to describe the same, where the additional one holds those who do not have any class (see for instance (Det Norske Veritas, 2011)). In both cases, the required equipment class depends on the specifics of the DP operation, and the main diversifier between the different classes is the redundancy of the hardware and software systems. Thus, the structure of the feedback loop implemented in software remains the same.

The most prominent hardware, regardless of class, is sensors, computer networks, computers, machinery, power systems, and actuators. Figure 3.2 shows an example of the system architecture from a commercial vendor. Some components are specific to the DP system, and some are shared with other ship systems. Since the DP control system is a tool that widens the vessel usability, the shared hardware may not be optimized for DP alone. An example of this is machinery, power system, and actuators which may be designed for minimizing fuel consumption during transit rather than stationkeeping. Naturally, this may impact the stationkeeping performance and capability in some environmental conditions.

The DP system software is divided between multiple computers solving different tasks at different hierarchical levels. It can be divided into:

- Actuator and hardware control. This is the lowest level of control software, and it sits in embedded computers on the various hardware components and is responsible for interacting with and controlling the hardware.
- Plant control. This runs on dedicated control computers and hold the actual implementation of the DP algorithm. The software structure, which today can be considered standard, is seen in Figure 3.3. With respect to Figure 3.2 the plant control runs on a computer in the control unit.
- Operator interface. This contains a human-machine interface in the form of levers, buttons, touch screens and graphical user interfaces

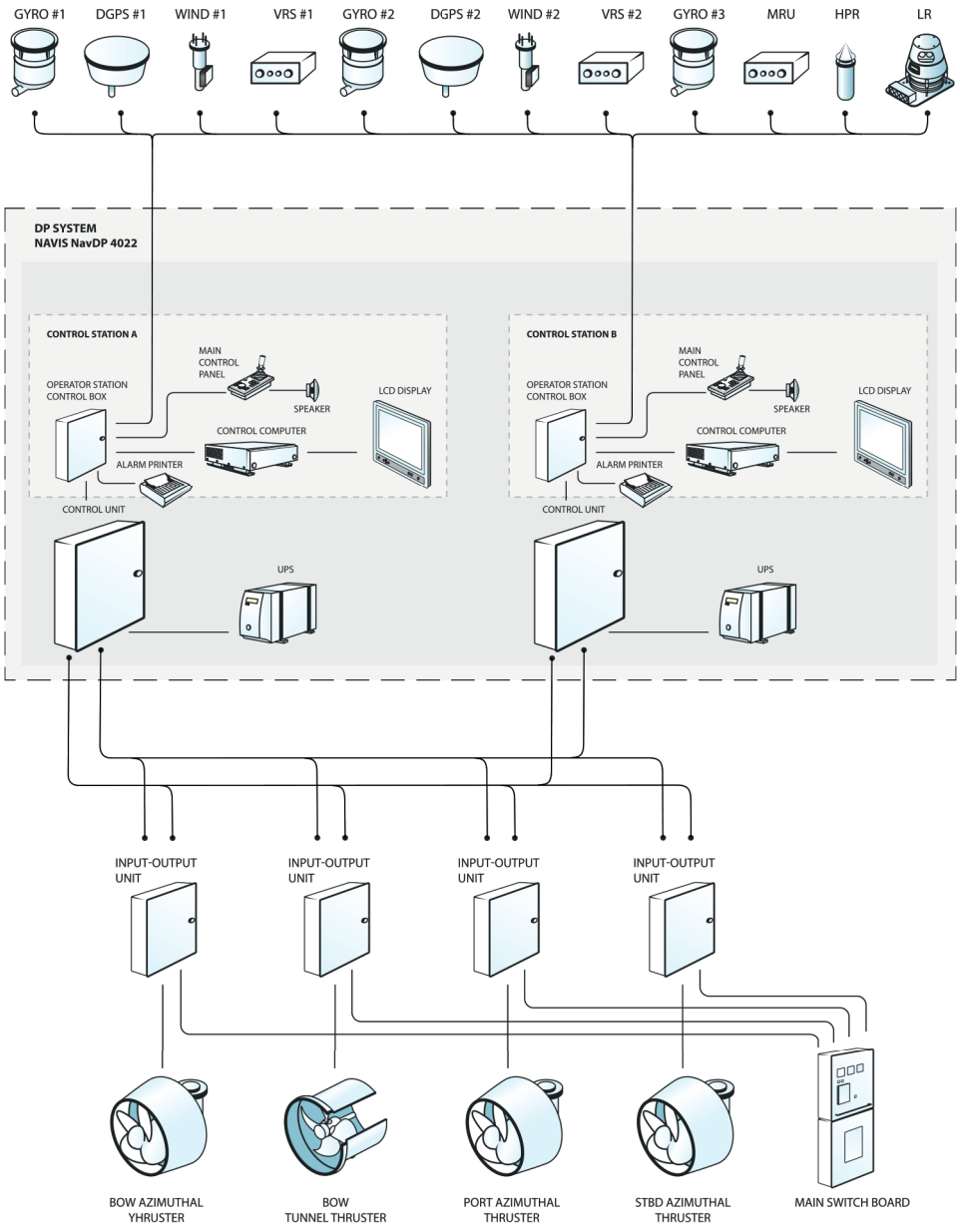

Figure 3.2: An example of DP control system architecture for a vessel with four thrusters and two identical operation stations. Adapted from (Navis Engineering, 2014).

providing the operator with input ability system status feedback. It runs on a separate computer in the operator station and communicates with the plant control computer over network. With respect to Figure 3.2 it runs on the control computer. Some commonly found functionality is: manual joystick operation, automatic positioning control of selected degrees of freedom in various modes (e.g. low, medium, or high gain positioning or weathervaning), trajectory tracking, waypoint tracking, or ROV tracking, autopilot. The system will also provide feedback of key parameters and provide analysis showing capability plots, consequence analysis, and alarms.

Although all the hardware components of the DP control system are important to the performance, the kernel plant control algorithm, seen schematically in Figure 3.3, is the imperative part. Since this is one of the main subjects in this thesis each of the components will now be introduced.

- Sensor suite: The sensor suite consists of a range of sensors to measure the vessel position, heading, motion, propulsion output, and operational environment. In general these can be divided in five groups:
  - Position reference systems. These are sensors that measure the position of the vessel in either global or local coordinates with respect to the NED frame. Examples include; global navigation satellite systems (GNSS), hydroacoustics systems, taut wire, and systems utilizing radar, microwave, or laser for position triangulation.
  - Attitude reference systems. These are sensors that measure the orientation of body frame with respect to the NED frame. Examples include; gyrocompass, magnetic compass, and GNSS compass.
  - Motion reference systems. These are sensors that measure the motion of the vessel in the body frame with respect to the NED frame. Examples include; inertial measurement systems (accelerometers and gyroscopes) for vertical reference and rate of turn, and Doppler velocity sensors.
  - Vessel propulsion measurements. These are sensors that measure the state of the actuators to determine the generated output propulsion in the body frame. Examples of measured variables include; RPM, torque, power, pitch angle, rudder angle, and azimuth angle.

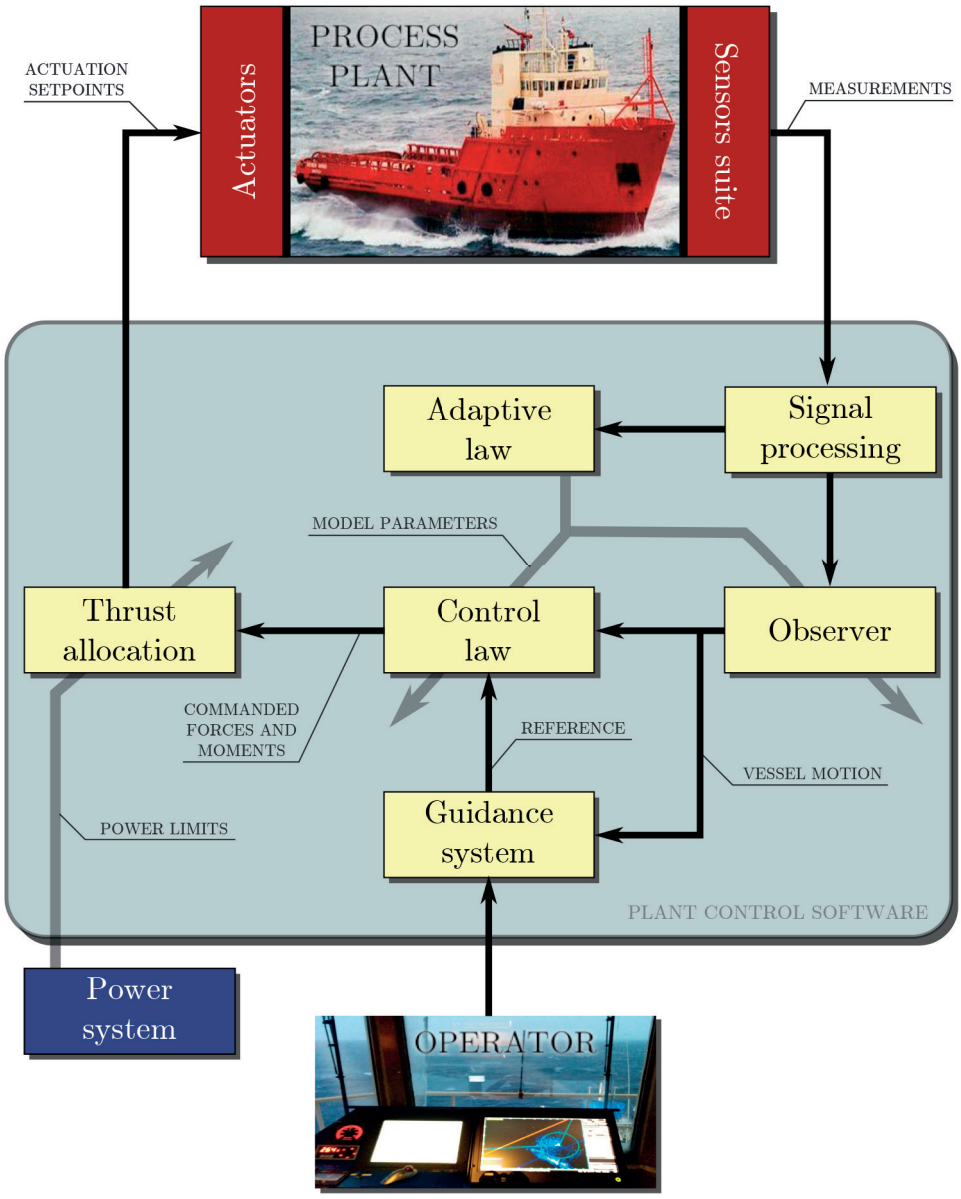

Figure 3.3: The modular structure of the DP control algorithm. Adopted from (Sørensen, 2012).

  - Environmental measurements. These are sensors that measure variables in the environment, either for direct or indirect application in the DP control system. Examples include; anemometer, wave radar, draught sensors, thermometers, and barometers.

  It must be emphasized that a DP control system will only need a subset of these sensors from each group to provide stationkeeping capability.

- Signal processing: The signal processing analyzes the raw measurements from the sensor suite and removes faulty readings so that they are not used in the feedback loop. It will do this by:
  - Monitoring the signals for wildpoints, high variance, high derivative, and frozen signals.
  - Apply voting between redundant measurements so detect biases.
  - Apply weighing to combine healthy redundant measurements.
- Adaptive law: The adaptive law updates the parameters of the mathematical model describing the vessel to different operational and environmental conditions. In a model-based observer and controller design, as displayed in Figure 3.3, the adaptive law should automatically provide the necessary corrections of the vessel model and controller gains subject to changes in vessel draught, wind area, and variations in the sea state.
- Observer: The observer, also known as state estimator, navigation filter, or vessel observer, is a structure that filters all measurements through a model of the vessel dynamics to remove noise, bias, and estimate unmeasured system states such as linear velocity and high frequency wave motion. The latter is done to obtain the low frequency motions of the vessel and avoid wave-frequency modulation in the feedback loop and the consequent wear-and-tear on the mechanical propulsion units. Another aspect of the observer is dead reckoning, which is the observers ability to provide reasonable state estimates for some time without position reference measurements. One famous and widely adopted method to implement the observer is by a Kalman filter (Breivik et al., 2015).
- Control law: The control law is a structure composed of a combination of feedback and feedforward terms that calculates the forces and moments needed to converge to and track the setpoint reference

provided by the guidance system while counteracting external disturbances. The feedback terms compare the observer motions to the setpoint reference and calculates a needed output based on the deviation. In order to avoid stationary deviations it contains a slowly adapting term, known as integral action. A common feedback implementation is nonlinear PID control. The feedforward terms provide a contribution based on direct application of calculated and/or measured signals. The most common and known are reference feedforward from the guidance system and wind feedforward where the measured wind speed and direction is translated into a load on the vessel through an aerodynamic model. For the latter the output is the opposite of the wind load. The result is that wind gusts can be countered directly and thereby does not push the vessel off position. The control law can be optimized and tailored for different objectives, and together with the guidance system it is the two structures implementing the different functionality modes.

- Guidance system: The guidance system, also known as the reference system, generates the control law setpoint reference signal needed to fulfill the operator set operation objective. Thus, its internal structure and implementation depends on the operation objective and system mode.

- Thrust allocation: The thrust allocation, also known as control allocation, calculates actuator commands to obtain the generalized forces and moments provided by the control law. This is often a challenging optimization problem as the vessels have more propulsion units than controlled DOFs. Also, the algorithm must take into account actuator type, fuel consumption, position in the hull, capacity, mechanical wear-and-tear, forbidden zones, and thruster loss effects. The module is the point of integration between the DP control system and the onboard power system.

- Power management system: The power management system controls the onboard power plant and ensures that enough power is available for the different consumers. It incorporates functionality to prevent overload and blackout, and for diesel-electric vessels, start and stop generators according to the power demand.

- Actuators: The onboard actuators are the units allowing the DP system to exert forces on the hull. Examples include conventional propellers, rudders, azimuth/azipod thrusters, tunnel thrusters, fins, and

Figure 3.4: Free floating DP experiment at HSVA during the Dynamic Positioning in Ice project. Courtesy of Statoil.

water jets, amongst others. These have their own local control system executing the commands of the thrust allocation (Smogeli, 2006; Ruth, 2008).

3.3 The Ice Challenge

The limited success of full scale automatic DP in though managed ice have given rise to research efforts to understand and solve the DP in ice challenge. By using model ice basins (as seen in Figure 3.4) or numerical methods for towing and free floating DP experiments the same conclusions as indicated by the full scale operations have been reached (covered in Section 2.4); that DP in managed ice will be possible given a sufficiently reactive control system (see e.g. (Jenssen et al., 2009; Hals and Efraimsson, 2011; Hals and Jenssen, 2012; Gash and Millan, 2012; Kerkeni et al., 2013)). This means that the control system is able to adapt and counteract changes in the environment in sufficiently short time to avoid severe setpoint deviations.

One of the keys to the success and precision of open water DP control systems is the description of the relationship between the vessel motion variables and the environment together with tailored robust multi-variable control methods. This is founded on years of quality research and experience. In managed ice this foundation is scarce at best as the operational

experience with DP is limited, and the ship-ice interaction is not well understood and described. Some insight can be gained from studies which describe and characterizes the loads and ice cover processes on floating or fixed structures (see for instance (Wright, 2001; Ettema and Nixon, 2005; Croasdale et al., 2009; Wang et al., 2010)), and it is clear that the ice loads have a complex relationship with the ship and ice cover variables involved (e.g. ship hull type, angle of attack, relative velocity, ice material properties, ice floe size distribution, ice concentration, ice drift properties, and ice floe configuration). Especially, the angle of attack, ice thickness, and ice concentration are found to play key roles on the mean loads (Comfort et al., 1999). An important characteristic of the load signal influencing the vessel is its variability in time (see (Jenssen et al., 2009) for examples). This constitutes one of the major differences from open water and also one of the main challenges with DP in ice.

To follow the conventional model-based control design approach would require descriptions of the ice impact on the dynamics of the vessel, similar to that of other environmental components (e.g. hydrodynamic damping). In the literature, the ice load descriptions are often empirical formulas lacking the time-varying nature of the phenomena, or numerical models taking into account each individual ice floe. Neither of these are well suited for DP control design, as differential equations relating the motion of the vessel (and other measurable variables) to the ice load is needed. Although these relations are present, their nature in the low velocity range is unclear (see e.g. (Valanto, 2001)). Jenssen et al. (2009) and Kerkeni et al. (2013) indicates that the state estimation capability of the observer is of great importance to achieving sufficient performance, and present some examples of improved performance in model scale DP experiments. However, the algorithmic details of the control system designs are not disclosed. It is also stressed that there is no experience with DP operations in heavy ice conditions and there is a demand for improved numerical tools for iterative development and system dimensioning. For level ice environments some simulation studies investigate adapting the conventional open water design model (Nguyen et al., 2009, 2011; Sørensen, 2012). It is shown that this improves performance somewhat even though no specific ice model is incorporated. The method provides a possible first approach to tackle the managed ice environment.

Operating in ice also puts limitations on the vessel's freedom of movement. In open water a ship on DP can move in any DOF independently. In severe ice, as experienced during ACEX, it may become underactuated. This

Figure 3.5: Icebreaker Fennica using her azimuth thrusters to clear ice in the North-West Passage 2015. Courtesy of Nordica Master Matti Westerlund and Arctia Ltd.

means that the vessels ability to move sideways is reduced, and to provide efficient transversal motion it may be necessary to apply forward and rotational motion (similar to parallel parking a car). In combination, an approach where spare thruster capacity is used create more open water around the vessel may be used (see Figure 3.5). Coupled with constantly changing ice drift direction (as seen in Figure 2.3) the reduced moveability caters for a challenging maneuvering task for an automatic system. Thus, it is critical to operate the vessel compliantly with the moving ice cover.

3.4 Towards the next generation control system

Since the introduction of nonlinear theory a few decades ago, the station-keeping algorithms have been without major new innovations in the model-based design methodology. The challenge of DP in ice is the perfect catalyst for researching new solutions. In many regards it is the ultimate challenge; operation in a hostile ever-changing dynamic environment with large load variations far away from port. Although there are multiple interdisciplinary

challenges, this section will focus on the following key points, believed to hallmark the next generation DP control systems;

- Precision and reactivity
- Power production and fuel utilization
- Autonomy and sensor integration

Today a conventional DP control system relies on position and heading measurement to pick up changes in the environment and adapt to them. In constant or slowly varying scenarios this works well, but when the environmental load changes rapidly, such as in severe ice, they struggle (Bray, 2011). Since a change of load on the vessel will materialize in acceleration, velocity, and position, respectively, this is completely in line with the conventional algorithm design. When the system senses change in environment through the position and heading measures it has already gained momentum that must be stopped and reversed. This does not mean that the system become unstable in the sense that the vessel will not pursue its setpoint, but rather that significant excursions will occur in the process. Thus, there is an inherent lag which can be improved by picking up changes earlier.

An aspect of this is the validity and precision of the kinetic model applied in the DP control design. It relies on measurements and assumptions to describe each load component separately. Inherently unmodelled and unmeasured dynamics will be present. The severity of this depends on the operational environment and the number of interacting phenomena. In order to counteract and adapt to these the observer and control law implements bias and integral action. Yet, relying on position and heading measurements implies the mentioned system lag. A system capable of sensing and reacting on the acceleration level (and correcting on position and heading) will be able to reduce this problem. It will not only apply to ice, but all sorts of operations where large unmodelled and unmeasured load variations occur. Examples include harsh weather, wave trains, equipment in the sea fixed to the vessel, current surges, and interaction effects with other vessels. Thus, introduction of inertial sensors for determining the dynamic acceleration (the acceleration resulting in motion), as seen in for instance (Lindegaard, 2003), may be highly beneficial to improve reactivity. Also acting on accelerations may cater for improved fuel consumption through not having to reverse gained momentum and cover ground each time a significant perturbation occurs.

Besides introducing inertial sensors to the feedback loop new advances in control theory may also allow for flexible and reactive control designs. Today, the DP algorithms are based on continuous mathematics. That implies a significant settling time as the system adapts to changes in the environment. By describing the vessel dynamics as a hybrid dynamical system, a mix of continuous and discrete states (Goebel et al., 2012), it enables to manipulate variables instantaneously in a consistent and analytical manner. It also opens for switching between algorithms for various operations and operational states. The latter has already received some attention (see for instance (Nguyen, 2006; Nguyen et al., 2007)). Such behavior may become important in order to create a control system able to automatically detect and select the optimal control method from a bank of available designs. For instance, the next generation of DP control systems should not be dedicated to just low speed positioning operations, it should handle also special maneuvering operations and transit.

If the control system is to become more reactive, it means that the power system must be able to cope with substantial thrust changes on short notice. That may be challenging as it takes some time to increase production. Naturally, it will depend on the magnitude of the change, but it may lead to not fulfilling the thrust demand, or causing a blackout. One potential solution that has caught some attention is diesel-electric power with batteries (see for instance (Zahedi and Norum, 2013)). Allowing the thrusters to draw from a reservoir of accumulated power will enable fast response without the abovementioned problems. The generators can then operate more optimally to ensure sufficiently high battery voltage. To a great extent this decouples the power and thrust production from each other, leaving both with improved working conditions.

IM operations require a wide range of parameters and variables to be monitored through remote sensing. This is tedious well suited for a computer system that does not tire or get bored with repetitive tasks. A system integrating the intelligence sources of Section 2.3 able to solve the IM surveillance task of detecting, monitoring, and forecasting, in addition to determining optimal vessel trajectories for the fleet will be of great help in decision support and operation planning. It will allow the operators to focus on strategic proactive choices and risk evaluation rather than data collection and interpretation. Such a system can also be seen in context of increasing vessel autonomy as it also coincides with generic tasks solved by autonomous robotic systems. These also plan and act according to dynamic operational environment in real-time. Especially the Mars Rovers (see for instance (Mai-

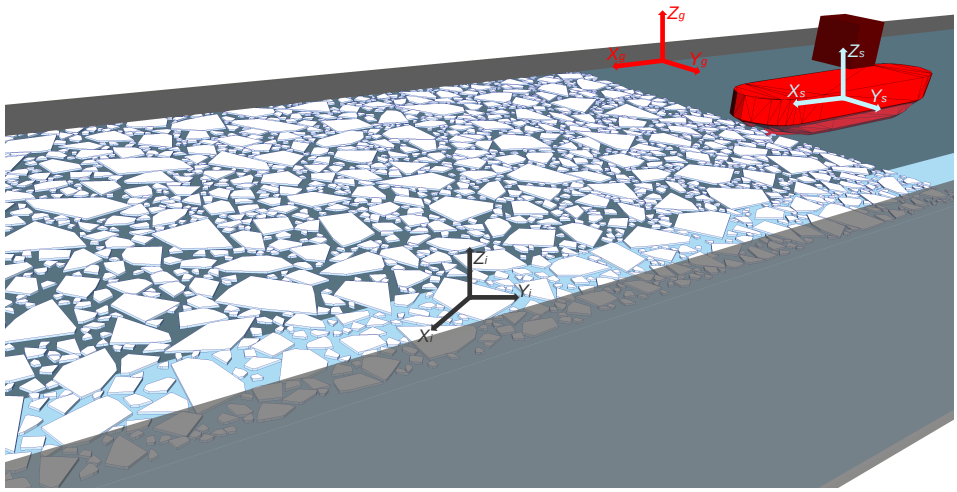

Figure 3.6: A simulation scene of the numerical model for simulating stationkeeping of a vessel in discontinuous ice found in (Metrikin, 2014).

mone et al., 2006)), and autonomous cars (see for instance (Urmson et al., 2008) and/or (Campbell et al., 2010)) show great capability when operating in complex hazardous environments. Although the applications are different, the approach to autonomy and sensor integration is similar. Thus, by extrapolating the design architecture it is possible to propose five tasks that must be solved to reach the level of autonomy where a ship can plan and act according to its spatial operational environment in real-time:

1. Create and update a navigational 3D model of the surrounding environment based on real-time sensor readings. This should include terrain above and below water, and classify moving and fixed objects according to their size and type.

2. Establish communication with other vessels in range to exchange information about vessel status, environment, hazards, and planned trajectories.

3. Predict the evolution of the surroundings based on the 3D model for a timeframe needed to alter the current operation of the vessel.

4. Determine safe and unsafe areas in the surroundings of the vessel with respect to the current operation.

5. Plan (and maneuver) efficient trajectories within the safe areas.

This type of sensor integration and analysis system will not only apply to operations in Polar regions, it may be beneficial in a wide range of marine application in complex environments with multiple ships and objects affecting the operation planning. Thus, even if stationkeeping operations in ice may never happen it can help push the technology to a new level.

A part of developing the next generation DP system capable of handling ice is the need for sophisticated numerical tools. Today, for open water, the development models for DP are often deterministic descriptive approximations of the actual physics. As such consists of a handful of differential equations they have the benefit of rapid implementation and simulation time. They are well suited for proof-of-concept and early development in well understood environments. For further assessment in a simulation model a numerical methods targeting the actual physics is needed. These may be used amongst other tasks for further fine-tuning of the system in the design phase (see e.g. (SIMA, 2014)), hardware in the loop simulations to detect faulty system behavior (see e.g. (Marine Cybernetics, 2014)), and training crew in system operation (see e.g. (Kongsberg Maritime, 2015)). For ice interactions high fidelity models are needed also in an early design phase in order to provide the coupled vessel-ice dynamics. The reason for this is the lack of deterministic descriptive approximations. Examples of high fidelity numerical models that may be coupled with a DP system are found in (Metrikin et al., 2015; Metrikin, 2015; Lubbad et al., 2015; Sayed et al., 2015; Septseault et al., 2015), and Figure 3.6 shows a snapshot of of a ship in managed ice.

Chapter 4

Research Overview

Each of the publications in Part II can stand alone. Yet, all are still part of a larger research effort comprising the thesis. This chapter presents the overarching research questions, scope of work, and red thread tying the publications together.

4.1 Scope of Work

The main scope of work is to investigate the challenges of DP in managed ice. That is investigating how to design the control system such that it counteracts the ice loads with sufficient precision while operating the vessel compliantly with the dynamic ice cover. Although a managed ice scenario is considered, the IM operation in itself is not considered. In summary, the following overarching research questions have been governing throughout the thesis work,

1. What is the load governing physics of the low velocity ship-managed ice interactions, and how does it relate to the ice condition and how does it affect the vessel motion dynamics?
2. How can the ship-ice interactions be modelled, and how can different approaches to increased reactivity be implemented in the DP control system?
3. What are feasible operation strategies, and how can proactive actions be implemented in the control system?

Although these are specific to solving the challenges of DP in ice, they fit well into the future predictions of how the DP control system may evolve.

4.2 List of Publications

During the period 2010-2015 a total of 13 papers have been produced, and in 10 of these I have been the first author. From these, 9 constitute the thesis. The publications are listed as they appear in Part II:

International Refereed Journal papers

(J.1) Kjerstad, Ø. K., Metrikin, I., Løset, S., and Skjetne, R. (2015). Experimental and phenomenological investigation of dynamic positioning in managed ice. *Cold Regions Science and Technology*, 111:6779.

(J.2) Kjerstad, Ø. K., and Skjetne, R. (2014). Modeling and control for dynamic positioned marine vessels in drifting managed sea ice. *Modeling, Identification and Control.*

(J.3) Kjerstad, Ø. K., and Skjetne, R. (2016). A resetting control design for dynamic positioning of marine vessels subject to severe disturbances. *IEEE Transactions on Control System Technology (submitted for 2nd review).*

(J.4) Kjerstad, Ø. K., and Skjetne, R. (2016). Disturbance rejection by acceleration feedforward for marine surface vessels. *IEEE Accesss (accepted for publication).*

International Refereed Conference papers

(C.1) Kjerstad, Ø. K., and Metrikin, I. (2015). Description and numerical simulations of dynamic positioning in reversing managed ice. In *Proceedings of POAC.*

(C.2) Kjerstad, Ø. K., Skjetne, R., and Berge B. O (2013). Constrained nullspace-based thrust allocation for heading prioritized stationkeeping of offshore vessels in ice. In *Proceedings of POAC.*

(C.3) Kjerstad, Ø. K., and Skjetne, R. (2012). Observer design with disturbance rejection by acceleration feedforward. In *Proceedings of ROCOND*.

(C.4) Kjerstad, Ø. K., and Skjetne, R. (2012). Feedforward linearization and disturbance rejection of mechanical systems using acceleration measurements. In *Proceedings of ROCOND*.

(C.5) Kjerstad, Ø. K., Skjetne, R., and Jenssen, N. A. (2011). Disturbance rejection by acceleration feedforward: Application to dynamic positioning. In *Proceedings of IFAC World Congress*.

Papers not included in the thesis

- Ren, Z., Skjetne, R., and Kjerstad, Ø. K. (2015). A Tension-based Position Estimation Approach for Moored Marine Vessels. In *Proceedings of IFAC MCMC*.
- Skjetne, R., and Kjerstad, Ø. K. (2013). Recursive nullspace-based control allocation with strict prioritization for marine craft. In *Proceedings of IFAC CAMS*.
- Su, B., Kjerstad, Ø. K., Skjetne, R., and Berg, T. E. (2013). Ice-going capability assessment and DP-ice capability plot for a double acting intervention vessel in level ice. In *Proceedings of POAC*.
- Kjerstad, Ø. K., and Breivik, M. (2010). Weather optimal positioning control for marine surface vessels. In *Proceedings of IFAC CAMS*.

4.3 The Red Thread

This section aim to provide the reader with the red thread of the above publications with some additional insight and comments. It does not go into great detail and discussion on the specific results, but outline the main findings as a whole. For the former, the reader is advised to the specific publications (given in Part II).

The development of any motion control system has separate stages depending on the previous available research and experience. As noted in Section 3.3, the fundamental understanding of the operational managed ice environment in context of DP control system design is to some extent lack-

ing. Therefore, (J.1) investigates multiple model scale low velocity towing datasets from the Dynamic Positioning in Ice (DYPIC) project. It found the following relations between the global loads and properties of the ice cover:

- Global ice loads contain rapid and significant transients that may abruptly inject energy into the stationkeeping system.
- Mean ice loads depend on the oblique angle between the vessel and the ice but not on the relative ice drift velocity (in the range of 0.130.51 m/s full-scale).
- Mean ice loads and standard deviations strongly depend on the ice floe size, ice concentration, and ice thickness

In an effort to link the processes in the ice cover to the observed loads the notion of ice floe contact networks and accumulated ice mass is introduced to explain the observed interaction dynamics (shown in Figure 4.1). However, towing experiments performed in a closed basin are restricted to investigating only parts of the dynamics involved in full-scale operations. Additional phenomena, such as ice drift direction changes, large intact ice features slipping through the IM system, compaction and pressure in the ice cover, are known challenges based on full-scale operational experience (Keinonen et al., 2006). Although these phenomena were not explicitly considered in (J.1), they are believed to further excite the ice floe contact networks and accumulated ice mass dynamics. Further research is needed to elaborate these relationships and to establish reliable quantitative models for managed ice actions on DP vessels. Regardless, the analysis presented in (J.1) provides a framework for understanding the major trends of the load signal. From this it is argued that the complexity of DP in managed ice requires a coherent design strategy for all core modules of the control system. (J.1) proposes the following, in line with Section 3.3:

- Control objectives that comply with the managed ice dynamics can act to minimize the ice floe contact networks and accumulated ice mass. Specifically, tracking the ice drift direction with the bow or stern of the vessel and reducing the direct transversal actuation by active ice vaning appears to be promising.
- The degraded performance of conventional open-water DP control systems in ice can be attributed to the lack of structures in the DP control algorithms capable of tracking the ice load signal and guiding the vessel in compliance with the managed ice dynamics.

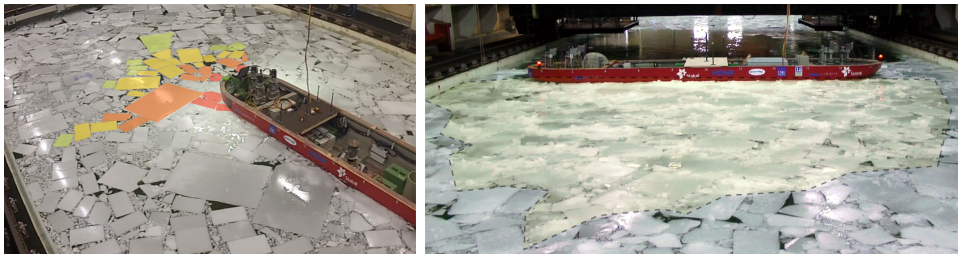

Figure 4.1: Left: Ice floe contact networks. Right: Accumulated ice mass. Both pictures are from the experimental testing at the Hamburg Ship Model Basin (HSVA).

- Improvements in the global ice load tracking performance may be obtained by introducing a control design model that incorporates the managed ice dynamics and/or adding ice load measurements. Inertial measurements appear to be particularly promising.

In order to investigate the proposals in (J.1), an experimental platform was needed. For early development a numerical model is better suited than physical experiments as it allows for rapid prototyping through iterative development. (J.2) presents such a tool where the state-of-the-art high fidelity numerical model of Metrikin (2014) is coupled with a control application layer to form a closed-loop simulation framework. This is able to produce a wide range of managed ice scenarios, including the challenging ice drift reversals. The framework structure is illustrated in Figure 4.2. The correspondence between experimental data from (J.1), numerical simulations, and an empirical formula for pack ice loads on stationkeeping vessels was investigated. This showed that the experimental load is replicated more accurately in the proposed framework than using the empirical formula. However, the match with the experimental data deviates as the ice concentration and oblique angle increases. This is especially evident in the transversal loads. There may be a number of interconnected reasons for this, but pinpointing the actual ones are challenging because the applied numerical model is an integrated environment where many physical processes are coupled. Thus, care must be taken in both experimental design and results interpretation when using the simulation framework. Yet, its main advantage is that it captures two of the fundamental vessel-ice and ice-ice processes described in (J.1), ice floe contact networks and accumulation of ice mass. This ability enables the simulation of the coupled vessel-ice dynamics, considered key for testing motion control systems.

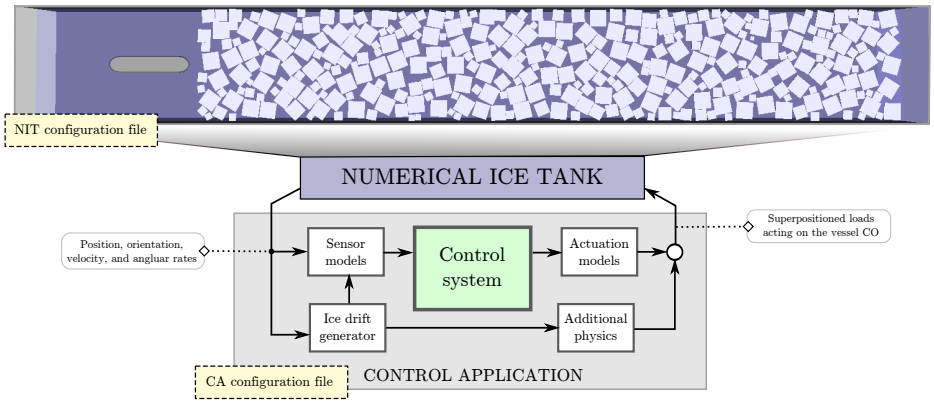

Figure 4.2: The modular structure of the closed-loop simulation platform for DP in managed ice.

(J.2) also investigates if a characteristic ice model applicable for control design can be synthesized to capture the ice dynamics, but this was found challenging as no specific measurable parameter linking the load variations to the ice cover was found. Therefore, ice-adapted control algorithms based on the conventional open water design model is presented. This can be seen as an increment step towards an ice mode from the open water systems in line with previous hash environments and level ice research (see (Nguyen et al., 2009, 2011; Sørensen, 2012)). In the proposed ice-adapted control algorithms the ice dynamics were included in the existing observer bias estimate, and handled using a conventional nonlinear PID control law. In summary, what separates the proposed enhancements from conventional open-water systems is the removal of the wave filter, and aggressive system tuning. Thus, the results are valid for other harsh operational scenarios than managed ice. The design was investigated using the developed simulation framework where it showed an ice concentration dependency on the stationkeeping capability. Incorporating additional vessel velocity and angular rate measurements aided this to some extent. However, the availability of the former is questionable as sensors providing these signals directly are not commonly found in marine applications.

Although modifying the conventional design methodology may give increased reactivity in some scenarios there is still a challenge with rapid unmodelled and umeasuresd external disturbances. Examples of such are wave trains, ship-to-ship interaction effects, current surges, and effects from operations with heavy equipment in the sea or at the sea floor such as towing, an-

chor handling, and sub-sea construction. The key challenge is to detect and act as early as possible. As also emphasized by Jenssen et al. (2009) and Kerkeni et al. (2013) this starts with increasing the state estimation capability of the observer. In line with Section 3.4, (J.3) proposes to improve stationkeeping performance of a state-of-the-art control design subject to harsh environment through a resetting mechanism in the observer. The state estimation is fundamental to both accurate positioning and trajectory generation, and these will suffer if the state estimates deviate. The reset is triggered when the observed estimation error reaches a threshold (indirectly indicating that substantial disturbance is present). Then, the state estimates are reset closer to their true value independent of time (ensured by the system model). This also instantaneously improves the precision of the control law output. The implication of improving the state estimation is enhanced stationkeeping precision under severe perturbations which may potentially extend the operational window of the vessel. As the resetting control design is a mix of continuous and discrete state descriptions, it is regarded and analyzed as a hybrid dynamic system (Goebel et al., 2012). A case study using simulations and model scale experiments verified that the transient state estimation error during transient severe disturbances was reduced and performance improved. The presented design is particularly interesting as it improves state estimation without gain adjustments, new measurements, or new dynamic models. Thus, it can be implemented by a minor update of the software algorithms. The use of hybrid theory, as presented in (J.3), may be seen as an intermediate step before including inertial sensors in the feedback loop. Although (J.3) targets harsh open water environments, the results can be adapted to ice as presented in (J.2) without loss of validity.

As proposed in (J.1), and discussed in Section 3.4, inertial sensors are a promising technology. The reason for this is that acceleration signals have a powerful disturbance rejection potential in rigid body motion control as they carry a measure proportional to the resulting force. Yet, these signals are seldom used, since measuring, decoupling, and utilizing the dynamic acceleration in the control design is not trivial. (J.4) discusses these topics and presents a solution for marine vessels building on conventional methods together with a novel control law design where the dynamic acceleration signals are used to form a dynamic disturbance compensation (similar to the approach of wind feedforward), named acceleration feedforward. A key enabler of improved performance is that the kinetic model used in conventional control design can be reformulated to use kinematic and sensor models for describing the velocity dynamics. This implies significant less

model uncertainty as all significant physical processes acting on the vessel are captured through the input of the inertial measurements. In the proposed design the acceleration feedforward replaces conventional integral action and enables unmeasured external loads and unmodeled dynamics to be counteracted with low time lag. The proposed design was investigated with both experimental data and the high-fidelity platform presented in (J.2), both showing feasibility and effectiveness of the proposed design methodology. (C.3), (C.4), and (C.5) provide additional insight on the design and feasibility of using acceleration measurements as feedforward.

The control system design methodology presented (J.4) offers a highly attractive solution to DP able of handling all unmodeled disturbances in an effective, robust, and tunable manner. In addition it has the following favorable properties (when compared to conventional designs):

- Rigorous hydrodynamical analysis is not needed for implementation of the algorithms as the kinetic vessel model is replaced with a model consisting of kinematics and sensor characteristics.
- Integral wind-up challenges are alleviated by reduced dependency on position and heading reference error in the disturbance rejection.
- Wind sensors and accompanying aerodynamic models are not needed to counter wind gusts as the effect on the vessel will be captured by the inertial sensors (and thereby accounted for).

The control designs presented in (J.2), (J.3), and (J.4) are complementary since they have different design methodologies and characteristics. Thus, they may be used in a redundant design, and/or in a scheme similar to the one proposed by Nguyen et al. (2007), which selects the most appropriate control systems in-situ.

While reactivity is key to DP in ice its also considered important to minimize the loads on the vessel through it's operational strategy. This is investigated though tracking the ice drift direction with the vessel's bow (or stern) since ice will accumulate on the hull at oblique headings. A potential consequence of not achieving ice drift tracking is loss of position as severe loading scenarios beyond the capability of the propulsion system may arise. As proposed in (J.1) the investigation and adaptation of weather optimal positioning control (WOPC) is promising for operations in managed ice because it incorporates the drift tracking directly without the need for additional measurements. Furthermore, it pro-actively exploits the environment for actuation. Therefore, (C.1) presents a WOPC system incorporating com-

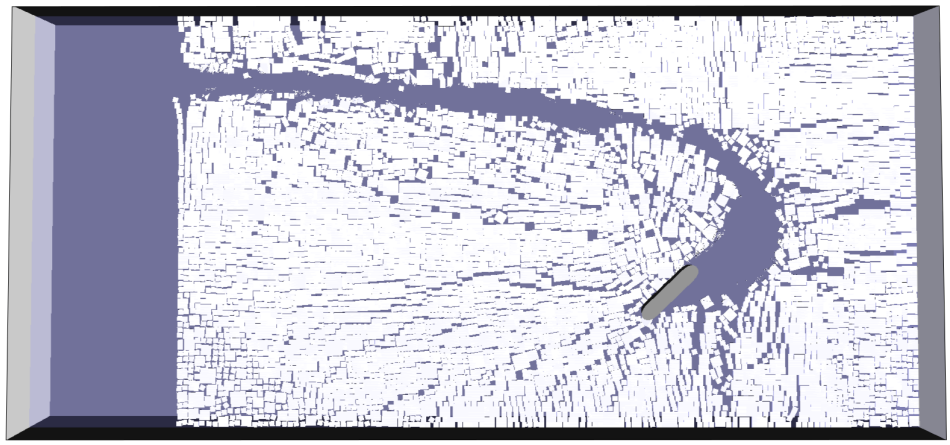

Figure 4.3: A simulation snapshot of WOPC in severe ice drift reversals. Notice that the ice drift is simulated by moving the vessel reference frame instead of the ice (as described in (J.2)).

ponents of (J.2) and (J.4). A case study using the simulation framework of (J.2) indicates that the concept works as intended for severe ice drift reversals in high ice concentrations (a simulation snapshot is seen in Figure 4.3). However, it is worth noting that WOPC is only applicable when no constraints are imposed on the heading of the vessel. Examples of scenarios with constraints are operations close to other structures or vessels and pipe-laying. In such scenarios the control designs of either (J.2), (J.3), or (J.4) may be applied directly.

Compliant ice cover behavior beyond tracking the ice drift direction may be achieved if the operational area is sufficiently large, and the vessel has freedom to maneuver. Then, two additional proactive measures can be incorporated in the control design:

- Seek the weakest path through the ice cover within the allowed operational area.
- Utilize the vessel momentum and inertia to address challenging ice features, e.g. as reported from full-scale stationkeeping operations in ice (Keinonen et al., 2006).

These two proposals are not investigated in this thesis, but for the sake of completeness mentioned here. Typically, such functionality would be incorporated in the guidance system.

The final part of the DP control system dealt with is thrust allocation. For this, it is considered key to prioritize yaw moment generation before surge and sway forces due to the importance of heading on the stationkeeping capability (as seen in (J.1)). Maintaining yaw and thereby tracking the ice drift direction will not cater for further severe load increase in scenarios with insufficient thrust available. (C.2) presents a novel recursive thrust allocation algorithm enabling such prioritization in addition to thrust magnitude constraints. It is important to note that the proposed design is intended as a simple and deterministic quick-to-implement method allowing for early control design evaluation (as used in (C.2) to assess the thrust capability using an experimental dataset from the construction and intervention vessel for Arctic operations (CIVARCTIC) project). It exceeds the feasibility of conventional constrained pseudo-inverse methods, but should not be compared to sophisticated optimization methods which obtains optimal solutions (as opposed to potentially sub-optimal). Another aspect of thrust allocation that is not dealt with in this thesis is the utilization of spare thrust capacity to flush near ice for self-IM and maneuvering (as seen in Figure 3.5). However, this is touched upon by Wold (2013).

In summary, this section shows that the presented research constitutes one development cycle (as illustrated in Figure 4.4) for a DP control system capable of operating in potentially harsh managed ice. A number of novel robust design enhancements are proposed based on characteristics of the ice environment. These show promise both theoretically as well as in simulations and model scale experiments. Thus, further research and evaluation should be undertaken. Additionally, the presented work showcases the importance of using high fidelity numerical tools as a DP control system development and assessment framework.

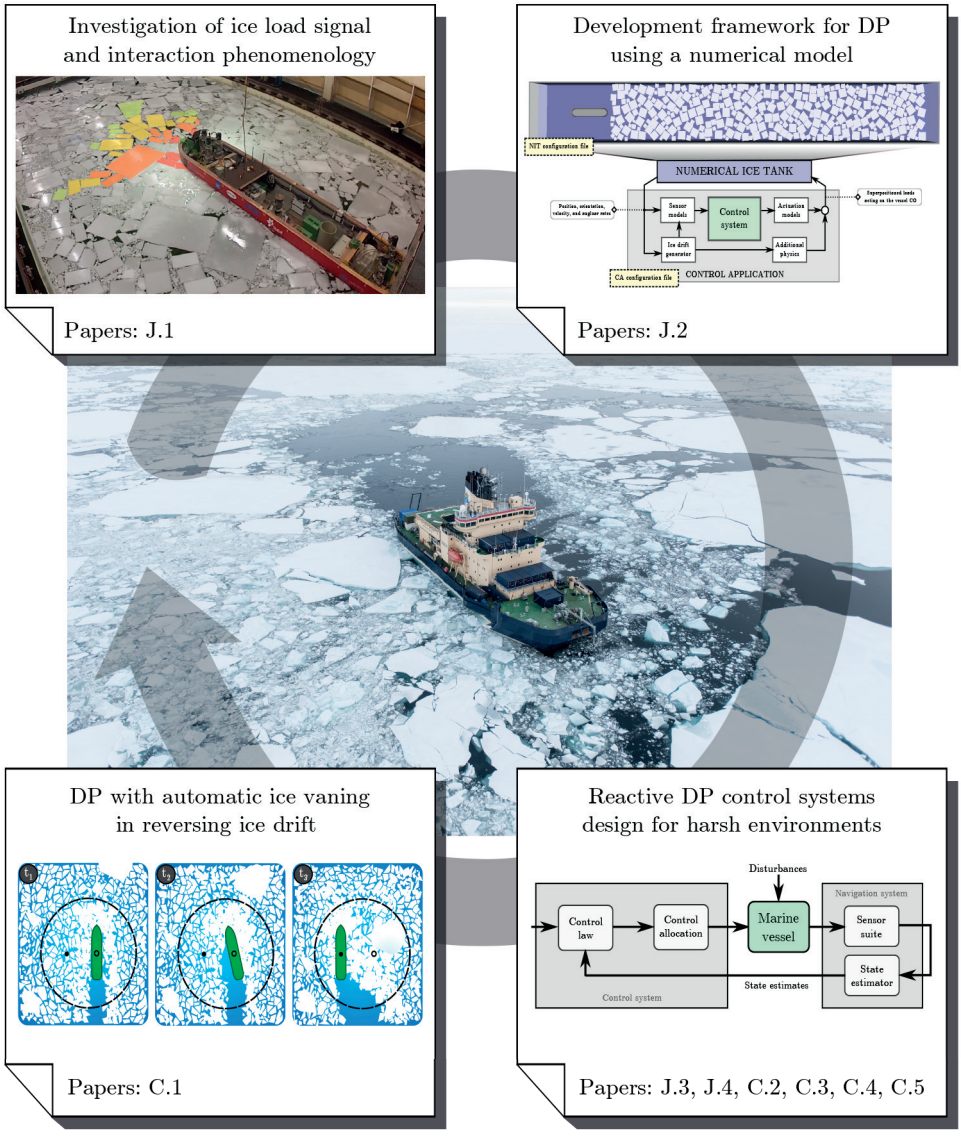

Figure 4.4: Illustration showing the relationship of the papers of Part II in context of developing a control system for DP in managed ice. The photo is from the Oden Arctic technology research cruise 2012.

Part II

Selected Publications

Chapter 5

International Refereed Journal papers

Experimental and Phenomenological Investigation of Dynamic Positioning in Managed Ice

Cold Regions Science and Technology 111 (2015) 67–79

Contents lists available at ScienceDirect

Cold Regions Science and Technology

journal homepage: www.elsevier.com/locate/coldregions

Experimental and phenomenological investigation of dynamic positioning in managed ice

Ø.K. Kjerstad [a,*], I. Metrikin [b,c], S. Løset [b], R. Skjetne [a]

[a] Department of Marine Technology, NTNU, Otto Nielsens vei 10, 7491 Trondheim, Norway
[b] Department of Civil and Transport Engineering, NTNU, Høyskoleringen 7A, 7491 Trondheim, Norway
[c] Arctic Design and Operations, Statoil ASA, Arkitekt Ebbells veg 10, 7053 Trondheim, Norway

ARTICLE INFO

Article history:
Received 30 August 2013
Received in revised form 13 November 2014
Accepted 26 November 2014
Available online 23 December 2014

Keywords:
Dynamic positioning
Managed ice
Global ice loads
Control systems
Model testing
Ice load estimation

ABSTRACT

This paper investigates the dynamic positioning of offshore vessels in managed ice conditions using a model-scale dataset from the large ice tank of the Hamburg Ship Model Basin. Experimental data obtained from the European research and development project DYPIC (DYnamic Positioning in ICe) are analyzed to determine the governing signal characteristics of ice loads acting on a drillship model in various managed ice conditions. The results indicate that the mean load level is strongly dependent on the oblique angle but independent of the relative velocity between the vessel and the ice (when it is below 0.51 m/s in full-scale). Furthermore, it is found that the managed ice cover characteristics (namely, the ice concentration, ice thickness, and floe size distribution) impact both the mean load level and the signal variation, leading to significant and rapid transients in the global load signal. These findings are investigated from a phenomenological perspective, and it is argued that *ice floe contact networks* and *accumulated ice mass* are responsible for the observed signal dynamics. Finally, both load signal and phenomenological analyses are used to discuss the implications of managed ice on conventional dynamic positioning control systems. It is shown that several core elements of the system are affected and require attention. Improved design considerations are proposed, but further work is required to implement and test the new concepts.

1. Introduction

According to the International Maritime Organization (1994), a dynamically positioned vessel automatically maintains its position (fixed location or predetermined track) exclusively through the use of thrusters. The existing control systems for dynamic positioning in open water have an established well-known structure (Fossen, 2011; Sørensen, 2005), and robust commercial solutions are available for different operational scenarios in the presence of wind, waves, and currents (see, e.g., Kongsberg Maritime, 2006; Rolls-Royce Marine, 2009; Sirehna, 2014). However, when the vessel interacts with sea ice, the environmental forces are substantially different, and conventional open-water systems are known to be insufficient (Gürtner et al., 2012; Hals and Jenssen, 2012; Jenssen et al., 2009; Kerkeni et al., 2013a). Nevertheless, full-scale, model-scale, and numerical experiments have demonstrated that high-uptime positioning is possible with ice management (IM) support (Hals and Jenssen, 2012; Keinonen and Martin, 2012; Liferov, 2014; Metrikin et al., 2013; Moran et al., 2006; Rohlén, 2009). IM involves all aspects of removing or reducing ice actions on the protected vessel (Eik, 2010). Actual IM activities are operation specific, but the main objective is to either transform the natural ice environment into an acceptable managed ice condition or to suspend the operation if that is not possible. Fig. 1 illustrates a physical IM operation: the operational fleet, the ice cover, and the ice drift direction. More details on stationkeeping operations in ice with an emphasis on IM are given in, e.g., Liferov (2014) and Riska and Coche (2013). Because IM is essential for successful operations, the scope of this paper is limited to the assessment of dynamic positioning (DP) in a channel of managed sea ice.

To investigate a DP operation from the control engineering perspective, this paper examines global managed ice load data from a model-scale dataset of the DYPIC project (DYnamic Positioning in ICe), which was performed in 2010–2012 (Kerkeni et al., 2014). The project consisted of an extensive set of experiments performed at the large ice tank of the Hamburg Ship Model Basin (HSVA) in 2011 and 2012. Details and the setup of those model tests are provided in Section 2 of this paper. Then, Section 3 investigates the resulting ice load signals and their characteristics in various managed ice conditions, accentuating important aspects of control system development. Next, Section 4 discusses the possible physical mechanisms responsible for the ice load signal dynamics, in which a *phenomenological* analysis of the

* Corresponding author. Tel.: +47 97745157.
E-mail addresses: oivind.k.kjerstad@ntnu.no (Ø.K. Kjerstad), ivan.metrikin@ntnu.no (I. Metrikin), sveinung.loset@ntnu.no (S. Løset), roger.skjetne@ntnu.no (R. Skjetne).

http://dx.doi.org/10.1016/j.coldregions.2014.11.015
0165-232X/

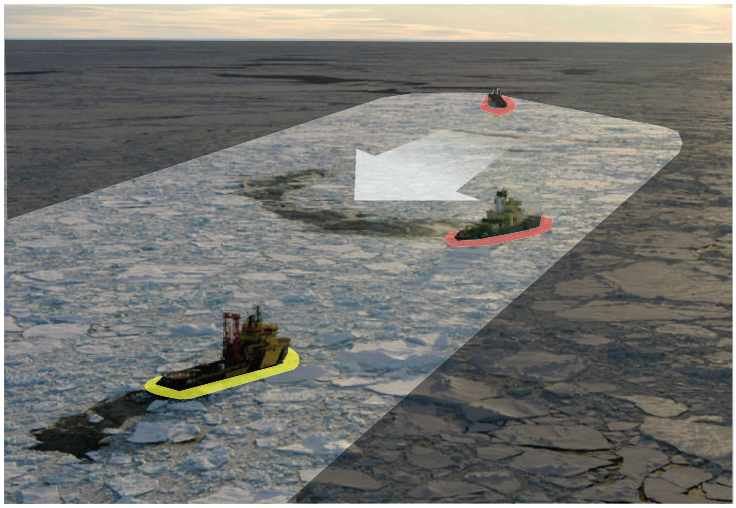

Fig. 1. Ice management concept featuring the protected DP vessel (enclosed in yellow) and the physical ice management fleet (enclosed in red). Adapted from Moran et al. (2006).

ice–structure interaction is performed that identifies and investigates key processes in the managed ice cover. Finally, Section 5 utilizes the ice load signal and phenomenological findings to identify the main weaknesses of conventional DP control systems and to propose specific improvements of control algorithms for operations in managed ice. The paper ends with a summary and conclusions in Section 6.

2. Model tests of the DYPIC project

The European research and development project DYPIC was a 3 year initiative (2010–2012) led by HSVA and financed by the national research agencies of Germany, France, and Norway. The program focused on various aspects of DP technology for offshore operations in ice-infested waters. Comprehensive project overviews can be found in Jenssen et al. (2012) and Kerkeni et al. (2014). This paper builds on the model testing data of DYPIC, in which almost 250 different scenarios were tested in broken ice conditions at the large ice model basin of HSVA (which is 72 m long and 10 m wide). In this section, model tests performed in 2011 and 2012 are described in terms of vessel data, experimental setup and managed ice field preparation routines.

Table 1
Primary characteristics of the ADS and illustration of the thruster arrangement.

Parameter	Full scale	Model scale
Length at design waterline (m)	200.13	6.67
Length between perpendiculars (m)	184	6.13
Breadth, moulded (m)	41.33	1.37
Draught at design waterline (m)	12	0.4
Stem angle at design waterline (°)	45	45
Frame angle at midship (°)	45	45
Displacement volume (m^3)	68457	2.535
Center of gravity from aft. perp. (m)	95.34	3.18
Block coefficient	0.75	0.75
Metacentric height (m)	10.71	0.357
Total thrust (N)	7.2×10^6	270

2.1. Vessel data

Two different vessels were tested in the DYPIC project: a Polar Research Vessel (PRV) and an Arctic Drill Ship (ADS). This paper investigates and analyzes the ADS data, whose primary characteristics are presented in Table 1 (the model was scaled by a factor of $\lambda = 30$). The hull shape of the vessel is shown in Fig. 2.

2.2. Experimental setup

Fig. 4 shows the two different testing modes used in DYPIC: carriage-fixed towing mode and free-floating DP mode. Because an extensive description of these testing modes can be found in Haase and Jochmann (2013b), only a brief overview will be provided in this section.

In the carriage-fixed towing mode, the vessel was rigidly connected to the ice tank's main carriage, which pushed it through the stationary ice field. A 6-component scale connected the vessel to the carriage, and the loads were measured using an arrangement of 3 horizontal and 3 vertical load cells. Therefore, these tests were instrumental in deriving the actual ice loads acting on the vessel. Different ice drift angles were modeled by adjusting the mounting angle between the model and the scale. The main difficulties of this setup were that the connection was not perfectly rigid and that the carriage itself was vibrating, which caused noise in the force signals (the vibrations were most likely coming from the carriage drive). Filtering such data is not trivial because the noise and the ice load frequency spectra may overlap. The specific filtering technique used in this paper is discussed in Section 3.

In the DP mode, the vessel was self-propelled by a system of 6 azimuth thrusters (3 in the bow and 3 in the stern, as shown in Table 1). The DP system was set to track and hold a fixed position/heading setpoint. The ice drift was simulated by either allowing the vessel to move through the ice, following a setpoint fixed to the moving carriage, or by pushing the ice field against the vessel. The position and heading of the vessel were measured using a Qualisys motion capture system with 4 infrared cameras. The thrusters were operated either manually by an operator or automatically by a DP control system. Two different DP vendors tested their systems in the DYPIC project: Kongsberg

Fig. 2. Hull shape of the Arctic Drill Ship. Left: bow view, right: stern view. White marks indicate the waterline.

Maritime and DCNS Research/Sirehna (Jenssen et al., 2012; Kerkeni et al., 2014). Some details of those systems and corresponding results are provided in Dal Santo and Jochmann (2012), Hals and Jenssen (2012), and Kerkeni et al. (2014). However, neither of the vendors provided the detailed algorithmic particulars of their systems. Therefore, external load estimates from the DP mode experiments will not be considered in this paper because they are a result of undisclosed commercial algorithms. Nevertheless, the datasets provide valuable insight into the physical behavior of the ice in the vicinity of the vessel, which is investigated in Section 4.

All test runs were segmented in sections with different ice drift velocities (exemplified in Fig. 3). The range of tested velocities was 0.13–0.51 m/s in full-scale, corresponding to 0.023–0.093 m/s in model-scale. These velocities are assumed to be representative of common ice drift velocities in the Arctic (Yulmetov et al., 2013a; Yulmetov et al., 2013b).

2.3. Managed ice field preparation

The preparation procedures for the broken ice fields in DYPIC are fully covered in Haase and Jochmann (2013a) and Haase et al. (2013), so only a brief overview will be provided here.

Preparation of the ice field began with cutting the intact level ice into longitudinal stripes that were as wide as the breadth of the target floes. Then, each stripe was cut into pieces corresponding to the length of the target floes. After the entire ice sheet had been cut according to the pattern, the floes were distributed along a certain area of the tank to reach the target ice concentration (*IC*). Finally, the floes were mixed to obtain a homogeneous floe size distribution over the entire test length, and brash ice was introduced by manually crushing some of the ice floes. Fig. 5 shows examples of the different broken ice fields as captured from the ceiling of the ice tank. The actual ice concentrations and floe size distributions in the experiments were determined using image processing techniques (Zhang et al., 2012; Zhang et al., 2014). The broken ice fields were reused after each test run such that four different ice field types could be utilized within one testing day. An example of the ice field evolution throughout a testing day is shown in Fig. 6 for DYPIC test series 5000. Finally, Table 2 defines all parameters of the DYPIC ice fields relevant for the analyses performed in the remainder of this paper.

3. Ice load signal analysis

This section investigates the ice load measurements of the DYPIC project to determine signal characteristics that can influence DP control system performance. The towing experiments specified in Table 3 are analyzed, in which the following notation is used: ψ_r is the oblique angle between the vessel and the ice, v_r is the relative velocity between the vessel and the ice in model-scale, N is the ice field number from Table 2; Fig. 5, IC is the ice concentration, h is the ice thickness in model-scale, σ_f is the flexural strength of the ice in model-scale, σ_c is the compressive strength of the ice in model-scale, and E is the Young's modulus of the ice. In tests 6300 and 6400, the flexural strength value is acquired from the previous test conducted on the same day (6200) because no dedicated measurements were performed for tests 6300 and 6400. In series 8000, the flexural strength was not measured. In series 4000, 6000 and 8000, the compressive strength measurements were performed only once, whereas in series 5000, two measurements were performed: for tests 5100 and 5300. The Young's modulus was only measured in series 6000 and 8000.

Because DP systems achieve the positioning objective by controlling the vessel's low-frequency motion dynamics (Fossen, 2011), a frequency analysis of the ice load signals was performed first. Two ice towing experiments are compared with two open-water towing experiments in Fig. 7. As shown, the main difference when moving from open

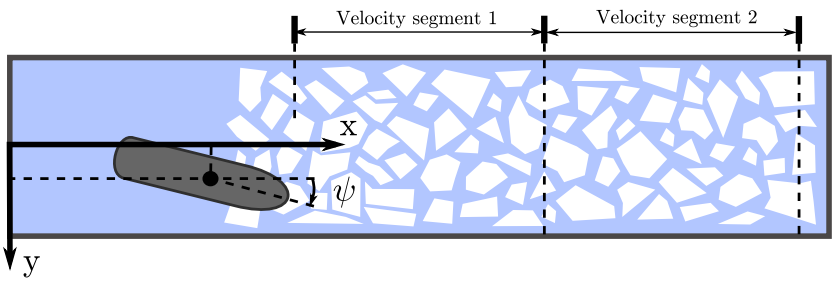

Fig. 3. Definition of the ice tank coordinate system and illustration of the velocity segmentation.

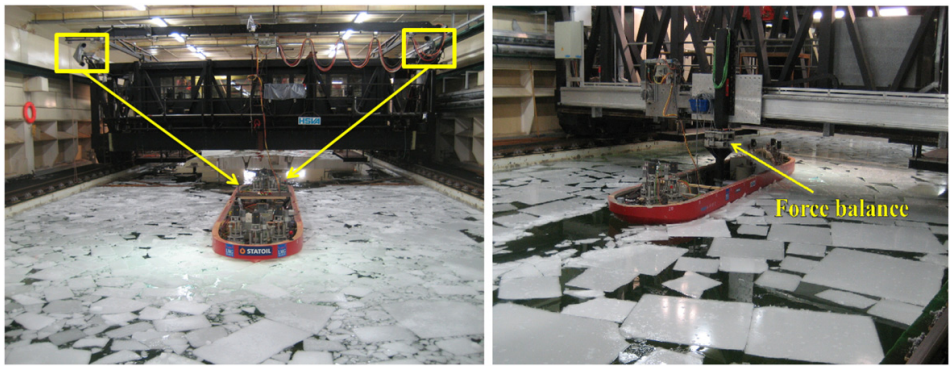

Fig. 4. Pictures of the two testing modes in the DYPIC project. Left: DP mode in which the vessel, the main carriage and the Qualisys motion tracking system can be observed. Right: carriage-fixed towing mode showing the fixed vessel, the carriage and the 6-component force balance.

water to ice lies in the low-frequency range (below 1 Hz). Therefore, the control system must actively counteract most of the ice loads by active thruster actuation. The energy peaks above 1 Hz, observed in both open water and in the ice signals, are believed to be noise originating from the experimental setup (as mentioned in the previous section). Therefore, in the remainder of this paper, the low pass filter specified in Table 4 is applied to the carriage-fixed towing datasets. Although such filtering suppresses both the noise and the potential high-frequency ice load signal components, it is justifiable from the DP perspective because the control system does not aim to compensate high-frequency ice loads.

During positioning of the vessel, the DP system has to determine the required actuation loads to counteract the environmental disturbances. The DP systems are proven technology in constant sea states. However, the open-water positioning capabilities are known to degrade in rapidly changing conditions (for instance, during quickly shifting tides or when affected by the thruster wake of other vessels (Bray, 2011)). Thus, it is critical to investigate how the ice load signal develops with respect to time. Therefore, Fig. 8 shows the ice load signals in time domain, as recorded in towing experiments 5100–5400 (ref. Tables 2 and 3). As shown, the load signal varies significantly in magnitude and contains rapid signal transients. These are particularly evident in the transversal direction and in the moment for high ice concentration (5100 and 5400) and for the ice cover with large square floes (5100 and 5200). Such rapidly fluctuating changes must be given special attention in the control system because significant energy (potentially threatening the positioning capabilities) is abruptly introduced into the system. The physical reasons for these signal dynamics will be explored in the following section of the paper.

The next step of the ice load signal analysis is to investigate the interconnections between the ice loads and the relative ice–vessel interaction velocity v_r because the load–velocity relationship is used by the DP control system. Fig. 9 shows the dependence between the mean ice loads and v_r for different oblique angles ψ_r. Cases of 0°, 10°, 170° and 180° are presented. The datapoints were produced by filtering the load time series and truncating them according to the experiments' velocity segmentation. To avoid potential transient dynamics associated with a change in velocity, the first and last 30% of the segments were discarded, leaving only the 40% steady-state middle section of each segment for further evaluation.

In Fig. 9, the experiments with two velocity segments apparently indicate a load–velocity dependence. However, because these experiments were performed in increasing velocity order with respect to the tank segmentation, care should be taken when interpreting their results. It is hypothesized that the increase in the load can be attributed to not only the velocity increase but also to the effect of increasing compaction of the ice cover when the vessel is towed through the tank. This hypothesis is confirmed by the observation of a reversed load–velocity trend in experiments 6300, 6400, and 8300, which were performed with three segments in decreasing velocity order. Hence, it is concluded that the investigated data show a velocity segmentation setup dependence that is most likely caused by the tank boundaries. This conclusion is further substantiated by the phenomenological analysis of the physical processes in the managed ice cover (see Section 4). The lack of a clear velocity dependence is also reported for full-scale operations (Wright, 2001) and in simulations (Sayed et al., 2014) and confirms the findings of Haase and Jochmann (2013a) previously reported for the DYPIC data.

In addition to the lack of a velocity dependence, the mean loads in Fig. 9 show a significant impact of the oblique angle on the load level; notably, the increase of the transversal load is evident. This result is important for DP control systems because it provides an indication of the feasible ice–vessel heading values for operations. The mean load data and standard deviations also indicate that there is a significant and complex influence of the floe size, the ice concentration, and the ice thickness, independent of the oblique angle and the relative velocity (for both bow-first and stern-first setups). An example of this complexity can be observed by comparing experiments 8300, 4100, and 5100. The first experiment was conducted with approximately 30% thicker ice than the latter two experiments; however, the mean load remains in the same range for all datapoints. The main reason for this result is believed to be the managed ice matrix composition of experiment 8300, which consisted of smaller floes and contained a significant amount of brash ice (see Table 2). A similar load dampening effect can also be observed by comparing large and small floe sets (experiments 4100 and 5100 with 4400 and 5400, respectively) and by the reduced standard deviation in tests in which brash ice was present. A similar effect of brash ice on the load level was also reported by Neville et al. (2013).

4. Phenomenological investigation of the managed ice–vessel interaction process

The primary managed ice load signal characteristics, which were identified in the previous section, indicate significant threats posed by managed ice actions on a stationary DP vessel. However, a pure signal analysis does not allow an efficient control system to be designed to overcome these challenges because it lacks a physical understanding of the managed ice interactions. Therefore, this section

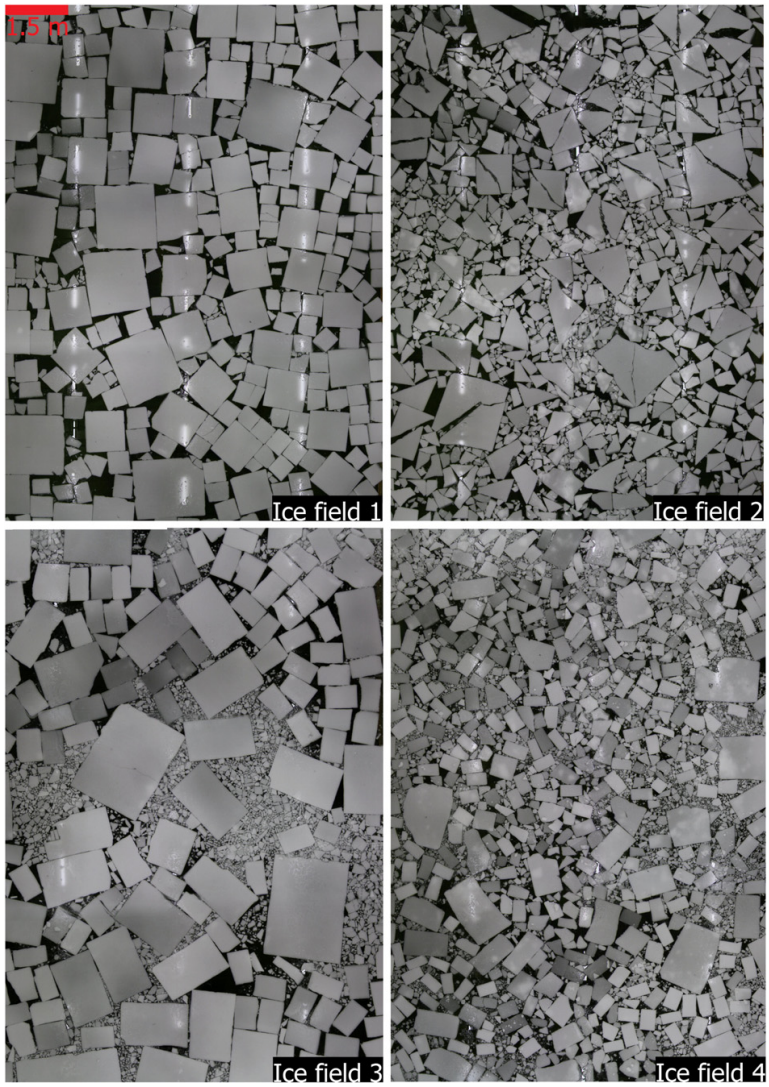

Fig. 5. Relevant ice fields of the DYPIC project, which were captured with a downward-facing camera installed at the ceiling of the ice tank. Ice field numbers refer to Table 2.

offers a phenomenological interpretation of the ice load signal characteristics and their relation to the dynamics of the vessel.

By investigating the video material from the DYPIC trials, it was found that as the vessel advances in the ice tank, it interacts with several ice floes, which in turn interact with even more ice floes, producing strings of interacting rigid bodies. This can be observed in Video 1, which shows a segment of experiment 4100 at 4× playback speed. In the remainder of this paper, these interconnected strings will be called *ice floe contact networks*. Fig. 10 shows a snapshot illustration of the vessel and several interconnected ice floe contact networks in a DP experiment. In general, these networks are in-plane phenomena, but their load-releasing mechanisms were observed to be both in- and out-of-plane(depending on the ice condition, sloping angle of the interface, ice concentration and floe size distribution). The observed release mechanisms include pushing and rearranging of the ice floes, rafting, splitting failures, bending failures, and under-hull ice rubble transport. The ice floe contact networks may partially explain the load signal variation because they consist of unique configurations of ice floes and brash ice that are being dynamically rearranged and cleared around the vessel. The ice floe contact network phenomenon has been reported on different scales in the studies of Herman (2013), Hopkins and Tuhkuri (1999), Liu et al. (2010), Paavilainen and Tuhkuri (2012), Riska and Coche (2013), and Woolgar and Colbourne (2010). The DYPIC experiments provide additional confirmation of the importance of this phenomenon, in this case, for stationkeeping operations in a channel of managed sea ice.

Although the ice floe contact networks can explain some transients in the ice load signal, the video materials indicate that the networks occasionally interact with the tank boundaries. This may create a

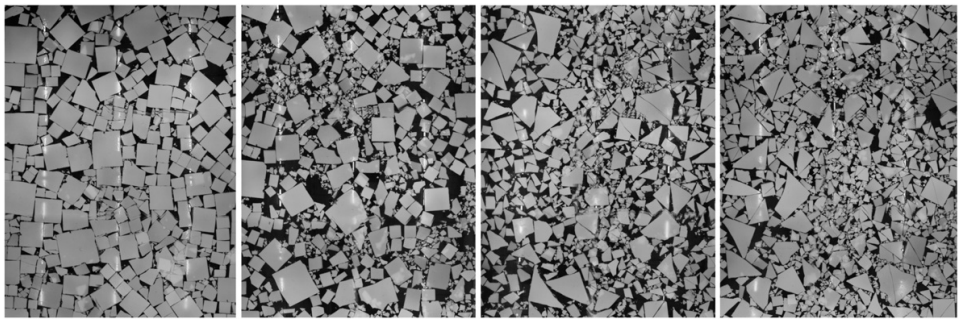

Fig. 6. Ice field evolution throughout one testing day of the DYPIC project. From left to right: series 5100, 5200, 5300 and 5400.

force chain (Paavilainen and Tuhkuri, 2012) in the managed ice cover that will temporarily increase the load even further. However, the timeframe of the load fluctuations in Fig. 8 is larger than could be attributed to a single force chain buckling event. Therefore, it is believed that there are more than one load-bearing networks acting simultaneously on the vessel. These networks are arising and buckling dynamically, leading to sustained changes in the load signal. This finding is important for assessing the required width of the managed ice channel and the guidance strategy of the vessel's control system because sufficient clearance should be provided to avoid severe ice floe interlocking and force chain formation processes during stationkeeping operations.

Observations of the physical processes in the ice floe contact networks can also explain the lack of load–velocity dependence found in Fig. 9. Video 1 and other evidence from the DYPIC project indicate that the load release mechanisms were the same at different velocities in the experiments. The geometrical characteristics of the ice cover (ice concentration and ice floe sizes, shapes and thickness) and the boundary conditions, but not the velocity, were primarily responsible for governing the release mechanisms. Because the release mechanisms govern the overall ice loads, it can be argued that the load level should be velocity-independent in the currently investigated range (below 0.51 m/s in full-scale). Although no quantitative data supporting these claims are presented, no other phenomena accountable for the load–velocity characteristics could be found in the DYPIC datasets. Further research is needed to understand the mechanisms and dynamics of these physical processes, as well as the interconnection between the mechanical properties of the ice (such as flexural strength, compressive strength and Young's modulus), relative velocity and the load release levels in managed ice.

In addition to the lack of velocity dependence, Fig. 9 shows that the load increases with the oblique angle. This result is believed to originate from the fact that the vessel constitutes a wider obstruction and acts as a tract, pressurizing the ice cover on its exposed side. Thus, more ice floe contact networks are forming. Furthermore, at high oblique angles, the environment may not be able to provide sufficient pressure for clearing the ice floes away from the vessel–ice interface. This situation is reflected in Fig. 11, in which rubble and ice floe accumulation are outlined in the upstream segment of the ice cover. In the remainder of the paper, this will be called the *accumulated ice mass*. This is an upstream area of a compacted ice mass that is captured by the obstructing vessel. In the literature, this is sometimes referred to as a false bow or a prow (Ettema and Nixon, 2005). For a ship-shaped vessel, the accumulated ice mass is only present when the exposed hull shape has sections that are sufficiently perpendicular to the ambient ice drift direction (e.g., in the case of high oblique angles). This phenomenon has significant out-of-plane ice rubble accumulation because a large volume of ice becomes broken and subsequently trapped by the obstructing vessel. For DP, this implies that the thrusters must push not only the vessel but also the accumulated ice mass. Hence, when present, the accumulated ice mass plays an important role with respect to both mean and transient ice loads. This is confirmed by both DYPIC data and by previous works in this field: Croasdale et al. (2009) and Wright (2001). A similar effect was also reported by Løset and Timco (1992) for oil spill recovery using a flexible boom and by Kulyakhtin et al. (2013) for underwater rubble accumulation in laboratory experiments.

This section described how the signal characteristics presented in Section 3 may relate to the physical phenomena in the ice cover

Table 2
Definitions of the broken ice fields in the DYPIC project.

No.	Type of floe	Share [%]	Shape	Floe size [m] Model-scale	Floe size [m] Full-scale	Description
1	Small	45	Square	0.5	15	Side of square
	Medium	40		1.0	30	
	Big	15		1.5	45	
2	Small	45	Triangle	0.5	15	Cathetus of 45°
	Medium	40		1.0	30	right triangle
	Big	15		1.5	45	
3	Small	30.3	Rectangle	0.5/0.3	15/9	Length/width of
	Medium	30.3		1.0/0.6	30/18	rectangle
	Big	15.3		1.5/1.0	45/30	
	Brash	24.1	–	–	–	–
4	Small	30.3	Rectangle	0.3/0.25	9/7.5	Length/width of
	Medium	30.3		0.6/0.5	18/15	rectangle
	Big	15.3		1.0/0.75	30/22.5	
	Brash	24.1	–	–	–	–

Table 3
Model-scale parameters of the towing experiments analyzed in this paper. Note that the velocity segmentation is listed in order of application for each experiment.

Exp.	ψ_r [°]	v_r [m/s]	N	IC [%]	h [mm]	σ_f [kPa]	σ_c [kPa]	E [MPa]
4100	170	0.023, 0.047	1	81.7	28.7	60.8	92	–
4200	170	0.023, 0.047	1	67.7	28.7	45.9	92	–
4300	170	0.023, 0.047	2	68.8	28.7	48.3	92	–
4400	170	0.023, 0.047	2	72.8	28.7	37.8	92	–
5100	180	0.023, 0.047	1	84.2	24.3	64.3	89	–
5200	180	0.023, 0.047	1	70.2	24.3	56.8	89	–
5300	180	0.023, 0.047	2	69.9	24.3	51.2	77	–
5400	180	0.023, 0.047	2	76.1	24.3	47.0	77	–
6300	0	0.094, 0.047, 0.023	4	77.2	23.8	25.1	87	10
6400	10	0.094, 0.047, 0.023	4	76.1	23.8	25.1	87	10
8300	10	0.094, 0.047, 0.023	4	75.6	35.9	–	48	22

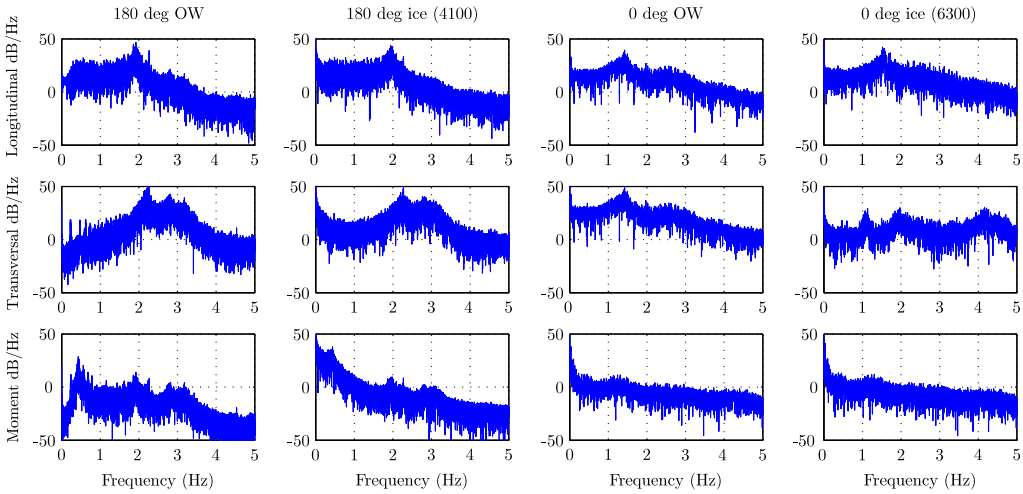

Fig. 7. Frequency spectra comparisons of DYPIC open water (OW) and ice towing experiments.

through the concepts of ice floe contact networks and accumulated ice mass. Because these phenomena exhibit a substantial dependence on the operation and maneuvering of the vessel, they should be considered in the control system design. However, towing experiments performed in a closed basin are restricted to investigating only parts of the dynamics involved in full-scale operations. Additional phenomena, such as ice drift direction changes, large intact ice features slipping through the IM system, compaction and pressure in the ice cover, are known challenges based on full-scale operational experience (Keinonen et al., 2006). Although these phenomena were not explicitly considered in this paper, they are believed to further excite the ice floe contact networks and accumulated ice mass dynamics. Further research is needed to elaborate these relationships and to establish reliable quantitative models for managed ice actions on DP vessels. Regardless, the phenomenological analysis presented in this section provides a sufficient framework for understanding the major trends of the load signal and for investigating implications on DP control system development.

5. Managed ice implications on DP control systems

The generalized equations of motion of a DP vessel can be written in the following form:

$$\dot{\boldsymbol{\eta}} = \mathbf{J}(\boldsymbol{\eta})\boldsymbol{\nu} \tag{1}$$

$$\mathbf{M}\,\dot{\boldsymbol{\nu}} = \boldsymbol{\tau}_{control} + \boldsymbol{\tau}_{hydro} + \boldsymbol{\tau}_{wind} + \boldsymbol{\tau}_{waves} + \boldsymbol{\tau}_{ice} \tag{2}$$

where $\boldsymbol{\eta}$ is the position and orientation vector expressed in an inertial frame, $\mathbf{J}(\boldsymbol{\eta})$ is the transformation matrix between the inertial frame and the body frame, $\boldsymbol{\nu}$ is the body frame velocity vector, $\mathbf{M}$ is the vessel rigid body mass matrix, $\boldsymbol{\tau}_{control}$ is the vessel actuation output, $\boldsymbol{\tau}_{hydro}$ is the hydrodynamic and hydrostatic loads acting on the vessel (including current loads), $\boldsymbol{\tau}_{wind}$ is the wind loads on the vessel, $\boldsymbol{\tau}_{waves}$ is the wave loads on the vessel, and $\boldsymbol{\tau}_{ice}$ is the ice loads from the interaction with the managed ice cover.

The fundamental challenge of DP is to fulfill the vessel control objective: tracking a fixed location or predetermined track through the use of active thrusters. Sections 3 and 4 indicate that severe ice floe interlocking, force chain formation, and added inertia of the accumulated ice mass can be reduced by minimizing the ice floe contact networks and ice mass accumulation. Therefore, to minimize the loads on the DP vessel, two additional control objectives for DP in managed ice can be formulated:

- Minimize the oblique angle between the vessel and the ice.
- Minimize the transverse actuated motion of the vessel.

This set of objectives is called the *reactive control objectives*. Interestingly, these objectives coincide with those of minimum-power DP applications in open water. Miyazaki et al. (2013) compared several specific open water design concepts for minimal power DP and concluded that zero transversal controllers, such as *weather optimal positioning control* (Fossen, 2011; Kjerstad and Breivik, 2010), present the best solution. This design appears to be promising for operations in managed ice because it incorporates both objectives directly without the need for additional measurements, and moreover, it exploits the environment for actuation. Fig. 13 explains this concept further. Implementation of the design concept in the control system can be achieved by applying the control system hierarchy shown in Fig. 12. This structure is conventional for open-water DP, and it has been successfully adopted for experiments in ice (Kerkeni et al., 2013a). It closes the loop between the sensor measurements and the thruster output, and it creates an autonomous system that requires only setpoint commands from the operator.

If the operational area is sufficiently large and the vessel has freedom to maneuver, two additional *proactive control objectives* may be beneficial:

- Seek the weakest path through the ice cover, e.g., as illustrated in Fig. 13.
- Utilize the vessel momentum and inertia to address challenging ice features, e.g., as reported for full-scale stationkeeping operations in ice (Keinonen et al., 2006).

Table 4
Low-pass filter specifications.

Filter type	Passband	Stopband	Passband ripple	Stopband attenuation
Butterworth	0.4 Hz	0.75 Hz	1 dB	60 dB

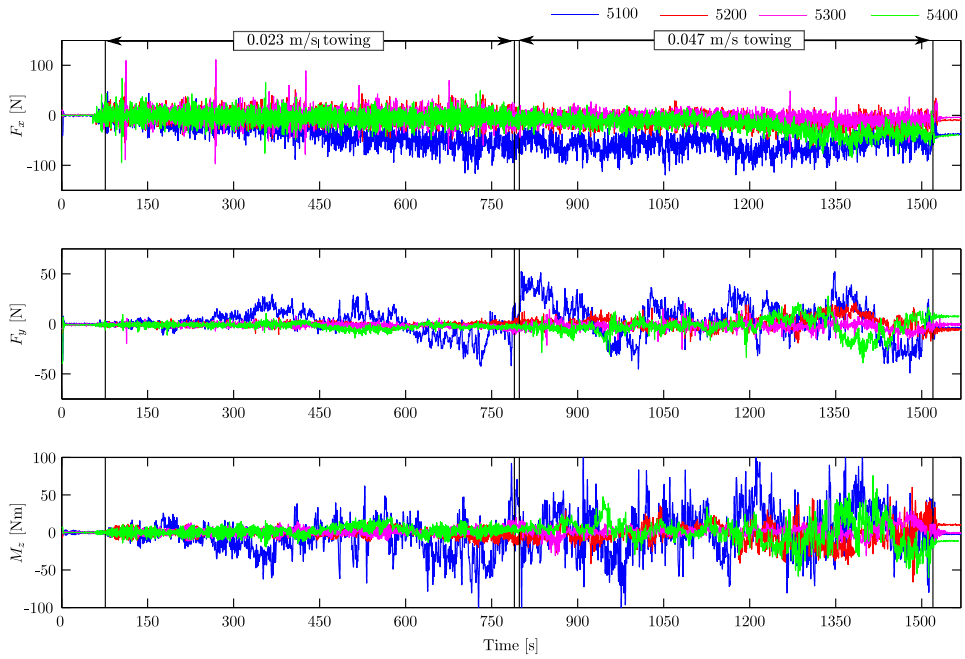

Fig. 8. Towing time series from experiments 5100 to 5400. Vertical black lines indicate the start and stop of the different velocity segments. All values are given in model-scale.

These strategies aim to minimize the future load on the system based on predictions of the ice environment in the operational region. However, there is currently no robust and thoroughly verified *ice observation system* (Haugen et al., 2011) capable of gathering the necessary measurements from the surrounding environment, and there are no autonomous prediction and decision systems available. Therefore, human operators will be needed to perform observations, evaluate information, assess risks, and initiate maneuvers as required by the proactive control objectives.

Although the control objectives can be met by a specific design concept, the overall performance of the DP system hinges on the ability of the state estimator to accurately predict the states of the system (position and orientation, linear and angular velocity, and external loads). If the state estimator is unable to track the ice loads accurately, the positioning capability will deteriorate (as shown experimentally by Jenssen et al. (2009) and Kerkeni et al. (2013a) in managed ice). This occurs because the estimator signals are directly used to calculate the thruster's actuation output. Thus, improving performance requires the mathematical *control plant model* (Sørensen, 2005), which is an explicit simplified approximation of Eqs. (1)–(2) used for state prediction, to better capture the dynamics of the vessel.

Incorporating the ice dynamics in the control plant model may be achieved by either introducing a directly measured ice load variable into the equations (using the measurement to capture the dynamics, as reported by Nguyen et al. (2009)) or by applying a mathematical model relying on indirect measurements (e.g., ice drift, ice concentration, and ice thickness) and the vessel motion states (as is common for hydrodynamic added mass and drag in open-water DP). Although identifying and developing the latter may be achieved using an extensive dataset (exceeding that of DYPIC), the robustness and accuracy are questionable for tracking the highly fluctuating ice load signal. Thus, although a descriptive model may predict the mean loads as a function of the particulars of the ice cover and vessel motion states, it will be challenging to predict the fluctuations originating from the in situ ice floe contact networks and accumulated ice mass.

The first option, i.e., incorporating ice load measurements into the control plant model, requires additional instrumentation. Such signals may be obtained through strain gauges (Leira et al., 2009; Ritch et al., 2008), external impact panels (Gagnon et al., 2008), or inertial measurements (Johnston et al., 2008; Nyseth et al., 2013). All these technologies have proven performance in ice load measurements on icebreaking ships, but inertial sensors are particularly interesting for DP because they constitute a non-invasive instrumentation system that resides inside the vessel and is able to capture the global loads acting from any oblique angle. Achieving the same sensing capability with strain gauges or external impact panels requires extensive instrumentation around the entire hull. Lindegaard (2003) shows and discusses how to incorporate inertial measurements into DP control systems for open water using a conventional control plant model. Alternatively, because all global loads perturbing the system are captured in the accelerations (linear and angular) of the vessel, the inertial sensors offer another approach to the state estimation problem. Rather than estimating the external loads through specific kinetic models, the state estimation problem can be reformulated to remove sensor bias and gravitational influence from the inertial sensor signals. This can be solved using established kinematic control plant models (Batista et al., 2011). Although these do not provide the load estimates directly, they can be determined and applied in the control system, as proposed in (Kjerstad et al., 2011; Kjerstad and Skjetne, 2012). Another challenge

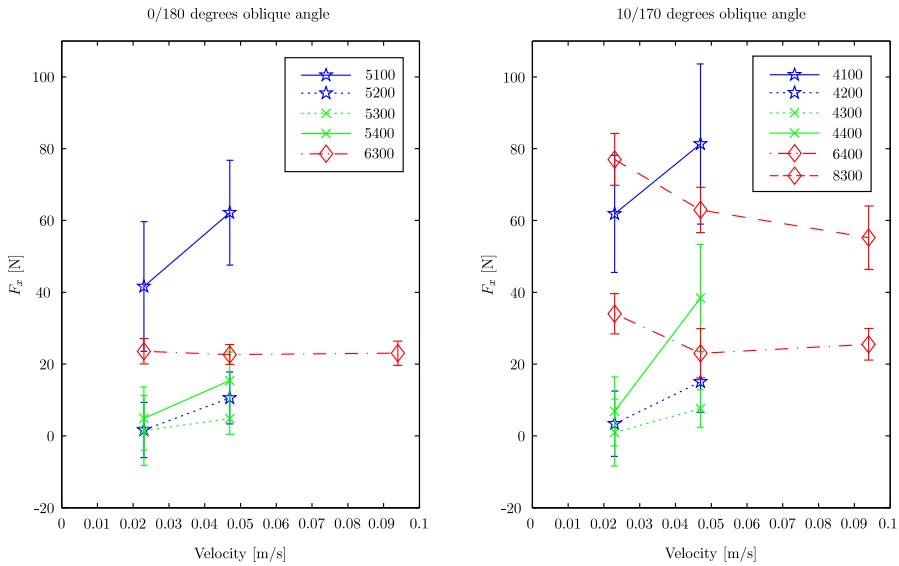

(a) The longitudinal loads

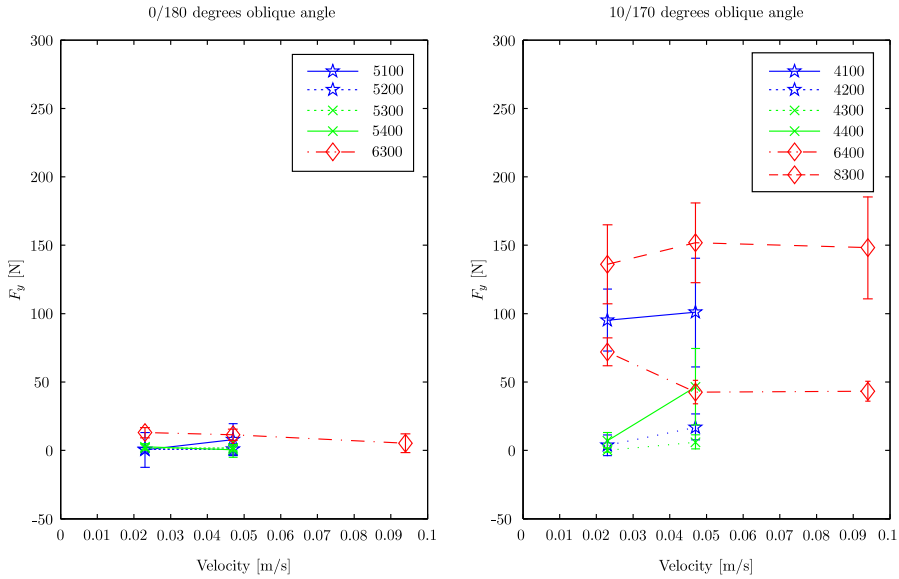

(b) The transversal loads

Fig. 9. The mean load and standard deviation given in the tank frame (defined in Fig. 3) as a function of velocity for the towing experiments of Table 3. Left: The datapoints from the 0/180° oblique angle experiments. Right: The datapoints from the 10/170° oblique angle experiments. All values are given in model-scale.

with this approach is the need for an angular acceleration measurement. These signals may be obtained by either an angular accelerometer (Titterton and Weston, 2005) or by a configuration of conventional linear accelerometers (Buhmann et al., 2006).

Conventional DP state estimators employ a wave filter to reduce high-frequency oscillatory wave motion (beyond the DP system bandwidth) on the state estimates. This filter may be disabled when operating well within the ice field because the ice cover dampens the wave energy exponentially with respect to distance from the ice edge (Broström and Christensen, 2008). This is beneficial for tracking the ice loads because it allows the remaining environmental components to be weighted higher.

Another aspect of DP operation in managed ice is related to the utilization of the thruster system of the vessel. The capability of the

Video 1. The Arctic Drill Ship observed from above as it advances in the ice field during experiment 4100. The Arctic Drill Ship observed from above as it advances in the ice field during experiment 4100. Supplementary data to this article can be found online at http://dx.doi.org/10.1016/j.coldregions.2014.11.015

thruster system in the various degrees of freedom is highly dependent on the ice conditions (Kerkeni et al., 2013b; Su et al., 2013). Therefore, it can be beneficial to prioritize the moment for heading control over longitudinal and transversal loads in the control allocation system (which determines how much load each thruster should produce) (Kjerstad et al., 2013; Skjetne and Kjerstad, 2013; Wold, 2013). It may also be beneficial to incorporate local ice management by using the thruster wakes. Notably, podded propulsors have shown significant ice clearing performance in high ice concentrations (Ferrieri et al., 2013; Keinonen and Lohi, 2000), which may help trigger release mechanisms in the ice floe contact networks and clear ice floes from the vessel. Wold (2013) shows how to utilize spare actuation capacity for this purpose without compromising the positioning of the vessel. The thruster wake ice management may be implemented as an automatic and/or operator-guided process.

6. Conclusions

This paper investigated the dynamic positioning of offshore vessels in managed ice conditions using a model-scale dataset from the large ice tank of HSVA. The analysis of signals from 25 towing experiment segments indicated the following:

- Global ice loads contain rapid and significant transients that may abruptly inject energy into the stationkeeping system.
- Mean ice loads depend on the oblique angle between the vessel and the ice but not on the relative ice drift velocity (in the range of 0.13–0.51 m/s full-scale).
- Mean ice loads and standard deviations strongly depend on the ice floe size, ice concentration, and ice thickness.

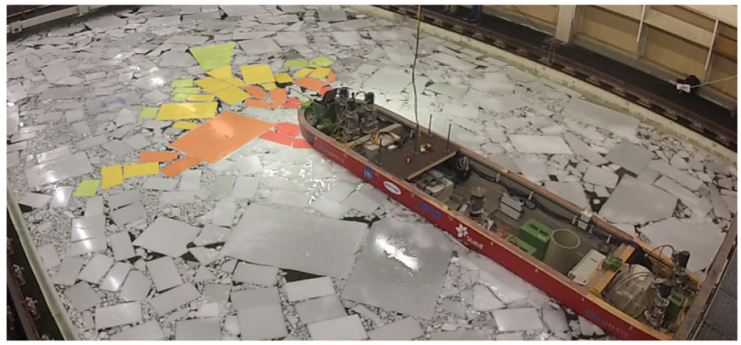

Fig. 10. A snapshot from a DYPIC DP mode experiment, in which a subset of contact networks was identified from video material and visualized by manually overlaying colors indicating movement of the ice floes.

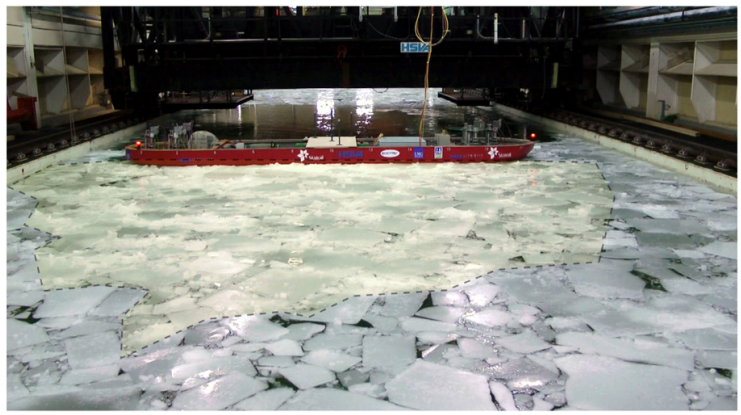

Fig. 11. A snapshot from a DYPIC DP mode experiment at a 90° oblique angle illustrating the accumulated ice mass. It is possible to observe a significant amount of ice rubble inside the yellow overlay outlined by a dashed line.

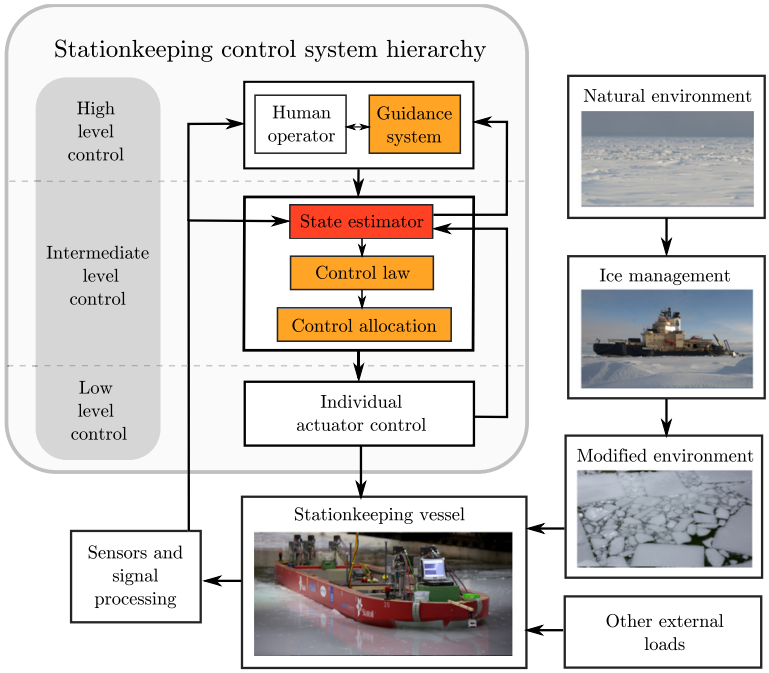

Fig. 12. Control system hierarchy for stationkeeping in managed sea ice.
Adapted from Breivik (2010, p. 127) and Kerkeni et al. (2013a).

These signal characteristics of the managed ice load were explained through the concepts of ice floe contact networks and accumulated ice mass. Finally, it was argued that managed ice poses the following implications for DP control systems:

- Control objectives that comply with the managed ice dynamics can act to minimize the ice floe contact networks and accumulated ice mass. Specifically, tracking the ice drift direction with the bow or stern of the vessel and reducing the direct transversal actuation by active ice vaning appears to be promising.
- The degraded performance of conventional open-water DP control systems in ice can be attributed to the lack of structures in the DP control algorithms capable of tracking the ice load signal and guiding the vessel in compliance with the managed ice dynamics.
- Improvements in the global ice load tracking performance may be obtained by introducing a control plant model that incorporates the managed ice dynamics and/or adding ice load measurements. Inertial measurements appear to be particularly promising.

It is concluded that the complexity of DP in managed ice requires a coherent design strategy for all core modules of the control system, where it is important to ensure both ice load signal tracking capability and control objectives that comply with the managed ice dynamics. Although no

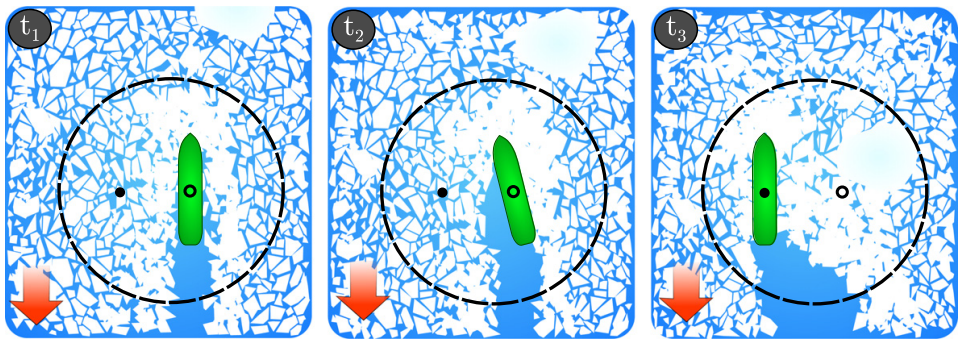

Fig. 13. Illustration of maneuvering to seek the weakest path in the ice and utilization of the drifting sea ice for vessel actuation. At t_1, a potentially significant ice load feature is approaching the vessel, and the position is changed from the hollow circle to the full black circle. At t_2, the vessel has created an oblique angle while maintaining its upstream position to acquire an actuating starboard ice load. At t_3, the vessel has utilized the ice load to move into the new position and minimized the oblique angle to minimize the load, allowing the hazardous ice feature to pass.

specific design was presented, the proposals and considerations of this paper can serve as the basis for further work on enabling safe and robust DP in managed ice conditions.

Acknowledgments

The authors would like to acknowledge the Research Council of Norway (RCN) for their financial support of the Arctic DP project at the Norwegian University of Science and Technology (RCN project no. 199567) and the MARTEC ERA-NET project: DYPIC — dynamic positioning in ice covered waters (RCN project no. 196897), which supplied experimental data from the Hamburg Ship Model Basin. The authors would also like to thank the Ministry of Ecology, Sustainable Development, Transport and Housing (France) and the Federal Ministry of Economics and Technology (Germany) for their financial support of the MARTEC ERA-NET project: DYPIC — dynamic positioning in ice covered waters. Additionally, the authors would like to thank industry partners in the mentioned projects: Statoil, Kongsberg Maritime, DNV GL, DCNS Research/Sirehna, and the Hamburg Ship Model Basin for their kind support, and Francesco Scibilia, Ulrik Jørgensen, and Biao Su for constructive feedback and insightful comments.

References

Batista, P., Silvestre, C., Oliveira, P., Cardeira, B., 2011. Accelerometer Calibration and Dynamic Bias and Gravity Estimation: Analysis, Design, and Experimental Evaluation. IEEE Transactions on Control Systems Technology 19 (5), 1128–1137.
Bray, D., 2011. The DP Operator's Handbook. The Nautical Institute.
Breivik, M., 2010. Topics in Guided Motion Control of Marine Vehicles. (Ph.D. thesis). Norwegian University of Science and Technologyp. 127.
Broström, G., Christensen, K., 2008. Waves in Sea Ice. Technical Report. Norwegian Meteorological Institute, Norway.
Buhmann, A., Peters, C., Cornils, M., Manoli, Y., 2006. A GPS Aided Full Linear Accelerometer Based Gyroscope-free Navigation System. Position, Location, and Navigation Symposium, 2006 IEEE/ION, pp. 622–629.
Croasdale, K., Bruce, J., Liferov, P., 2009. Sea ice Loads Due to Managed Ice. Proceedings of the 20th International Conference on Port and Ocean Engineering Under Arctic Conditions.
Dal Santo, X., Jochmann, P., 2012. Model DP System for Ice-tank Research. Proceedings of the ASME 2012 31st International Conference on Ocean, Offshore and Arctic Engineering.
Eik, K.J., 2010. Ice Management in Arctic Offshore Operations and Field Developments. (Ph.D. thesis). Norwegian University of Science and Technology, Trondheim, Norway.
Ettema, R., Nixon, W.A., 2005. Ice Tank Tests on Ice Rubble Loads Against a Cable-Moored Conical Platform. J. Cold Reg. Eng. 19 (4), 103–116.
Ferrieri, J.M., Veitch, B., Akinturk, A., 2013. Experimental Study on Ice Management Through the Use of Podded Propeller Wash. Proceedings Third International Symposium on Marine Propulsors.
Fossen, T.I., 2011. Handbook of Marine Craft Hydrodynamics and Motion Control. Wiley.
Gagnon, R., Cumming, D., Ritch, R., Browne, R., Johnston, M., Frederking, R., McKenna, R., Ralph, F., 2008. Overview accompaniment for papers on the bergy bit impact trials. Cold Reg. Sci. Technol. 52 (1), 1–6.
Gürtner, A., Baardson, B.H.H., Kaasa, G.O., Lundin, E., 2012. Aspects of Importance Related to Arctic DP Operations. Proceedings of the ASME 2012 31st International Conference on Ocean, Offshore and Arctic Engineering.
Haase, A., Jochmann, P., 2013a. DYPIC — Dynamic Positioning in Ice — Second Phase of Model Testing. Proceedings of the ASME 2013 32nd International Conference on Ocean, Offshore and Arctic Engineering.
Haase, A., Jochmann, P., 2013b. Different Ways of Modeling Ice Drift Scenarios in Basin Tests. Proceedings of the ASME 2013 32nd International Conference on Ocean, Offshore and Arctic Engineering.
Haase, A., van der Werff, S., Jochmann, P., 2013. DYPIC — Dynamic Positioning in Ice — First Phase of Model Testing. Proceedings of the ASME 2013 32nd International Conference on Ocean, Offshore and Arctic Engineering.
Hals, T., Jenssen, N.A., 2012. DP Ice Model Tests of Arctic Drillship and Polar Research Vessel. Proceedings of the ASME 2012 31st International Conference on Ocean, Offshore and Arctic Engineering.
Haugen, J., Imsland, L., Løset, S., Skjetne, R., 2011. Ice Observer System for Ice Management Operations. Proceedings of the Twenty-first (2011) International Offshore and Polar Engineering Conference.
Herman, A., 2013. Numerical modeling of force and contact networks in fragmented sea ice. Ann. Glaciol. 54 (62), 114–120.
Hopkins, M.A., Tuhkuri, J., 1999. Compression of floating ice fields. J. Geophys. Res. 104 (C7), 15,815–15,825.
International Maritime Organization, 1994. Guidelines for Vessels with Dynamic Positioning Systems. MSC/circ.645.
Jenssen, N.A., Muddesitti, S., Phillips, D., Backstrom, K., 2009. DP In Ice Conditions. Proceedings of the Dynamic Positioning Conference.
Jenssen, N.A., Hals, T., Haase, A., Santo, X., Kerkeni, S., Doucy, O., Gürtner, A., Hetschel, S.S., Moslet, P.O., Metrikin, I., Løset, S., 2012. A Multi-national R&D Project on DP Technology in Ice. Proceedings of the Dynamic Positioning Conference.
Johnston, M., Timco, G., Frederking, R., Miles, M., 2008. Measuring global impact forces on the CCGS Terry Fox with an inertial measurement system called MOTAN. Cold Reg. Sci. Technol. 52 (1), 67–82.
Keinonen, A., Lohi, P., 2000. Azimuth and Multi Purpose Icebreaker Technology for Arctic and Non-Arctic Offshore. Proceedings of the Tenth (2000) International Offshore and Polar Engineering Conference.
Keinonen, A., Martin, E.H., 2012. Modern Day Pioneering and Its Safety in the Floating Ice Offshore. Proceedings of the International Conference and Exhibition on Performance of Ships and Structures in Ice.
Keinonen, A., Shirley, M., Liljeström, G., Pilkington, R., 2006. Transit and Stationary Coring Operations in the Central Polar Pack. 7th International Conference and Exhibition on Performance of Ships and Structures in Ice.
Kerkeni, S., Dal Santo, X., Metrikin, I., 2013a. Dynamic Positioning in Ice — Comparison of Control Laws in Open Water and Ice. Proceedings of the ASME 2013 32st International Conference on Ocean, Offshore and Arctic Engineering.
Kerkeni, S., Metrikin, I., Jochmann, P., 2013b. Capability Plots of Dynamic Positioning in Ice. Proceedings of the ASME 2013 32st International Conference on Ocean, Offshore and Arctic Engineering.
Kerkeni, S., dal Santo, X., Doucy, O., Jochmann, P., Haase, A., Metrikin, I., Løset, S., Jenssen, N.A., Hals, T., Gürtner, A., Moslet, P.O., Støle Hetschel, S., 2014. DYPIC Project: Technological and Scientific Progress Opening New Perspectives. Proceedings of the Arctic Technology Conference.
Kjerstad, Ø., Breivik, M., 2010. Weather Optimal Positioning Control for Marine Surface Vessels. Proceedings of IFAC CAMS (Rostock, Germany).
Kjerstad, Ø., Skjetne, R., 2012. Observer Design with Disturbance Rejection by Acceleration Feedforward. Proceedings of ROCOND12 (Aalborg, Denmark).
Kjerstad, Ø., Skjetne, R., Jenssen, N.A., 2011. Disturbance Rejection by Acceleration Feedforward: Application to Dynamic Positioning. Proceedings of IFAC World Congress, Milan Italy.
Kjerstad, Ø., Skjetne, R., Berge, B., 2013. Constrained Nullspace-based Thrust Allocation for Heading Prioritized Stationkeeping of Offshore Vessels in Ice. Proceedings of 22st International Conference on Port and Ocean Engineering Under Arctic Conditions.
Kongsberg Maritime, 2006. Kongsberg K-Pos Dynamic Positioning — Optimizing Complex Vessel Operations. Brochure.
Kulyakhtin, S., Høyland, K.V., Astrup, O.S., Evers, K.U., 2013. Rubble Ice Transport on Arctic Offshore Structures (RITAS), Part III: Analysis of Model Scale Rubble Ice Stability. Proceedings of 22st International Conference on Port and Ocean Engineering Under Arctic Conditions.
Leira, B., Børsheim, L., Espeland, Ø, Amdahl, J., 2009. Ice-load Estimation for a Ship Hull Based on Continuous Response Monitoring. Proceedings of the Institution of Mechanical Engineers, Part M: Journal of Engineering for the Maritime Environment.
Liferov, P., 2014. Station-keeping in Ice — Normative Requirements and Informative Solutions. Proc. Arctic Technology Conference 2014.
Lindegaard, K.P.W., 2003. Acceleration Feedback in Dynamic Positioning. (Ph.D. thesis). Norwegian University of Science and Technology.
Liu, L., Zhan, D., Spencer, D., Molyneux, D., 2010. Pack Ice Forces on Floating Offshore Oil and Gas Exploration Systems. In Proceedings of the 9th International Conference and Exhibition on Performance of Ships and Structures in Ice.
Løset, S., Timco, G.W., 1992. Laboratory Testing of a Flexible Boom for Ice Management. Ocean, Offshore and Arctic Engineering, pp. 289–295.
Metrikin, I., Løset, S., Jenssen, N.A., Kerkeni, S., 2013. Numerical simulation of dynamic positioning in ice. Mar. Technol. Soc. J. 47 (2), 14–30.
Miyazaki, M.R., Tannuri, E.A., de Oliveria, A.C., 2013. Minimum Energy DP Heading Control: Critical Analysis and Comparison of Different Strategies. Proceedings of the ASME 2013 32st International Conference on Ocean, Offshore and Arctic Engineering.
Moran, K., Backman, J., Farrell, J.W., 2006. Deepwater Drilling in the Arctic Ocean's Permanent Sea Ice. Proceedings of the Integrated Ocean Drilling Program.
Neville, M., Brown, J., Martin, E., Keinonen, A., Liljeström, F.E.G., 2013. Influence of Modeling Full Scale Based Managed Ice Conditions in DP Ice Model Tests. Proceedings of the 22nd International Conference on Port and Ocean Engineering Under Arctic Conditions.
Nguyen, D.T., Sørbø, A.H., Sørensen, A.J., 2009. Modelling and Control for Dynamic Positioned Vessels in Level Ice. Proceedings of Conference on Manoeuvring and Control of Marine Craft, pp. 229–236.
Nyseth, H., Frederking, R., Sand, B., 2013. Evaluation of Global Ice Load Impacts Based on Real-time Monitoring of Ship Motions. Proceedings of 22st International Conference on Port and Ocean Engineering Under Arctic Conditions.
Paavilainen, J., Tuhkuri, J., 2012. Pressure Distributions and Force Chains During Simulated Ice Rubbling Against Sloped Structures. Cold Reg. Sci. Technol. 85, 157–174.
Riska, K., Coche, E., 2013. Station Keeping in Ice — Challenges and Possibilities. Proceedings of the 22nd International Conference on Port and Ocean Engineering Under Arctic Conditions.
Ritch, R., Frederking, R., Johnston, M., Browne, R., Ralph, F., 2008. Local ice pressures measured on a strain gauge panel during the CCGS Terry Fox bergy bit impact study. Cold Reg. Sci. Technol. 52 (1), 29–49.
Rohlén, Å., 2009. Relationship Between Ice-management and Station Keeping in Ice. Presentation at Dynamics Positioning Conference.
Rolls-Royce Marine, 2009. Icon DP — A Positioning Product From Rolls-Royce. Brochure.
Sayed, M., Kubat, I., Wright, B., Millan, J., 2014. Numerical Simulations of Ice Forces on Moored and Thruster-assisted Drillships. Arctic Technology Conference.
Sirehna, 2014. EASY-DP — Sirehna Brochure. Brochure.

Skjetne, R., Kjerstad, Ø., 2013. Recursive Nullspace-based Control Allocation With Strict Prioritization for Marine Craft. Proceedings of IFAC CAMS, Osaka, Japan.
Sørensen, A.J., 2005. Lecture Notes Marine Cybernetics: Modeling and Control. Faculty of Engineering Science and Technology. NTNU, Trondheim, Norway.
Su, B., Kjerstad, Ø.K., Skjetne, R., Berg, T.E., 2013. Ice-going Capability Assessment and DP-ice Capability Plot for a Double Acting Intervention Vessel in Level Ice. Proceedings of the 22th International Conference on Port and Ocean Engineering Under Arctic Conditions.
Titterton, D., Weston, J., 2005. Strapdown Inertial Navigation Technology. Progress in Astronautics and Aeronautics Second ed. AIAA.
Wold, H.E., 2013. Thrust Allocation of DP in Ice. (Master's thesis). Norwegian University of Science and Technology, Trondheim, Norway.
Woolgar, R.C., Colbourne, D.B., 2010. Effects of hull-ice friction coefficient on predictions of pack ice forces for moored offshore vessels. Ocean Eng. 37 (2), 296–303.
Wright, B.D., 2001. Ice Loads on the Kulluk in Managed Ice Conditions. Proceedings of the 16th International Conference on Port and Ocean Engineering Under Arctic Conditions.
Yulmetov, R., Løset, S., Eik, K., 2013a. Analysis of Drift of Sea Ice and Icebergs in the Greenland Sea. Proceedings of the 22th International Conference on Port and Ocean Engineering Under Arctic Conditions.
Yulmetov, R., Marchenko, A., Løset, S., 2013b. Ice Drift and Sea Current Analysis in the Northwestern Barents Sea. Proceedings of the 22th International Conference on Port and Ocean Engineering Under Arctic Conditions.
Zhang, Q., Werff, S., Metrikin, I., Løset, S., Skjetne, R., 2012. Image Processing for the Analysis of an Evolving Broken-ice Field in Model Testing. Proceedings of the ASME 2012 31st International Conference on Ocean, Offshore and Arctic Engineering.
Zhang, Q., Skjetne, R., Metrikin, I., Løset, S., 2014. Image Processing for Ice Floe Analyses in Broken-ice Model Testing. Cold Reg. Sci. Technol. http://dx.doi.org/10.1016/j.coldregions.2014.12.004.

Modeling and Control for Dynamic Positioned Marine Vessels in Drifting Managed Sea Ice

Modeling, Identification and Control, Vol. 35, No. 4, 2014, pp. 249–262, ISSN 1890–1328

Modeling and Control for Dynamic Positioned Marine Vessels in Drifting Managed Sea Ice

Øivind Kåre Kjerstad Roger Skjetne

Department of Marine Technology, Norwegian University of Science and Technology, N-7491 Trondheim, Norway.
E-mail: {oivind.k.kjerstad,roger.skjetne}@ntnu.no

Abstract

This paper presents a development framework for dynamic positioning control systems for marine vessels in managed ice. Due to the complexity of the vessel-ice and ice-ice interactions a configurable high fidelity numerical model simulating the vessel, the ice floes, the water, and the boundaries is applied. The numerical model is validated using experimental data and coupled with a control application incorporating sensor models, control systems, actuator models, and other external dynamics to form a closed loop development platform. The ice drift reversal is simulated by moving the positioning reference frame in an elliptic trajectory, rather than moving each individual ice floe. A control plant model is argued, and a control system for managed ice is proposed based on conventional open water design methods. A case study shows that dynamic positioning in managed ice is feasible for some moderate ice conditions.

Keywords: Dynamic positioning, Numerical simulation, Control design, Nonlinear systems

1 Introduction

According to Gautier et al. (2009) the Arctic region holds approximately 30 % of the undiscovered gas, and 13 % of the undiscovered oil in the world. Such resources coupled with diminishing supplies of conventional oil and higher oil prices have resulted in an intensified focus on research and development work to qualify, enable, and mature technological solutions required for Arctic offshore operations. One of the major challenges is the fact that many of the undrilled prospectives lies below 100 m water-depth (Hamilton, 2011). To reach these requires floating prouction units that are capable of operating in the harsh Arctic environemnt. A key system enabling this is the station-keeping system that ensures that the vessel maintains position within a given operational area. Stationkeeping ranges from passive moored structures which do not have its own actuation to dynamic positioning (DP) where a onboard control system calculates the thruster actuation needed to automatically maintain position (fixed location or predetermined track) in the presence of external disturbances (IMO, 1994). Although floating production units in the Arctic are foreseen to be thruster assisted moored structures, where a control system works together with the moorings to enable efficient and robust positioning, DP will be an essential component during the exploration phase, connection and disconnection from the mooring, and for support and intervention.

When vessels interacts with high concentrations of sea ice (above 6/10th), the environmental forces are substantially different and conventional open-water DP systems are known to be insufficient (Kerkeni et al., 2013; Gürtner et al., 2012; Hals and Jenssen, 2012; Jenssen et al., 2009). Nevertheless, it has been demonstrated by full-scale, model-scale, and numerical experiments that high-uptime positioning is possible with ice management (IM) support (Rohlén, 2009; Keinonen and Martin, 2012; Hals and Jenssen, 2012; Metrikin et al., 2013; Liferov, 2014). IM involves all aspects of removing or reducing ice actions on the protected

doi:10.4173/mic.2014.4.3

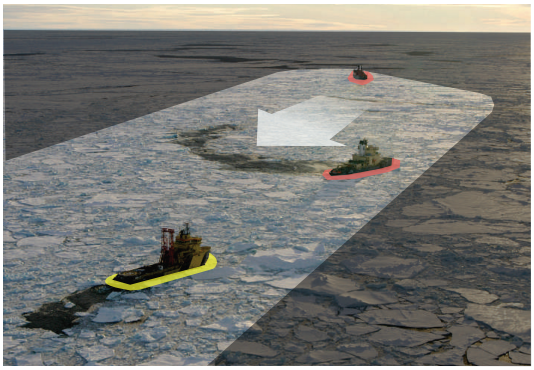

Figure 1: Ice management concept featuring the protected DP vessel (enveloped in yellow) and the physical ice management fleet (enveloped in red). Adapted from (Moran et al., 2006).

Figure 2: A vessel at DP in the large ice basin at HSVA during DYPIC. Courtesy of DYPIC.

vessel (Eik, 2010). Actual IM activities are operation-specific, but the main objective is to either transform the natural ice environment into an acceptable managed ice condition or suspend the operation if that is not possible. Figure 1 illustrates a modern physical IM operation: the operational fleet, the ice cover, and the ice drift direction.

During development of control systems, models of the vessel dynamics are needed for simulation and control systems design. Sørensen (2012) defines two levels of model fidelity: *process plant models* and *control plant models*. The process plant model describes the actual physics involved with high fidelity and replaces costly deployments during development and testing. There are several benefits to computer simulations, but most notably it enables rapid design iterations in a controllable and repeatable environment. The control plant model is typically a simplification of the process plant model capturing the important characteristics of the process. It is the foundation of model-based control design and used in analytical stability analysis. This is usually obtained by identifying the plant dynamics from first principles and experimental data.

Today, the development of ice-enabled DP systems heavily depend on experimental testing and tuning in laboratory basins (see for instance (Hals and Efraimsson, 2011) and (Jenssen et al., 2012)) where a model scale vessel controlled by a DP system is propelled through an ice cover frozen and cut to match the ice conditions. Figure 2 shows a DP test at the Hamburg Ship Model Basin (HSVA). Although model ice tanks create realistic ice environments for linear motion, testing of phenomena or maneuvers requiring some transversal space is challenging. Also, the overhead and expenses involved with each experiment is high, and each frozen ice cover is constrained to a few tests with limited repeatability. Therefore, applying simulation models relieving laboratory experiments is considered highly beneficial.

This paper presents a development platform for DP in ice which applies the numerical model presented in (Metrikin, 2014) and data from the European research project DYnamic Positioning In iCe (DYPIC). The latter was a 3 year initiative (2010-2012) led by HSVA and financed by the national research agencies of Germany, France, and Norway. The program focused on various aspects of DP technology for offshore operations in ice-infested waters, where almost 250 different scenarios were performed in broken ice conditions in the large ice tank of the HSVA (which is 72 m long and 10 m wide). Comprehensive project overviews can be found in (Jenssen et al., 2012) and (Kerkeni et al., 2014).

The contribution of this paper is: (1) description, application, and investigation of a numerical tool as a process model for control system development in managed ice; (2) simulation of ice drift reversals by elliptic trajectories; (3) derivation of a control design model and control algorithms for DP in managed sea-ice; and (4) investigation of the proposed design by a case study.

1.1 Scope

The planar 3 degrees of freedom (DOF) equations of motion of a DP vessel are:

$$\dot{\boldsymbol{\eta}} = \mathbf{R}(\psi)\boldsymbol{\nu} \tag{1}$$

$$\mathbf{M}_{RB}\dot{\boldsymbol{\nu}} = \boldsymbol{\tau} + \boldsymbol{\tau}_{hydro} + \boldsymbol{\tau}_{wind} + \boldsymbol{\tau}_{waves} + \boldsymbol{\tau}_{ice} \tag{2}$$

where $\boldsymbol{\eta} \in \mathbb{R}^3$ is the position and orientation vector expressed in an inertial frame, $\mathbf{R}(\psi) \in \mathbb{R}^{3\times3}$ is the rotation matrix between the inertial frame and the body frame where $\psi \in \mathbb{R}$ is the vessel heading, $\boldsymbol{\nu} \in \mathbb{R}^3$ is the body frame velocity vector, $\mathbf{M}_{RB} \in \mathbb{R}^{3\times3}$ is the

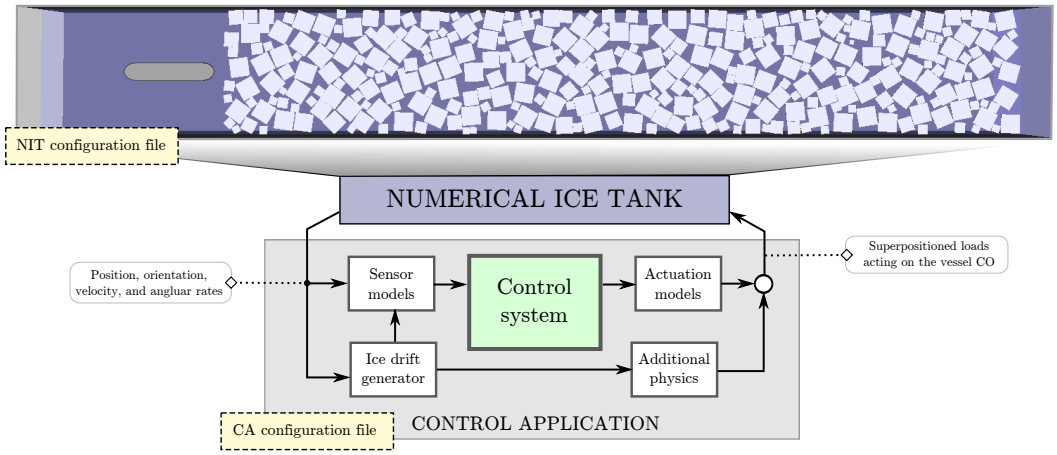

Figure 3: The modular structure of the closed-loop simulation platform for DP in managed ice.

rigid body mass matrix, $\boldsymbol{\tau} \in \mathbb{R}^3$ is the vessel actuation, $\boldsymbol{\tau}_{hydro} \in \mathbb{R}^3$ is inertial, hydrodynamic, and hydrostatic loads (including current loads), $\boldsymbol{\tau}_{wind} \in \mathbb{R}^3$ is the wind loads, $\boldsymbol{\tau}_{waves} \in \mathbb{R}^3$ is the wave loads, and $\boldsymbol{\tau}_{ice} \in \mathbb{R}^3$ is the ice loads from the interaction with the managed ice cover. In this paper the variable notation found in (SNAME, 1950) is applied.

Unfortunately, no analytical dynamic models for the managed ice loads $\boldsymbol{\tau}_{ice}$ exist (Eik, 2010), and deriving one able to relate the in-situ load variations to measurable variables is challenging (Kjerstad et al., 2014). This mainly affects the derivation of a control design model for managed ice. Numerical methods have shown promise as process models when simulating each individual ice floe as a body (see for instance (Metrikin et al., 2013) and (Metrikin, 2014)). Therefore, the first problems treated in this paper are:

1. Apply and validate a numerical managed ice model as a process model and simulation framework for DP in managed ice;

2. Establish a control design model for DP control systems development in managed ice.

Although DP in managed ice have been proven feasible, the control algorithms have not been exposed. Also, it is uncertain which elements of the operation is most challenging for the DP control system. Thus, the final problem treated here is:

3. Adapt conventional DP control systems technology for operations in managed ice and illustrate challenges involved with the operation.

2 Process Model and Closed Loop Simulation Platform

Numerical models based on first principles describing the vessel and the ice floes as interacting bodies with their respective spatial geometries and material properties are considered necessary to simulate the complex vessel-ice and ice-ice interactions and capture the time varying load transients. As managed ice can consist of high amounts of coupled ice floes, the computational complexity of simulating these may also become high. However, models applying physics engines have shown great promise for handling this, see e.g. (Lubbad and Løset, 2011),(Metrikin et al., 2012b,a, 2013).

As mentioned above, the numerical model described in (Metrikin, 2014) is applied as the process model for DP in managed ice. It is implemented as a fixed timestep model based on nonsmooth 6 degrees of freedom (DOF) multi-body dynamics with contacts, friction, and material properties. In the following it will be referred to as the Numerical Ice Tank (NIT), and Section 2.2 elaborates further on its capabilities and validity. Each simulation is comprised of the following five interconnected elements: the rigid body vessel, the towing carriage, the ice floes, the water volume, and the tank boundaries. The NIT can be set up in three different simulation modes:

- *Free running*, where the vessel is forced through the ice cover by a fixed input force and moment vector.

- *Towing*, where the vessel is forced through the ice cover by the carriage at a given velocity.

- *DP*, where the vessel is propelled by a body force and moment vector defined at each time step.

For development of DP control systems the latter two modes are used. Towing is applied to study the ice dynamics without the additional vessel dynamics and calibrate the numerical model through replicating HSVA ice basin experiments. The DP mode is used to close the loop between the simulator vessel motion output and the body force and moment vector to test various control algorithms. Figure 3 provides an overview the closed-loop simulation platform.

2.1 Kinematics

The NIT vessel motion variables are defined in two reference frames:

- *The tank-fixed frame* $\{t\}$ which is non-rotational and fixed to the stationary tank boundaries;
- *The body frame* $\{b\}$ is fixed to the vessel body.

For development of DP a third reference frame is introduced to simulate ice drift in the numerical ice tank:

- *The positioning frame* $\{n\}$ which is non-rotational and following a pre-defined trajectory to simulate ice drift in the stationary ice cover. The DP vessel will be set to track a fixed position in this frame.

Figure 4 illustrates the reference frames. In this paper {n} is considered inertial. The main reason for this approximation is that it is common in ice tank testing (Haase and Jochmann, 2013), and thereby enables a basis for comparison for calibration and validation. The position and orientation vector $\boldsymbol{\eta}$ given in the {n} frame relates to the {t} frame as

$$\boldsymbol{\eta} = \boldsymbol{\eta}_t - \boldsymbol{\eta}_{id} \tag{3}$$

where $\boldsymbol{\eta}_t \in \mathbb{R}^3$ is the position and orientation vector in the tank frame, and $\boldsymbol{\eta}_{id} \in \mathbb{R}^3$ is the position of {n} in {t}. The dynamics of $\boldsymbol{\eta}_{id}$ will be treated in-depth in Section 2.4. The body frame {b} relates to {n} as

$$\dot{\boldsymbol{\eta}} = \mathbf{R}(\psi)\boldsymbol{\nu}. \tag{4}$$

2.2 The Numerical Ice Tank

As the NIT is treated in-depth in (Metrikin, 2014), only a brief summary of its capabilities relevant for describing the closed-loop simulation platform is given.

The NIT computes the vessel dynamics in 6 DOF without wind and waves, using a physics engine with tailored routines for handling the ice material properties. Each simulation is comprised of the following five

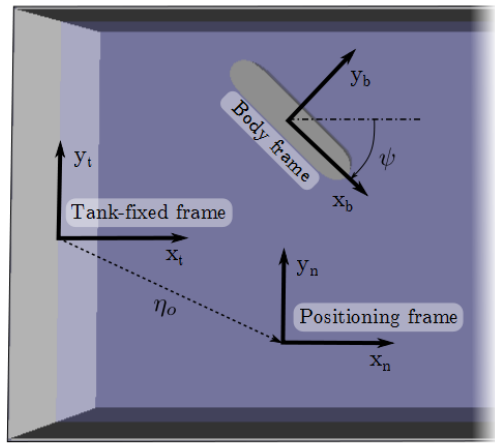

Figure 4: The reference frames of the closed loop simulation platform for DP in managed ice.

interconnected elements: the vessel, the towing carriage, the ice floes, the water volume, and the tank boundaries. The vessel is simulated as a rigid body in 6 DOF without deformations. Throughout this paper a 3D model of an Arctic Drillship (ADS), which was experimentally tested in DYPIC, is used (see Section 4.1). The towing carriage is simulated by a prismatic joint that restricts the motions of the vessel in 5 DOF and allows only the heave displacement. As the towing progresses, the prismatic joint measures the global loads on the vessel from the ice and the fluid by calculating the constraint forces in all DOFs. This mimics the six-component scale commonly used in model testing. It should be noted that the towing carriage is only included in the simulation in towing mode.

The ice floes are simulated as breakable bodies with uniform thickness in 6 DOF. The initial ice floe sizes and floe positions are generated by a ice field generation algorithm that aims to produce a specificed ice field. The water is simulated as a static plane that produces buoyancy and drag loads on the vessel and the ice floes. Tables 1 and 2 summarize the processes in the NIT. The tank boundaries are simulated as stationary rigid bodies. The interface to the model is a XML file that specifies vessel model properties, tank dimensions, ice field properties, ice material properties, water properties, and boundary properties.

2.3 Calibration and Precision

To calibrate the NIT and evaluate its precision the DYPIC towing experiments shown in Table 3 were

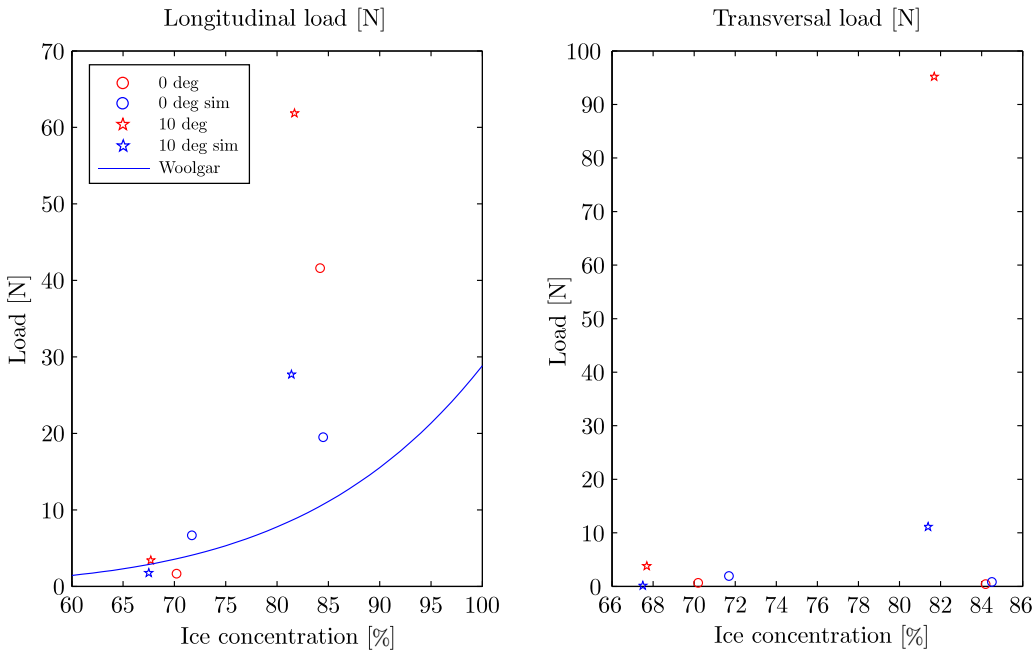

Figure 5: Comparison between model scale data of the experiments seen in Table 3, numerical simulations, and the empirical formula found in (Woolgar and Colbourne, 2010).

Table 1: NIT physical processes and coefficients.

Physical process	Coef. value
Ice-ice static friction	0.2
Ice-ice dynamic friction	0.2
Ice-wall static friction	0.2
Ice-wall dynamic friction	0.2
Ice-vessel static friction	0.0976
Ice-vessel dynamic friction	0.0976
Linear form drag coefficient	0.4
Angular form drag coefficient	0.6
Skin friction	0.01

Table 2: Simulator parameters.

Parameters	Symbol	Unit
Water density	ρ_w	kg/m^3
Ice density	ρ_c	kg/m^3
Ice flexural strength	σ_f	kPa
Ice compressive strength	σ_c	kPa
Ice elastic modulus	E	Mpa
Ice concentration	c	%
Ice thickness	h	mm

replicated. Towing experiments simplify the comparison and interpretation of the simulation results with the experimental data as it is independent of vessel dynamics (and control system). In this study the dynamic friction coefficients of Table 1 were identified from experiments in the ice laboratory at HSVA. In reality this normally differs from the static friction coefficients. However, the NIT applies the same value for both dynamic and static friction. The linear and angular form drag coefficients, and the skin friction were found by trial and error. As it is not possible to exactly replicate the experimental ice floe configuration of the ice cover in the NIT (floe positions and orientations), an ice cover with the same properties was used. See Figure 6 for a comparison. Further, the elastic modulus was set to 10 MPa for all runs, the water and ice densities were set to 1000 and 900 kg/m^3, respectively.

Figure 5 shows the correspondence between experimental data, numerical simulations, and the empirical formula for pack ice loads on stationkeeping vessels for the presented parameters. This shows that the longitudinal load is replicated better in the NIT than using the empirical formula. However, the match of the NIT from the experimental data is seemingly deviating as the ice concentration and oblique angle increases. This is especially evident in the transversal loads. There

Table 3: DYPIC towing experiments. Exp. denotes the experiment number, ψ_r in $[deg]$ is the oblique angle, v_r in $[m/s]$ is the vessel velocity in {t}, c is the ice concentration, h is the ice thickness, σ_f is the ice flexural strength, and σ_c is the ice compressive strength.

Exp.	ψ_r	v_r	c	h	σ_f	σ_c
4100	170	0.023,0.047	81.7	28.7	60.8	92
4200	170	0.023,0.047	67.7	28.7	45.9	92
5100	180	0.023,0.047	84.2	24.3	64.3	89
5200	180	0.023,0.047	70.2	24.3	56.8	89

may be a number of interconnected reasons for this, but pinpointing the actual ones are challenging because the NIT is an integrated environment where many physical processes are coupled. Thus, care must be taken in both experimental design and results interpretation. However, it must be mentioned that the precision can be improved by tuning the linear and angular form drag coefficients for each individual experiment.

The main advantage of the NIT is that it captures two of the fundamental vessel-ice and ice-ice processes described in (Kjerstad et al., 2014): *Ice floe contact networks* and *accumulation of ice mass*. Both relates to the behavior of the drifting ice cover when an obstructing vessel is present and are considered highly important to capture the in-situ time-varying dynamical behavior of the vessel and the ice. This is not captured in any other available model (i.e., statistical or empirical models).

2.4 Closed-Loop Simulation Platform

The control application (CA) of Figure 3 is a collection of interconnected models which enable testing of control algorithms during execution of the NIT (in DP mode). Although it's specific implementation depends on the control system in question, it is divided into the following five general modules: sensor models, ice drift generator, control system, actuator models, and additional physics.

The sensor models simulate onboard equipment measuring the vessel motion, consisting of a coordinate transformation and sensor modeling. First, the NIT vessel motion output (position, orientation, linear velocity, and angular rate) is transformed from {t} to {n} and {b}, and then sensor dynamics and noise is added to the signals. Besides the NIT motion variables, signals originating from the other CA components are possible. The specific sensor implementations are dependent on the application and sensor characteristics.

The ice drift generator models the ice drift in the basin. Typically, linear ice drift, where the vessel tracks

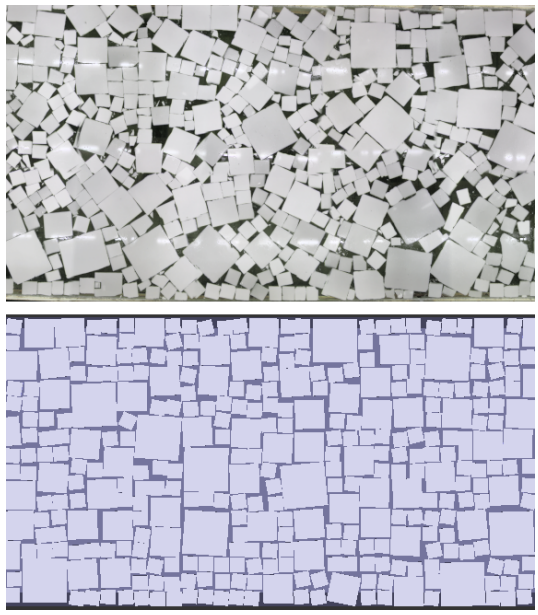

Figure 6: A comparison between the HSVA ice cover and the NIT ice cover for experiment 4100.

a point moving from one side of the basin to the other is considered. However, Keinonen and Martin (2012) reports that the ice drift reversals originating from tides and Coriolis forcing are a major challenge to positioning. Therefore, such a drift scenario is considered in this paper. From the drift patterns in Figure 8 an elliptic trajectory was selected. This is realized by the following motion of {n} in {t},

$$\boldsymbol{\eta}_{id} = \boldsymbol{\eta}_0 + \boldsymbol{\eta}_e \tag{5}$$

where $\boldsymbol{\eta}_0 \in \mathbb{R}^3$ is the initial position of {n} and $\boldsymbol{\eta}_e \in \mathbb{R}^3$ describes the elliptic trajectory as

$$\dot{\boldsymbol{\eta}}_e = \boldsymbol{\Psi} \tag{6}$$

$$\dot{\boldsymbol{\Psi}} = \begin{bmatrix} -a\alpha^2 sin(\alpha t) \\ -b\alpha^2 cos(\alpha t) \\ 0 \end{bmatrix} \tag{7}$$

where a and b are coefficients determining the spatial size of the ellipse, and $\alpha = \frac{v_i}{a}$ where v_i is the maximum ice drift velocity. Figure 7 illustrates the concept. Note that only one half of the ellipse is applied, where the velocity along this decreases until the positioning frame reaches the pivot. Then, the velocity starts to increase again. This complies with observations in nature.

The control system module contains the implemen-

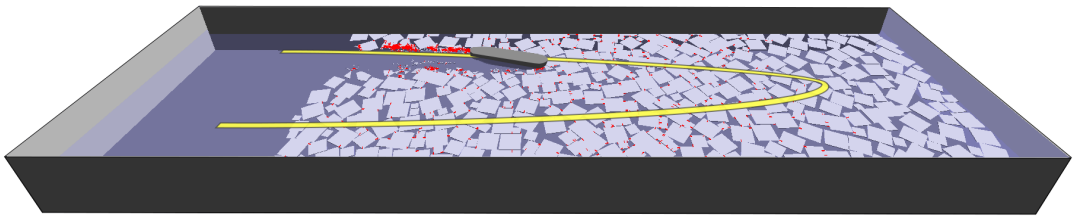

Figure 7: Illustration of the elliptic ice drift trajectory in the closed loop simulation platform.

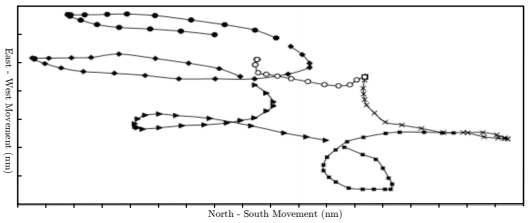

Figure 8: The reversing ice drift as reported by Keinonen et al. (2000).

tation of the control algorithms, and a specific implementation is given in Section 3. The actuator models implement the dynamics of the thruster system onboard the vessel. Experience obtained from full-scale experiments indicates that first-order models are well suited (Sørensen et al., 1996). Thus,

$$\dot{\boldsymbol{\tau}} = -\mathbf{A}_t^{-1}\left(\boldsymbol{\tau} - \mathbf{T}\mathbf{u}\right), \tag{8}$$

where $\mathbf{A}_t$ is a diagonal matrix of time constants, $\mathbf{T} \in \mathbb{R}^{3\times 12}$ is the thruster configuration matrix, and $\mathbf{u}$ is the commanded thrust input from each individual thruster.

The additional physics module contains vessel specific dynamics which are not modeled explicitly in the NIT. Examples of such are wind loads, additional vessel drag, and mooring loads. These are added to the body force and moment vector together with the actuation forces. However, neither was implemented in this study.

It is important to note that the closed-loop system does not enable models implemented in the CA to apply forces on other bodies in the simulation than the vessel. For instance, the thruster wake which is known to affect the ice cover, is not captured. Depending on the vessel and it thruster system, this may be of importance. Therefore, care must be taken when interpreting the simulation results.

2.4.1 Implementation and Experimental Design Considerations

The NIT comes as an object file library (.lib). For convenience, the CA is also generated as an object file library from it's initial implementation in Matlab/Simulink. Both the NIT and the CA libraries are accessed by a C++ interface. Using this, a simulation executable is created. The simulator pseudo code is seen in Algorithm 1.

```
initialize;
read configuration files;
while not at end of simulation do
    Data = Step NIT (Actuation);
    Actuation = Step App. Module (Data);
    save results;
end
```

Algorithm 1: The closed-loop simulator's main program loop.

Although the closed-loop simulator can generate a wide range of scenarios, there are two experimental design considerations, besides the ones already mentioned, that must be recognized:

1. *The number of bodies in the simulation.* This will affect the run-time of the simulation as packed ice field will be computationally heavier than lower concentration scenarios.

2. *The boundary conditions.* These can severely impact the load dynamics if the ice floe contact networks of the vessel interacts with them. However, in some cases this may be a part of the experimental design, i.e., stationkeeping in a narrow managed ice channel.

Judging the capabilities of the closed-loop simulation platform it is found to be a feasible for early development and testing of conceptual control algorithms for specific and confined maneuvers. With respect to load

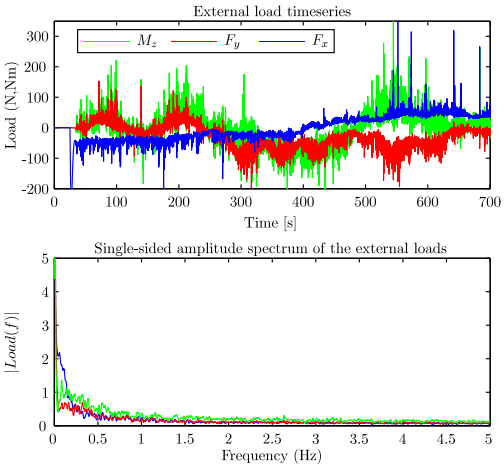

Figure 9: The time-varying nature and frequency spectrum of the external loads of the NIT. The spectrum is low-pass filtered using a moving average filter to show trends.

precision and validity, the applicability depends on the objective of the experiment. For instance, if the precision of the loads is critical, such as for tuning, then the range of applicable ice conditions are lower than for proof-of-concept simulations where the objective may be investigating stability and parameter sensitivity.

3 DP Control System Design

In this section a control design model is derived and used to synthesize a DP control system for managed ice. Both the model and control system consider the planar motion of the vessel; surge, sway, and yaw. Further, it is assumed that the velocity range of DP is sufficiently low such that phenomena such as centripetal forces and Coriolis effects can be neglected.

3.1 Ice Loads and the Control Plant Model

To design a model-based control law a control design model description of (1)-(2) is needed. For open water this is established and several model exist (see (Fossen, 2011)). In this study the following model is chosen as a starting point,

$$\dot{\boldsymbol{\xi}} = \mathbf{A}_w \boldsymbol{\xi} + \mathbf{E}_w \mathbf{w}_w \tag{9}$$

$$\dot{\boldsymbol{\eta}} = \mathbf{R}(\psi)\boldsymbol{\nu} \tag{10}$$

$$\dot{\mathbf{b}}_o = \mathbf{w}_o \tag{11}$$

$$\mathbf{M}\dot{\boldsymbol{\nu}} = \boldsymbol{\tau} - \mathbf{D}\boldsymbol{\nu} + \mathbf{R}(\psi)^\top \mathbf{b}_o + \boldsymbol{\tau}_{wind} + \boldsymbol{\tau}_{ice} + \mathbf{w}_v \tag{12}$$

where $\boldsymbol{\xi} \in \mathbb{R}^6$ is a first order wave response state, $\mathbf{A}_w \in \mathbb{R}^{6\times 6}$ and $\mathbf{E}_w \in \mathbb{R}^{6\times 3}$, are constant matrices describing the sea state, and $\mathbf{M} := \mathbf{M}_{RB} + \mathbf{M}_a$ where $\mathbf{M}_a$ is the added mass from accelerating the fluid around the ships hull. Notice that the rotation matrix in (10) only depends on the heading ψ. This comes fo the assumption that roll and pitch angles of the vessel are small. The bias term $\mathbf{b}_o \in \mathbb{R}^3$ is a non-physical quantity that incorporates several effects such as ocean current loads, modeling errors, unmodeled dynamics, and wave drift. The variables $\mathbf{w}_i$ $(i = w, o, v)$ are zero-mean Gaussian noise vectors representing model uncertainty and measurement noise. $\boldsymbol{\tau} \in \mathbb{R}^3$ is the control input, and $\boldsymbol{\tau}_{wind} \in \mathbb{R}^3$ is the wind loads (assumed measured). See Fossen (2011) for further information.

Figure 9 shows the external loads (hydrodynamics and ice) from one closed-loop simulation. The frequency analysis shows that the loads appear in the low end of the spectrum. This complies well with the findings in (Kjerstad et al., 2014), and imply that integral control may be sufficient to deal with the disturbances.

Although it has been found that the mean ice loads on a stationkeeping vessel depend on the oblique angle, ice concentration, ice properties, floe size distribution, and ice thickness, no applicable dynamic model describing the time variations exists (Eik, 2010; Kjerstad et al., 2014). There are several reasons for this. Mainly, the signals have high variance and rapid transients (as seen in Figure 9) that are not described well by neither the given ice parameters nor the vessel states. This stems from the fact that the in-situ configuration, dynamics, and boundary conditions of the ice floe contact networks heavily impact the load. Nevertheless, the load may be divided into the following components,

$$\boldsymbol{\tau}_{ice} = \boldsymbol{\tau}_i + \boldsymbol{\tau}_f + \boldsymbol{\tau}_p, \tag{13}$$

where $\boldsymbol{\tau}_i$ are inertial load components that originate from the added ice mass which the vessel must actuate and the de-acceleration of incoming ice floes, $\boldsymbol{\tau}_f$ is additional friction originating from hydrodynamic phenomena on the ice floes, vessel-ice friction, and ice-ice friction. $\boldsymbol{\tau}_p$ is loads from large scale ice cover pressure.

Although (13) is rooted in highly complex and multibody nature it seems reasonable to assume that the ice induces both added inertia and friction to the dynamic system. Thus, a mass-damper model can be argued

$$\boldsymbol{\tau}_{ice} = -\mathbf{M}_{ice}\dot{\boldsymbol{\nu}} + \mathbf{d}_{ice}(\boldsymbol{\nu}) + \mathbf{R}^\top \mathbf{b}_{ice} + \mathbf{w}_{ice} \tag{14}$$

$$\dot{\mathbf{b}}_{ice} = \mathbf{w}_b, \tag{15}$$

where $\mathbf{M}_{ice} \in \mathbb{R}^{3\times 3}_{\geq 0}$ is added ice mass and $\mathbf{d}_{ice}(\boldsymbol{\nu}) \in \mathbb{R}^3$ is a damping function describing the ice condition, $\mathbf{b}_{ice}$ is a Wiener process, and $\mathbf{w}_b$ and $\mathbf{w}_{ice}$ are zero-

mean Gaussian noise vectors. A major downside of this model is the fact that $\mathbf{M}_{ice}$ and $\mathbf{d}_{ice}(\boldsymbol{\nu})$ are highly dependent on the in-situ ice floe contact networks, accumulated ice mass, and boundary conditions which requires them to be determined on-line if to be used in control. This adds complexity to system in the form of additional integrators. However, if a high quality ice load measurement is available this approach may be feasible, as seen in (Østhus, 2014). If no such signal is available, and alternative is to linearize $\mathbf{d}_{ice}(\boldsymbol{\nu}) \approx \mathbf{D}_{ice}\boldsymbol{\nu}$ and use fixed $\mathbf{M}_{ice}$ and $\mathbf{D}_{ice}$ matrices. However, practice has shown that estimating these matrices off-line is challenging and no significant improvement in tracking capabilities is gained with respect to incorporating all ice loads in one bias estimate such as,

$$\boldsymbol{\tau}_{ice} = \mathbf{R}(\psi)^\top \mathbf{b}_{ice} + \mathbf{w}_{ice} \tag{16}$$

$$\dot{\mathbf{b}}_{ice} = \mathbf{w}_b. \tag{17}$$

Therefore, (16)-(17) is selected as the design model in the remainder of this study.

Another aspect of the ice environment is the exponential attenuation of high frequency oscillatory wave loads (Broström and Christensen, 2008). This allows for removing the wave model (9). For the subsequent control design this will be beneficial as it reduces the number states and model uncertainty. Hence, the following adaptation of (9)-(12) can be applied as a control plant model for managed ice,

$$\dot{\boldsymbol{\eta}} = \mathbf{R}(\psi)\boldsymbol{\nu} \tag{18}$$

$$\dot{\mathbf{b}} = \mathbf{w}_1 \tag{19}$$

$$\mathbf{M}\dot{\boldsymbol{\nu}} = -\mathbf{D}\boldsymbol{\nu} + \boldsymbol{\tau} + \boldsymbol{\tau}_{wind} + \mathbf{R}(\psi)^\top \mathbf{b} + \mathbf{w}_2 \tag{20}$$

where $\mathbf{b} = \mathbf{b}_o + \mathbf{b}_{ice}$. For simplicity this model can be written in compact for as

$$\dot{\mathbf{x}} = \mathbf{A}(\psi)\mathbf{x} + \mathbf{B}\boldsymbol{\zeta} + \mathbf{E}\mathbf{w} \tag{21}$$

where $\mathbf{x} = \begin{bmatrix}\boldsymbol{\eta} & \boldsymbol{\nu} & \mathbf{b}\end{bmatrix}^\top \in \mathbb{R}^9$ is the state vector and $\boldsymbol{\zeta} = \begin{bmatrix}\boldsymbol{\tau} & \boldsymbol{\tau}_{wind}\end{bmatrix}^\top \in \mathbb{R}^{3\times 2}$ is a input vector. $\mathbf{A}(\psi) \in \mathbb{R}^{9\times 9}$, $\mathbf{B} \in \mathbb{R}^{3\times 2}$, and $\mathbf{E} \in \mathbb{R}^{9\times 3}$ are matrices describing the system according to (18)-(20).

3.2 Control Design

For the control design we apply the conventional DP approach found in for instance (Fossen, 2011) and (Sørensen, 2012), where the main goal is to develop a control law that can be used to investigate and pinpoint elements that need further development. To achieve this, two sensor suites are considered:

1. Position and heading measurements only.
2. Position, heading, linear velocity, and angular rate measurements.

In conventional DP control systems the linear velocity measurement is not commonly considered. These signals are here assumed available through technologies such as GNSS Doppler systems and inertially aided hydroacustic positioning systems. However, it is still considered necessary to employ a controller-observer structure where the observer will provide sensor fusion, filter measurements, estimate the bias state, and provide dead-reckoning in the case of measurement loss. Thus, we consider the following components:

- Observer
- Control law and reference system
- Control allocation

3.2.1 Observer

Traditionally, either a Kalman filter or a nonlinear passive DP observer (Fossen, 2011) is used. As the tuning parameters of the latter are more intuitively connected to the physics of the system (Sørensen, 2012) this approach is selected. Copying (18)-(20) and introducing an injection term gives,

$$\dot{\hat{\mathbf{x}}} = \mathbf{A}(\psi)\hat{\mathbf{x}} + \mathbf{B}\boldsymbol{\xi} + \mathbf{L}(\psi)(\mathbf{y} - \mathbf{C}\hat{\mathbf{x}}), \tag{22}$$

where $\mathbf{L}(\psi) \in \mathbb{R}^{9\times n}$ is a nonlinear injection gain matrix, and n is either 3 or 6 depending on the sensor suite. For the second sensor suite, $\mathbf{L}(\psi)$ is proposed as

$$\mathbf{L}(\psi) = \begin{bmatrix} \mathbf{K}_1 & \mathbf{K}_4\mathbf{R}(\psi) \\ \mathbf{K}_2\mathbf{R}(\psi)^\top & \mathbf{K}_5 \\ \mathbf{K}_3 & \mathbf{K}_6\mathbf{R}(\psi) \end{bmatrix}. \tag{23}$$

UGAS stability of the proposed observer is established using the Lyapunov function candidate $V = \mathbf{x}^\top\mathbf{P}\mathbf{x}$, where $\mathbf{P} = \mathbf{P}^\top > 0$. For the first sensor suite, $\mathbf{L}(\psi)$ becomes the first column of (23), and becomes identical to the nonlinear passive DP observer. UGAS is ensured by Theorem 11.2 in (Fossen, 2011).

Both Kerkeni et al. (2013) and Jenssen et al. (2009) report deficient performance of open water observers in managed ice experiments. Judging the proposed observers it is clear that the only option to improve the tracking performance is to apply more aggressive tuning than what is common in open water. Especially for the bias estimate. However, this approach is constrained by the the quality of the measurements. If high injection gains are used with noisy measurements the estimation performance may deteriorate.

3.2.2 Control Law and Reference Model

The control law determines the 3 DOF generalized forces and moment that is required for fulfilling the control objectives (tracking a fixed location or a predefined path). Traditionally, the structure of the control law is a nonlinear PID with anti-windup of the integral action (Sørensen, 2012). In this study the windup routines are disregarded for simplicity, and the control structure is chosen as

$$\boldsymbol{\tau} = \boldsymbol{\tau}_{FF} + \boldsymbol{\tau}_{FB}, \tag{24}$$

where $\boldsymbol{\tau}_{FF}$ are feedforward terms and $\boldsymbol{\tau}_{FB}$ are feedback terms. These are assigned as

$$\boldsymbol{\tau}_{FF} = \mathbf{M}\dot{\boldsymbol{\nu}}_d - \boldsymbol{\tau}_{wind} \tag{25}$$

$$\boldsymbol{\tau}_{FB} = -\mathbf{K}_p\mathbf{R}(\psi)^\top\tilde{\boldsymbol{\eta}} - \mathbf{K}_d\tilde{\boldsymbol{\nu}} - \mathbf{K}_i\mathbf{R}(\psi)^\top\int_0^t \tilde{\boldsymbol{\eta}}dt \tag{26}$$

where $\tilde{\boldsymbol{\eta}} := \hat{\boldsymbol{\eta}} - \boldsymbol{\eta}_d$ is the position error, $\tilde{\boldsymbol{\nu}} := \hat{\boldsymbol{\nu}} - \boldsymbol{\nu}_d$ is the velocity error, and $\mathbf{M}\dot{\boldsymbol{\nu}}_d$ constitutes a desired motion feedforward. $\boldsymbol{\eta}_d$, $\boldsymbol{\nu}_d$, and $\dot{\boldsymbol{\nu}}_d$ are determined using a third order reference filter for the setpoint.

3.2.3 Control Allocation

DP vessels are usually over-actuated which means that the vessel has more actuators than degrees of freedom. This requires a control allocation algorithm to determine the output each actuator such that the generalized control vector $\boldsymbol{\tau}$ is produced. The following linear mapping is applied

$$\boldsymbol{\tau} = \mathbf{T}\mathbf{u} \tag{27}$$

where $\mathbf{u} \in \mathbb{R}^n$ is a vector of thrust forces and $\mathbf{T} \in \mathbb{R}^{3\times n}$ it the thruster configuration matrix, where n is the number of thrust components. Here, the allocation algorithm found in (Skjetne and Kjerstad, 2013) is used.

4 Simulation Case Study

In this case study, DP subject to managed ice drift reversals in medium and high ice concentration is investigated. This is done to shed light on the proposed control system's performance and understand the relation to the severity of the ice condition.

4.1 The Arctic Drillship

The vessel applied is the conceptual ADS seen in Figure 2. This is optimized for operations in ice and experimentally tested in the DYPIC project. The vessel has three azimuth thrusters in the bow and three in the stern, making it suitable for DP. Its main particulars and specific azimuth thruster arrangement are found in tables 4 and 5. Further description of the ADS is found in (Gürtner et al., 2012; Hals and Jenssen, 2012; Metrikin et al., 2013; Kjerstad et al., 2014).

Table 4: ADS main particulars and illustration of the thruster arrangement.

Parameter	Model scale
Length in design waterline (m)	6.67
Length between perpendiculars (m)	6.13
Breath, modeled (m)	1.37
Draught at design waterline (m)	0.4
Stem angle at design waterline (°)	45
Frame angle at midship (°)	45
Displacement volume (m^3)	2535
Center of gravity from aft. perp. (m)	3.18
Block coefficient	0.75
Metacentric height (m)	0.357
Total thrust (N)	201

Table 5: The ADS azimuth thruster arrangement.

No.	Comment	x [mm]	y [mm]	F [N]
1	Port-Bow	2272	316	22
2	Center-Bow	2644	0	22
3	Stb-Bow	2272	-316	22
4	Center-Stern	-3102	0	45
5	Port-Stern	-2664	190	45
6	Stb-Stern	-2664	-190	45

The proposed control design of Section 3 require the matrices $\mathbf{M}$ and $\mathbf{D}$ to be determined. Here, the rigid body matrix is applied as the system inertia matrix $\mathbf{M}$. This follows directly from the vessel's dry mass and is

$$\mathbf{M} = \mathrm{diag}\left(\begin{bmatrix}2535 & 2535 & 8485\end{bmatrix}\right). \tag{28}$$

Commonly in DP control design, the applied system inertia matrix is a summation of the dry mass and an approximation of the added mass gained from accelerating fluid around the hull. However, since the added mass effects are not incorporated in the NIT it is not considered in this study.

$\mathbf{D}$ were approximated experimentally in the NIT by running the vessel to steady state in open water using constant input. This resulted in

$$\mathbf{D} = \mathrm{diag}\left(\begin{bmatrix}75 & 100 & 3205\end{bmatrix}\right). \tag{29}$$

4.2 Experiment Setup

The two cases considered were:

Table 6: State estimator and control law gains.

Gain	Surge	Sway	Yaw
K_1	4	4	4
K_2	1000	1500	5000
K_3	30	60	500
K_4	1	1	1
K_5	1000	1500	5000
K_6	400	750	4000
K_p	200	200	400
K_d	1000	1000	3000
K_i	6	6	14

- Case 1: Elliptic drift reversal in 55% managed ice.
- Case 2: Elliptic drift reversal in 80% managed ice.

In both cases the ice strength properties and floe size distribution were set to replicate experiment 4100 (see Table 3) in a 75x18x2.5 m basin. The ice drift ellipse parameters in (7) were set to $a = 45$ and $b = 4.5$ with a maximum ice drift of 0.2 m/s. Gaussian white noise with standard deviations of 0.01 m (and m/s) were used for the position and linear velocity measurements. The standard deviation for the heading and angular rate measurements were 0.1 deg (and deg/s). The control system gains seen in Table 6 were obtained by trial and error in order to achieve a feasible trade-off between noise filtering, state tracking, setpoint tracking, and thruster usage. The closed-loop bandwidth was found to be $f_b = \begin{bmatrix}1.83 & 1.83 & 1.45\end{bmatrix}\ Hz$. With respect to Figure 9 this is well above the main frequency range of the external loads.

Three simulations were performed based in the two sensor suites described above: Case 1 with sensor suite 1, case 2 with sensor suite 1, and case 2 with sensor suite 2. All were performed with identical initial conditions, where the control objective is to track {n} keeping the heading constant at $\psi = 0$. Effectively this means tracking a fixed location. The positioning frame was initialized at $\boldsymbol{\eta}_0 = \begin{bmatrix}10.5 & -4.5 & 0\end{bmatrix}^\top$ in {t}. Wind loads were not included in the simulations. To quantify the performance of the observers, the following cost function is applied

$$Q(t) = \int_0^t \tilde{\mathbf{x}}^\top \mathbf{W} \tilde{\mathbf{x}}, \tag{30}$$

where $\tilde{\mathbf{x}} \in \mathbb{R}^9$ is the observer error state, and $\mathbf{W} \in \mathbb{R}^{9\times 9}$ is a static diagonal positive definite normalization matrix. (30) gives the cumulative error of the state estimates as a function of time, where low value indicates high precision.

4.3 Results and Discussion

Figure 10 shows the simulation results where it can be seen that the positioning and heading keeping capabilities in 55% ice concentration is fair. One important reason for this is that the vessel deflects and pushes incoming ice floes away and no severe ice floe contact networks nor ice mass accumulation forms. Thus, the load variations are contained to minor perturbations which are well tracked and counteracted. In 80% ice concentration these phenomena are more evident causing a severe load regime. This is indirectly shown by the control input norms for case 2, and causes performance deterioration of the suite 1 control system. The main reason for this is the fact that the point of attack and magnitude of the ice loads are constantly changing. This creates a continous change of the vessel momentum which must be sensed though the double time integrals of the force (position and heading measurements). As the momentum is already gained when it materialized in the measurements it causes a sustained transient deviation in the observer (for all states). In turn it causes inaccurate thruster output calculation and results in poor positioning. Therefore, it makes sense to incorporate velocity and angular rate measures as these capture the momentum earlier. This is verified by the case 2: suite 2 results. With the NIT capabilities in mind, it may be that the ice loads are underpredicted causing a somewhat optimistic positioning performance for both runs of case 2. Nevertheless, the ice concentration dependency complies well with reports of open-water DP systems, which work in light conditions, but struggles as the ice condition toughens (see (Keinonen et al., 2006) and (Rohlén, 2009)). It should also be noted that the conditions toughens as the oblique angle increases. This is seen in the tank frame position plot of Figure 10.

The heading tracking of the vessel does not show the same degree of improvement as the positioning in case 2: suite 2. A combination of sub-optimal control law (both in its structure and tuning) and the brute force operation strategy, resulting in sustained high oblique angle for most of the simulation, is believed to be the main reasons for this. In general, if allowed by the operation, the DP vessel should act to prevent the oblique angle from becoming high.

In sum this study indicates that classical DP control architecture with the proposed modifications is feasible for conditions without high ice concentration. It is also believed to extend the operational window with respect to conventional open-water systems. This is achieved mainly through removing the wave filter from the observer, re-tuning it and the control law more aggressively, and when available adopting velocity and angular rate measurements. Still, it is uncertain whether

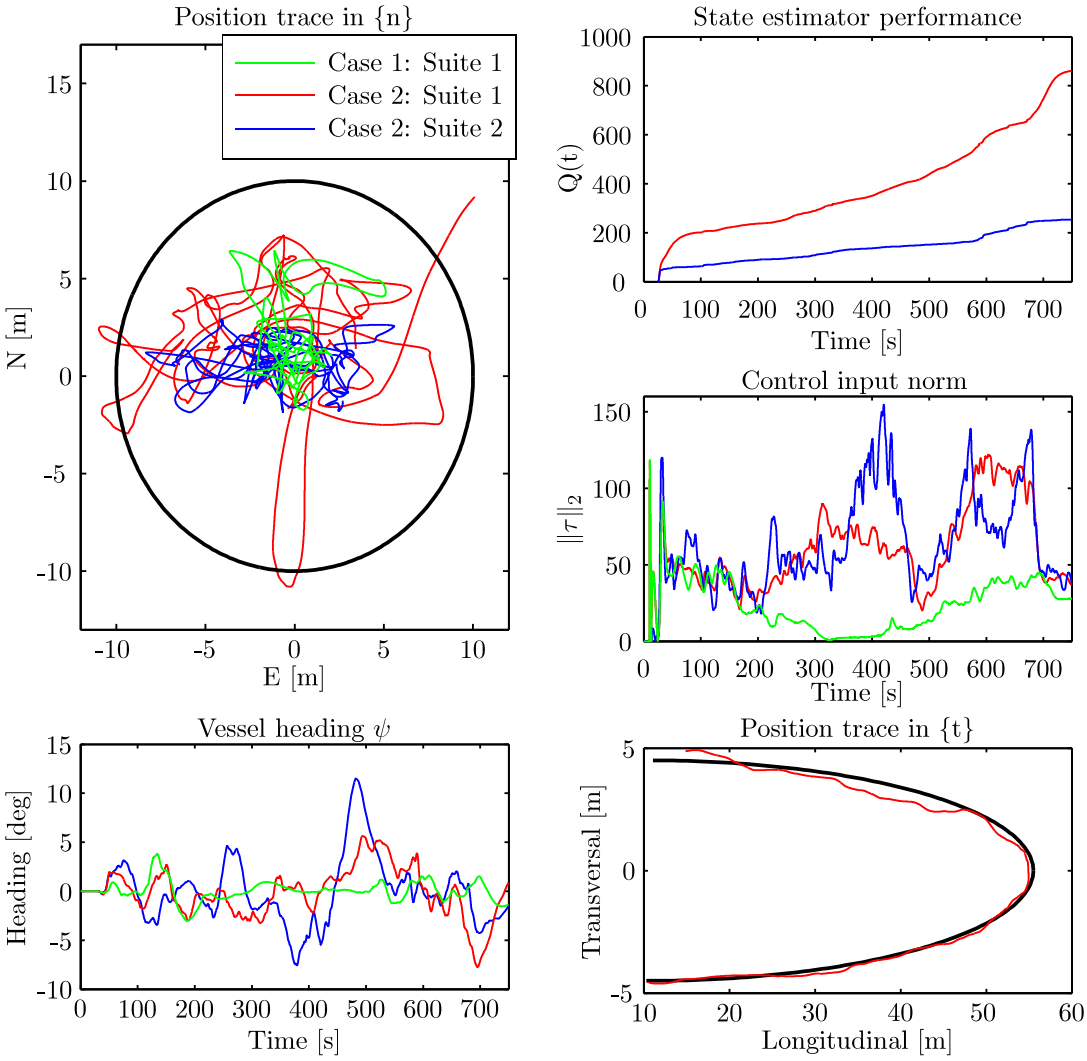

Figure 10: A comparison of the two control systems setups. The positioning frame trace plot is scaled to full scale using $\lambda = 30$. The observer performance plot shows the performance measure for case 2: suite 1, where the suite 2 observer was run in parallel. The initial position of the vessel in {t} was $x = 10.5$ m and $y = -4.5$ m.

this provides sufficient reactivity to handle high ice concentrations, ice pressure, and large or abnormal ice features slipping through the IM. Thus, it may be required to improve the reactivity of the system further and implement proactive ice handling measures to take on such conditions. Kjerstad et al. (2014) provides an overview of some possible improvements.

5 Summary and Conclusions

This paper have described and motivated the use of a given numerical tool as a process model for developing DP control systems. Its precision exceeds that of a comparable empirical model, but some underprediction is seemingly occurring at high ice concentrations and oblique angles. The strength of the model, in DP development context, is its ability to capture the time-varying variation in the loads from processes in the ice cover. This is considered key for testing control systems.

A development framework closing the loop of the numerical model was presented. This incorporates important components such as sensors characteristics, actuator dynamics, and ice drift. For the latter, an elliptic trajectory was chosen to model both the temporal and spatial dynamics.

Ice-adapted control algorithms were proposed based on a control design model. The ice dynamics were included in the observer bias estimate, and handled using a conventional nonlinear PID control law as no ice specific parameter nor vessel state were considered to describe the load variations. In summary, what separates the proposed enhancements from conventional open-water systems is the removal of the wave filter, and aggressive system tuning. The control system was tested using the developed simulation platform where it showed an ice concentration dependency on the positioning capability. Incorporating additional vessel velocity and angular rate measurements aided this to some extent.

Acknowledgments

Research partly funded by the Research Council of Norway (RCN) KMB project no. 199567: "Arctic DP", with partners Kongsberg Maritime, Statoil, and DNV GL, and partly by RCN project no. 203471: CRI SAMCoT. Additionally, the authors would like to thank Nils Albert Jenssen and Lars Imsland for constructive feedback, and Ivan Metrikin for providing the numerical model, technical support, and constructive feedback.

References

Broström, G. and Christensen, K. Waves in sea ice. Technical report, Norwegian Meteorological Institute, Norway, 2008.

Eik, K. J. *Ice Management in Arctic Offshore Operations and Field Developments*. Ph.D. thesis, NTNU, Norway, 2010.

Fossen, T. I. *Handbook of Marine Craft Hydrodynamics and Motion Control*. Wiley, 2011. doi:10.1002/9781119994138.

Gautier, D. L., Bird, K. J., Charpentier, R. R., Grantz, A., Houseknecht, D. W., Klett, T. R., Moore, T. E., Pitman, J. K., Schenk, C. J., Schuenemeyer, J. H., Sørensen, K., Tennyson, M. E., Valin, Z. C., and Wandrey, C. J. Assessment of Undiscovered Oil and Gas in the Arctic. *Science*, 2009. 324(5931):1175–1179. doi:10.1126/science.1169467.

Gürtner, A., Baardson, B. H. H., Kaasa, G.-O., and Lundin, E. Aspects of importance related to Arctic DP operations. In *Proc. 31th Int. Conf. on Ocean, Offshore and Arctic Engineering (OMAE)*. 2012. doi:10.1115/OMAE2012-84226.

Haase, A. and Jochmann, P. Different ways of modeling ice drift scenarios in basin tests. In *Proc. 32th Int. Conf. on Ocean, Offshore and Arctic Engineering (OMAE)*. 2013. doi:10.1115/OMAE2013-10793.

Hals, T. and Efraimsson, F. DP Ice Model Test of Arctic Drillship. In *Proc. of the Dynamic Positioning Conference*. 2011.

Hals, T. and Jenssen, N. A. DP ice model tests of Arctic drillship and polar research vessel. In *Proc. 31th Int. Conf. on Ocean, Offshore and Arctic Engineering*. 2012. doi:10.1115/OMAE2012-83352.

Hamilton, J. M. The Challenges of Deep-Water Arctic Development. *Int. Journal of Offshore and Polar Engineering*, 2011. 21(4):241–247.

International Maritime Organization (IMO). *Guidelines for Vessels with Dynamic Positioning Systems*. 1994. MSC/circ.645.

Jenssen, N. A., Hals, T., Haase, A., Santo, X., Kerkeni, S., Doucy, O., Gürtner, A., Hetschel, S. S., Moslet, P. O., Metrikin, I., and Løset, S. A Multi-National R&D Project on DP Technology in Ice. In *Proc. of the Dynamic Positioning Conference*. 2012.

Jenssen, N. A., Muddesitti, S., Phillips, D., and Backstrom, K. DP In Ice Conditions. In *Proc. of the Dynamic Positioning Conference*. 2009.

Keinonen, A. and Martin, E. H. Modern day pioneering and its safety in the floating ice offshore. In *Proc. 10th Int. Conf. and Exhibition on Performance of Ships and Structures in Ice (ICETECH)*, volume 1. 2012.

Keinonen, A., Shirley, M., Liljeström, G., and Pilkington, R. Transit and Stationary Coring Operations in the Central Polar Pack. In *Proc. 7th Int. Conf. and Exhibition on Performance of Ships and Structures in Ice (ICETECH)*. 2006.

Keinonen, A., Wells, H., Dunderdale, P., Pilkington, R., Miller, G., and Brovin, A. Dynamic positioning operation in ice, offshore Sakhalin, May–June 1999. In *Proc. of the 10th Int. Offshore and Polar Engineering Conf. (ISOPE)*. 2000.

Kerkeni, S., Dal Santo, X., and Metrikin, I. Dynamic Positioning in Ice - Comparison of Control Laws in Open Water and Ice. In *Proc. 32th Int. Conf. on Ocean, Offshore and Arctic Engineering (OMAE)*. 2013. doi:10.1115/OMAE2013-10918.

Kerkeni, S., dal Santo, X., Doucy, O., Jochmann, P., Haase, A., Metrikin, I., Løset, S., Jenssen, N. A., Hals, T., Gürtner, A., Moslet, P. O., and Støle Hetschel, S. DYPIC project: Technological and scientific progress opening new perspectives. In *Proc. of the Arctic Technology Conference (ATC)*. 2014.

Kjerstad, Ø., Metrikin, I., Løset, S., and Skjetne, R. Experimental and phenomenological investigation of dynamic positioning in managed ice. *Cold Regions Science and Technology*, 2014.

Liferov, P. Station-keeping in ice - normative requirements and informative solutions. In *Proc. Arctic Technology Conference (ATC)*. 2014.

Lubbad, R. and Løset, S. A numerical model for real-time simulation of ship-ice interaction. *Cold Regions Science and Technology*, 2011. 65(2):111 – 127.

Metrikin, I. A Software Framework for Simulating Stationkeeping of a Vessel in Discontinuous Ice. *Modeling, Identification and Control*, 2014. 35(4):211–246. doi:10.4173/mic.2014.4.2.

Metrikin, I., Borzov, A., Lubbad, R., and Løset, S. Numerical Simulation of a Floater in a Broken-Ice Field - Part II: Comparative Study of Physics Engines. In *Proc. 31th Int. Conf. on Ocean, Offshore and Arctic Engineering (OMAE)*. 2012a. doi:10.1115/OMAE2012-83430.

Metrikin, I., Løset, S., Jenssen, N. A., and Kerkeni, S. Numerical Simulation of Dynamic Positioning in Ice. *Marine Technology Society Journal*, 2013. 47(2):14–30. doi:10.4031/MTSJ.47.2.2.

Metrikin, I., Lu, W., Løset, S., and Kashafutdinov, M. Numerical Simulation of a Floater in a Broken-Ice Field - Part I: Model Description. In *Proc. 31th Int. Conf. on Ocean, Offshore and Arctic Engineering (OMAE)*. 2012b. doi:10.1115/OMAE2012-83938.

Moran, K., Backman, J., and Farrell, J. W. Deepwater drilling in the Arctic Ocean's permanent sea ice. In *Proc. of the Integrated Ocean Drilling Program (IODP)*. 2006.

Østhus, V. *Robust Adaptive Control of a Surface Vessel in Managed Ice Using Hybrid Position and Force Control*. Master's thesis, NTNU, Norway, 2014.

Rohlén, Å. Relationship Between Ice-Management and Station Keeping in Ice. Presentation at Dynamics Positioning Conference, 2009.

Skjetne, R. and Kjerstad, Ø. Recursive nullspace-based control allocation with strict prioritization for marine craft. In *Proc. of 9th IFAC Conf. on Control Applications in Marine Systems*. 2013. doi:10.3182/20130918-4-JP-3022.00052.

Sørensen, A. J. *Marine Control Systems: Propulsion and Motion Control of Ships and Ocean Structures*. Department of Marine Technology, NTNU, Norway, 2012.

Sørensen, A. J., Sagatun, S. I., and Fossen, T. I. Design of a dynamic positioning system using model-based control. *Control Engineering Practice*, 1996. 4(3):359 – 368. doi:10.1016/0967-0661(96)00013-5.

The Society of Naval Architects Marine Engineers. Nomenclature for treating the motion of a submerged body through a fluid. Technical report, 1950. Technical and Research Bulletin, 1-5.

Woolgar, R. C. and Colbourne, D. B. Effects of hull-ice friction coefficient on predictions of pack ice forces for moored offshore vessels. *Ocean Engineering*, 2010. 37:296 – 303. doi:10.1016/j.oceaneng.2009.10.003.

A Resetting Control Design for Dynamic Positioning of Marine Vessels Subject to Severe Disturbances

A Resetting Control Design for Dynamic Positioning of Marine Vessels Subject to Severe Disturbances

Øivind Kåre Kjerstad and Roger Skjetne

***Abstract*—This paper presents a resetting control design for dynamic positioning of marine vessels which applies a state-of-the-art continuous algorithm as a design basis. It is motivated by the fact that conventional designs can experience reduced transient performance when subject to unmodeled and unmeasured changes in the environment. The design employs a control law and an observer in a separation principle, and it combines continuous-time and discrete-time state descriptions to allow the state estimate of the observer to make a favorable jump when the measured estimation error violates a threshold. This instantaneously improves the state estimation error without compromising the continuous observer properties, resulting in an instantaneous improvement of the feedback control precision. Simulations and model scale experiments validating the design and improved performance, are presented.**

***Index Terms*—Dynamic positioning; Nonlinear systems; Hybrid systems; State observer**

I. Introduction

Dynamic positioning (DP) of a marine vessel is defined as keeping location (either a fixed position and heading or low-speed tracking) exclusively by means of onboard thrusters [1]. State-of-the-art marine control systems employ the structure of Fig.1 and are designed using continuous model-based control methods relying on measurements of position, heading, and sometimes angular velocity [2], [3]. A separation principle using an observer together with a control law is employed to remove unwanted wave-frequency (WF) motion captured in the measurements and estimate the low frequency (LF) position and velocity for application in the control law. Fig.2 defines the WF and LF components of the total motion. It is important to remove the WF component, because if it enters the feedback loop it will modulate the propulsion commands and cause inefficient use of and unwanted wear-and-tear on the actuation system.

In general, marine motion control systems have good track records and are proven stable and robust in a wide range of sea states (see [2] and [3]). Yet, their ability to handle unmodeled dynamics and environmental disturbances is typically limited to integral action (in both observer and control law). To avoid instabilities the update process must be done relatively slow.

Ø. K. Kjerstad is affiliated with the Department of Marine Technology, the Department of Civil and Transport Engineering, and the Arctic Technology Department. The two former are at the Norwegian University of Science and Technology (NTNU), Trondheim, Norway, and the latter is at the The University Centre in Svalbard, Longyearbyen, Norway. R. Skjetne is with the Department of Marine Technology at NTNU. E-mails: oivind.k.kjerstad@ntnu.no, roger.skjetne@ntnu.no.

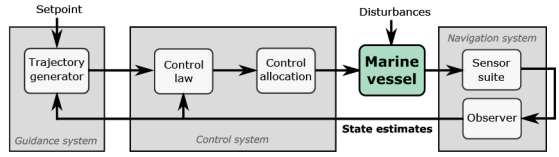

Fig. 1. Signal flow in guidance, navigation, and control of marine vessels. Adapted from [2].

The trade-off is degraded transient performance during integral action convergence [4], [5]. In many cases this degraded performance is unacceptable. Providing the control system with more information about the environment, either in the form of measurements or through more precise dynamical models is the conventional approach to reduce the problem. Examples include wind measurements to handle wind gusts and mooring models to handle mooring loads. As a further optimization it can be beneficial to construct a bank of dynamic models for the observers and control laws with different parameters and continuously choose the one that fits the measurements best. For DP, the latter is known as hybrid control through a supervisory switching mechanism [3], [6]. Common to these methods are that all require the environment to be measured and/or characterized with some uncertainty. Thus, they fall short when the vessel is influenced by substantial, complex, and abrupt phenomena that are hard to model and measure. Examples of such are wave trains, ship-ice interaction effects, ship-to-ship interaction effects, current surges, and effects from operations with heavy equipment in the sea or at the sea floor such as towing, anchor handling, and sub-sea construction.

In this paper we focus on the control law and observer of Fig.1, and propose to improve positioning performance of a state-of-the-art control design subject to harsh environment through a resetting mechanism in the observer. The state estimation is fundamental to both accurate positioning and trajectory generation, and these will suffer if the state estimates deviate. The reset is triggered when the observed estimation error reaches a threshold (indirectly indicating substantial disturbances are present). Then, the state estimates jump closer to their true value independent of time. This will also instantaneously improve the precision of the control law output. The implication of improving the state tracking is enhanced positioning precision under severe perturbations potentially extending the operational window of the vessel. As

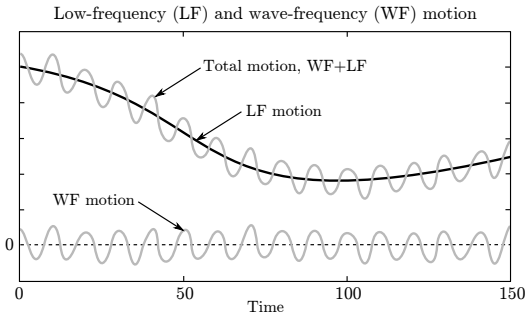

Fig. 2. The total motion of a ship is modeled as a LF response with the WF response added as an output disturbance. Adapted from [3].

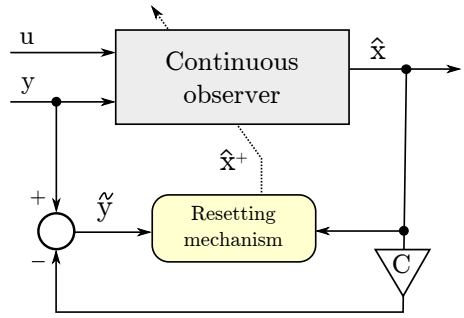

Fig. 3. The resetting observer concept. The resetting is only invoked when the observed estimation error is larger than a defined threshold.

the resetting control design is a mix of continuous and discrete state descriptions, it is regarded and analyzed as a hybrid dynamic system [7]. We develop and analyze the theory for realizing the aforementioned resetting mechanism for a state-of-the-art observer, and present experimental data to validate the resulting closed-loop response. Since the method is novel, a motivational example is presented to further illustrate the design concept.

Terminology and notation: In UGS, UGAS, UGpAS, UGES, etc., stands G for Global, S for Stable, U for Uniform, A for Asymptotic, E for Exponential, and p for pre. According to the hybrid framework of [7], the continuous system $\dot{x} = f(x)$ is called the *flow map*, and its domain is a *flow set*, $x \in \mathcal{C}$. The discrete jumps $x^+ = g(x)$ is called the *jump map*, and its domain is the *jump set*, $x^+ \in \mathcal{D}$.

A. Motivational example

Consider the scalar second order system for which an origin regulation controller is to be designed,

$$m\ddot{q} + a\dot{q} = u + b \tag{1a}$$
$$\dot{b} = d(t) \tag{1b}$$
$$y = q \tag{1c}$$

where q, $\dot{q}$, $\ddot{q} \in \mathbb{R}$ is the position, velocity, and acceleration, respectively, $m, a \in \mathbb{R}_{>0}$ are known system parameters, $d(t) \in \mathbb{R}$ is an unknown time-varying disturbance, and $y \in \mathbb{R}$ is the measured output. By $x := col(q, \dot{q}, b)$ the system can be written on state space form. In lack of a disturbance model, we replace (1b) with $\dot{b} = 0$ for the observer design model. Using this, a separation principle control law and observer can be designed as

$$u = -K\hat{x} \tag{2}$$
$$\dot{\hat{x}} = A\hat{x} + Bu + L(y - C\hat{x}) \tag{3}$$

where $\hat{x} := col(\hat{q}, \dot{\hat{q}}, \hat{b})$ is the estimate of x, $K := diag(k_p, k_d, 1) \in \mathbb{R}^{3\times3}_{>0}$ is a control gain matrix, $A \in \mathbb{R}^{3\times3}$, $B \in \mathbb{R}^3$, and $C \in \mathbb{R}^{1\times3}$ are the state space system matrices of (1), and $L \in \mathbb{R}^{3\times3}_{>0}$ is a Luenberger observer injection gain matrix. The observer error dynamics, derived from $\tilde{x} := x - \hat{x}$, can be written as

$$\dot{\tilde{x}} = (A - LC)\tilde{x} + \Lambda d(t), \tag{4}$$

where $\Lambda \in \mathbb{R}^{3\times1}$ is a matrix in accordance with (1).

From a resetting perspective it is reasonable to allow $\hat{x}$ to evolve according to (3) when the observed state estimation error $\tilde{y} := y - C\hat{x}$ is low, and reset and jump the states so that the error is reduced when it reaches a threshold, $|\tilde{y}| \geq \epsilon > 0$. We implement this as seen in Fig.3 with the following jump map,

$$\hat{x}^+ = \hat{x} + \gamma, \tag{5}$$

where $\hat{x}^+ \in \mathbb{R}^3$ is the state vector after the jump and $\gamma \in \mathbb{R}^3$ is the length of the jump. The key for improved performance (and stability) of the resetting, is to design γ ensuring that the error is reduced, i.e.

$$|x - \hat{x}^+| \leq |x - \hat{x}|. \tag{6}$$

By the derivation of γ in Section III, we propose

$$\gamma = (A - LC)^{-1}\Lambda(C(A - LC)^{-1}\Lambda)^{-1}\tilde{y}, \tag{7}$$

and note that (6) holds for any $\epsilon > 0$.

Fig.4 shows the results of two closed-loop simulations of (1) with and without resetting of the observer. The plant dynamics were implemented with $m = 10$, $a = 1$, and b as a recurring step disturbance with varying magnitude (changing at 5, 10, and 15 seconds). Both runs were performed with identical initial conditions and static K and L matrices designed using pole placement. For the resetting $\epsilon = 0.02$ was used. Fig.4 shows that the resetting controller reduces the errors in the state estimates with increased reactivity when the disturbance triggers resets of the observer (multiple occasions after 10 and 15 s). However, it is important to emphasize that the closed-loop velocity behavior cannot be directly compared as the trajectories differ. Nevertheless, the proposed extension improves performance while maintaining low gains without additional measurements or disturbance models. Combining low gains with high reactivity is often a desired property in control design. It should be noted that (7) affects and improves all states. This subsequently improves the precision of the regulation controller.

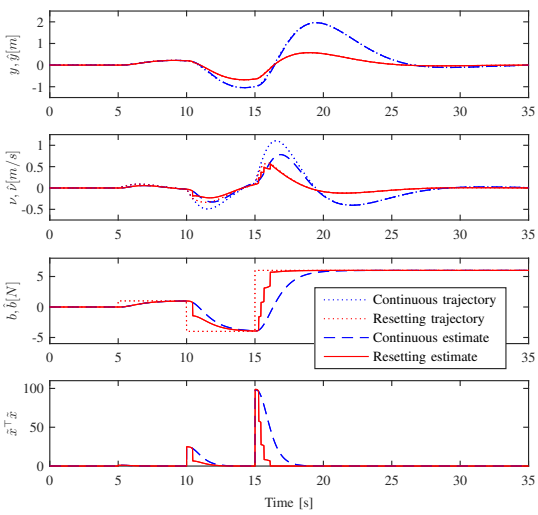

Fig. 4. The results of the simulation example, illustrating the effect of the resetting mechanism of the observer for equal gains. The top plot shows the actual and estimated position trajectory of the system, the two middle show the actual and estimated velocity and bias states, and the bottom plot shows the quadratic state estimate error for the individual simulations.

II. Problem Formulation

We consider the control plant model established as state-of-the-art for DP [2], [3],

$$\dot{\xi} = \Omega(\omega_0)\xi \tag{8a}$$
$$\dot{\eta} = R(\psi)\nu \tag{8b}$$
$$\dot{b} = -T^{-1}b + d(t) \tag{8c}$$
$$M\dot{\nu} + D\nu = \tau + R^\top(\psi)b \tag{8d}$$
$$y = \eta + C_w\xi \tag{8e}$$

where $\xi \in \mathbb{R}^6$ models the WF motion, $\Omega \in \mathbb{R}^{6\times 6}$ describes the sea-state, $\omega_0 \in \mathbb{R}$ is the wave peak frequency (assumed known), $\eta := \begin{bmatrix} N & E & \psi \end{bmatrix}^\top \in \mathbb{R}^3$ is the LF position and heading given in the North-East-Down (NED) frame, $R(\psi) \in \mathbb{R}^{3\times 3}$ is the rotation matrix between the NED and vessel's body fixed frame, $b \in \mathbb{R}^3$ is a bias state capturing external loads and unmodeled dynamics where $T \in \mathbb{R}^{3\times 3}$ is a diagonal time constant matrix, $d(t) \in \mathbb{R}^3$ is an unknown perturbation disturbance, $M \in \mathbb{R}^{3\times 3}_{>0}$ is the vessel inertia and added mass matrix, $\nu := \begin{bmatrix} u & v & r \end{bmatrix}^\top \in \mathbb{R}^3$ is the vessel's body fixed linear and angular velocity, $D \in \mathbb{R}^{3\times 3}_{\geq 0}$ is a linear damping matrix, $\tau \in \mathbb{R}^3$ is the control input, $y \in \mathbb{R}^3$ is the measurement of the total motion, and $C_\omega \in \mathbb{R}^{3\times 6}$ is a selection matrix. It is assumed that the solutions to (8) is forward complete, which is reasonable since in practice τ and $d(t)$ are bounded inputs.

To achieve DP we consider the following UGES state feedback control law proposed in [8],

$$\tau = -R(\psi)^\top K_p(\eta - \eta_d) - K_d\nu - R(\psi)^\top b \tag{9}$$

where $K_p, K_d \in \mathbb{R}^{3\times 3}$ are positive definite matrices, and $\eta_d \in \mathbb{R}^3$ is the setpoint position. As mentioned above, a observer is needed to obtain the signals needed to implement the control law. As in [8] we apply the following state-of-the-art experimentally verified nonlinear passive UGES state observer,

$$\dot{\hat{\xi}} = \Omega\hat{\xi} + K_1(\omega_o)\tilde{y} \tag{10a}$$
$$\dot{\hat{\eta}} = R(y_3(t))\hat{\nu} + K_2\tilde{y} \tag{10b}$$
$$\dot{\hat{b}} = -T^{-1}\hat{b} + K_3\tilde{y} \tag{10c}$$
$$M\dot{\hat{\nu}} + D\hat{\nu} = \tau + R^\top(y_3(t))\hat{b} + R^\top(y_3(t))K_4\tilde{y} \tag{10d}$$
$$\hat{y} = \hat{\eta} + C_\omega\hat{\xi} \tag{10e}$$

where $\hat{\xi}$, $\hat{\eta}$, $\hat{b}$, and $\hat{\nu}$ are the estimated states, K_{1-4} are positive definite fixed injection gain matrices, and the observed error $\tilde{y} := y - \hat{y}$. Notice that $y_3(t) = \psi(t)$ is directly applied in the rotation matrices as it is assumed to be known precisely (for instance by a gyrocompass). This is a common assumption in marine control design which will be exploited in the design of the resetting mechanism also (y_3 is the third element of y).

Since the control law and observer are designed separately, the separation principle must hold for overall stability to be ensured. In [8] the presented continuous control design is analyzed, and it is found that the estimation and control error dynamics can be tuned separately, and that the cascaded system is UGAS. For further details, see [2], [8], [9], and [3].

Conventionally, the observer is designed for conditions with high value elements in T and $d(t) = w$ in (8c), where $w \in \mathbb{R}^3$ is zero mean white noise. This describes a slowly-varying first order Markov process. Practice has shown that it performs well for slowly varying disturbance. However, if $d(t)$ is substantial with non-zero mean for an interval of time the observer will experience significant transient errors before it again converges (as the environment calms down and $d(t) \to 0$). It is important to note that the estimation error is bounded as the observer is UGES, and thereby input-to-state-stable (ISS). Since we assume that $d(t)$ is rooted in complex phenomena that are both difficult to measure and define characteristically (for control purposes), we propose to improve the transient performance by observer resetting similar to that of the introductory example. By jumping $\hat{\eta}$, $\hat{\nu}$, $\hat{b}$, and $\hat{\xi}$ closer to their correct values, an instantaneous improvement of the estimation error is gained. The objective of the paper is therefore to design and experimentally verify this with the flow map,

$$\dot{x} = f(x, d) \tag{11a}$$
$$\dot{\hat{x}} = f(\hat{x}, 0) + h(\hat{x}, y) \tag{11b}$$

where $x := col(\xi, \eta, b, \nu) \in \mathbb{R}^{15}$ is the actual state, $\hat{x} := col(\hat{\xi}, \hat{\eta}, \hat{b}, \hat{\nu}) \in \mathbb{R}^{15}$ is the state estimate, and $f \in \mathbb{R}^{15}$ and $h \in \mathbb{R}^{15}$ are given by (8) and (10), respectively. Resetting the observer, without changes in x, gives the jump maps,

$$x^+ = x, \tag{12a}$$
$$\hat{x}^+ = \hat{x} + \gamma, \tag{12b}$$

where $\gamma \in \mathbb{R}^{15}$ is a vector added to the state estimate vector when the measured error $\tilde{y}$ moves from the flow set $\mathcal{C}$ to the jump set $\mathcal{D}$. These sets are defined as,

$$\mathcal{C} = \{(x, \hat{x}) : |\tilde{y}_1| < \epsilon_1 \text{ and } |\tilde{y}_2| < \epsilon_2 \text{ and } |\tilde{y}_3| < \epsilon_3\} \quad (13a)$$
$$\mathcal{D} = \{(x, \hat{x}) : |\tilde{y}_1| \geq \epsilon_1 \text{ or } |\tilde{y}_2| \geq \epsilon_2 \text{ or } |\tilde{y}_3| \geq \epsilon_3\}, \quad (13b)$$

where $\epsilon_{1,2,3} > 0$ are individual thresholds defining the maximum allowed observed estimation errors for the different degrees of freedom. During jumps we will enforce,

$$|x - \hat{x}^+| \leq |x - \hat{x}|. \quad (14)$$

To analyze the properties of the resetting observer and the closed-loop, γ must be defined. This is done in Section III. Section IV presents a case study with simulations and experiments. Finally, Section V presents the conclusions.

III. Resetting control design

A. Observer resetting mechanism

To derive the jump map vector γ, we evaluate the observer error dynamics given by $\tilde{x} := x - \hat{x}$ as

$$\dot{\tilde{x}} = (A(t) - L(t)C)\tilde{x} + \Lambda d(t), \quad (15)$$

where $A(t)$, $L(t)$, C, and Λ follows directly from (8) since the system is forward complete. Although the error dynamics are nonlinear due to the rotation matrices, we exploit the fact that $A(t)$ and $L(t)$ do not change when the estimated states jump, as they are a function of the measurement y_3. Thus, in the jump instance, (15) can be treated as LTI,

$$\dot{\tilde{x}} = H_t\tilde{x} + \Lambda d(t), \quad (16)$$

where $H_t \in \mathbb{R}^{15\times 15}$ is a constant matrix given by the value of y_3 at the time t of the jump. A key aspect to be aware of is that (16) is only used to derive γ such that the state estimates jump closer to the correct values when $(x, \hat{x}) \in \mathcal{D}$. It is not used to evolve the continuous dynamics of the states. Since (15) have been shown to be UGES [2], H_t is Hurwitz for all values of y_3. The solution of (16) with respect to a time variable t' is,

$$\tilde{x}(t') = e^{H_t t'}\tilde{x}_0 + \int_0^{t'} e^{H_t(t'-\tau)}\Lambda d(\tau)d\tau. \quad (17)$$

By assuming that the norm of the initial error $|\tilde{x}_0|$ is dominated by $|\tilde{b}_0|$, and that the initial errors $\xi_0 - \hat{\xi}_0$, $\eta_0 - \hat{\eta}_0$, and $\nu_0 - \hat{\nu}_0$ can be neglected, the solution can be approximated as

$$\tilde{x}(t') \approx e^{H_t t'}\Lambda\tilde{b}_0 + \int_0^{t'} e^{H_t(t'-\tau)}\Lambda d(\tau)d\tau. \quad (18)$$

These assumptions are reasonable, as ξ and η are measured and ν is close to zero for a low velocity DP operation, all catering for small bounded errors that are quickly dissipated by the error dynamics after the first initialization of the observer.

Generalizing (18) by a function $\beta(t', \tilde{b}_0, d) \in \mathbb{R}^3$ describing the impact of the initial condition and the disturbance on the estimation error yields,

$$|\tilde{x}(t')| = \int_0^{t'} e^{H_t(t'-\tau)}\Lambda\beta(t', \tilde{b}_0, d(\tau))d\tau \quad (19)$$
$$\geq \int_0^{t'} e^{H_t(t'-\tau)}\Lambda\zeta d\tau \quad (20)$$
$$\geq (e^{H_t t'} - I)H_t^{-1}\Lambda\zeta \quad (21)$$

where $|\beta(t', \tilde{b}_0, d)| \geq |\zeta|$, $\zeta \in \mathbb{R}^3$. Notice that (21) is a candidate for γ. However, it is not practical as it is an explicit function of t'. Thus, we choose

$$\gamma = -H_t^{-1}\Lambda\varsigma \quad (22)$$
$$\tilde{y}(t) = -CH_t^{-1}\Lambda\varsigma \quad (23)$$

where $\varsigma \in \mathbb{R}^3$ is a conservative estimate of ζ through the fact that (23) assumes that the measured value is the steady-state error. Combining (22) and (23) gives

$$\gamma = H_t^{-1}\Lambda(CH_t^{-1}\Lambda)^{-1}\tilde{y}, \quad (24)$$

which comply with (14) for all $\epsilon_{1,2,3} > 0$ since $|\tilde{x}| \geq |\gamma|$. This is important as it gives freedom to set the thresholds independent of γ. However, these are typically chosen so that resets occur only when the system is severely perturbed. Also, notice that $\tilde{y} = 0$ after the jump. Thus, $(x, \hat{x}) \in \mathcal{C}$ in the instance of the completion of the reset. The resetting observer can be summarized as,

$$\dot{\hat{x}} = A(t)\hat{x} + B\tau + L(t)\tilde{y} \quad (25a)$$
$$\hat{x}^+ = \hat{x} + H_t^{-1}\Lambda(CH_t^{-1}\Lambda)^{-1}\tilde{y}. \quad (25b)$$

Proposition III.1. *For $(x, \hat{x}) \in \mathcal{D}$ the (time-frozen) system (15) with jump map (12) and (24) will comply with (14).*

The sufficient Lyapunov conditions to claim stability for the proposed hybrid system is given by Theorem 3.18 of [7], for convenience restated here.

Lemma III.2. (Theorem 3.18 in [7]) *Let $\mathcal{H} = (\mathcal{C}, f, \mathcal{D}, g)$ be a hybrid system, and let $\mathcal{A} \subset \mathbb{R}^n$ be closed. If V is a Lyapunov function candidate for $\mathcal{H}$, and there exists $\alpha_1, \alpha_2 \in \mathcal{K}_\infty$ and a continuous $\rho \in \mathcal{PD}$ such that*

$$\alpha_1(|x|_\mathcal{A}) \leq V(x) \leq \alpha_2(|x|_\mathcal{A}) \quad \forall x \in C \cup D \cup g(D) \quad (26)$$

$$\langle \nabla V(x), f(x) \rangle \leq -\rho(|x|_\mathcal{A}) \quad \forall x \in C \quad (27)$$

$$V(g) - V(x) \leq -\rho(|x|_\mathcal{A}) \quad \forall x \in D \quad (28)$$

then $\mathcal{A}$ is UGpAS for $\mathcal{H}$.

When a hybrid system is UGpAS it implies that all solution trajectories can be continued and will converge to a set $\mathcal{A}$ independent of future jumps. Here, the stability of the total

system is analyzed by investigating the error dynamics $\tilde{x}$. Thus,

$$\mathcal{A} = \left\{(x, \tilde{x}) \in \mathbb{R}^{15} \times \mathbb{R}^{15} : \tilde{x} = 0\right\}. \tag{29}$$

Theorem III.3. *The resetting observer (25) error dynamics $\tilde{x}$ is under the stated assumptions, with $d(t) \equiv 0$, UGpAS with respect to the set $\mathcal{A}$.*

Proof. Conditions (26) and (27) are established by the fact that the observer (10) has been shown to be UGES by a quadratic Lyapunov function [2]. Condition (28) is established by Proposition III.1. □

Most importantly this result ensures that the resetting mechanism does not compromise the stability and properties of the continuous observer dynamics. When $d(t) \neq 0$ is included in the analysis the same result is achieved, but for larger uniformly ultimately bounded set given as a function of the maximum value of $d(t)$.

B. Control law design and separation principle

To ensure the intended system stability, the plant, resetting observer, and control law must be investigated in closed-loop. This implies that the states in the control law (9) is replaced with the state estimates as,

$$\tau = -R(y_3)^\top K_p(\hat{\eta} - \eta_d) - K_d\hat{\nu} - R(y_3)^\top \hat{b}. \tag{30}$$

Notice that the same assumption as for the observer rotation matrices is applied here. The closed-loop stability is analyzed by defining $e := col(\xi, \eta - \eta_d, \nu, b) \in \mathbb{R}^{15}$ and

$$\mathcal{A}' = \left\{(e, \tilde{x}) \in \mathbb{R}^{15} \times \mathbb{R}^{15} : e = 0 \text{ and } \tilde{x} = 0\right\}. \tag{31}$$

Theorem III.4. *The closed loop error dynamics $(e, \tilde{x})$ are under the stated assumptions, with $d(t) \equiv 0$, UGpAS with respect to the set $\mathcal{A}'$.*

Proof. Conditions (26) and (27) are established by the fact that the closed-loop error dynamics has been shown to be UGAS by a quadratic Lyapunov function [2], [8]. Condition (28) is established by Proposition III.1 and Theorem III.3 through resetting of the observer state estimates. □

As with the resetting observer design the most important aspect of this result is that the resetting respects the separation principle and does not compromise the stability and properties of the continuous dynamics of the closed-loop. As above, when $d(t) \neq 0$ the analysis can be found to render the the same result, but for larger uniformly ultimately bounded set.

IV. Case study: DP in severe perturbations

The proposed resetting control design was tested using simulations and experiments. The former provide an environment where all states are known and thereby enables improved assessment of performance. The latter complements the simulations as it contains the actual vessel in the loop, and not a mathematical model. In both cases the model scale offshore vessel Cybership III (CS3) was set to keep a fixed station. Fig.5 shows the vessel and it's thruster configuration, and Table I presents a summary of the main hull parameters

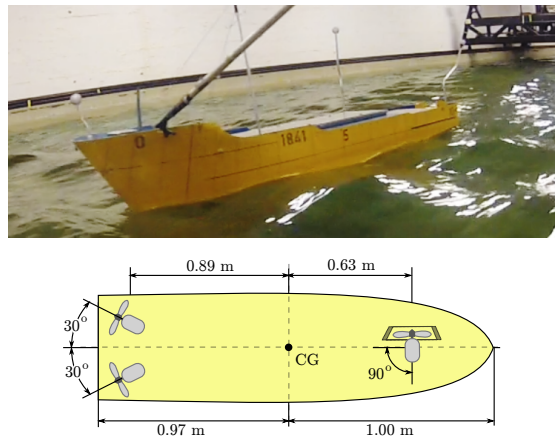

Fig. 5. Top: Cybership 3 in MC-Lab during the experiments. Bottom: The fixed azimuth thruster configuration of CS3 applied in this study.

[6], [10], [11]. CS3 has two azimuth thrusters in the stern and one ducted azimuth in the bow. Here, these were used with fixed azimuth. For control allocation, which converts τ to individual thruster setpoints, the inverse thruster configuration matrix T_τ was calculated as described in [2]. This relates the generalized forces of τ to thruster setpoints $\mu \in \mathbb{R}^3$ as

$$T_\tau^{-1}\tau = \mu. \tag{32}$$

For the experiment μ was converted to revolutions per second by a second order mapping as described in [3] and [12]. This was needed as input to each thruster.

TABLE I
CyberShip 3 main parameters.

Parameter	Model Scale	Full Scale
Length between perp.	2.275 m	68.28 m
Breadth at water line	0.437 m	13.11 m
Draught	0.153 m	4.59 m
Weight (normal load)	74,2 kg	2262 tons

A. Control parameters

The control matrices K_p and K_d were set to be,

$$K_p = \begin{bmatrix} 6.5 & 0 & 0 \\ 0 & 6.5 & 0 \\ 0 & 0 & 3.1 \end{bmatrix}, \quad K_d = \begin{bmatrix} 66.4 & 0 & 0 \\ 0 & 97.5 & 0 \\ 0 & 0 & 30 \end{bmatrix}.$$

By investigation of the linearized system, without observer and assuming state feedback, as described in [2], it was found that the closed-loop corresponds to system time constants in the range 20-30s from reference to position/heading. This is considered reasonable for DP with CS3.

The continuous observer gains K_1, K_2 were set according to the wave frequency as described in [2]. K_3 and K_4 were found by trial and error to be,

$$K_3 = \begin{bmatrix} 10 & 0 & 0 \\ 0 & 16 & 0 \\ 0 & 0 & 6 \end{bmatrix}, \quad K_4 = \begin{bmatrix} 50 & 0 & 0 \\ 0 & 96 & 0 \\ 0 & 0 & 42 \end{bmatrix}.$$

These comply with the requirement that $K_{3i}/K_{4i} < \omega_0$ (where the subscript i denotes the diagonal term $i \in [1, 2, 3]$, and ω_0 is given below). In regard to K_3 and K_4, these should not be set too high as this may cause unwanted oscillations in the position, velocity, and bias estimates due to WF motion perturbations.

The resetting mechanism were incorporated as described in Section III with $\epsilon_1 = 0.0167$, $\epsilon_2 = 0.0167$, and $\epsilon_3 = 0.01$. Scaled to full size these correspond to 0.5 m tracking error in position and 0.01 rad ($\approx$ 0.6 deg) in heading. These are considered to be reasonable to trigger jumps in severe conditions only.

B. Simulation

To simulate the vessel, environment, and control system, the Marine Cybernetics Simulator (MCSim) was used. MCSim is a modular multi-disciplinary simulator based on MATLAB/Simulink [13], and it can be regarded as a process plant model [3]. In this study it was set up to describe the vessel and environment with thruster dynamics without saturation effects, hydrodynamic effects, generalized Coriolis and centripetal forces, nonlinear damping forces, current forces, wave forces with a JONSWAP wave spectrum [2] using a significant wave height $H_s = 0.04$ m and $\omega_0 = 4.66$ rad/s, generalized restoring forces, and an external time-varying disturbance force serving as the unknown and unmeasured perturbation. The latter was set to act between 25 s and 40 s. Two identical scenarios were run, only separated by activation of the resetting of the observer.

Fig.6 compares position, heading, and thruster output norm of the two simulations. It can be seen that the positioning error is significantly improved and the heading error slightly improved when using observer resetting with the given parameters. The increased reactivity is also seen in the outputted thrust norm as more effort is applied to counteract the disturbance. The reason for this is more precise state estimation in the observer, especially for ν and b. Fig.7 shows the state estimates compared to the actual states when resetting is active and confirms that the state jumps contribute to tracking the signals.

C. Experiment

An experiment was conducted in the 40m x 6.45m x 1.5m basin at the Marine Cybernetics Laboratory (MC-Lab) at the Department of Marine Technology at the Norwegian University of Science and Technology (NTNU). There, CS3 was free-floating, battery powered, and controlled by an onboard Compact RIO target from National Instruments (NI) running a VxWorks real-time operating system at 50Hz. The high level control system (control law, observer, and thrust allocation) was developed using MATLAB/Simulink and coupled and downloaded to vessel hardware using NI LabView and NI Veristand software. In order to compare the resetting observer and its continuous counterpart they were run in parallel and it was manually switched between which was active in the feedback loop. For the control law, the one proposed in (30), and a conventional nonlinear PID, as seen in [3], was tested

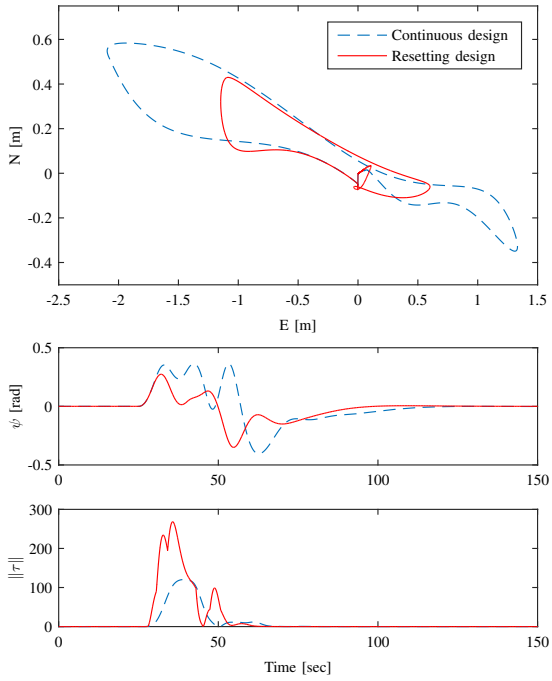

Fig. 6. Comparison of position, heading, and output thrust norm for the simulations with and without resetting of the observer.

and also manually switched between (independent of the active observer). To measure position and heading of the vessel in the tank frame the MC-Lab's Qualisys motion capture system (MCS) was used. This provides Earth-fixed position and heading of the vessel. The MCS consists of 3 onshore cameras and reflective markers mounted on the vessel. To simulate the different sea conditions, a computer controlled hydraulic wave maker system was used. In this experiment, regular waves with $H_s = 0.04$ m and $\omega_0 = 4.66$ rad/s was applied. To introduce severe disturbance, the vessel was manually perturbed by a stick as illustrated in Fig.5.

An aspect for resetting the observer is contamination of bias and noise on the measurements. Static or slowly varying bias will not affect the resetting, as it will not emulate any fast changes in the system. But additive noise may cause premature jumps with lower precision as $\tilde{y}$ does not reflect the disturbance well. This may be mitigated by increasing $\epsilon_{1,2,3}$, requiring $\tilde{y}$ to be in $\mathcal{D}$ for some time, and/or filtering $\tilde{y}$ for triggering the reset and in the calculation of γ. In this experiment the latter was chosen, and a lowpass filter was incorporated in the resetting mechanism as,

$$\dot{y}_f = -T_f^{-1} y_f + T_f^{-1} \tilde{y} \tag{33}$$

$$y_f^+ = 0 \tag{34}$$

where $y_f \in \mathbb{R}^3$ is the filtered observed error state replacing $\tilde{y}$ in (13) and (24), and $T_f \in \mathbb{R}^{3\times 3}$ is a diagonal time constant matrix, set to 0.1s for all degrees of freedom. This filter

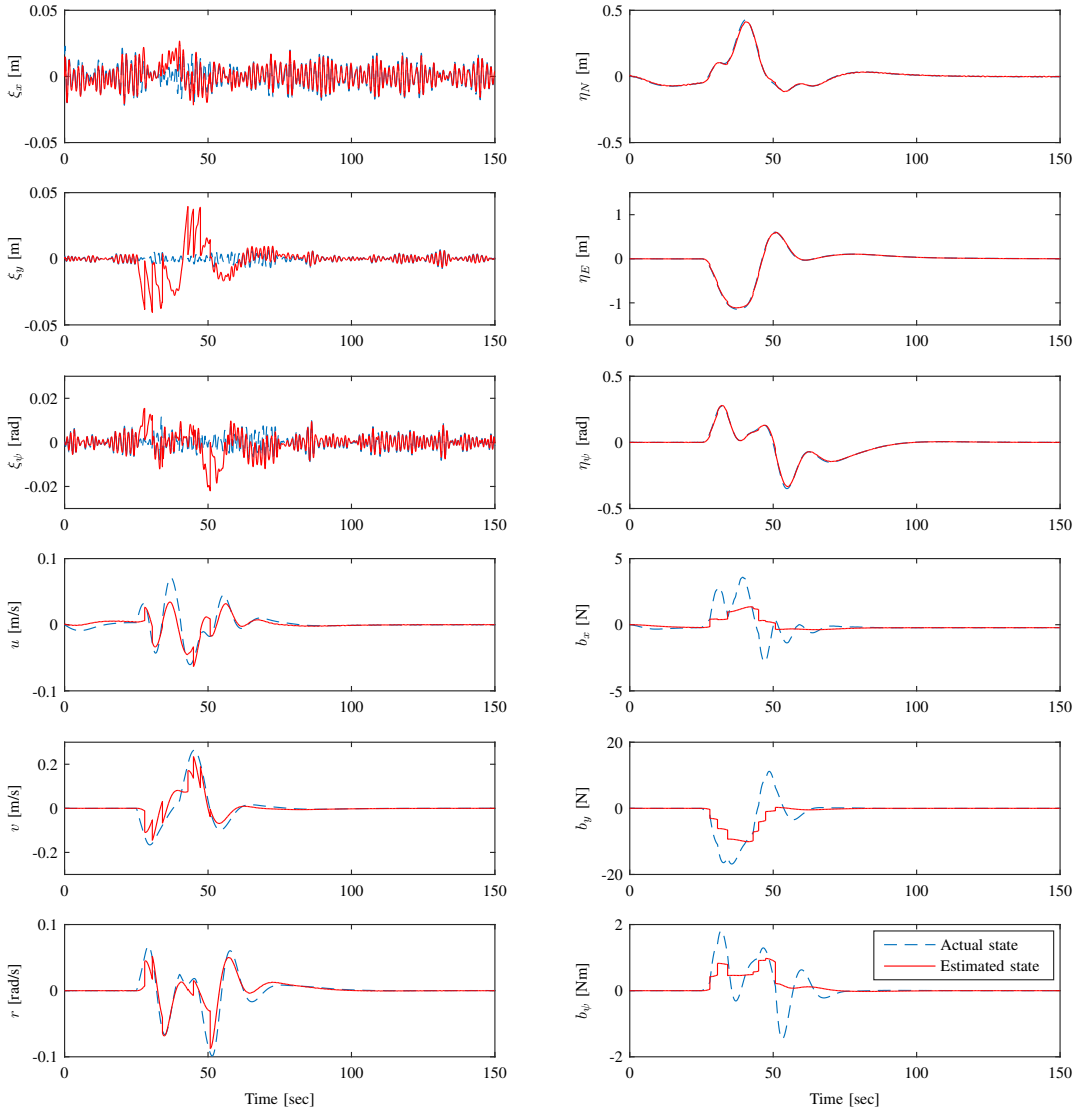

Fig. 7. The state estimates compared to the true states in the simulation with resetting of the observer.

does not conflict with the observer stability nor the separation principle, as it adds more conservativeness to γ. Also, the resetting mechanism was implemented with the restriction that only the degree of freedom that violated its threshold was reset. The remaining were in the reset instance treated as if zero. This adds further conservativeness to γ.

The results are shown in Fig.8, featuring the recorded magnitude of the perturbations in the right column, and the normalized cumulative error norm for the measured states in the left. The latter shows that the resetting observer applied in the experiment reduces the cumulative error by 45%, indicating improved state estimation.

V. Conclusions

This paper has presented a resetting control design which extends a state-of-the-art time continuous algorithm with an additional resetting mechanisms in the observer. The resetting has been designed so that when the state estimation error violates a threshold, indicating severe external unmodeled and unmeasured disturbances, the state estimates are jumped according to the system model to reduce the the error without compromising the properties of the continuous algorithm or requiring changes to it. The improvement in state estimation subsequently enhances the positioning capability as the control

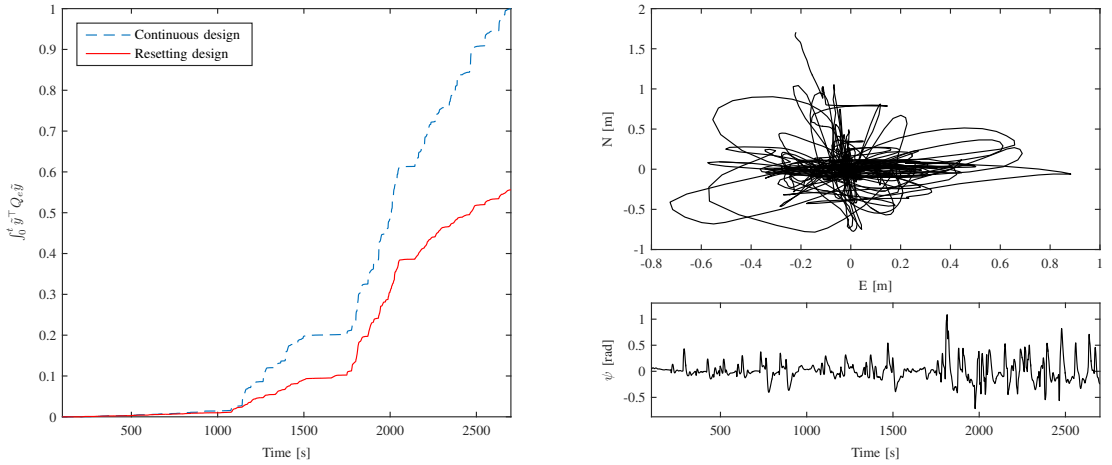

Fig. 8. The experimental results obtained in MC-Lab with CS3. Left is the comparison of the cumulative estimation error, where Q is a diagonal normalization matrix. Right is the recorded position and heading trace of the vessel.

output precision increases.

A case study using simulations and experiments verified that the transient tracking performance during transient severe disturbances was improved. The presented design is particularly interesting as it improves state estimation without gain adjustments, new measurements, or new dynamic models.

ACKNOWLEDGMENT

Research partly funded by the Research Council of Norway (RCN) KMB project no. 199567: "Arctic DP", with partners Kongsberg Maritime, Statoil, and DNV GL, and partly by RCN project no. 203471: CRI SAMCoT, and partly by RCN project no. 223254: CoE AMOS. Additionally, the authors would like to thank Prof. Andrew Teel and Svenn Are Tutturen for constructive discussions.

REFERENCES

[1] International Maritime Organization (IMO), *Guidelines for Vessels with Dynamic Positioning Systems*, June 1994, MSC/circ.645.

[2] T. I. Fossen, *Handbook of Marine Craft Hydrodynamics and Motion Control*. Wiley, 2011.

[3] A. J. Sørensen, *Marine Control Systems: Propulsion and Motion Control of Ships and Ocean Structures*. Department of Marine Technology, NTNU, Norway, 2012.

[4] D. Bray, *The DP Operator's Handbook*. The Nautical Institute, 2011.

[5] Ø. Kjerstad, I. Metrikin, S. Løset, and R. Skjetne, "Experimental and phenomenological investigation of dynamic positioning in managed ice," *Cold Regions Science and Technology*, 2014.

[6] N. T. Dong, "Design of hybrid marine control systems for dynamic positioning," Ph.D. dissertation, National University of Singapore, 2006.

[7] R. Goebel, R. G. Sanfelice, and A. R. Teel, *Hybrid Dynamical Systems: Modeling, Stability, and Robustness*. Princeton University Press, 2012.

[8] A. Loria, T. Fossen, and E. Panteley, "A separation principle for dynamic positioning of ships: theoretical and experimental results," *Control Systems Technology, IEEE Transactions on*, vol. 8, no. 2, pp. 332–343, 2000.

[9] T. I. Fossen and J. P. Strand, "Passive nonlinear observer design for ships using lyapunov methods: full-scale experiments with a supply vessel," *Automatica*, vol. 35, no. 1, pp. 3 – 16, 1999.

[10] E. Ruth, "Propulsion control and thrust allocation on marine vessels," PhD Thesis, NTNU, Dept. Marine Technology, Trondheim, Norway, 2008.

[11] V. Hassani, A. M. Pascoal, and A. J. Sørensen, "A Novel Methodology for Marine Vessel Adaptive Wave Filtering: Theory and Experiments," in *Proc. of the 52nd IEEE Conference on Decision and Control*, 2013.

[12] R. Skjetne, Ø. N. Smogeli, and T. I. Fossen, "A Nonlinear Ship Manoeuvering Model: Identification and adaptive control with experiments for a model ship," *Modeling, Identification and Control*, no. 25, 2004.

[13] A. J. Sørensen, E. Pedersen, and Ø. Smogeli, "Simulation-based design and testing of dynamically positioned marine vessels," in *Proc. of International Conference on Marine Simulation and Ship Maneuverability*, 2003.

Øivind Kåre Kjerstad was born in Norway 1985, and started his career as a factory worker in the maritime industry in Western Norway in 2001. In 2005 after receiving the skilled craftsmanship diploma he began studying cybernetics at NTNU. In 2010 he received his M.Sc. and joined the research project *KMB Arctic DP* to pursue a PhD. During this, he has participated in research cruises to Svalbard and East Greenland, and model scale experiments in ice. His research interests are within marine motion control systems and Arctic technology.

Roger Skjetne Professor Roger Skjetne received in 2000 his MSc degree in control engineering at the University of California at Santa Barbara and in 2005 his PhD degree at NTNU, for which the thesis was awarded the Exxon Mobil prize for best PhD thesis in applied research. Prior to his studies, he worked as an electrician for Aker Elektro AS on installations in the North Sea. In 2004-2009 he was employed in Marine Cybernetics AS, working on Hardware-In-the-Loop simulation for testing safety-critical marine control systems. From August 2009 he has held the position of Professor in Marine Control Engineering at the Department of Marine Technology at NTNU, where he presently is the leader of the research group on Marine Structures. His research interests are within Arctic stationkeeping operations and Ice Management systems for ships and rigs, environmentally robust control of shipboard electric power systems, and nonlinear control theory for motion control of single and groups of marine vessels. Roger Skjetne managed the *KMB Arctic DP* research project, is leader of the ice management work package in the CRI Sustainable Arctic Marine and Coastal Technology (SAMCoT), and is an associated researcher in the CoE Centre for Ships and Ocean Structures (CeSOS) and CoE Autonomous Marine Operations and Systems (AMOS).

Disturbance Rejection by Acceleration Feedforward For Marine Surface Vessels

Disturbance rejection by acceleration feedforward for marine surface vessels

Øivind Kåre Kjerstad and Roger Skjetne

***Abstract*—Acceleration signals have a powerful disturbance rejection potential in rigid body motion control as they carry a measure proportional to the resulting force. Yet, they are seldom used, since measuring, decoupling, and utilizing the dynamic acceleration in the control design is not trivial. This paper discusses these topics and presents a solution for marine vessels building on conventional methods together with a novel control law design where the dynamic acceleration signals are used to form a dynamic reference-less disturbance feedforward compensation. This replaces conventional integral action and enables unmeasured external loads and unmodel dynamics to be counteracted with low time lag. A case study shows feasibility of the proposed design using experimental data and closed-loop high fidelity simulations of dynamic positioning in a harsh cold climate environment with sea-ice.**

***Index Terms*—Feedback control; Feedforward control; State estimation; Disturbance rejection.**

I. Introduction

In marine motion control the main objective is typically to control the position and velocity of a ship to a desired state. This is usually achieved with the structure seen in Figure 1 through model-based control design relying on state measurements of position, heading, and sometimes angular velocity. Such systems have a good track record and are proven stable and robust in a wide range of sea states; see [1] and [2]. Yet, their ability to handle unmodeled dynamics and environmental disturbances is limited to integral action based on state feedback. However, since the state measurements hold time integrals of the force, there is an inherent lag before it propagates significantly to adapt the system. This works well for slowly varying forces, but when rapid and substantial force transients occur the control precision can be severely affected [3]–[5]. How to handle harsh and rapidly varying exogenous disturbances due to loads from sea-ice on a dynamically positioned vessel was the objective of the Arctic DP project [6] that initiated this study.

In general, there are two approaches to dealing with this challenge. The first is extending the model used in control design to describe the additional physics. Yet, modelling phenomena such as harsh weather, wave trains, equipment in the sea connected to the vessel, current surges, interaction effects with other vessels, and sea-ice interaction may be challenging for control purposes as they are results of complex physical processes. The second approach, which is the topic of this paper, is extending the sensor suite of the vessel to capture the phenomena in question. Here acceleration signals are investigated. These are especially attractive as they carry a proportional measure of the resulting force. Special emphasis is put on dynamic positioning (DP), defined by [7] as automatically maintaining position (fixed location or predetermined track) exclusively through the use of the ship's thrusters alone. It is used in low velocity operations when a precise geo-fixed or relative position is needed. Examples include cargo transfer between ships and platforms, subsea construction, diving support, drilling, pipelaying, etc.

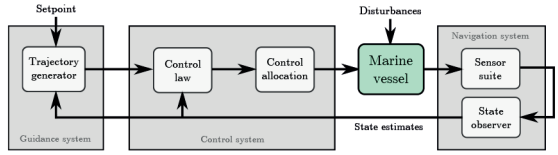

Fig. 1. Signal flow in guidance, navigation, and control of marine craft. Adapted from [1].

To apply acceleration signals in the control design require a sensor suite containing accelerometers. The technology itself is well established; see e.g. [8] and found in a variety of applications such as consumer electronics, vibration sensing of large structures, impact detection, and navigation. In some cases inertial measurement units (IMUs), containing accelerometers, gyroscopes, and magnetometers are part of marine vessel sensor suites to supply onboard systems with roll and pitch measurements (these are calculated based on the strong influence of gravity on the measurements; see [1]). However, these measurements are not commonly used in closed-loop motion control. There are several reasons for this, but foremost that the sensor output is not a direct measure of the dynamic acceleration (i.e., the acceleration resulting in motion). The output is dependent on the location of the sensor in the vessel hull and affected by gravity, measurement bias, and sensor noise. An exception is found in [9] where linear motion acceleration signals are used to enhance the state observer for DP and introduce an additional acceleration feedback term in the control law. In our paper the distinction is that the full acceleration vector is found. This enables use of kinematic and sensor models in the state observer, and for forming an acceleration feedforward (AFF) signal used in the control law to directly compensate a disturbance, as previously proposed by the authors in [10] and [11]. This provides

Ø. K. Kjerstad is affiliated with the Department of Marine Technology, the Department of Civil and Transport Engineering, and the Arctic Technology Department. The two former are at the Norwegian University of Science and Technology (NTNU), Trondheim, Norway, and the latter is at the The University Centre in Svalbard, Longyearbyen, Norway. R. Skjetne is with the Department of Marine Technology at NTNU. E-mails: oivind.k.kjerstad@ntnu.no, roger.skjetne@ntnu.no.

a powerful and reactive tool for developing robust control systems operating in harsh environments, where traditional control designs are not well suited.

The main contributions of this paper are the design methodology incorporating AFF in the control law to compensate disturbances and unmodeled dynamics, and experimental verification of the load estimation and the measurement setup showing feasibility of these methods. As the proposed control law design method is novel, a motivating example is given below to showcase its main concept.

Mathematical notation: In UGS, UGAS, UGES, etc., stands G for Global, S for Stable, U for Uniform, A for Asymptotic, and E for Exponential. Total time derivatives of $x(t)$ are denoted $\dot{x}, \ddot{x}, x^{(3)}, \ldots, x^{(n)}$. The Euclidean vector norm is $|x|$, the induced matrix 2-norm is denoted $\|A\|$, while the signal norm is denoted $\|u\| := sup\{|u(t)| : t \geq 0\}$. Stacking several vectors into one is denoted $\text{col}(x, y, \ldots) \triangleq \left[x^\top, y^\top, \ldots\right]^\top$. The smallest and largest eigenvalues of $A > 0$ is denoted $\lambda_{\min}(A) > 0$ and $\lambda_{\max}(A) > 0$, respectively.

A. Motivating example

To illustrate how AFF is applied in control design, consider a scalar mechanical system with unity mass and nonlinear damping,

$$\ddot{x} + \dot{x}^3 = u + d(t), \tag{1}$$

where $(x, \dot{x}, \ddot{x})$ is the position, velocity, and acceleration – all measured quantities, u is a control input force, and $d(t)$ is an external disturbance force. The objective is to control $x(t)$ to accurately track a desired position $x_d(t)$, where $(x_d(t), \dot{x}_d(t), \ddot{x}_d(t))$ are all bounded and available signals. We assume the disturbance is bounded, absolutely continuous, and $\exists d_m > 0$ such that $\left|\dot{d}(t)\right| \leq d_m$ a.a. $t \geq 0$.

Let the control law be divided into a nominal term Γ and a term Δ to compensate the disturbance, that is,

$$u = \Gamma - \Delta, \tag{2}$$

where the objective of Γ is to ensure nominal closed-loop performance that satisfies the specification of the control problem when $d(t) = 0$, and the objective of Δ is to handle the disturbance $d(t)$.

To design Γ we define a Hurwitz matrix

$$A = \begin{bmatrix} 0 & 1 \\ -k_1 & -k_2 \end{bmatrix}, \tag{3}$$

and let $P = P^\top > 0$ satisfy the Lyapunov equation $PA = A^\top P = -qI$ with $q > 0$. Using $k = [k_1, k_2]$ we assign the nominal term

$$\Gamma(\ddot{x}_d, \dot{x}, e, t) := -ke + \dot{x}^3 + \ddot{x}_d(t), \tag{4}$$

where $e := \text{col}(x - x_d(t), \dot{x} - \dot{x}_d(t))$. Differentiating $V_0(e) = e^\top Pe$ along the solutions of the closed-loop system

$$\dot{e} = Ae + b\left(d(t) - \Delta\right), \tag{5}$$

where $b = \text{col}(0, 1)$, gives

$$\dot{V}_0 = -qe^\top e + 2e^\top Pb\left(d(t) - \Delta\right), \tag{6}$$

and it follows for $d(t) - \Delta = 0$ that $\{e = 0\}$ is UGES. To design Δ we propose two options, direct and filtered acceleration feedforward.

1) Direct acceleration feedforward: Assume $a(t) = \ddot{x}(t - \delta)$ is the acceleration measurement for (1), where δ is a small known time delay due to signal processing and communication. Then, by direct feedforward, we assign the signal

$$\Delta(t) := a(t) + \dot{x}(t - \delta)^3 - u(t - \delta), \tag{7}$$

which from (1) implies that $\Delta(t) = d(t - \delta)$. Using $p_M = \lambda_{\max}(P)$ it now follows that

$$\begin{aligned} \dot{V}_0 &\leq -q\left|e\right|^2 + 2p_M\left|e\right|\left|d(t) - d(t - \delta)\right| \\ &\leq -\frac{q}{2}\left|e\right|^2 + \Lambda\delta^2, \end{aligned} \tag{8}$$

where $\Lambda := 2\frac{p_M^2 d_m^2}{q}$, and using the Global Lipschitz property $|d(t) - d(\tau)| \leq d_m\left|t - \tau\right|$ (following from absolute continuity of $d(t)$ and boundedness of $\dot{d}(t)$). Letting $\tilde{d}(t) := d(t) - d(t - \delta)$, (8) implies that the resulting closed-loop system

$$\dot{e} = Ae + b\tilde{d}(t) \tag{9}$$

is input-to-state stable (ISS) with respect to $\tilde{d}(t)$ and, correspondingly, the delay δ. A small delay $\delta \ll 1$ will from (8) result in a small impact by the disturbance on the tracking performance. In the limit as $\delta \to 0$ the difference $\tilde{d}(t)$ vanishes and the nominal performance is recovered.

Note that an alternative to (4) and (7) is to use the simpler control law

$$\Gamma(\ddot{x}_d, e, t) := -ke + \ddot{x}_d(t) \tag{10a}$$

$$\Delta(t) := a(t) - u(t - \delta) \tag{10b}$$

$$= d(t - \delta) - \dot{x}(t - \delta)^3, \tag{10c}$$

which shows that the feedforward term Δ can be realized model-free, without knowledge of the velocity. Instead, the nonlinear damping term is accounted for in the extended disturbance $\bar{d}(t) = d(t) - \dot{x}(t)^3$ such that $\tilde{d}(t) = \bar{d}(t) - \bar{d}(t - \delta)$, and the same conclusion follows. This is important as it allows for handling uncertain or unmodeled dynamics.

2) Filtered acceleration feedforward: Now let Δ be the state of a filter to track $d(t)$ as closely as possible. In this case, the control law (2) becomes dynamic, where Γ is defined in (4). Letting $\varepsilon := d(t) - \Delta$ be the disturbance tracking error, and differentiating

$$V(e, \varepsilon) = V_0(e) + \frac{1}{2}\varepsilon^2 \tag{11}$$

along the solutions of (5) and $\dot{\Delta}$ gives

$$\dot{V} = -qe^\top e + \left(2e^\top Pb + \dot{d}(t) - \dot{\Delta}\right)\varepsilon. \tag{12}$$

Assuming now there is no time delay on the state measurements, and using $a(t) = \ddot{x}(t)$, we notice from (1) and (2) that $\varepsilon = \ddot{x} + \dot{x}^3 - \Gamma$. We assign

$$\begin{aligned} \dot{\Delta} &= 2b^\top Pe - \mu\left(\Gamma - a - \dot{x}^3\right) \\ &= 2b^\top Pe - \mu\varepsilon. \end{aligned} \tag{13}$$

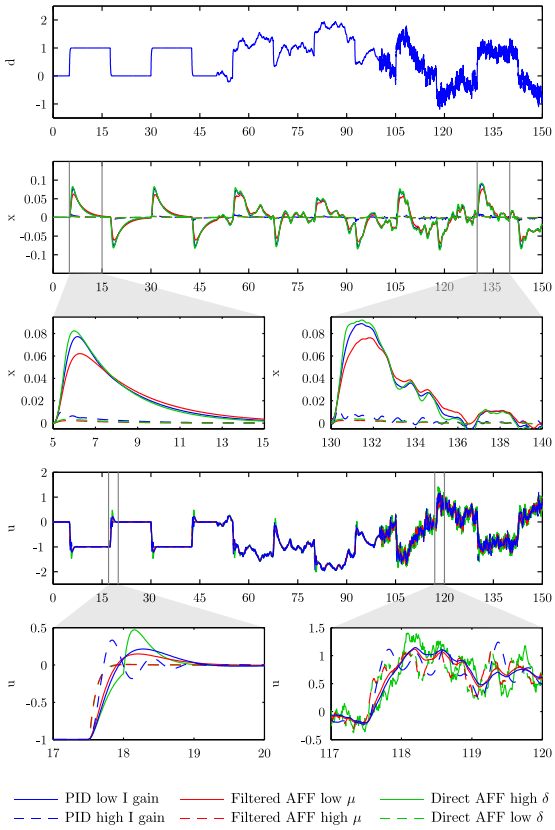

Fig. 2. Top: the time development of the state subject to different control strategies. Notice that the disturbance signal is marked by light blue. Bottom: A close-up of the control input.

The derivative of (11) along the solutions of the resulting closed-loop system

$$\dot{e} = Ae + b\varepsilon \tag{14}$$
$$\dot{\varepsilon} = -2b^\top Pe - \mu\varepsilon + \dot{d} \tag{15}$$

now becomes

$$\begin{aligned}\dot{V} &= -qe^\top e - \mu\varepsilon^2 + \varepsilon\dot{d}(t) \\ &\leq -q\left|e\right|^2 - \frac{\mu}{2}\left|\varepsilon\right|^2 + \frac{1}{2\mu}\left|\dot{d}(t)\right|^2,\end{aligned} \tag{16}$$

which shows that the system is ISS with respect to $\dot{d}(t)$ as a disturbance input, where the filter gain μ can be used to attenuate its impact on the closed-loop tracking performance.

Note again that we can remove the nonlinear damping term $\dot{x}^3$ from (4) and (13), incorporate it into the extended disturbance $\bar{d}(t) = d(t) - \dot{x}(t)^3$, and arrive at a model-free control law with Γ from (10a) and

$$\dot{\Delta} = 2b^\top Pe - \mu\left(\Gamma - a\right) \tag{17a}$$
$$u = \Gamma - \Delta. \tag{17b}$$

Inserting (10a) into (17a) we notice that Δ serves as an integral action state on the augmented error $\bar{e} = \mathrm{col}(e,\ \ddot{x} - \ddot{x}_d(t))$.

3) Simulation comparison: To further showcase AFF control design, a simulation of (1) with $d(t)$ of increasing severity is presented. Three control laws, each with two parameter variations, were used for a point stabilization objective ($x_d = 0$). The compared control laws were:

- The nominal control law (4) together with direct AFF (7), using high and low δ.
- The nominal control law (4) together with filtered AFF (13), using high and low μ.
- A PID control law, $u = -ke - k_i \int e dt$, where $k_i = [k_{i1}, k_{i2}]$, with high and low k_i.

All of the above were simulated using fixed common nominal control gains $k = [2, 5]$. Figure 2 shows $d(t)$ in the top plot, and the tracking performance of x and control input u in the subsequent. The AFF control laws with low disturbance attenuation (high δ or low μ) offers no real advantage over PID as the performance is comparable. However, increasing the integral action of the PID to improve the disturbance rejection eventually results in control input oscillations. This is best seen in the lower left plot. The AFF control laws with high disturbance attenuation (low δ and high μ) does not have this problem. They are able to accurately attenuate the disturbance, recovering the nominal performance, without control input oscillations. Improved control precision is thus obtained.

II. Problem formulation

For 3 degrees-of-freedom (DOF) motion control of a rigid-body marine surface vessel, we consider a generalization of the state-of-the-art models [1], [2],

$$\dot{\eta} = R(\psi)\nu \tag{18a}$$
$$M\dot{\nu} = \tau + \rho(\eta, \nu) + d(t) \tag{18b}$$

where $\eta = \mathrm{col}\,(x, y, \psi) \in \mathbb{R}^3$ is the position and orientation of the body in the inertial frame, $\nu = \mathrm{col}\,(u, v, r) \in \mathbb{R}^3$ is the body-fixed linear and angular velocity of the body, $M = M^\top > 0$ is the rigid body inertia matrix, $\tau \in \mathbb{R}^3$ is the body-fixed control input, $\rho : \mathbb{R}^3 \times \mathbb{R}^3 \to \mathbb{R}^3$ is a locally Lipschitz function containing nonlinear dynamics (Coriolis, damping, and restoring forces), and $d : \mathbb{R}_{\geq 0} \to \mathbb{R}^3$ accounts for external time-varying disturbances. We assume $\exists d_m > 0$ such that $\max\{\|d(t)\|, \left\|\dot{d}(t)\right\|\} \leq d_m$. $R(\psi) \in SO(3)$ is the rotation matrix between the body frame and the inertial frame. This has the following properties,

$$R(\psi)^\top R(\psi) = R(\psi)R(\psi)^\top = I \tag{19}$$
$$\dot{R} = R(\psi)S(r) \tag{20}$$

where $S(r) \in \mathbb{R}^{3\times 3}$ is a skew symmetric matrix with the following properties,

$$S(r) = \begin{bmatrix} 0 & -r & 0 \\ r & 0 & 0 \\ 0 & 0 & 0 \end{bmatrix} = -S(r)^\top. \tag{21}$$

For control design we assume that the following signals are available: The vessel position, $p = \mathrm{col}\,(x, y, z) \in \mathbb{R}^3$, measured in the assumed inertial north-east-down (NED) frame.

The vessel orientation, $\Theta = \text{col}\,(\phi, \theta, \psi) \in \mathbb{R}^3$, measured in the body frame relative to the NED frame. The vessel rate of turn, $\omega = \text{col}\,(p, q, r) \in \mathbb{R}^3$, measured in the body frame relative to the NED frame. And finally, accelerometer output $a_m = \text{col}\,(a_x, a_y, a_z)$ measured on the rigid body in its sensor frame relative to the NED frame.

In this paper we refer to an accelerometer as a body-fixed three axis orthogonal linear sensor. By assuming that the accelerometer is aligned with the body frame, and that the sensor scale-factor, cross-coupling, and misalignment errors are negligible after calibration, we modeled it as in [12],

$$a_m = a_l + \omega \times v + g + b + w \tag{22a}$$
$$\dot{g} = -\omega \times g \tag{22b}$$

where $a_m \in \mathbb{R}^3$ is the sensor output, $a_l \in \mathbb{R}^3$ is the linear dynamic acceleration in the sensor mounting point, $\omega = \text{col}\,(p, q, r)$ is the angular rate of the body relative to the inertial frame, and $v = \text{col}\,(u, v, w)$ is linear velocity of the body. Notice that ν in (18) contains elements of both v and ω. Furthermore, $g \in \mathbb{R}^3$ is the gravitational component expressed in the body frame, $b \in \mathbb{R}^3$ is the sensor bias, and $w \in \mathbb{R}^3$ is the sensor noise.

To enable use of the dynamic acceleration in control design, three challenges must be overcome. The first is that it may be impractical, or even impossible, to mount a sensor in the point of control. Here the point of control will be referred to as origin (CO) of the body frame. What arises is a dependency on the distance between CO and the sensor mounting position given by

$$a_l = a_{\text{co}} + \alpha \times l + \omega \times (\omega \times l) \tag{23}$$

where $a_{\text{co}} \in \mathbb{R}^3$ is the linear dynamic acceleration in CO, $\alpha \in \mathbb{R}^3$ is the angular acceleration, and $l \in \mathbb{R}^3$ is the body frame distance vector between the points of measure and CO. The latter will be referred to as the accelerometer lever arm, or just lever arm.

The second challenge is the fact that $a_{\text{co}} \neq \dot{\nu}$. The dynamic acceleration a_l captured in an accelerometer (along with other effects) does not contain the angular acceleration α. It should be mentioned that sensors capable of measuring α exists [8], but they are not common in marine applications. Therefore, such are not considered here. We propose to obtain α through exploiting the lever arm dependency of four distributed accelerometers. Thus, the third challenge is that of acquiring $\dot{\nu}$ from these.

The main objective is to design a 3 DOF control law τ for (18) utilizing $\dot{\nu}$, using the state-of-the-art structure of Figure 1, such that the vessel accurately tracks a predefined time-parametrized trajectory given by $\{\eta_d(t), \nu_d(t), \dot{\nu}_d(t)\}$ while subject to unmodeled dynamics and rapidly varying disturbances. Although the control design will provide the main contribution, the application of acceleration measurements must be given attention to tackle the aforementioned challenges in both the sensor suite and the state estimation.

Since solving the three challenges to obtain the dynamic acceleration is a prerequisite for the control design, the paper is structured likewise. Chapter 3 presents the reconstruction of the dynamic acceleration through multiple accelerometers and a state observer. Chapter 4 derives and analyzes dynamic tracking control laws based on filtered AFF. Chapter 5 features a case study investigating DP subject to severe ice interaction in an Arctic operation. Finally, Chapter 6 summarizes and concludes the results of the paper.

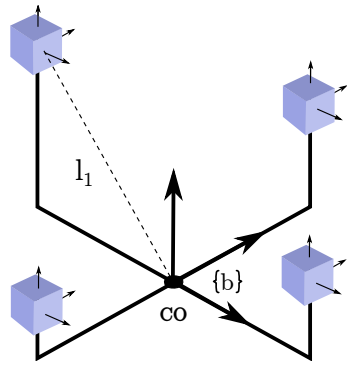

Fig. 3. An illustration of one possible setup of the accelerometers for measuring the full state acceleration vector.

III. Reconstructing the Dynamic Acceleration

To overcome the two first challenges of using accelerometers we exploit four spatially distributed sensors and the relation between them. This enables use of well known, matured, and relatively cheap and rugged conventional accelerometers in a spatial configuration to setup a virtual 6 DOF accelerometer in CO. Similar schemes are seen in [13] and [14]. The final accelerometer challenge of obtaining $\dot{\nu}$ is handled by reformulating the state observer. Although the control objective of this paper does not require the 6 DOF acceleration vector, it is practical for the removal of gravity and for generality to include it.

A. 6 DOF acceleration measurement

Consider parameterizing (23) as a product of its static and dynamic variables

$$a_l = \begin{bmatrix} I_{3\times3} & S(l)^\top & H(l) \end{bmatrix} \begin{bmatrix} a_{\text{co}} \\ \alpha \\ \bar{\omega} \end{bmatrix} \tag{24a}$$
$$= W(l) z. \tag{24b}$$

where $I_{3\times3} \in \mathbb{R}^{3\times3}$ is an identity matrix, $S(l)$ is given in (21), and

$$H(l) = \begin{bmatrix} 0 & -l_x & -l_x & l_y & l_z & 0 \\ -l_y & 0 & -l_y & l_x & 0 & l_z \\ -l_z & -l_z & 0 & 0 & l_x & l_y \end{bmatrix}, \tag{25}$$

is a sub-matrix of the accelerometer configuration matrix $W(l) \in \mathbb{R}^{3\times12}$, and $z \in \mathbb{R}^{12}$ is the linear acceleration, angular acceleration, and angular rate cross product vector. The latter contains $\bar{\omega} \in \mathbb{R}^6$ defined as

$$\bar{\omega} = \begin{bmatrix} \omega_x^2 & \omega_y^2 & \omega_z^2 & \omega_x\omega_y & \omega_x\omega_z & \omega_y\omega_z \end{bmatrix}^\top. \tag{26}$$

MRU 5+

Fig. 4. R/V Gunnerus and a MRU 5+. Courtesy of Fredrik Skoglund, and Kongsberg Seatex.

TABLE I
PLACEMENT OF MRUS IN R/V GUNNERUS RELATIVE TO CO.

Nr.	X [m]	Y [m]	Z [m]	Note
1	0.358	0.804	-4.321	Technical room
2	14.978	0.039	0.568	Bow bulb
3	-7.454	4.123	-0.012	Engine room stb.
4	-7.545	-4.251	-0.730	Engine room port

As mentioned, by measuring in one location $W(l)$ cannot be inverted to find z. Therefore, we propose to use a configuration of four sensors, as illustrated in Figure 3, such that (24b) can be extended to

$$\begin{bmatrix} a_{l1} \\ a_{l2} \\ a_{l3} \\ a_{l4} \end{bmatrix} = \begin{bmatrix} W(l_1) \\ W(l_2) \\ W(l_3) \\ W(l_4) \end{bmatrix} z \tag{27}$$

$$a_c = G(l_c) z \tag{28}$$

where $a_c \in \mathbb{R}^{12}$ is the combined linear acceleration vectors in the sensor mounting positions, $G(l_c) \in \mathbb{R}^{12\times 12}$ is the combined sensor configuration matrix and $l_c = col(l_1, l_2, l_3, l_4)$ is the combined sensor lever arm vector. To calculate z it is important to ensure that the static matrix $G(l_c)$ is nonsingular. According to [15], this is achieved when the sensors are oriented equally and their positions are not co-planar, that is at least one sensor must not lie in the same plane as the three others. Then, by substituting in the four accelerometer equations in (22a) for a_c, we get

$$G^{-1} a_{mc} = z + G^{-1} \begin{bmatrix} \omega \times v + g + b_1 + w_1 \\ \omega \times v + g + b_2 + w_2 \\ \omega \times v + g + b_3 + w_3 \\ \omega \times v + g + b_4 + w_4 \end{bmatrix}, \tag{29}$$

where $a_{mc} = col(a_{m1}, a_{m2}, a_{m3}, a_{m4})$. This shows that the setup with four spatially distributed accelerometers constitutes a virtual 6 DOF sensor placed in CO. Notice that it still has the same sensor effects as (22a) on the measurements.

B. Experimental verification

In November 2013 a series of maneuvering experiments were carried out with the NTNU research vessel Gunnerus offshore mid-Norway. Four Kongsberg Seatex 5+ Motion-Refecence Units (MRUs) [16] were installed onboard. The vessel and sensor are seen in Figure 4. Prior to the campaign, the MRU's lever arms and orientation were accurately measured using laser-based industrial surveying techniques [17]. Table I shows the MRU positions.

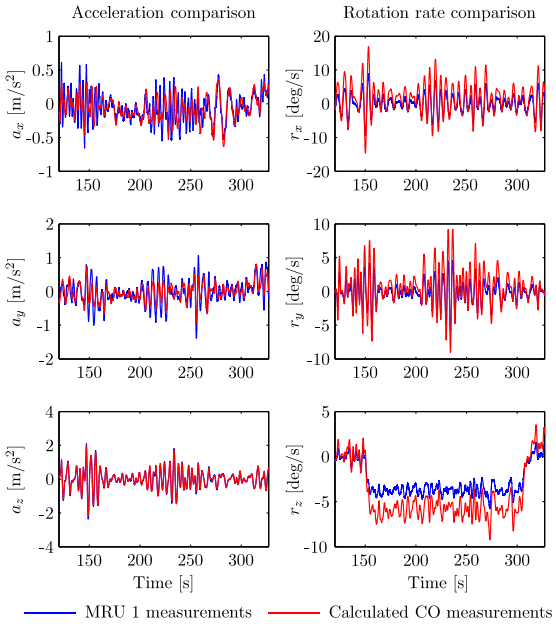

Fig. 5. Comparison of the obtained acceleration vector with data output of MRU 1. Left column: The multi-sensor linear accelerations vs. MRU 1 output. Right column: The multi-sensor integration of the angular accelerations vs. MRU 1 gyroscope output.

The MRUs were placed in the vessel hull such that $G(l_c)$ was nonsingular and spatially large. By investigation of the eigenvalues of $G(l_c)^{-1}$ it was found that they were of magnitude less than one. From (29) this implies improved noise and bias attenuation. Both a_l and ω were logged from each MRU at 100 Hz by a Kongsberg Seatex Vessel Motion Monitor (VMM). Notice that a_l, and not a_m was logged. This was due to a proprietary undisclosed algorithm providing the necessary compensation internally in the MRUs.

Figure 5 features the output of the 6 DOF measurement setup compared to MRU 1 data from when Gunnerus performed a turning circle in multi-directional swell waves with significant wave height of 2.1 m and period of 8.5 s. The left column shows the calculated a_{co} compared to MRU 1 a, and the right, $\int \alpha \, dt$ compared to MRU 1 ω.

The results show that the oscillatory wave induced components of the calculated output match well. The deviations in magnitude are believed to stem from the MRU 1 elevated position coupled with roll and pitch motions. In the right column, the angular acceleration is compared to the MRU 1 gyroscope by integration. Although seemingly biased and deviating in magnitude, the oscillatory components of the signals match well, indicating the feasibility of measuring the angular acceleration component.

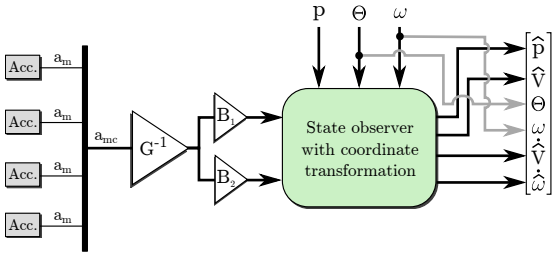

Fig. 6. Block diagram showing the relation between the accelerometer sensor suite and the state observer.

C. State observer

In order to solve the last accelerometer challenge, and obtain $\dot{\nu}$, the state observer of Figure 1 is redefined from an implementation of (18) [2] to a model including and exploiting the acceleration measurement system. The structure applied is shown in Figure 6, and the model is

$$\dot{p}_v = -S(\omega(t))p_v + v \tag{30a}$$
$$\dot{v} = -S(\omega(t))v - b_l - g + B_1 G^{-1} a_{mc} \tag{30b}$$
$$\dot{g} = -S(\omega(t))g \tag{30c}$$
$$\dot{b}_l = 0 \tag{30d}$$
$$\dot{\omega} = b_\omega + B_2 G^{-1} a_{mc} \tag{30e}$$
$$\dot{b}_\omega = 0, \tag{30f}$$

where $p_v := R(\Theta)^\top p$ is the position rotated to the body frame, $v = col(u, v, w) \in \mathbb{R}^3$ is the linear velocity subsystem, $a_{mc} \in \mathbb{R}^{12}$ is the collective accelerometer measurement vector, as seen in (29), $b_l \in \mathbb{R}^3$ and $b_\omega \in \mathbb{R}^3$ are the linear and rotational accelerometer bias originating from the sensor transformation, and $B_{1,2} \in \mathbb{R}^{3\times 12}$ are selection matrices for a_{co} and α, respectively.

This redefinition has two important aspects. The first is that it allows for full state feedback control design including $\dot{\nu}$. Thus, AFF designs similar to those presented in the motivational example can be applied. The second is that it improves the tracking capability of the observer. If unmodeled dynamics and harsh disturbances are not handled, poor state estimation will occur, which in turn results in reduced control accuracy. By replacing the kinetic model (18b) with a model composed of kinematic and sensor characteristics (30b)-(30f) the acceleration signal, capturing the system dynamics through measurements, acts as input to the state observer. The performance is therefore not dependent on model assumptions and validity for the given environment, but rather on the quality of the sensor suite. For DP this is especially attractive as reduced state estimation performance has been reported [3], [5], [18].

As the above model contains cross products between the states ω and p_v, v, and g, respectively, it is nonlinear. State-of-the-art observer designs for nonlinear systems includes various nonlinear extensions of the Kalman filter. The downside with these is the lack of established convergence and stability properties. Here a work around is applied. In (30) the objective of the ω state is to remove bias from α. It is assumed that ω is available with high precision and low noise characteristics. This is reasonable as most marine crafts carry a high end attitude systems capable of supplying both Θ and ω. Therefore, by regarding it as a time-varying signal in the position and linear velocity subsystems (30a)-(30c) the nonlinear model can be regarded as linearly time varying (LTV), and written as

$$\dot{x} = A(t)x + BG^{-1}a_m \tag{31}$$
$$y = \begin{bmatrix} p_v & \omega \end{bmatrix}^\top, \tag{32}$$

where $x = \text{col}(p_v, v, b_l, g, \omega, b_\omega)$. For LTV systems a wide range of Kalman-related results are available; see [19], [20], and [21]. The solution in [22], with the state vector extended by ω and b_ω, is chosen to solve the estimation problem.

An aspect of (30b) is that it holds two competing integrators in b_l and g. In [12], the subsystem (30a)-(30d) is found uniformly completely observable iff $\omega(t)$ has sufficient perturbations (with $y = p_v$). Although this cannot be guaranteed at all times, it does not constitute a problem as the collective bias $b_l + g$ is uniformly completely observable. Thus, the estimation performance of determining p_v, v, a_{co}, and α is not compromised.

In summary, all the three accelerometer challenges have been investigated and solved, catering for realization of AFF control law designs utilizing full state feedback including $\dot{\nu}$.

IV. Control design

The role of the control law in Figure 1 is to calculate the 3 DOF control efforts needed to fulfill the control objective of making η track a desired vector $\eta_d((t)$ in NED. Thus, the control designs presented in this section employ only the planar subset of signals supplied by the sensor suite and state observer (i.e., η, ν, and $\dot{\nu}$).

Since marine vessels propulsion typically are unsymmetrical with respect to the yz-plane, it is convenient to tune the positioning response of the control law with respect to vessel-parallel (VP) coordinates. Correspondingly, we transform the position/heading vector η from NED to VP, that is, $\eta_v := R(\psi)^\top \eta$.

We define $\eta_{v,d} := R(\psi)^\top \eta_d(t)$, resulting in the VP error state

$$\begin{aligned}\tilde{\eta}_v &= \eta_v - \eta_{v,d} \\ &= R(\psi)^\top (\eta - \eta_d(t)) \\ &= R(\psi)^\top \tilde{\eta},\end{aligned} \tag{33}$$

where $\tilde{\eta} := \eta - \eta_d(t)$. We similarly define

$$\nu_d := R(\psi)^\top \dot{\eta}_d(t) \tag{34a}$$
$$a_d := \dot{\nu}_d = -S(r)\nu_d + R(\psi)^\top \ddot{\eta}_d(t), \tag{34b}$$

and $\tilde{\nu} := \nu - \nu_d(t)$, where we used $\dot{R} = R(\psi)S(r)$ and $S(r) = -S(r)^\top$. This yields the error dynamics

$$\dot{\tilde{\eta}}_v = -S(r)\tilde{\eta}_v + \tilde{\nu} \tag{35a}$$
$$M\dot{\tilde{\nu}} = \tau + \rho(\eta, \nu) + d(t) - Ma_d. \tag{35b}$$

To achieve disturbance rejection by AFF, we propose the following control law

$$\tau = \Gamma - \Delta \tag{36}$$

where $\Gamma : \mathbb{R}_{\geq 0} \times \mathbb{R}^n \times \mathbb{R}^n \to \mathbb{R}^n$ is a nominal control law, and $\Delta \in \mathbb{R}^n$ is a dynamic disturbance attenuation state. Correspondingly, $\varepsilon := d(t) - \Delta$ defines a disturbance rejection error signal.

A. Nominal tracking design

We consider first the nominal design, where ε is considered a disturbance input from which we want to render the system input-to-state stable (ISS). The design of the term Δ is left for later. The objective is thus to design a nominal control law for Γ that renders the closed-loop system UGES for the case $\varepsilon = 0$ and ISS for $\varepsilon \neq 0$.

A common approach to achieve UGES is to apply a backstepping-based transformation of the state. Accordingly, we define the linear state transformation $z := \mathrm{col}(z_1, z_2)$ with $z_1 := \tilde{\eta}_v$ and $z_2 := \tilde{\nu} + K_1 \tilde{\eta}_v$. Defining $\tilde{x} := \mathrm{col}(\tilde{\eta}_v, \tilde{\nu})$, and letting $K_1 = K_1^\top > 0$ and $K_2 = K_2^\top > 0$ be feedback gain matrices, we get the following proposition based on conventional backstepping.

Proposition IV.1. There exist positive constants k, λ, and γ such that the solutions of the closed-loop system (35) with the control (36) and

$$\begin{aligned}\Gamma = &- [I + K_2 K_1 - M K_1 S(r)]\, \tilde{\eta}_v \\ &- [K_2 + M K_1]\, \tilde{\nu} - \rho(\eta, \nu) + M a_d,\end{aligned} \tag{37}$$

satisfies the uniform bound

$$|\tilde{x}(t)| \leq \max\left\{ k\, |\tilde{x}(t_0)|\, e^{-\lambda(t-t_0)},\ \gamma \sup_{t_0 \leq \tau \leq t} \|\varepsilon(\tau)\| \right\}. \tag{38}$$

Proof. The control law (37) can be rewritten in the z-states as

$$\begin{aligned}\Gamma = &- z_1 - K_2 z_2 - \rho(\eta, \nu) + M a_d \\ &- M K_1 \left(\tilde{\nu} - S(r) \tilde{\eta}_v\right),\end{aligned} \tag{39}$$

such that the closed-loop system becomes

$$\dot{z}_1 = -S(r) z_1 - K_1 z_1 + z_2 \tag{40a}$$

$$M \dot{z}_2 = -z_1 - K_2 z_2 + \varepsilon. \tag{40b}$$

Differentiating the Lyapunov function

$$V(z) = \frac{1}{2} z_1^\top z_1 + \frac{1}{2} z_2^\top M z_2 \tag{41}$$

along the solutions of (40), we get

$$\begin{aligned}\dot{V} &= -z_1^\top K_1 z_1 - z_2^\top K_2 z_2 + z_2^\top \varepsilon \\ &\leq -2 c_3 |z|^2 + |z|\, |\varepsilon| \\ &\leq -c_3 |z|^2, \qquad \forall\, |z| \geq \frac{1}{c_3} |\varepsilon|\end{aligned} \tag{42}$$

where $c_3 = \frac{1}{2} \lambda_{\min}(K_1, K_2)$. We also have $c_1 |z|^2 \leq V(z) \leq c_2 |z|^2$ where $c_1 = \frac{1}{2} \min\{1, \lambda_{\min}(M)\}$ and $c_2 = \frac{1}{2} \max\{1, \lambda_{\max}(M)\}$. It follows from ISS theorems [23, Theorem 4.6] that the solutions in the z-coordinates satisfy

$$|z(t)| \leq max\left\{ \sqrt{\frac{c_2}{c_1}} |z(t_0)| e^{-\frac{c_3}{c_2}(t-t_0)}, \frac{c_2}{c_1 c_3} \sup_{t_0 \leq \tau \leq t} \|\varepsilon(\tau)\| \right\}. \tag{43}$$

The state transformation can be written $z = T\tilde{x}$ where

$$T := \begin{bmatrix} I & 0 \\ K_1 & I \end{bmatrix}, \qquad T^{-1} = \begin{bmatrix} I & 0 \\ -K_1 & I \end{bmatrix}, \tag{44}$$

and

$$T^\top T = \begin{bmatrix} I + K_1^\top K_1 & K_1^\top \\ K_1 & I \end{bmatrix} > 0. \tag{45}$$

Letting $\sigma_1 := \sqrt{\lambda_{\min}(T^\top T)}$ and $\sigma_2 := \sqrt{\lambda_{\max}(T^\top T)}$ gives[1] the equivalence relation

$$\sigma_1 |\tilde{x}| \leq |z| \leq \sigma_2 |\tilde{x}|. \tag{46}$$

For the exponential convergence bound in (43) we get

$$|\tilde{x}(t)| \leq \frac{\sigma_2}{\sigma_1} \sqrt{\frac{c_2}{c_1}}\, |\tilde{x}(t_0)|\, e^{-\frac{c_3}{c_2}(t-t_0)}, \tag{47}$$

and for the input bound we get

$$|\tilde{x}(t)| \leq \frac{c_2}{\sigma_1 c_1 c_3} \sup_{t_0 \leq \tau \leq t} \|\varepsilon(\tau)\|. \tag{48}$$

Hence, we take $k = \frac{\sigma_2}{\sigma_1} \sqrt{\frac{c_2}{c_1}}$, $\lambda = \frac{c_3}{c_2}$, and $\gamma = \frac{c_2}{\sigma_1 c_1 c_3}$. □

A slightly different control law can be derived from LgV-backstepping [24].

Proposition IV.2. There exist positive constants k, λ, and γ such that the solutions of the closed-loop system (35) with the control (36) and

$$\begin{aligned}\Gamma = &- [K_2 K_1 - M K_1 S(r)]\, \tilde{\eta}_v - [K_2 + M K_1]\, \tilde{\nu} \\ &- \rho(\eta, \nu) + M a_d,\end{aligned} \tag{49}$$

satisfies the uniform bound (38), where $K_1 = C_1 + \kappa_1 I$ and $K_2 := C_2 + \frac{1}{4\kappa_1} I$ with $C_1 = C_1^\top > 0$, $C_2 = C_2^\top > 0$, and $\kappa_1 > 0$.

Proof. We use $z = \mathrm{col}(z_1, z_2)$, $z = T\tilde{x}$ where T is defined by (44), such that the control law (49) becomes

$$\Gamma = -K_2 z_2 - \rho + M a_d - M K_1 \left(\tilde{\nu} - S \tilde{\eta}_v\right), \tag{50}$$

such that the closed-loop system becomes

$$\dot{z}_1 = -S(r) z_1 - K_1 z_1 + z_2 \tag{51a}$$

$$M \dot{z}_2 = -K_2 z_2 + \varepsilon. \tag{51b}$$

Differentiating the Lyapunov function (41) along the solutions of (51), we get

$$\begin{aligned}\dot{V} &\leq -z_1^\top C_1 z_1 - z_2^\top C_2 z_2 + z_2^\top \varepsilon \\ &\leq -\bar{c}_3 |z|^2, \qquad \forall\, |z| \geq \frac{1}{\bar{c}_3} |\varepsilon|\end{aligned} \tag{52}$$

where $\bar{c}_3 = \frac{1}{2} \lambda_{\min}(C_1, C_2)$. The proof hereafter follows the proof of Proposition IV.1, resulting in the constants $k = \frac{\sigma_2}{\sigma_1} \sqrt{\frac{c_2}{c_1}}$, $\lambda = \frac{\bar{c}_3}{c_2}$, and $\gamma = \frac{c_2}{\sigma_1 c_1 \bar{c}_3}$. □

Contrary to (40), we notice that the closed-loop system (51) makes out a cascade, where the z_2-subsystem for $\varepsilon = 0$ independently converges exponentially to zero while driving the exponentially stable z_1-subsystem. The disturbance rejection error ε will affect this exponential convergence, where ε is first lowpass-filtered through the z_2-dynamics with steady-state gain K_2^{-1} before affecting the tracking error $z_1 = \tilde{\eta}_v$.

[1] Note that σ_1 and σ_2 correspond to the minimum and maximum singular values of $T^\top T$.

B. Closing the loop with disturbance rejection

While the static part of the control law is given by (36) with either (37) or (49), we will now consider a dynamic filtered design to make the disturbance rejection AFF term Δ track the disturbance $d(t)$ as closely as possible. Towards this end we will apply the 3 DOF dynamic acceleration signal vector $a(t) = \dot{\nu}(t) \in \mathbb{R}^3$ as a feedforward signal for disturbance rejection.

By applying (36) with either of the control laws in propositions IV.1 or IV.2, we get the error dynamics

$$\dot{z} = A(r)z + B\varepsilon \tag{53}$$

where $A(r)$ and B are defined from (40) or (51), respectively. Moreover, letting $P := \frac{1}{2}\operatorname{diag}(I, M)$ and $Q := \operatorname{diag}(K_1, K_2)$ for (42) or $Q := \operatorname{diag}(C_1, C_2)$ for (52), then in both cases above we have

$$V(z) = z^\top P z \tag{54}$$

$$\dot{V} \leq -z^\top Q z + 2z^\top P B \varepsilon, \tag{55}$$

and we have shown that the system is UGES for $\varepsilon = 0$ and ISS with linear gain from ε as input.

1) Direct filtered design: With ε defined above as the disturbance rejection error state, we get

$$\dot{\varepsilon} = -\dot{\Delta} + \dot{d}(t). \tag{56}$$

Noting that

$$\varepsilon = d - \Delta = Ma(t) - \Gamma - \rho(\eta, \nu) \tag{57}$$

is an available feedforward signal due to the acceleration measurement, this gives the immediate choice

$$\dot{\Delta} = \mu\left(Ma(t) - \Gamma - \rho(\eta, \nu)\right) \tag{58a}$$

$$= \mu\varepsilon \tag{58b}$$

$$= -\mu\left(\Delta - d(t)\right) \tag{58c}$$

which results in the closed-loop system (53) and

$$\dot{\varepsilon} = -\mu\varepsilon + \dot{d}(t). \tag{59}$$

Theorem IV.1. The origin $(z, \varepsilon) = (0, 0)$ of the closed-loop system (53) and (59) is UGES for $\dot{d}(t) = 0$ and ISS with $\dot{d}(t)$ as a bounded input.

Proof. UGES of the origin for $\dot{d} = 0$ is concluded since the closed-loop error system (53) and (59) is a cascade of two UGES subsystems connected with linear gain [23, Appendix C]. From converse Lyapunov theorems [23] there then exists a quadratic Lyapunov function, which becomes an ISS-Lyapunov function with $\dot{d}$ as input. □

With the disturbance rejection filter (58), Δ will attempt to track $d(t)$ with accuracy dependent on the gain μ. If $\dot{d}(t) = 0$ then Δ will exponentially converge to and track d as a type of integral action. For $\dot{d}$ nonzero there will be a tracking error, tunable by the gain μ; however, the previous section shows that the nominal DP control laws (37) or (49) render the DP closed-loop system robust to this deviation.

Another choice is to define the CLF

$$W(z, \varepsilon) := V(z) + \frac{1}{2\mu}\varepsilon^\top\varepsilon. \tag{60}$$

Taking the total time derivative along (53) and (59) yields

$$\dot{W} \leq -z^\top Q z + \varepsilon^\top\left(\frac{1}{\mu}\dot{d} - \frac{1}{\mu}\dot{\Delta} + 2B^\top P z\right).$$

Noting that $PB = \frac{1}{2}\operatorname{col}(0, I)$, we assign

$$\dot{\Delta} = \mu\left[Ma(t) - \Gamma - \rho(\eta, \nu) + z_2\right] \tag{61a}$$

$$= \mu\left[\varepsilon + z_2\right] \tag{61b}$$

$$= -\mu\left(\Delta - d(t)\right) + z_2, \tag{61c}$$

which gives

$$\dot{W} \leq -z^\top Q z - \varepsilon^\top\varepsilon + \frac{1}{\mu}\varepsilon^\top\dot{d}. \tag{62}$$

The resulting closed-loop error system becomes (53) and

$$\dot{\varepsilon} = -\mu\varepsilon - \mu z_2 + \dot{d}. \tag{63}$$

Theorem IV.2. The origin $(z, \varepsilon) = (0, 0)$ of the closed-loop system (53) and (63) is UGES for $\dot{d}(t) = 0$ and ISS with $\dot{d}(t)$ as a bounded input.

Proof. The conclusion follows from $W(z, \varepsilon)$ being a quadratic ISS-Lyapunov function with $\dot{d}$ as input. □

2) Filtered design based on a disturbance model: Suppose the disturbance is generated by an exogenous model

$$\dot{\xi} = A_d\xi + E_d w \tag{64a}$$

$$d = C_d\xi \tag{64b}$$

where $\xi \in \mathbb{R}^q$, $q \geq 3$, is the disturbance state, d is the output that affects the DP control system, w is Gaussian white noise, (A_d, E_d, C_d) are linear matrices, and (C_d, A_d) is an observable pair.

Assuming $w = 0$, we design a Luenberger-type disturbance observer

$$\dot{\hat{\xi}} = A_d\hat{\xi} + L_d\varepsilon \tag{65a}$$

$$\Delta = C_d\hat{\xi}, \tag{65b}$$

where the injection signal $\varepsilon = C_d\tilde{\xi} = C_d(\xi - \hat{\xi})$ is generated from (57), and L_d is designed such that $F_d := A_d - L_dC_d$ is Hurwitz. Correspondingly, let $P_d = P_d^\top > 0$ satisfy $P_dF_d + F_d^\top P_d = -Q_d$. This gives the closed-loop system

$$\dot{z} = A(r)z + BC_d\tilde{\xi} \tag{66a}$$

$$\dot{\tilde{\xi}} = F_d\tilde{\xi}. \tag{66b}$$

Theorem IV.3. The origin $(z, \tilde{\xi}) = (0, 0)$ of the closed-loop system (66) is UGES.

Proof. A cascade of two UGES subsystems connected through a linear gain is UGES [23, Appendix C]. □

We note that the disturbance rejection filter (65) can be rewritten as

$$\dot{\hat{\xi}} = F_d\hat{\xi} + L_d d(t) \tag{67a}$$

$$\Delta = C_d\hat{\xi}. \tag{67b}$$

Comparing this to the direct filter design in (58), we recognize $C_d = I$, $L_d = \mu I$, and $A_d = 0$ (such that $F_d = -\mu I$). This

indicates that (65) is a general filter that, even if the model (64) is uncertain or unknown, can be designed to improve the filtering performance of the acceleration feedforward-based injection signal ε from (57). However, the more accurately (64) models the disturbance, the better tracking of the disturbance is achieved.

C. A note on the separation principle

Since the vessel dynamics (18) is nonlinear and the control law and state observer is used together in a separation principle, the stability of the complete feedback loop must be considered. Stability follows in our case directly from [23, Appendix C] as the UGES control law and the UGES state observer are cascaded.

V. DP IN ICE CASE STUDY

When marine vessels interact with high concentrations of sea-ice (above 6/10th surface coverage), the dynamics are substantially different from open water conditions, and conventional open water DP systems are known to be insufficient [3], [18], [25]–[27]. However, full-scale, model-scale, and numerical experiments have demonstrated that high-uptime positioning is possible given feasible ice conditions and a reactive DP system [26], [28]–[31]. The first is ensured by an icebreaker support fleet that breaks up the incoming natural ice cover and creates a channel of small ice floes for the protected DP vessel to operate in. A reactive DP system can be synthesized by removing the wave filtering and retuning the control system more aggressively [5]. However, since this is based on a simplified open water model lacking the complex and rapidly varying ice dynamics, it will struggle to track and counteract the external loads as these increase. In [32], [33] this problem is alleviated by assuming an accurate ice load measurement. However, practical and reliable measurement systems are not available today. Neither are sufficiently accurate control models capturing the ice dynamics [27], [34]. One reason for this is that the ice loads depend on the complex in-situ state and properties of the ice floes in direct and indirect contact with the vessel. As the presented AFF methodology avoids the ice load specific measurement and modelling challenges, it is seen as a candidate solution for a reactive system.

A. Preliminaries

This study is divided into two cases. The first investigates a dataset from a model scale experiment performed at the Hamburg Ship Model Basin (HSVA) as a part of the European research and development project DYnamic Positioning in ICe (DYPIC). Project overviews can be can be found in [35], [36]. The second case is a closed-loop numerical simulation using a state-of-the-art high-fidelity numerical program.

For both cases the conceptual and experimentally tested Arctic drillship (ADS) is considered. This was one of two vessels tested during DYPIC, and it is seen in Figure 7. Its main particulars and azimuth thruster arrangement are found in tables II and III. In the model ice basin at HSVA the position and orientation of the vessel was measured using a Qualisys position reference system. The linear accelerations and rotation rates were measured using an onboard IMU, and the actuation output was measured by load cells in each thruster. All data were logged with 50 Hz. Further description of the ADS is found in [27].

Fig. 7. The model scale Arctic Drillship during experimental testing at HSVA. Courtesy of DYPIC.

TABLE II
THE ADS MAIN PARTICULARS. FS DENOTES FULL SCALE, MS MODEL SCALE.

Parameter	FS	MS
Length in design waterline (m)	197.73	6.67
Length between perp. (m)	184	6.13
Breath, moudled (m)	41.33	1.37
Draught at design waterline (m)	12	0.4
Stem angle at design waterline (°)	45	45
Frame angle at midship (°)	45	45
Displacement volume (m^3)	68457	2.535
Centre of gravity from aft. p. (m)	95.34	3.18
Block coefficient	0.75	0.75
Metacentric height (m)	10.71	0.357
Total thrust (N)	$7.2{\cdot}10^6$	270

B. Case 1: Open-loop disturbance estimation

Model scale trials in ice basins are often used since full scale trials are both impracticality and expensive as it is performed in an uncontrollable environment [3], [37], [38]. The foundation for this part of the case study is the free floating DP experiment 5200 dataset. This was a free floating DP

TABLE III
THE ADS AZIMUTH THRUSTER ARRANGEMENT.

No.	Comment	x [mm]	y [mm]	F_{max} [N]
1	Port-Bow	2272	316	45
2	Center-Bow	2644	0	45
3	Stb-Bow	2272	-316	45
4	Center-Stern	-3102	0	45
5	Port-Stern	-2664	190	45
6	Stb-Stern	-2664	-190	45

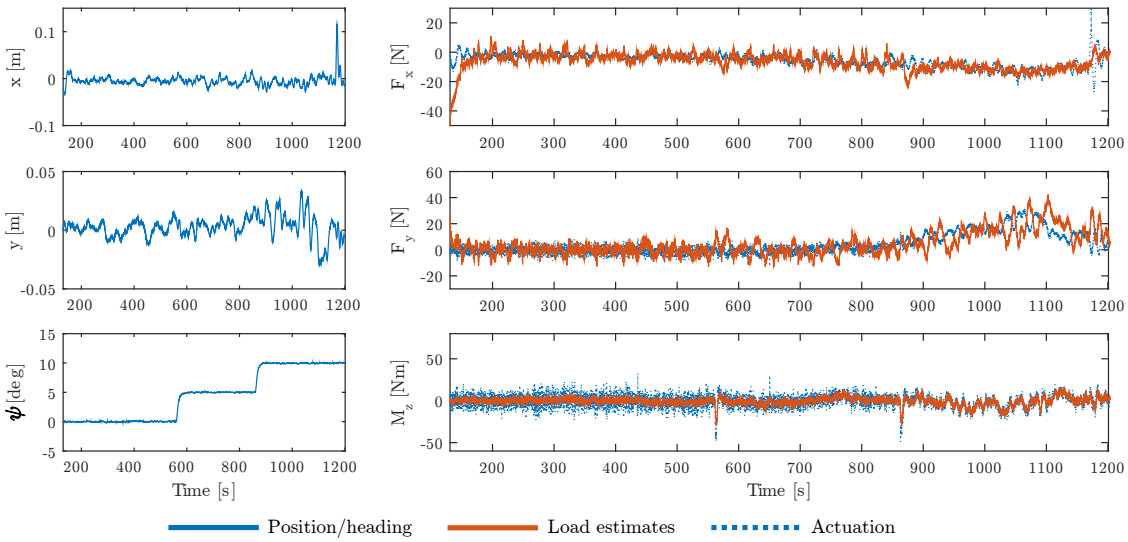

Fig. 8. Left: the recorded position and heading of DYPIC experiment 5200 with respect to the moving reference frame. Right: the body frame open-loop disturbance estimates compared to the vessel actuation (in opposite sign for eased interpretation). All data in model scale.

TABLE IV
DYPIC EXPERIMENT 5200 ICE FIELD PROPERTIES.

Property	Value
Ice concentration	70 %
Ice thickness	0.025 m
Min floe size	0.5 x 0.5 m
Max floe size	1.5 x 1.5 m
Ice drift velocity	0.047 m/s

TABLE V
DYPIC EXPERIMENT 5200 DP SETPOINT SEGMENTATION.

No.	Setp. (x [m] ,y [m],ψ [deg])	Length [m]
1.	0, 0, 0°	17
2.	0, 0, 5°	17
3.	0, 0, 10°	17

test where the vessel tracked a reference frame moving with constant velocity through the basin. A commercial ice-adapted DP system controlled the vessel. As the vessel progressed in the basin, the heading setpoint was altered to obtain an oblique angle with respect to the ice drift. It should also be mentioned that the vessel maintained position and heading within allowed tolerances, for all setpoints. However, the ice conditions were relatively mild and the ice concentration then allows the ice floes to be pushed away, rather than broken or rafted by the advancing ship. Key experimental parameters are given in tables IV and V. For a more in-depth treatment of the experimental setup, see [27].

As the ADS IMU only contained one accelerometer, the rotational components of the acceleration vector could not be determined. However, the short IMU lever arm together with an experimental setup catering for low rotational rates enables to assume that the measured linear accelerations are close to the ones at CO. Thus, a Kalman filter applying a subset of the model (30a)-(30d) was implemented. To get an idea of the angular acceleration a differentiation of the IMU gyro measurement was performed.

The load estimation was performed using the following filter, derived from (58a) by employing the τ actuation signal and assuming $\rho(\eta, \nu) = 0$,

$$\dot{\Delta} = \mu(Ma(t) - \tau_o - \Delta) \tag{68}$$

where $\Delta \in \mathbb{R}^3$ is the disturbance estimate, and $\tau_o \in \mathbb{R}^3$ is the measured actuation vector. For this case study $\mu = 1$ was used.

Figure 8 shows the recorded position and heading of the vessel in the moving reference frame and the planar loads found by the open-loop disturbance estimation compared to the actuation output. It can be seen that the estimates correspond well with the actuation level, but are not identical. This may be attributed to the fact that the vessel experienced perturbations which were not effectively handled by the control system, causing minor deviation from the setpoint (as seen in the position and heading data). These are especially evident towards the end of the experiment in y. Interestingly, the AFF load estimates seem to capture the disturbances. The physical explanation for the increase in load and variation is compaction of the ice cover as the vessel advances towards the end of the basin.

The results indicates that the methodology is able to estimate the dynamic acceleration from an accelerometer with the previously mentioned challenges, and calculate the external load including rapidly varying dynamics. However, no definitive verification of the method is possible with this dataset as no independent measurement system was used.

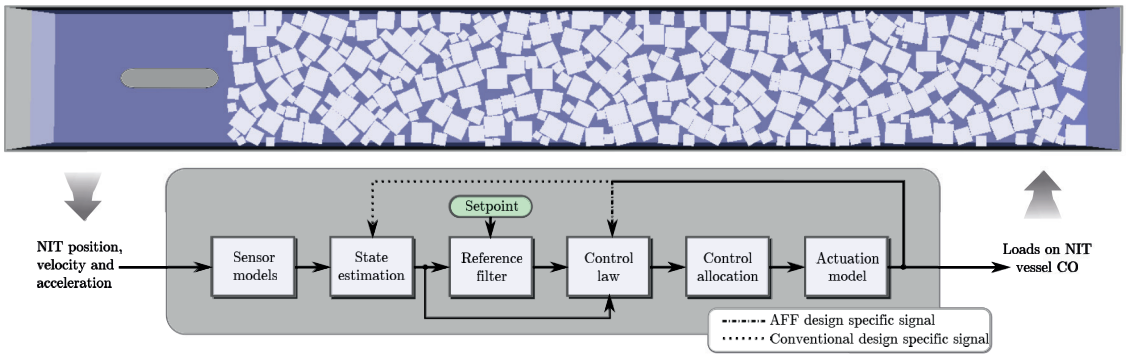

Fig. 9. Illustration featuring a rendering from the numerical ice tank indicating the experimental setup, and the overall topology of the simulation program.

C. Case 2: Closed-loop simulation

This study uses the DP in ice development framework featured in [5]. It closes the loop between a control system and the numerical model of [39], which hereafter will be referred to as the Numerical Ice Tank (NIT). Figure 9 provides an overview. As the aforementioned references treat both the setup in-depth, only a brief summary is given together with the case setup.

The NIT computes the vessel's dynamics in 6 DOF without wind and waves using a physics engine with tailored routines for ice material modelling. Each simulation is comprised of the following five interconnected elements: the vessel, the towing carriage, the ice floes, the water volume, and the ice tank boundaries. The vessel is simulated as a rigid body in 6 DOF without deformations. The towing carriage is not used in this paper as only free-floating DP mode is considered. The ice floes are simulated as breakable bodies with uniform thickness in 6 DOF. The initial ice floe sizes and floe positions are generated by an ice field generation algorithm that aims to produce a specified ice field. The water is simulated as a static plane that produces buoyancy and drag loads on the vessel and the ice floes.

The motion variables of the vessel in NIT are defined in three reference frames: the tank-fixed frame $\{t\}$ which is non-rotational and fixed to the stationary tank boundaries; the body frame $\{b\}$ which is fixed to the vessel; and the ice floe frames $\{i\}$ which are fixed to each individual ice floe. For DP, a fourth reference frame, the positioning frame $\{n\}$, is introduced. This is non-rotational and follows a pre-defined trajectory to simulate ice drift in the stationary ice cover. For DP development, $\{n\}$ is considered inertial, and in this study the DP vessel will be set to track a fixed setpoint in this frame. This approximation is common for simulating ice drift in ice tank testing [36].

The sensor models simulate onboard equipment for measuring the motions of the vessel. They are implemented by first transforming the NIT vessel motion output (i.e. position, orientation, linear velocity, and angular rate) from $\{t\}$ to $\{n\}$ and $\{b\}$. Then, sensor dynamics and noise are added to the signals. The accelerometers are simulated realistically with both gravity and bias errors. The actuator models implement the dynamics of the thruster system onboard the vessel. This is approximated with first order dynamics as described by [2].

TABLE VI
PLACEMENT OF ACCELEROMETERS IN THE ADS RELATIVE TO CO FOR THE NUMERICAL SIMULATION.

ACC nr.	X [m]	Y [m]	Z [m]	Note
1	3	0	0.3	Bow
2	0	0.6	0	Starboard
3	-3	0	0.3	Stern
4	0	-0.6	0	Port

TABLE VII
NUMERICAL SIMULATION ICE CONDITIONS.

Parameters	Value	Unit
Water density	1000	kg/m^3
Ice density	900	kg/m^3
Ice flexural strength	45.9	kPa
Ice compressive strength	92	kPa
Ice elastic modulus	10	Mpa
Ice concentration	85	%
Ice thickness	40	mm
Ice drift velocity	0.047	m/s
Max. floe size	1.5	m
Min. floe size	0.5	m

Two control systems are compared, one with AFF using the accelerometer configuration as seen in Table VI, a state observer as described in Section III-C, the control law of Proposition 4.2, and the direct disturbance rejection filter in (68). For comparison, a state-of-the-art nonlinear PID-type (nPID) control law combined with a nonlinear DP observer, both adapted to ice conditions as described in [5]. In practice this is a more aggressively tuned DP controller where the wave filter has been removed. The challenges with such a control system in harsh environments has been covered above. Two simulations are run with identical ice covers. One for each control system.

The control objective of the scenario is identical to that of experiment 5200. However, the ice concentration is more severe which constitute a significantly more challenging operational environment than in the model scale experiment. A summary of the ice parameters used are found in Table VII.

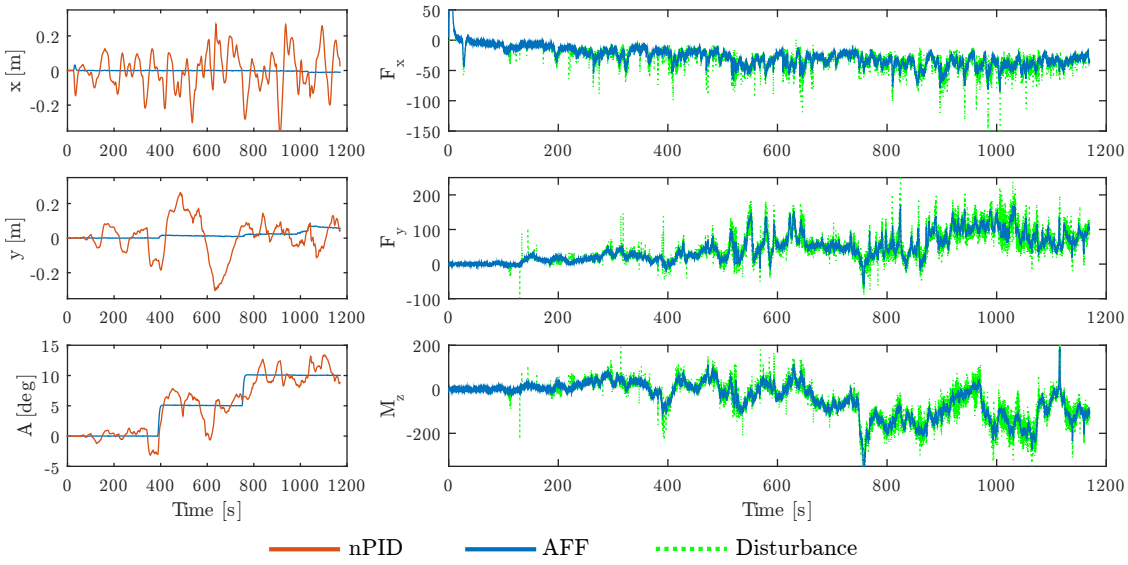

Fig. 10. Left: Comparison between ice-adapted nPID and the proposed AFF controller. Right: The estimated disturbance by the rejection filter compared to the simulated disturbance.

The simulation results are shown in Figure 10 where the left column present the position and heading accuracy. This shows that the positioning capabilities of AFF system outperforms the nPID. The right column of Figure 10 presents the disturbance estimation accuracy of the AFF system. It shows that it is able to track and filter the external load well.

VI. Conclusions

This paper presented a control system design that uses acceleration measurements for rigid body marine motion control subject to harsh environments. The challenges of obtaining a full state measure of the dynamic acceleration was addressed with a setup of four accelerometers placed in a specific configuration that serves as input to the state observer. The main contribution of the paper is the novel method for integrating the dynamic acceleration as an acceleration feedforward in the control law. The proposed design was investigated with both experimental data and high-fidelity simulations, both showing feasibility and effectiveness of the proposed control setup.

VII. Acknowledgments

Research partly funded by the Research Council of Norway (RCN) KMB project no. 199567: Arctic DP, with partners Kongsberg Maritime, Statoil, and DNV GL, and partly by RCN projects no. 203471: CRI SAMCoT and no. 223254: COE AMOS. Additionally, the authors would like to thank the MARTEC ERA-NET project: DYPIC - Dynamic positioning in ice covered waters (RCN Project no. 196897), which supplied experimental data from the Hamburg Ship Model Basin, and PhD Ivan Metrikin for providing the numerical model and great support.

References

[1] T. I. Fossen, *Handbook of Marine Craft Hydrodynamics and Motion Control*. Wiley, 2011.

[2] A. J. Sørensen, *Marine Control Systems: Propulsion and Motion Control of Ships and Ocean Structures*. Department of Marine Technology, NTNU, Norway, 2012.

[3] N. A. Jenssen, S. Muddesitti, D. Phillips, and K. Backstrom, "DP In Ice Conditions," in *Dynamic Positioning Conference, Houston, Texas, USA*, 2009.

[4] D. Bray, *The DP Operator's Handbook*. The Nautical Institute, 2011.

[5] Ø. Kjerstad and R. Skjetne, "Modeling and Control for Dynamic Positioned Marine Vessels in Drifting Managed Sea Ice," *Modeling, Identification and Control*, 2014.

[6] R. Skjetne, L. Imsland, and S. Løset, "The Arctic DP Research Project: Effective Stationkeeping in Ice," *Modeling, Identification and Control*, 2014.

[7] International Maritime Organization, *Guidelines for Vessels with Dynamic Positioning Systems*, June 1994, MSC/circ.645.

[8] D. Titterton and J. Weston, *Strapdown Inertial Navigation Technology, Second Edition (Progress in Astronautics and Aeronautics)*. AIAA, 2005.

[9] K.-P. W. Lindegaard, "Acceleration feedback in dynamic positioning," Ph.D. dissertation, Norwegian University of Science and Technology, 2003.

[10] Ø. Kjerstad, R. Skjetne, and N. A. Jenssen, "Disturbance rejection by acceleration feedforward: Application to dynamic positioning," in *Proceedings of IFAC World Congress, Milan, Italy*, 2011.

[11] Ø. Kjerstad and R. Skjetne, "Observer design with disturbance rejection by acceleration feedforward," in *Proceedings of ROCOND12, Aalborg, Denmark*, 2012.

[12] P. Batista, C. Silvestre, and P. Oliveira, "On the observability of linear motion quantities in navigation systems," *Systems & Control Letters*, vol. 60, no. 2, pp. 101 – 110, 2011.

[13] A. Buhmann, C. Peters, M. Cornils, and Y. Manoli, "A GPS aided Full Linear Accelerometer Based Gyroscope-free Navigation System," in *Position, Location, And Navigation Symposium, 2006 IEEE/ION*, 2006, pp. 622–629.

[14] C.-W. Tan and S. Park, "Design of accelerometer-based inertial navigation systems," *Instrumentation and Measurement, IEEE Transactions on*, vol. 54, no. 6, pp. 2520–2530, 2005.

[15] B. Zappa, G. Legnani, A. van den Bogert, and R. Adamini, "On the Number and Placement of Accelerometers for Angular Velocity and Acceleration Determination," *Transactions of the ASME*, 2001.
[16] Kongsberg Maritime AS, "MRU 5+ - The ultimate marine motion sensor," Brochure, 2014.
[17] Parker Maritime AS, "R/V Gunnerus Summary Report," Technical Report, 2013.
[18] S. Kerkeni, X. Dal Santo, and I. Metrikin, "Dynamic Positioning in Ice - Comparison of Control Laws in Open Water and Ice," in *Proceedings of the 32nd Int. Conf. Ocean, Offshore and Arctic Engineering*, 2013.
[19] R. E. Kalman and R. S. Bucy, "New results in linear filtering and prediction theory," *Transactions of the ASME. Series D, Journal of Basic Engineering*, vol. 83, pp. 95–107, 1961.
[20] J.-P. Gauthier and I. Kupka, *Deterministic Observation Theory and Applications*. Cambridge University Press, 2001.
[21] G. Besançon, "Observer design for nonlinear systems," in *Advanced Topics in Control Systems Theory: Lecture Notes from FAP 2005 (Lecture Notes in Control and Information Sciences)*. Springer, 2006.
[22] P. Batista, C. Silvestre, P. Oliveira, and B. Cardeira, "Accelerometer calibration and dynamic bias and gravity estimation: Analysis, design, and experimental evaluation," *Control Systems Technology, IEEE Transactions on*, vol. 19, no. 5, pp. 1128–1137, 2011.
[23] H. K. Khalil, *Nonlinear Control*. Pearson Education Ltd., 2015.
[24] M. Arcak and P. Kokotović, "Redesign of backstepping for robustness against unmodelled dynamics," *IJRNC*, vol. 11, no. 7, pp. 633–643, 2001, robustness in identification and control.
[25] A. Gürtner, B. H. H. Baardson, G.-O. Kaasa, and E. Lundin, "Aspects of importance related to Arctic DP operations," in *Proceedings of the ASME 2012 31st International Conference on Ocean, Offshore and Arctic Engineering OMAE2012, July 1-6, 2012, Rio de Janeiro, Brazil*, 2012.
[26] T. Hals and N. A. Jenssen, "DP ice model tests of Arctic drillship and polar research vessel," in *Proceedings of the ASME 2012 31st International Conference on Ocean, Offshore and Arctic Engineering OMAE2012, July 1-6, 2012, Rio de Janeiro, Brazil*, 2012.
[27] Ø. Kjerstad, I. Metrikin, S. Løset, and R. Skjetne, "Experimental and phenomenological investigation of dynamic positioning in managed ice," *Cold Regions Science and Technology*, vol. 111, pp. 67–79, 2015.
[28] A. Keinonen and E. H. Martin, "Modern day pioneering and its safety in the floating ice offshore," in *Proceedings of the International Conference and Exhibition on Performance of ships and structures in ice*, vol. 1, 2012.
[29] P. Liferov, "Station-keeping in ice - normative requirements and informative solutions," in *Proc. Arctic Technology Conference 2014, Houston, Texas, USA*, 2014.
[30] I. Metrikin, S. Løset, N. A. Jenssen, and S. Kerkeni, "Numerical Simulation of Dynamic Positioning in Ice," *Marine Technology Society Journal*, vol. 47, no. 2, pp. 14–30, 2013.
[31] Å. Rohlén, "Relationship Between Ice-Management and Station Keeping in Ice." Presentation at Dynamics Positioning Conference, Houston, Texas, USA, 2009.
[32] D. T. Nguyen, A. H. Sørbø, and A. J. Sørensen, "Modelling and control for dynamic positioned vessels in level ice," in *Proceedings of Conference on Manoeuvring and Control of Marine Craft*, 2009, pp. 229 – 236.
[33] D. H. Nguyen, D. T. Nguyen, S. T. Quek, and A. J. Sørensen, "Position-moored drilling vessel in level ice by control of riser end angles," *Cold Regions Science and Technology*, vol. 66, no. 2–3, pp. 65 – 74, 2011.
[34] K. J. Eik, "Ice Management in Arctic Offshore Operations and Field Developments," Ph.D. dissertation, Norwegian University of Science and Technology, Trondheim, Norway, 2010.
[35] N. A. Jenssen, T. Hals, A. Haase, X. Santo, S. Kerkeni, O. Doucy, A. Gürtner, S. S. Hetschel, P. O. Moslet, I. Metrikin, and S. Løset, "A Multi-National R&D Project on DP Technology in Ice," in *Proceedings of the Dynamic Positioning Conference, Houston, Texas, USA*, 2012.
[36] A. Haase and P. Jochmann, "Different ways of modeling ice drift scenarios in basin tests," in *Proceedings of the ASME 2013 32nd International Conference on Ocean, Offshore and Arctic Engineering, June 9-14, 2013, Nantes, France*, 2013.
[37] D. Deter, W. Doelling, L. Lembke-Jene, and A. Wegener, "Stationkeeping in solid drift ice," in *Dynamic Positioning Conference, Houston, Texas, USA*, 2009.
[38] W. L. Kuehnlein, "Philosophies for Dynamic Positioning in Ice-Covered Waters," in *Proceedings of Offshore Technology Conference, Houston, Texas, USA*, 2009.
[39] I. Metrikin, "A Software Framework for Simulating Stationkeeping of a Vessel in Discontinuous Ice," *Modeling, Identification and Control*, 2014.

Chapter 6

International Refereed Conference Papers

Description and Numerical Simulations of Dynamic Positioning in Reversing Managed Ice

POAC'15
Trondheim, Norway

Proceedings of the 23rd International Conference on
Port and Ocean Engineering under Arctic Conditions
June 14-18, 2015
Trondheim, Norway

DESCRIPTION AND NUMERICAL SIMULATIONS OF DYNAMIC POSITIONING IN REVERSING MANAGED ICE

Øivind Kåre Kjerstad[1], Ivan Metrikin[2,3] and Roger Skjetne[1]
[1]Dept. of Marine Technology, Norwegian University of Science and Technology
[2] Dept. of Civil and Transport Engineering, Norwegian University of Science and Technology
[3]Arctic Design and Operations, Statoil ASA, Trondheim, Norway

ABSTRACT

This paper discusses and describes the design of dynamic positioning control systems for drifting managed sea ice environments. Compared to open water conditions, the presence of ice imposes complex dynamics on the motions of the vessel, which must be accounted for in the control algorithms. Foremost this relates to estimating and tracking variations of the global loads with sufficient precision, and, if possible, automatically vaning the vessel into the ice drift direction. In this paper, several approaches and design possibilities for this is explored, and two distinctly different designs are proposed. These are compared in a high-fidelity numerical tool which simulates the ship-ice interaction in managed ice. The case investigated is an 180 degree elliptic ice drift reversal with severe curvature, where the ice drift velocity decreases until the ellipse pivot point is reached, and then it increases again. Both proposed systems demonstrate positioning and vaning capabilities in moderate and severe ice conditions, but with different performance. These differences are discussed in the paper. Additionally, the study showcases the importance of using high-fidelity numerical models as a control system development tool.

INTRODUCTION

One of the major challenges faced by the oil and gas industry in the Arctic is that many undrilled prospects lie beyond the 100 m water-depth limit where sea ice intrusion is possible (Hamilton, 2011). Potential operations in those regions will require floating platforms with robust station-keeping capabilities. Existing solutions range from passive mooring systems without thruster use to fully automated dynamic positioning (DP) systems which automatically maintain position (fixed location or predetermined track) by the propulsion system of the vessel alone (IMO, 1994). Although it is expected that floating production units in the Arctic will be thruster-assisted moored structures, free floating DP solutions will still be an essential component of the operations. Such will be needed whenever short-term positioning is required. This encompasses, for instance, early hook up operations in the exploration phase, connection and disconnection from deployed moorings, and associated support and intervention. Furthermore, since thruster-assisted moored systems essentially are DP systems tailored and adapted to work with moorings, research on one topic will in many cases benefit both.

When vessels interact with high concentrations of sea ice (above 6/10th), the global loads are substantially different from open water conditions, and conventional open water DP systems

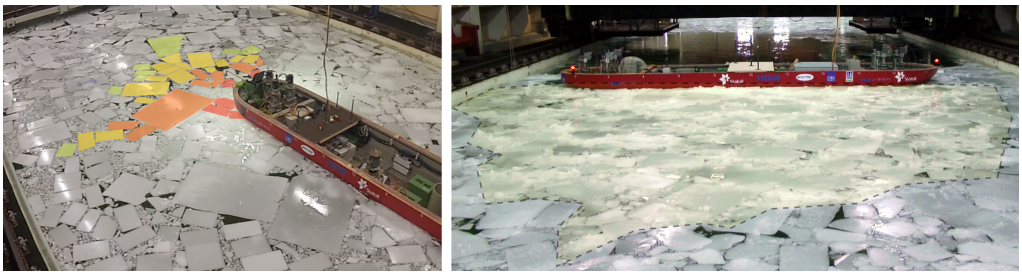

Figure 1. Left: Ice floe contact networks. Right: Accumulated ice mass. Both pictures are from the experimental testing at the Hamburg Ship Model Basin (HSVA). See Kjerstad et al. (2015) for further information.

are known to be insufficient (Kjerstad et al., 2015; Kerkeni et al., 2013a; Gürtner et al., 2012; Hals and Jenssen, 2012; Jenssen et al., 2009). Nevertheless, it has been demonstrated by full-scale, model-scale, and numerical experiments that high-uptime positioning is possible with ice management (IM) support (Rohlén, 2009; Keinonen and Martin, 2012; Hals and Jenssen, 2012; Metrikin et al., 2013; Liferov, 2014). Practically, this implies transforming the natural environment by a fleet of ice breaking vessels to a state where the global loads on the protected DP vessel are reduced (compared to no IM). Furthermore, it is critically important that the DP control system itself is able to tackle the complex and dynamic vessel-ice interactions. This may range from processes in the managed ice, such as *ice floe contact networks* and *accumulation of ice mass* (Kjerstad et al., 2015) (both seen in Figure 1), to ice pressure or challenging under-managed ice slipping by the IM fleet. From the control system perspective, efficient performance requires tracking and counteraction of the global loads, and application of an operational strategy that complies with (and, if possible, exploits) the ice interactions (Kjerstad et al., 2015).

Since the sea ice environment is substantially different from open water, the whole positioning system must be revised (Kjerstad et al., 2015). Issues range from winterization of sensory equipment, situation awareness and decision support for ice operations, tailored ice-capable actuators to the mentioned requirements to the DP control system. This paper focuses mainly on the latter, including selection of sensors systems, operational strategy, and design of the control algorithms. To gain further insight into the functionality of different control designs, a case study investigating an ice drift reversal scenario in managed ice is presented. The study is performed in the development platform described in (Kjerstad and Skjetne, 2014) which applies the numerical model presented in (Metrikin, 2014). Numerical models based on first principles describing the vessel and the ice floes as interacting bodies with their respective spatial geometries and material properties are considered necessary to simulate the complex vessel-ice and ice-ice interactions. These processes are not well captured in any other available model types (i.e. statistical or empirical models). Furthermore, experimental testing of scenarios which require significant space is challenging in the existing ice basins, because of the high scale factor needed for correct ice property scaling.

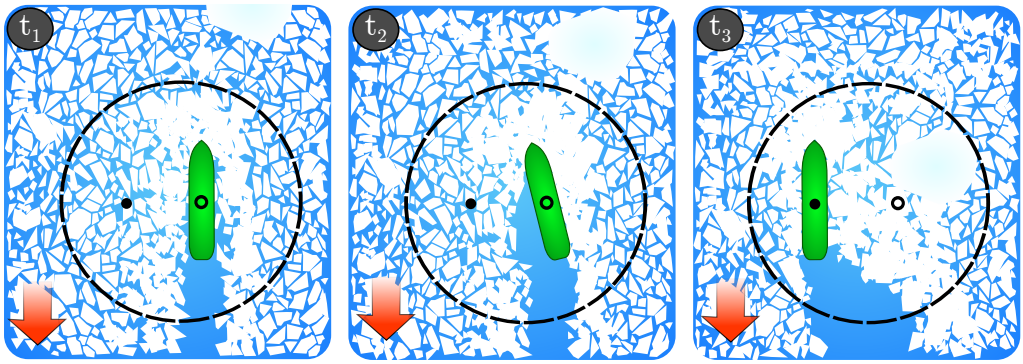

Figure 2. Illustration of manoeuvring to seek the weakest path through the ice, and corresponding utilization of the drifting sea ice for vessel actuation. At t_1, a potentially significant ice load feature is approaching the vessel, and the position is changed from the hollow circle to the full black circle. At t_2, the vessel has created an oblique angle while maintaining its upstream position to acquire an actuating starboard ice load. At t_3, the vessel has utilized the ice load to move into the new position and minimized the oblique angle to minimize the load, allowing the hazardous ice feature to pass.

DYNAMIC POSITIONING CONTROL DESIGN CONSIDERATIONS

The generalized 6 DOF equations of motion of a DP vessel can be written in the following form:

$$\dot{\boldsymbol{\eta}} = \mathbf{J}(\boldsymbol{\eta})\boldsymbol{\nu} \tag{1}$$

$$\mathbf{M}\dot{\boldsymbol{\nu}} = \boldsymbol{\tau}_{control} + \boldsymbol{\tau}_{hydro} + \boldsymbol{\tau}_{wind} + \boldsymbol{\tau}_{waves} + \boldsymbol{\tau}_{ice} \tag{2}$$

where $\boldsymbol{\eta} \in \mathbb{R}^6$ is the position and orientation vector expressed in an inertial frame, $\mathbf{J}(\boldsymbol{\eta}) \in \mathbb{R}^{6\times6}$ is the transformation matrix between the inertial frame and the body frame, $\boldsymbol{\nu} \in \mathbb{R}^{\mathbf{6}}$ is the body frame velocity vector, $\mathbf{M} \in \mathbb{R}^{6\times6}$ is the vessel rigid body mass matrix, $\boldsymbol{\tau}_{control} \in \mathbb{R}^6$ is the vessel actuation output, $\boldsymbol{\tau}_{hydro} \in \mathbb{R}^6$ is the hydrodynamic and hydrostatic loads acting on the vessel (including current loads), $\boldsymbol{\tau}_{wind} \in \mathbb{R}^6$ is the wind loads on the vessel, $\boldsymbol{\tau}_{waves}$ is the wave loads on the vessel, and $\boldsymbol{\tau}_{ice} \in \mathbb{R}^6$ is the global ice loads.

Normally, a DP system for a ship-shaped vessel in open water controls three out of the six DOFs (the planar position and the heading). The main reason for this is the fact that the remaining DOFs are inherently stable and do not need control. The fundamental challenge of the DP system is then to fulfill the so-called vessel control objective: track a fixed location (and heading) or predetermined track through the use of active thrusters (i.e. $\boldsymbol{\tau}_{ice}$). The same applies in ice. However, based on the phenomenological analysis in (Kjerstad et al., 2015), two additional control objectives for DP in managed ice are formulated:

- Minimize the oblique angle between the vessel and the ice.
- Minimize the transverse actuated motion of the vessel.

These objectives need to be fulfilled in order to reduce the global ice loads which are dictated by for instance ice floe interlocking and force chain formation in the ice floe contact networks, and added inertia of the accumulated ice mass.

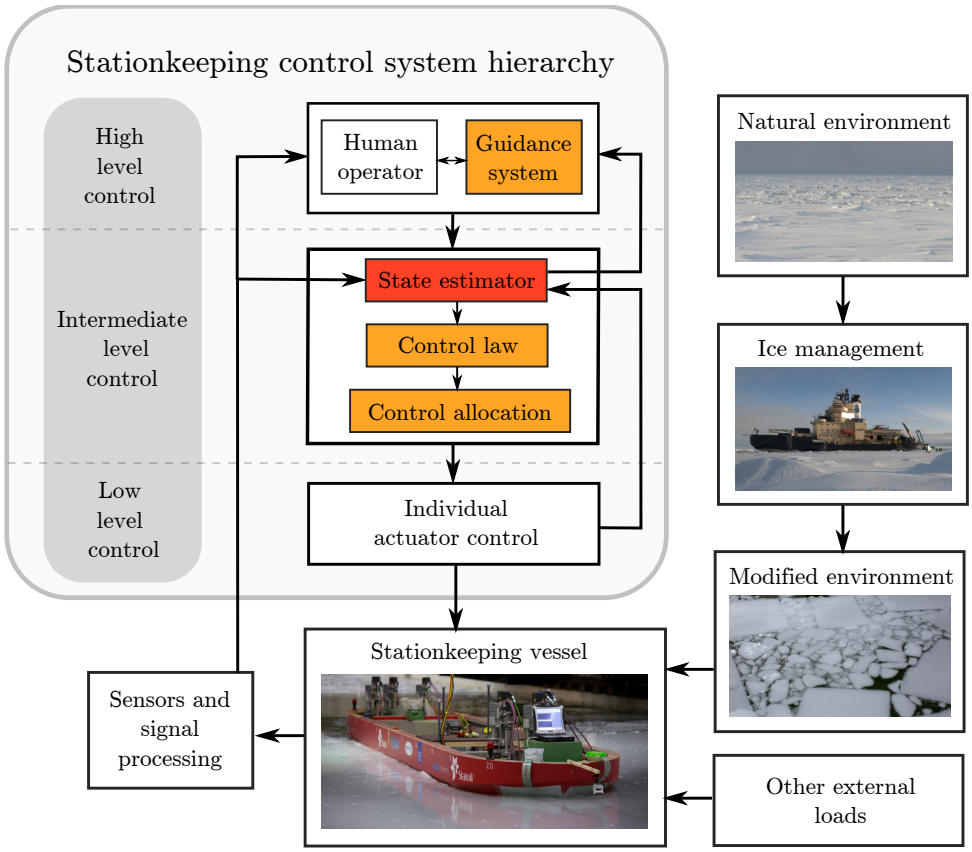

Figure 3. Control system hierarchy for stationkeeping in managed sea ice. Adapted from Breivik (2010, p. 127) and Kerkeni et al. (2013a). Also provided in Kjerstad et al. (2015).

This combined set of objectives is called the *reactive control objectives*. Interestingly, it coincides with objectives of the minimum-power DP applications in open water. Miyazaki et al. (2013) compares several specific open water design concepts for minimal power DP and concludes that zero transversal controllers, such as *weather optimal positioning control* (WOPC) (Fossen, 2011; Kjerstad and Breivik, 2010), provide the best solution. This design appears to be promising for operations in managed ice, because it incorporates the objectives directly, i.e. without the need for additional measurements. Furthermore, it pro-actively exploits the environment for actuation. Figure 2 explains this concept further. Here it is important to note that such a strategy is only applicable when no constraints are imposed on the heading of the vessel. Examples of scenarios where this may not be possible is operations close to other structures or vessels and pipe-laying. Implementation of the *reactive* design concept in the control system can be achieved by applying the hierarchy shown in Figure 3. This structure is conventional for open-water DP, and it has been successfully adopted for operations in ice (Kerkeni et al., 2013a). It closes the loop between the sensor measurements and the thruster output, and it creates an autonomous system that requires only setpoint commands from the operator.

If the operational area is sufficiently large, and the vessel has freedom to manoeuvre, two additional *proactive control objectives* may be beneficial:

- Seek the weakest path through the ice cover, e.g. as illustrated in Figure 2.
- Utilize the vessel momentum and inertia to address challenging ice features, e.g. as reported from full-scale stationkeeping operations in ice (Keinonen et al., 2006).

These strategies aim to minimize the future load on the system based on predictions of the ice environment in the operational region. However, there is currently no robust and thoroughly verified *ice observation system* (Haugen et al., 2011) capable of gathering the necessary measurements from the surrounding environment, and there are no autonomous prediction and decision systems available. Therefore, human operators will be needed to perform observations, evaluate information, assess risks, and initiate manoeuvres as required by the proactive control objectives. However, ice observation systems are an active field of research, and if a real-time system becomes available then elements of the proactive control objectives may be automated. One example is continuous evaluation and prediction of the most feasible setpoint within the operational area which would take into account the ice floe configuration around the vessel, ice drift conditions, and vessel dynamics.

Although the reactive control objectives can be met by a specific design concept, the overall performance of the DP system hinges on the ability of the state estimator to accurately predict the states of the system (position and orientation, linear and angular velocity, and external loads), and the control law to calculate the appropriate actuation output. These are actually two sides of the same challenge. If the state estimator is unable to track the ice loads accurately, the positioning capability will deteriorate (as shown experimentally by Kerkeni et al. (2013a) and Jenssen et al. (2009) in managed ice). It happens because the estimator signals are directly used to calculate the thruster's actuation output. Thus, improving positioning performance requires the mathematical *control plant model* (Sørensen, 2012), which is an explicit simplified approximation of (1)-(2) used for state prediction and control design, which are needed to better capture the dynamics of the vessel. For open water conditions those control plant models are well established (see (Fossen, 2011)). In this study, the following model of Fossen (2011) is chosen as a starting point. Then, ice loads are imposed as follows:

$$\dot{\boldsymbol{\xi}} = \mathbf{A}_w \boldsymbol{\xi} + \mathbf{E}_w \mathbf{w}_w \tag{3}$$

$$\dot{\boldsymbol{\eta}} = \mathbf{R}(\psi)\boldsymbol{\nu} \tag{4}$$

$$\dot{\mathbf{b}}_o = \mathbf{w}_o \tag{5}$$

$$\begin{aligned}(\mathbf{M} + \mathbf{M}_a)\dot{\boldsymbol{\nu}} = \boldsymbol{\tau}_{control} - \mathbf{D}\boldsymbol{\nu} + \mathbf{R}(\psi)^\top \mathbf{b}_o \\ + \boldsymbol{\tau}_{wind} + \boldsymbol{\tau}_{ice} + \mathbf{w}_v\end{aligned} \tag{6}$$

where $\boldsymbol{\xi} \in \mathbb{R}^6$ is the first order wave response state, $\mathbf{A}_w \in \mathbb{R}^{6\times6}$ and $\mathbf{E}_w \in \mathbb{R}^{6\times3}$ are matrices describing the sea state, $\mathbf{M}_a \in \mathbb{R}^{3\times3}$ is the added mass from accelerating the fluid around the ship's hull, and $\mathbf{D} \in \mathbb{R}^{3\times3}$ is a linear damping matrix approximating the damping in the system. $\mathbf{R}(\psi) \in \mathbb{R}^{3\times3}$ is the rotation matrix between the inertial and body frame. This is the reduction of $\mathbf{J}(\boldsymbol{\eta})$ in (1) when the mentioned subset of DOFs are evaluated. Notice that it only depends on the heading $\psi \in \mathbb{R}$. This comes from the assumption that roll and pitch angles of the vessel are

small. The bias term $\mathbf{b}_o \in \mathbb{R}^3$ is a non-physical quantity that incorporates several effects such as ocean current loads, modelling errors, unmodelled dynamics and wave drift (all defined in the inertial frame). The variables $\mathbf{w}_i$ $(i = w, o, v)$ are zero-mean Gaussian noise vectors representing model uncertainty and measurement noise. $\boldsymbol{\tau}_{control} \in \mathbb{R}^3$ is the control input, $\boldsymbol{\tau}_{wind} \in \mathbb{R}^3$ is the wind loads (assumed to be measured by appropriate sensors), and $\boldsymbol{\tau}_{ice} \in \mathbb{R}^3$ are the global ice loads.

Conventional DP systems employ a wave filter to reduce high-frequency oscillatory wave motion from entering the feedback loop and causing additional wear-and-tear. This is achieved by estimating $\boldsymbol{\xi}$ and removing its impact on the position and heading signals. When operating well within the ice field, this filter may be removed because the ice cover dampens the wave energy exponentially with respect to distance from the ice edge (Broström and Christensen, 2008). This is beneficial for tracking the ice loads, because it allows the bias state to be weighted higher in the estimator equations.

Incorporating the ice dynamics in (6) may be achieved in 2 ways. The first one is to introduce a direct measurement to capture the external load dynamics, similar to how wind is handled (Nguyen et al., 2009). The second one is to apply a mathematical model relying on indirect measurements (e.g. ice drift, ice concentration, ice thickness, etc.) and the vessel motion states. This is common for hydrodynamic added mass and drag in open-water DP. Although $\boldsymbol{\tau}_{ice}$ is highly complex, it seems reasonable to assume that the ice induces both added inertia and friction in the dynamical system. Thus, a mass-damper control model in the following form can be suggested:

$$\boldsymbol{\tau}_{ice} = -\mathbf{M}_{ice}\dot{\boldsymbol{\nu}} + \mathbf{d}_{ice}(\boldsymbol{\nu}) + \mathbf{R}(\psi)^\top \mathbf{b}_{ice} + \mathbf{w}_{ice} \tag{7}$$

$$\dot{\mathbf{b}}_{ice} = \mathbf{w}_b, \tag{8}$$

where $\mathbf{M}_{ice} \in \mathbb{R}^{3\times3}_{\geq 0}$ is added ice mass and $\mathbf{d}_{ice}(\boldsymbol{\nu}) \in \mathbb{R}^3$ is a damping function describing the ice condition, $\mathbf{b}_{ice} \in \mathbb{R}^3$ is a Wiener process, and $\mathbf{w}_b \in \mathbb{R}^3$ and $\mathbf{w}_{ice} \in \mathbb{R}^3$ are zero-mean Gaussian noise vectors.

A major downside of (7)-(8) is the fact that $\mathbf{M}_{ice}$ and $\mathbf{d}_{ice}(\boldsymbol{\nu})$ have their own non-linear time-varying dynamics. Those dynamics are highly dependent on the in-situ ice floe contact networks, accumulated ice mass and boundary conditions. Although it can be possible to develop a model for this case, using an extensive full-scale dataset, the robustness and accuracy of such model would be anyway questionable for tracking the highly fluctuating ice load signal. Specifically, a descriptive model may be able to predict the mean loads as a function of the particulars of the ice cover and the vessel motion states, but it will be very challenging for such model to predict the signal fluctuations. This is the key challenge, because the slowly varying loads are already well handled in existing DP systems through the bias estimate. To avoid using a specific model for $\boldsymbol{\tau}_{ice}$, its dynamics can be assigned to the bias estimate $\mathbf{b}_o$. Such methodology is common practice for unmeasured and unmodelled loads. Efforts can then be spent on optimizing the estimation of $\mathbf{b}_o$ through advances in control theory and additional motion sensors. One promising approach based on observer resetting is proposed in (Kjerstad and Skjetne, 2015a).

The other option - incorporating ice load measurements into the control plant model - requires additional instrumentation. Necessary signals can be obtained through strain gauges (Ritch et al., 2008; Leira et al., 2009), external impact panels (Gagnon et al., 2008) or inertial measurements

(Johnston et al., 2008; Nyseth et al., 2013). All those technologies have proven performance in ice load measurements on icebreaking ships, but inertial sensors are particularly interesting for DP because they constitute a non-invasive instrumentation system that resides inside the vessel and is able to capture the global loads acting from any oblique angle. Achieving the same sensing capability with strain gauges or external impact panels requires extensive instrumentation around the entire hull. Today, inertial measurements are not directly incorporated in DP systems and the conventional sensor suite is comprised of various position reference systems: global navigation systems, hydroacoustic systems, taunt-wire, laser and radar reflection systems; heading reference systems such as gyrocompasses, and other systems such as wind sensors, draught sensors, vertical reference units, etc. Lindegaard (2003) demonstrated how to incorporate inertial measurements into DP control systems for open water using a conventional control plant model. Alternatively, as all global loads perturbing the system are captured in the accelerations of the vessel (linear and angular), the inertial sensors offer another approach to the state estimation problem. Rather than estimating the external loads through specific kinetic models (as (6)), the state estimation problem can be reformulated to remove sensor bias and gravitational influence from the inertial sensor signals. This can be solved using kinematic control plant models (Batista et al., 2011). A challenge with this approach is the need for an angular acceleration measurement. Those signals are not commonly available, but can be obtained by either an angular accelerometer (Titterton and Weston, 2005) or by a configuration of conventional linear accelerometers (Buhmann et al., 2006; Kjerstad and Skjetne, 2015b).

Both (Kjerstad et al., 2015) and (Kjerstad and Skjetne, 2014) provide frequency analysis of model-scale data and simulator data which show that the global ice loads appear in the low end of the spectrum. It implies that integral action in the control law may be sufficient to deal with the ice load (in addition to proportional and derivative terms). However, compared to open water, the integral action should be more reactive such that a rapid change in load does not push the vessel off position, or cause it to drive off. In conventional DP control law design the main tool for achieving this is tuning the integral action tougher. Unfortunately, this will only provide some improvement before oscillations (and in the end instability) occur in the system. Nevertheless, with recent development in control theory and application of sensors not conventionally considered there are several ways of achieving this challenge may be solved. One example is integrator resetting as proposed in (Kjerstad and Skjetne, 2015a; Tutturen and Skjetne, 2015). Another is to determine the global loads signals from inertial measurements (Kjerstad et al., 2011, 2012) :

$$\mathbf{M}\mathbf{a} - \boldsymbol{\tau}_{control} = \sum \boldsymbol{\tau}_i \tag{9}$$

where $\mathbf{a} \in \mathbb{R}^3$ is the measured and bias-corrected acceleration vector, and $\boldsymbol{\tau}_i$ denotes all other external forces. Thus, this method is actually a combination of the two existing measurements with knowledge of the vessel's rigid mass matrix. This signal can then be applied as feedforward in the control law, in order to directly counteract all external disturbances (Kjerstad et al., 2011; Kjerstad and Skjetne, 2012, 2015b). This method is known as acceleration feedforward.

Another aspect of DP operation in managed ice is related to the utilization of the thruster system of the vessel. Since the global loads are highly fluctuating, the thruster usage will, to some extent, be likewise. This may be challenging with respect to wear-and-tear, and must be accounted for during vessel's design. Furthermore, the vessel's capability in the various degrees of freedom is highly dependent on the ice conditions (Kerkeni et al., 2013b; Su et al., 2013). Therefore, it

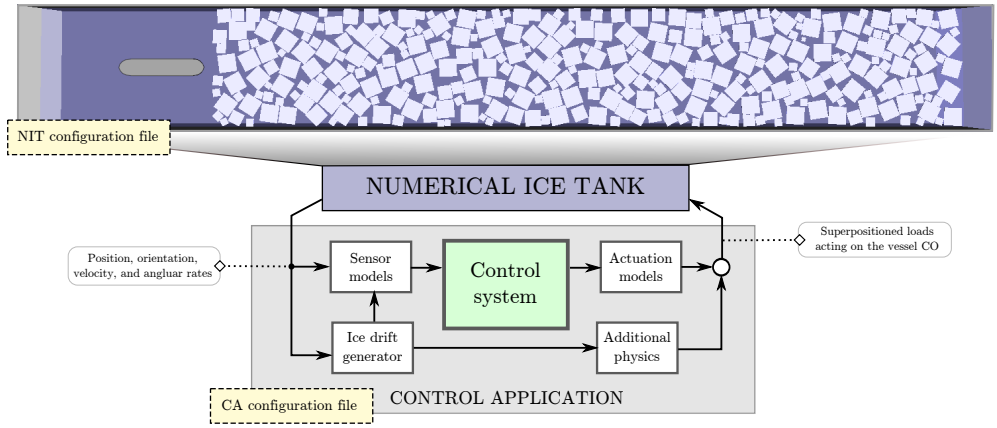

Figure 4. The modular structure of the closed-loop simulation platform for DP in managed ice.

can be beneficial to prioritize the moment for heading control over longitudinal and transversal loads in the control allocation system (which determines how much load each thruster should produce), and especially when a vaning strategy is used. This ensures that the vessel heading tracks the ice drift direction and is the last to be compromised in high-load scenarios (Kjerstad et al., 2013; Skjetne and Kjerstad, 2013; Wold, 2013). It may also be beneficial to incorporate local ice management by using the thruster wakes. For this task podded propulsors have shown significant ice clearing performance in high ice concentrations (Ferrieri et al., 2013; Keinonen and Lohi, 2000), which may help triggering release mechanisms in the ice cover and clearing ice floes away from the vessel. Wold (2013) shows how to utilize spare actuation capacity for this purpose without compromising the positioning performance of the vessel. In principle, thruster wake ice management can be implemented as an automatic and/or operator-guided process.

CLOSED LOOP SIMULATION PLATFORM

The development framework of Kjerstad and Skjetne (2014) is used in this paper for investigating control system designs. The framework employs the numerical model of Metrikin (2014), which will be referred to as the Numerical Ice Tank (NIT). Figure 4 provides an overview of the main components of the framework. As the aforementioned reference articles treat both the development framework and the numerical model in-depth, only a brief summary will be given herein.

The NIT computes the vessel's dynamics in 6 DOF without wind and waves using a physics engine with tailored routines for ice material modelling. Each simulation is comprised of the following five interconnected elements: the vessel, the towing carriage, the ice floes, the water volume and the ice tank boundaries. The vessel is simulated as a rigid body in 6 DOF without deformations. The towing carriage is not used in this paper as only free-floating DP mode is considered. The ice floes are simulated as breakable bodies with uniform thickness in 6 DOF. The initial ice floe sizes and floe positions are generated by an ice field generation algorithm that aims to produce a specified ice field. The water is simulated as a static plane that produces buoyancy and drag loads on the vessel and the ice floes.

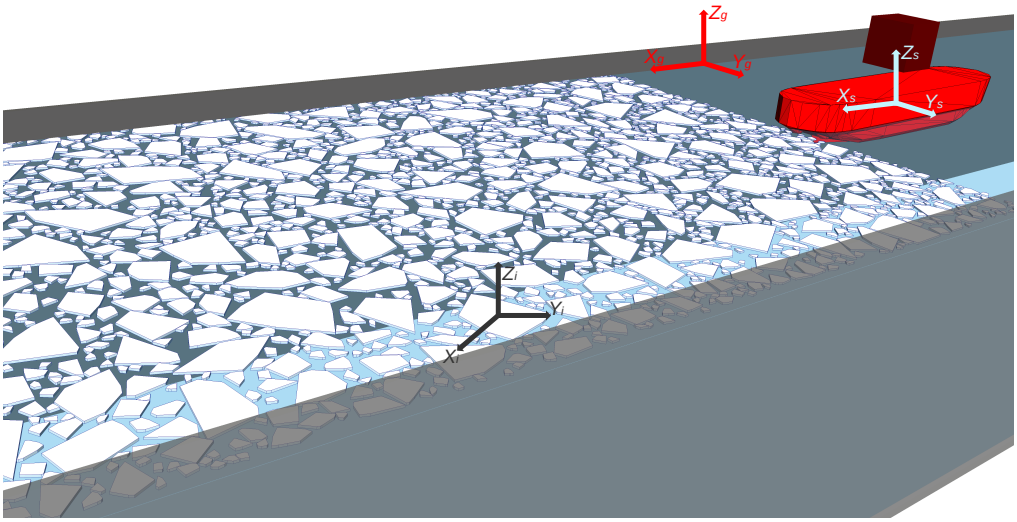

Figure 5. The reference frames of the closed loop simulation platform for DP in managed ice. Courtesy Metrikin (2014).

The motion variables of the vessel in NIT are defined in three reference frames: *the tank-fixed frame {t}* which is non-rotational and fixed to the stationary tank boundaries; *the body frame {b}* which is fixed to the vessel; and *the ice floe frames {i}* which are fixed to each individual ice floe. Figure 5 illustrates the NIT reference frames. For development of DP, a fourth reference frame is introduced through control application (CA). This is *the positioning frame {n}* which is non-rotational and follows a pre-defined trajectory to simulate ice drift in the stationary ice cover. This is done in the ice drift generator module as described in (Kjerstad and Skjetne, 2014). In this paper {n} is considered inertial, and the DP vessel will be set to track a fixed position in this frame. The main reasons for this approximation is that it is a common way to simulate ice drift in ice tank testing (Haase and Jochmann, 2013), and the current version of NIT does not inherently provide ice drift functionality. Furthermore, this method enables a basis for comparison for calibrating simulation results against model-scale data.

Besides the ice drift generator, the CA is a collection of interconnected models which enable testing of control algorithms during execution of the NIT in DP mode. Although the specific implementation of CA depends on the control system in question, it is generally divided into the following five modules: sensor models, ice drift generator, control system, actuator models and additional physics.

The sensor models simulate on-board equipment for measuring the motions of the vessel. They are implemented by first transforming the NIT vessel motion output (i.e. position, orientation, linear velocity and angular rate) from {t} to {n} and {b}. Then, sensor dynamics and noise are added to the signals. Besides the NIT motion variables, signals originating from other CA components are possible to simulate. The specific sensor implementations however depend on the application and sensor characteristics.

The control system module contains the implementation of the control algorithms, and a specific implementation will be given in the next section of this paper. The actuator models implement the dynamics of the thruster system on-board the vessel. The additional physics module contains vessel-specific dynamics which are not modelled explicitly in the NIT. Examples of such dynamics are the wind loads, additional vessel drag and loads from the mooring system. These loads are added to the body force and moment vector together with the actuation forces, and then supplied to the NIT.

It is important to note that the closed-loop system does not allow applying forces to any other bodies than the vessel. For instance, the thruster wake which is known to affect the ice cover, is not captured. Depending on the vessel and it's thruster system this may be of importance. This is one example of why care must be taken when interpreting the simulation results. Additional information on the validity range of NIT and other aspects of the CA implementation and coupling with NIT can be found in Kjerstad and Skjetne (2014).

NUMERICAL SIMULATION CASE STUDY

In this section we describe and test two different control systems in various reversing ice drift conditions. Only the reactive part of the control system is investigated, and all simulations are performed in model-scale.

Control systems

As mentioned previously, one of the key aspects affecting the control system design is the sensor suite. Here we consider an idealized setup where only those measurements that are used directly in the feedback loop are considered:

- **Sensor suite 1**: Position and heading reference systems.
- **Sensor suite 2**: Position and heading reference systems, and inertial measurements.

Two control systems are designed based on those sensor suites: the conventional system and the candidate system. Both comply with the topology shown in Figure 3.

The conventional system is based on an adaptation of a state-of-the-art open water design based on (4)-(6). The difference from the conventional design is that it contains neither the wave model nor a specific ice model, and the ice load is estimated as a part of the bias. It is fully described in Kjerstad and Skjetne (2014). The candidate system uses the kinematic state estimator described in Kjerstad and Skjetne (2015b). As opposed to the conventional system, it does not estimate the external loads, but rather the gravity and sensor bias corrupting the inertial measurements.

In order to achieve the reactive control objectives, the WOPC control principle is applied in both systems. It means that the vessel directs it's heading towards a virtual point away from it, at all times. From the dynamical system perspective this mimics the dynamics of a pendulum in a force field, and allows the vessel to move along a circular arc around the virtual point of suspension. In this mode of operation, often called *weather optimal heading control*, the vessel's position will not converge to a specific desired point, but will remain somewhere on the circular arc (depending on the direction of the environmental forces). Therefore, the virtual point of suspension is also moved in such a fashion that the desired position is reached and maintained. This allows environmental vaning of the vessel, without additional sensors or systems

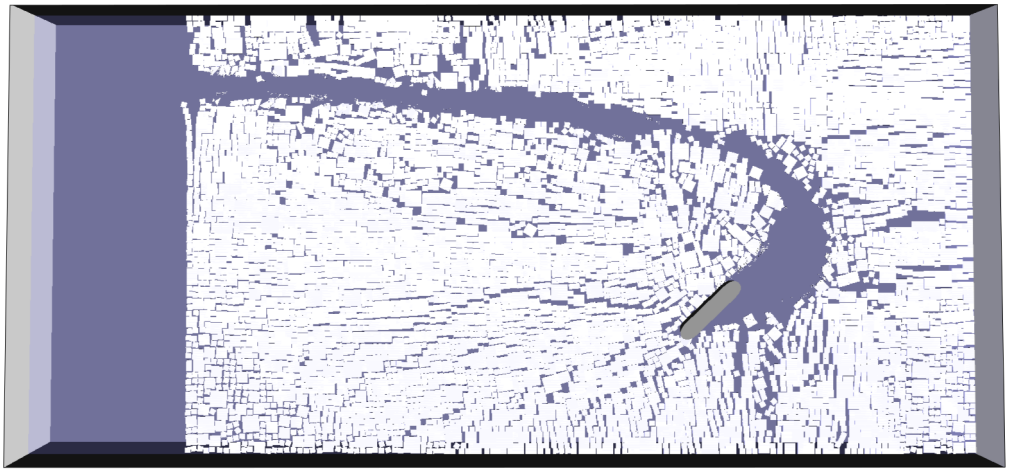

Figure 6. The model basin during simulation of the candidate DP system in high ice concentration. The basin size is 85x40x2.5 m, and the ellipse is 60 m long and 28 m wide.

computing the direction of the environmental forces. For drifting sea ice conditions this is particularly important, because a system providing reliable real-time and robust measurements of the ice drift drift direction currently does not exist. For both the conventional and the candidate systems, the nominal WOPC control law (proportional and derivative control) is implemented as described in Fossen (2011). However, integral action is needed to control the vessel in a meaningful way. For the conventional system, the pendulum length integral action described in Fossen (2011) is extended by integral action in heading acting on the deviation between the current and desired values. For the candidate system the integral action is replaced by acceleration feedforward (Kjerstad and Skjetne, 2015b) for longitudinal pendulum length and heading control. In summary, the two control systems tested here are:

- **Conventional modified DP system**: Uses sensor suite 1, a modified conventional state estimator, and the WOPC control law with additional integral action.
- **Candidate DP system**: Uses sensor suite 2, a kinematic state estimator, the WOPC control law with acceleration feedforward in both longitudinal and heading control.

Both systems apply control allocation algorithm from Skjetne and Kjerstad (2013), which prioritizes the moment generation over longitudinal and transversal thrust in case of thruster saturation.

Numerical Experiment Setup

In this study the Arctic Drillship (ADS) from Figure 1 is considered. This vessel is thoroughly described in (Gürtner et al., 2012; Hals and Jenssen, 2012; Metrikin et al., 2013; Kjerstad et al., 2015; Kjerstad and Skjetne, 2014). Therefore, only a brief overview of the most important parameters are given in this paper (Table 1). The vessel has three azimuth thrusters in the bow and three in the stern, making it suitable for DP. In this study all thrusters are considered to have equal power, delivering 45 N maximum thrust. However, this limit is not explicitly incorporated in the allocation, in order to better understand the capabilities of the algorithms. The dynamics

of the thruster system is modelled as in Kjerstad and Skjetne (2014), where thruster effects such as hull-wake interaction phenomena, ventilation, and thruster-ice interaction are not considered.

Table 1: ADS main particulars with scale factor $\lambda = 30$.

Parameter	Full scale	Model scale
Length between perpendiculars (m)	184	6.13
Breath, moulded (m)	41.33	1.37
Frame angle at midship (°)	45	45
Displacement volume (m^3)	68457	2.535
Center of gravity from aft. perp. (m)	95.34	3.18
Total thrust (N)	7.2×10^6	270

The linear transversal damping coefficient of 100, found experimentally in (Kjerstad and Skjetne, 2014), is herein considered to be too low. Therefore, an additional linear damping is added through the additional physics module of the CA. Hence, the coefficient considered in the control implementations is 600. This was set based on a qualified judgement and comparison with similar vessel designs. The other vessel control model parameters are the same as described in Kjerstad and Skjetne (2014).

Figure 6 shows the model basin and the size of the ice drift ellipse during a simulation run. The ice drift velocity was set to 0.2 m/s in model-scale ($\approx$ 2 knots in full-scale) at the beginning and end of the ellipse, and 0.02 m/s in model-scale ($\approx$ 0.2 knots in full-scale) at the pivot point of the ellipse. The maximum curvature radius of the ellipse is 3.2 m, which, together with the pivot velocity, comply well with measured data from (Yulmetov et al., 2013a,b), and may be considered as an extreme curvature. The simulated ice floe distribution can be seen in Figure 6. All floes are square, with side lengths 0.5, 1.0, and 1.5 m. These are distributed with 55, 40, and 15% in the broken ice cover, respectively. For the case study, two variations of ice concentration and ice thickness are considered:

- **Case 1**: Moderate ice concentration, 60% coverage, with 0.028 m ice thickness in model-scale.
- **Case 2**: High ice concentration, 85% coverage, with 0.04 m ice thickness in model-scale.

The reason for selecting these conditions is that the ice concentration and ice thickness are considered to be key parameters defining the "toughness" of the ice environment for DP. Table 2 shows the remaining simulation parameters, which are constant for both cases. For further information on the setup of the simulator the reader is referred to Kjerstad and Skjetne (2014).

Table 2: Fixed ice condition parameters.

Parameter	Model scale
Compressive strength (kPa)	92
Flexural strength (kPa)	45.9
Elastic Modulus (MPa)	10
Ice density (kg/m^3)	900

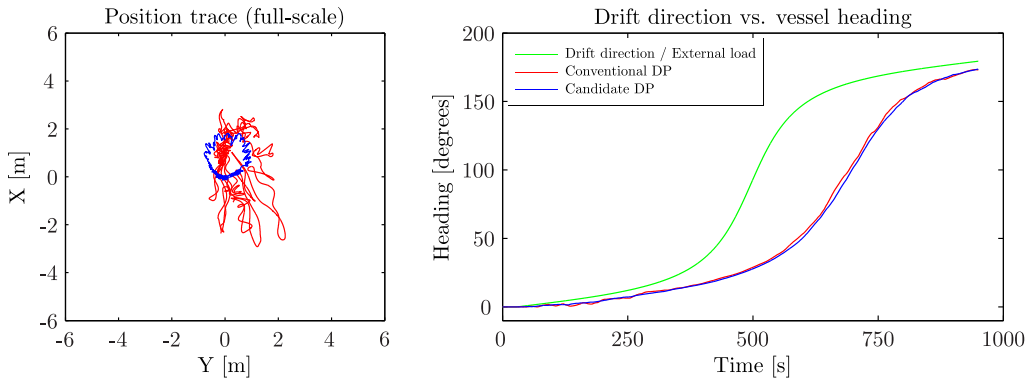

Figure 7. Case 1 position and heading trace for the two control systems in *{n}*.

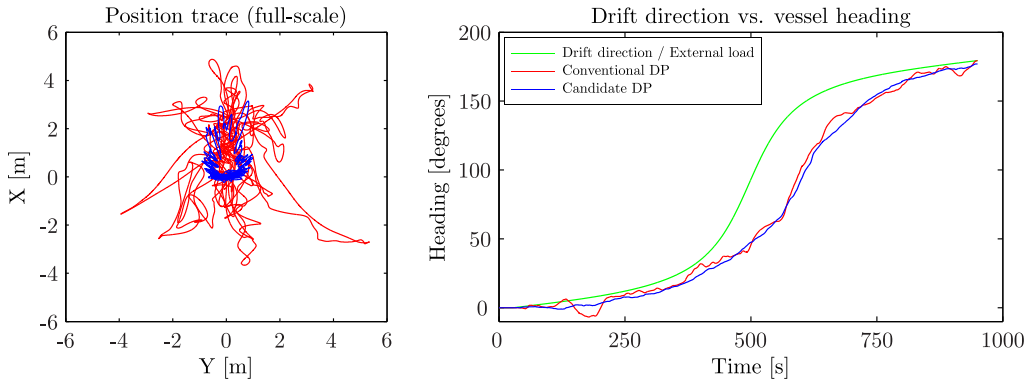

Figure 8. Case 2 position and heading trace for the two control systems in *{n}*.

The on-board position, orientation, and angular rate sensor measurements are considered to be idealistic without noise, and located at the centre of gravity of the vessel. The accelerometers however are simulated with noise, bias, and gravity. Here the four linear accelerometer setup from (Kjerstad and Skjetne, 2015b) is considered. These inertial sensors are placed in the bow, stern, and in the mid-ship of the vessel on both sides. When combined, they measure both the linear and angular accelerations at the centre of gravity.

For both cases the control objective is to track the position (0,0) in *{n}* and allow the heading to automatically vane using a 4 m virtual pendulum. Here, it is important to emphasize that the control systems has no information about the ice drift, ice condition, or other parameters besides the signals coming from the aforementioned sensor suites.

Results and Discussion

Figure 7 shows the position and heading of the vessel for case 1 simulations. It is clear that both systems are able to maintain position with high accuracy and vane as the ice drift changes. Since the environment forcing is moderate, and the oblique angle is initially zero, it takes some time for the load to build up on the ship's side, and to re-orient the vaning heading according to the pendulum principle. In case 2 however (Figure 8), the forcing is tougher and the vaning is

closer to the actual ice drift. This illustrates well that the harsher the environment, the quicker the re-orientation of the vessel will be.

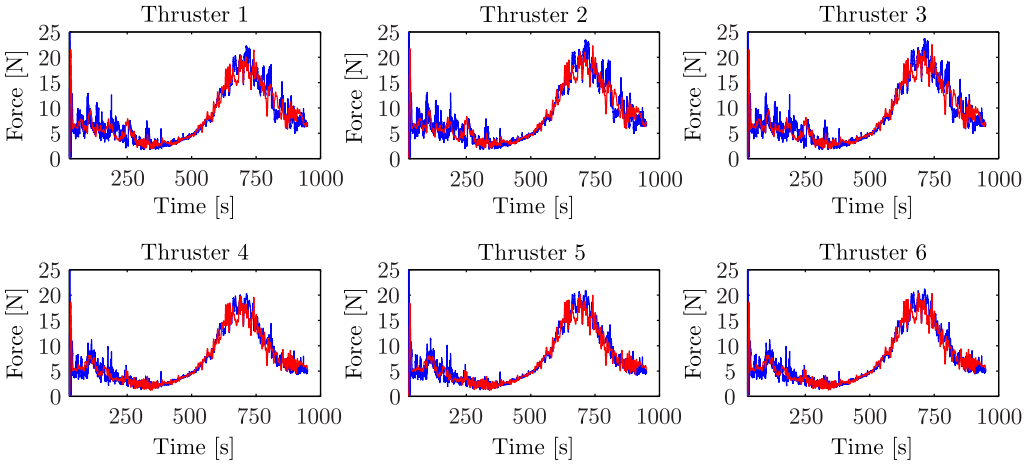

Figure 9. Case 1 actuation of the ADS thrusters. Plot colors relate to Figure 7.

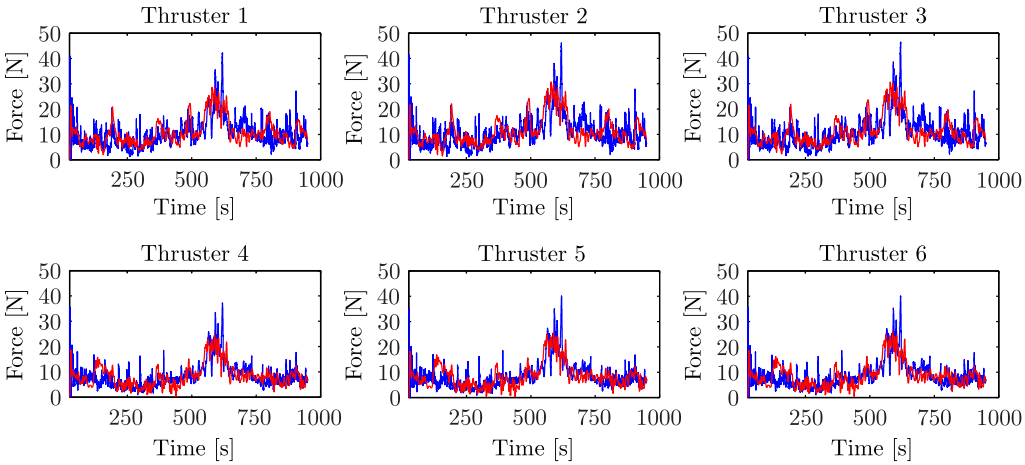

Figure 10. Case 2 actuation of the ADS thrusters. Plot colors relate to Figure 8.

Another factor which impacts the vaning performance is the virtual pendulum length. The shorter it is, the more accurate and reactive the vaning becomes (at the cost of higher thruster usage). Thus, it may be beneficial to research adaptive pendulum length control, where the pendulum is set long in low curvature, and short in high curvature. This will allow the control system to both relax the thruster usage in nominal operation, but at the same time be highly reactive when needed. Sensing the curvature can be done through the transversal position deviation.

Overall, the positioning performance is good for both cases and both systems. Compared, the candidate system provides the lowest position deviations and most stable heading control. This

is particularly evident in case 2. This result is due to the enhanced ability of the candidate system to estimate and counteract the external global loads. The trade-off for the improved accuracy is higher thrust output variation. This is seen in figures 9 and 10. Again it is most evident in the tougher ice conditions of case 2. The potential challenge of this is additional wear-and-tear of the actuator system. It must be mentioned, however, that the commanded thrust output variation can be adjusted to some extent through tuning the control law, but this will lower the positioning and heading tracking capabilities. Hence, a trade-off between allowed thrust output variation and positioning and heading capabilities must be found. Another notice is that greater difference in thruster usage among the installed thrusters is expected once an allocation system accounting for more of the aforementioned physical propeller and actuator dynamics is applied.

Besides the software algorithms, the only physical difference between the two control systems are the additional inertial sensors employed by the candidate system. This makes them complimentary in the sense that if a failure occurs on the inertial measurement system, the conventional system can be used as a fall-back option.

The cases presented here only test the control systems capability in scenarios where the ice does not contain any features which deviate from the nominal ice cover in size or material properties. Thus, further research is needed to both incorporate such ice features in the simulation platform, and evaluate the control system performance. Furthermore, in the presence of ice pressure, more complex ice interactions may take place (such as ridging). Additional research is needed to study how this would influence the feasibility and functioning of the DP system.

CONCLUSIONS

This paper discusses and describes the design of DP control systems for drifting managed sea ice environments and presents two specific implementations based on different sensor suites. A high fidelity numerical development tool were used to test these in a challenging 180 degree elliptic ice drift reversal scenario with moderate and though ice conditions. Both designs were able to keep position and vane, but the system including inertial sensors showed improved capabilities.

The results indicate that the control system design needed for an operation depends on the required positioning precision and severity of the ice conditions. For light and moderate conditions, a design based on current conventional systems with ice tuning and without the wave filter may suffice. In heavy ice conditions, or in cases with strict position or reactivity requirements, a system incorporating inertial measurements may be needed. The results also indicate that significant thrust variations, potentially imposing significant wear-and-tear on the thruster system, may be a consequence of DP in moderate and though ice conditions.

Besides the specific discussion around control system design, this paper showcases the importance of using high fidelity numerical models as a DP control system development tool.

ACKNOWLEDGEMENTS

Research partly funded by the Research Council of Norway (RCN) KMB project no. 199567: “Arctic DP”, with partners Kongsberg Maritime, Statoil, and DNV GL, and partly by RCN project no. 203471: CRI SAMCoT. Statoil is gratefully acknowledged for permitting publication.

REFERENCES

Batista, P., Silvestre, C., Oliveira, P., and Cardeira, B. (2011). Accelerometer calibration and dynamic bias and gravity estimation: Analysis, design, and experimental evaluation. *Control Systems Technology, IEEE Transactions on*, 19(5):1128–1137.

Breivik, M. (2010). *Topics in Guided Motion Control of Marine Vehicles*. PhD thesis, Norwegian University of Science and Technology. (p. 127).

Broström, G. and Christensen, K. (2008). Waves in sea ice. Technical report, Norwegian Meteorological Institute, Norway.

Buhmann, A., Peters, C., Cornils, M., and Manoli, Y. (2006). A GPS aided Full Linear Accelerometer Based Gyroscope-free Navigation System. In *Position, Location, And Navigation Symposium, 2006 IEEE/ION*, pages 622–629.

Ferrieri, J. M., Veitch, B., and Akinturk, A. (2013). Experimental study on ice management through the use of podded propeller wash. In *Proceedings Third International Symposium on Marine Propulsors, Launceston, Australia May 2013*.

Fossen, T. I. (2011). *Handbook of Marine Craft Hydrodynamics and Motion Control*. Wiley.

Gagnon, R., Cumming, D., Ritch, R., Browne, R., Johnston, M., Frederking, R., McKenna, R., and Ralph, F. (2008). Overview accompaniment for papers on the bergy bit impact trials. *Cold Regions Science and Technology*, 52(1):1 – 6.

Gürtner, A., Baardson, B. H. H., Kaasa, G.-O., and Lundin, E. (2012). Aspects of importance related to Arctic DP operations. In *Proc. 31th Int. Conf. on Ocean, Offshore and Arctic Engineering (OMAE)*.

Haase, A. and Jochmann, P. (2013). Different ways of modeling ice drift scenarios in basin tests. In *Proc. 32th Int. Conf. on Ocean, Offshore and Arctic Engineering (OMAE)*.

Hals, T. and Jenssen, N. A. (2012). DP ice model tests of Arctic drillship and polar research vessel. In *Proc. 31th Int. Conf. on Ocean, Offshore and Arctic Engineering*.

Hamilton, J. M. (2011). The Challenges of Deep-Water Arctic Development. *Int. Journal of Offshore and Polar Engineering*, 21(4):241–247.

Haugen, J., Imsland, L., Løset, S., and Skjetne, R. (2011). Ice Observer System for Ice Management Operations. In *Proceedings of the Twenty-first (2011) International Offshore and Polar Engineering Conference Maui, Hawaii, USA, June 19-24, 2011*.

International Maritime Organization (IMO) (1994). *Guidelines for Vessels with Dynamic Positioning Systems*. MSC/circ.645.

Jenssen, N. A., Muddesitti, S., Phillips, D., and Backstrom, K. (2009). DP In Ice Conditions. In *Proc. of the Dynamic Positioning Conference*.

Johnston, M., Timco, G., Frederking, R., and Miles, M. (2008). Measuring global impact forces on the CCGS Terry Fox with an inertial measurement system called MOTAN. *Cold Regions Science and Technology*, 52(1):67 – 82.

Keinonen, A. and Lohi, P. (2000). Azimuth and Multi Purpose Icebreaker Technology for Arctic and Non-Arctic Offshore. In *Proceedings of the Tenth (2000) International Offshore and Polar Engineering Conference, Seattle, USA, May 28-June 2, 2000*.

Keinonen, A. and Martin, E. H. (2012). Modern day pioneering and its safety in the floating ice offshore. In *Proc. 10th Int. Conf. and Exhibition on Performance of Ships and Structures in Ice (ICETECH)*, volume 1.

Keinonen, A., Shirley, M., Liljeström, G., and Pilkington, R. (2006). Transit and Stationary

Coring Operations in the Central Polar Pack. In *Proc. 7th Int. Conf. and Exhibition on Performance of Ships and Structures in Ice (ICETECH)*.

Kerkeni, S., Dal Santo, X., and Metrikin, I. (2013a). Dynamic Positioning in Ice - Comparison of Control Laws in Open Water and Ice. In *Proc. 32th Int. Conf. on Ocean, Offshore and Arctic Engineering (OMAE)*.

Kerkeni, S., Metrikin, I., and Jochmann, P. (2013b). Capability plots of dynamic positioning in ice. In *Proc. of the ASME 32th Int. Conf. on Ocean, Offshore and Arctic Engineering, June 9-14, 2013, Nantes, France*.

Kjerstad, Ø. and Breivik, M. (2010). Weather optimal positioning control for marine surface vessels. In *Proceedings of IFAC CAMS, Rostock, Germany*.

Kjerstad, Ø., Metrikin, I., Løset, S., and Skjetne, R. (2015). Experimental and phenomenological investigation of dynamic positioning in managed ice. *Cold Regions Science and Technology*, 111:67–79.

Kjerstad, Ø. and Skjetne, R. (2012). Observer design with disturbance rejection by acceleration feedforward. In *Proceedings of ROCOND12, Aalborg, Denmark*.

Kjerstad, Ø. and Skjetne, R. (2014). Modeling and Control for Dynamic Positioned Marine Vessels in Drifting Managed Sea Ice. *Modeling, Identification and Control*.

Kjerstad, Ø. and Skjetne, R. (2015a). A Resetting Observer for Dynamic Positioning of Marine Vessels Subject to Severe Disturbances. *IEEE Transactions on Control System Technology (submitted)*.

Kjerstad, Ø. and Skjetne, R. (2015b). Acceleration feedforward control for control of marine surface vessels. *Automatica (submitted)*.

Kjerstad, Ø., Skjetne, R., and Berge, B. (2013). Constrained Nullspace-based Thrust Allocation for Heading Prioritized Stationkeeping of Offshore Vessels in Ice. In *Proceedings of 22st International Conference on Port and Ocean Engineering under Arctic Conditions (POAC), Espoo, Finland*.

Kjerstad, Ø., Skjetne, R., and Jenssen, N. A. (2011). Disturbance rejection by acceleration feedforward: Application to dynamic positioning. In *Proceedings of IFAC World Congress, Milan, Italy*.

Leira, B., Børsheim, L., Espeland, Ø., and Amdahl, J. (2009). Ice-load estimation for a ship hull based on continuous response monitoring. *Proceedings of the Institution of Mechanical Engineers, Part M: Journal of Engineering for the Maritime Environment*.

Liferov, P. (2014). Station-keeping in ice - normative requirements and informative solutions. In *Proc. Arctic Technology Conference (ATC)*.

Lindegaard, K.-P. W. (2003). *Acceleration Feedback in Dynamic Positioning*. PhD thesis, Norwegian University of Science and Technology.

Metrikin, I. (2014). A Software Framework for Simulating Stationkeeping of a Vessel in Discontinuous Ice. *Modeling, Identification and Control*.

Metrikin, I., Løset, S., Jenssen, N. A., and Kerkeni, S. (2013). Numerical Simulation of Dynamic Positioning in Ice. *Marine Technology Society Journal*, 47(2):14–30.

Miyazaki, M. R., Tannuri, E. A., and de Oliveria, A. C. (2013). Minimum Energy DP Heading Control: Critical Analysis and Comparison of Different Strategies. In *Proceedings of the ASME 2013 32st International Conference on Ocean, Offshore and Arctic Engineering OMAE2013, June 9-14, 2013, Nantes, France*.

Nguyen, D. T., Sørbø, A. H., and Sørensen, A. J. (2009). Modelling and control for dynamic positioned vessels in level ice. In *Proceedings of Conference on Manoeuvring and Control of Marine Craft*, pages 229 – 236.

Nyseth, H., Frederking, R., and Sand, B. (2013). Evaluation of global ice load impacts based on real-time monitoring of ship motions. In *Proceedings of 22st International Conference on Port and Ocean Engineering under Arctic Conditions (POAC), Espoo, Finland*.

Ritch, R., Frederking, R., Johnston, M., Browne, R., and Ralph, F. (2008). Local ice pressures measured on a strain gauge panel during the CCGS Terry Fox bergy bit impact study. *Cold Regions Science and Technology*, 52(1):29 – 49.

Rohlén, Å. (2009). Relationship Between Ice-Management and Station Keeping in Ice. Presentation at Dynamics Positioning Conference.

Skjetne, R. and Kjerstad, Ø. (2013). Recursive nullspace-based control allocation with strict prioritization for marine craft. In *Proc. of 9th IFAC Conf. on Control Applications in Marine Systems*.

Sørensen, A. J. (2012). *Marine Control Systems: Propulsion and Motion Control of Ships and Ocean Structures*. Department of Marine Technology, NTNU, Norway.

Su, B., Kjerstad, Ø. K., Skjetne, R., and Berg, T. E. (2013). Ice-going capability assessment and DP-ice capability plot for a double acting intervention vessel in level ice. In *Proceedings of the 22th International Conference on Port and Ocean Engineering under Arctic Conditions, Helsinki, Finland*.

Titterton, D. and Weston, J. (2005). *Strapdown Inertial Navigation Technology, Second Edition (Progress in Astronautics and Aeronautics)*. AIAA.

Tutturen, S. A. and Skjetne, R. (2015). Hybrid control approach to improve transient response of integral action in Dynamic Positioning of vessels. In *Manoeuvring and Control of Marine Craft, Copenhagen, Denmark*.

Wold, H. E. (2013). Thrust allocation of DP in ice. Master's thesis, Norwegian University of Science and Technology, Trondheim, Norway.

Yulmetov, R., Løset, S., and Eik, K. (2013a). Analysis of drift of sea ice and icebergs in the Greenland sea. In *Proceedings of the 22th International Conference on Port and Ocean Engineering under Arctic Conditions, Helsinki, Finland*.

Yulmetov, R., Marchenko, A., and Løset, S. (2013b). Ice drift and sea current analysis in the northwestern Barents sea. In *Proceedings of the 22th International Conference on Port and Ocean Engineering under Arctic Conditions, Helsinki, Finland*.

Constrained Nullspace-based Thrust Allocation for Heading Prioritized Stationkeeping of Offshore Vessels in Ice

POAC'13
Espoo, Finland

Proceedings of the 22nd International Conference on
Port and Ocean Engineering under Arctic Conditions
June 9-13, 2013
Espoo, Finland

CONSTRAINED NULLSPACE-BASED THRUST ALLOCATION FOR HEADING PRIORITIZED STATIONKEEPING OF OFFSHORE VESSELS IN ICE

Øivind K. Kjerstad[1], Roger Skjetne[1], Bjørn Ola Berge[2]

[1] Department of Marine Technology, NTNU, 7491 Trondheim, NORWAY

[2] MARINTEK, POB 4125 Valentinlyst, 7450 Trondheim, NORWAY

ABSTRACT

The positioning capability is a crucial property for safe and reliable operations of a dynamically positioned (DP) offshore vessel. The limiting factor in such is the vessels thruster configuration and the maximum resultant forces and turning moment this can produce in all directions. Based on the vessels position and velocity deviations, the DP control law computes a desired resultant load set as correction. This is distributed by the DP thrust allocation algorithm to individual thruster forces based on rated power, thruster type (force direction capability), and hull position. In this paper, a novel and computationally light constrained thrust allocation algorithm which offers eased thruster weighting and prioritization between the degrees of freedom (surge, sway, and yaw), is developed. It is motivated by the importance of maintaining the heading directly against the ice drift, such that the projection of the vessel in the ice is minimized. Thus, first the yaw moment is allocated to the thrusters with a given fraction of the capability at its disposal. Then, the total remainder is distributed to surge and then sway. If the loads on the vessel are beyond the capability of the thrusters, then sway is affected first, then surge, and last yaw. Due to its simplicity, this method provides a convenient tool to evaluate and compare ice loads from model testing with the thrust capability of the DP vessel. In order to enable a DP-ice capability analysis, the quantification of loss of capability is investigated. This introduces three descriptive measures of the ice loads of a given ice condition; peak load, significant load, and mean load. As a case study, a towing tank dataset of an experimental intervention vessel (the CIVArctic vessel) in broken ice is investigated and discussed.

INTRODUCTION

The International Maritime Organization (1994), defines a vessel with dynamic positioning (DP) as: "*A vessel that maintains its position and heading (fixed location or predetermined track) exclusively by means of active thrusters*", which in essence is to determine the actuator forces which produce environmental compensation and appropriate position correction. This must be done while taking into account the type, constraints, and state of the actuators.

When a vessel is enclosed in drifting ice, the characteristics of the environmental load changes drastically. Although the mean load might be within acceptable limits of the vessel capability, unfeasible features or events in the ice cover can impose peak loads which are not. Hence, a strategy to prioritize the vessel output must be incorporated to better handle such scenarios. By investigation, the movement potential of a DP vessel is constrained and coupled with the ice due to the rigid body interaction. Here, the relative heading towards the ice drift is important as it governs both the hull interaction geometry and the exposure. In turn these govern the ice load

level. This effect is also emphasized by Moran et al. (2006) from a full scale DP operation in heavy ice conditions. Hence, in order to contain the overall loads imposed during positioning it is crucial to maintain the heading against the ice drift and prioritize yaw foremost in the thrust allocation. As the bow have significantly better ice handling capabilities than the ship sides, the allocation should prioritize surge before sway. Thus, the motivation of the paper is to introduce this prioritized allocation and enable for evaluation of the vessel DP-ice capability.

In the literature, thrust allocation for open-water is solved in a variety of ways, ranging from the pseudo-inverse of the thrust matrix (Fossen, 2011; Sørensen, 2005), not considering any of the constraints, to complex optimization problems including all constraints and rate limitations (Johansen & Fossen, 2013; Fossen, 2011).

The main contribution of this paper is a novel and computationally light magnitude constrained thrust allocation algorithm which offers eased thruster weighting and prioritizes between the planar degrees of freedom (surge, sway, and yaw). Secondly, a set of ice load definitions enables for quantification of the capability of the vessel subject to a given ice load time-series. Due to its simplicity, this method provides a convenient tool to evaluate and compare the ice loads from model testing or simulations with the thrust capability of the DP vessel. The DP-Ice Capability Plots are also investigated in the companion paper by (Su et al., 2013). A case study of the performance of the algorithm and methodology is included after the derivation of the allocation algorithm.

MATHEMATICAL MODELING

First, an unconstrained thrust allocation algorithm is derived and presented. This serves as an introduction to the problem and a basis for the constrained thrust allocation design.

Unconstrained allocation

The relationship between the general body fixed loads, and the thruster output can be defined as

$$\boldsymbol{\tau} = \mathbf{B}\mathbf{u}, \tag{1}$$

where $\boldsymbol{\tau} = \begin{bmatrix} F_x & F_y & M_z \end{bmatrix}^\top$ are the generalized body fixed control forces, $\mathbf{B} \in \mathbb{R}^{3\times 2n}$ is the actuator configuration matrix, and $\mathbf{u} \in \mathbb{R}^{2n}$ is the individual thruster forces. Thus, the goal of the allocation is to find $\mathbf{u}$ given $\mathbf{B}$ and $\boldsymbol{\tau}$.

Any actuator can be decomposed into an x and y component in the vessel body frame as

$$\mathbf{u} = \begin{bmatrix} u_{x1} & u_{y1} & u_{x2} & u_{y2} & \dots u_{xn} & u_{yn} \end{bmatrix}^\top \in \mathbb{R}^{2n}, \tag{2}$$

where n is the number of thrusters. By constructing a linear thrust configuration matrix based on Fossen (2011), the following decomposition is possible,

$$\mathbf{B} = \begin{bmatrix} \mathbf{b}_x^\top \\ \mathbf{b}_y^\top \\ \mathbf{b}_z^\top \end{bmatrix}, \tag{3}$$

where $\mathbf{b}_x$, $\mathbf{b}_y$, and $\mathbf{b}_z \in \mathbb{R}^{2n}$ are the row vectors of $\mathbf{B}$.

By investigation of (1) and (3), it can be seen that the generalized control forces $\boldsymbol{\tau}$ is related to the row vectors of $\mathbf{B}$ as

$$F_x = \mathbf{b}_x^\top \mathbf{u}, \qquad F_y = \mathbf{b}_y^\top \mathbf{u}, \qquad M_z = \mathbf{b}_z^\top \mathbf{u}. \tag{4}$$

The individual thruster forces $\mathbf{u}$ can be treated as a superposition of the three contributions,

$$\mathbf{u} = \mathbf{u}_z + \mathbf{u}_x + \mathbf{u}_y, \tag{5}$$

where $\mathbf{u}_z$, $\mathbf{u}_x$, and $\mathbf{u}_y$ are thruster contributions required to obtain $\boldsymbol{\tau}$ in yaw, surge, and sway respectively. In order to prioritize yaw, we ensure that both $\mathbf{u}_x$ and $\mathbf{u}_y$ are defined in the nullspace of $\mathbf{b}_z^\top$. Thus, $\mathbf{b}_z^\top \mathbf{u}_x = 0$ and $\mathbf{b}_z^\top \mathbf{u}_y = 0$ holds. Hence, $\mathbf{u}_z$ must be allocated first. This is done by rearranging (4) as,

$$\mathbf{u}_z = (\mathbf{b}_z^\top)^\dagger_{W_z} M_z, \tag{6}$$

where the weighted pseudoinverse is defined as

$$(\mathbf{b}_z^\top)^\dagger_{\mathbf{W}_z} = \mathbf{W}_z^{-1}\mathbf{b}_z(\mathbf{b}_z^\top \mathbf{W}_z^{-1}\mathbf{b}_z)^{-1}. \tag{7}$$

Each element in $\mathbf{b}_z^\top$ corresponds to a momentum produced by each thruster component. Thus, it allows for direct weighting of the thruster usage through a diagonal weighting matrix defined as

$$\mathbf{W}_z = diag(\begin{bmatrix} w_{1x} & w_{1y} & w_{2x} & w_{2y} & \dots & w_{nx} & w_{ny} \end{bmatrix}) \in \mathbb{R}^{2n\times 2n}, \tag{8}$$

where it can be seen that each thruster occupies two column vectors in the matrix, corresponding to the weighting in x and y. Although providing the possibility to weight the contribution from each thruster, it is challenging to obtain an optimal weighting. In the next subsection, when dealing with the saturation problem, a more comprehensible strategy of distributing the thruster forces will be presented.

After the calculation of $\mathbf{u}_z$, then $\mathbf{u}_x$ and $\mathbf{u}_y$ are decomposed as,

$$\mathbf{u}_x = \mathbf{N}_z \mathbf{c}_x \tag{9}$$
$$\mathbf{u}_y = \mathbf{N}_z \mathbf{c}_y, \tag{10}$$

where $\mathbf{N}_z \in \mathbb{R}^{2n\times 2n-1}$ is the nullspace matrix of $\mathbf{b}_z^\top$, and $\mathbf{c}_x, \mathbf{c}_y \in \mathbb{R}^{2n-1}$ are coefficient vectors of the magnitude of each respective nullvector in order to construct $\mathbf{u}_x$ and $\mathbf{u}_y$.

In order to obtain $\mathbf{u}_x$ and $\mathbf{u}_y$, the coefficient vectors $\mathbf{c}_x$ and $\mathbf{c}_y$ must be found. Here, the prioritization order applies. Both yaw-surge-sway and yaw-sway-surge are possible, but for a ship-shaped vessel a yaw-surge-sway is recommended. By defining the force balance for surge and sway, $\mathbf{u}_x$ and $\mathbf{u}_y$ can be found,

$$F_x = \mathbf{b}_x^\top(\mathbf{u}_{zy} + \mathbf{N}_z \mathbf{c}_x) \tag{11}$$
$$F_y = \mathbf{b}_y^\top(\mathbf{u}_{zx} + \mathbf{N}_z \mathbf{c}_y) \tag{12}$$

which can be rewritten to find $\mathbf{c}_x$ and $\mathbf{c}_y$ as,

$$\mathbf{c}_x = \left(\mathbf{b}_x^\top \mathbf{N}_z\right)^\dagger \left(F_x - \mathbf{b}_x^\top \mathbf{u}_{zy}\right) \tag{13}$$
$$\mathbf{c}_y = \left(\mathbf{b}_y^\top \mathbf{N}_z\right)^\dagger \left(F_y - \mathbf{b}_y^\top \mathbf{u}_{zx}\right), \tag{14}$$

where $\mathbf{u}_{zx}$ and $\mathbf{u}_{zy}$ are yet to be defined.

This enables the completion of the unconstrained allocation vector $\mathbf{u}$ as $\mathbf{u}_x$ and $\mathbf{u}_y$ can be found. Notice that the realization of $\mathbf{u}_{zy}$ and $\mathbf{u}_{zx}$ determines the prioritization order between surge and sway,

$$\mathbf{u}_{zy} = \begin{cases} \mathbf{u}_z & \textit{surge is prioritized.} \\ \mathbf{u}_z + \mathbf{u}_y & \textit{sway is prioritized.} \end{cases} \quad \mathbf{u}_{zx} = \begin{cases} \mathbf{u}_z + \mathbf{u}_x & \textit{surge is prioritized.} \\ \mathbf{u}_z & \textit{sway is prioritized.} \end{cases}. \tag{15}$$

Constrained thrust magnitude

Unfortunately, allocation without respect to the individual thruster saturation levels might impose unfeasible behavior and instabilities in the positioning system as it enables for a potential mismatch between commanded and achieved actuation. Hence, to avoid this the saturation level of the individual thrusters must be incorporated in the above unconstrained design.

As $\mathbf{u}_z$ is independent of $\mathbf{u}_x$ and $\mathbf{u}_y$, the required forces to obtain M_z can be distributed freely among the thrusters. Hence, (6) can be reformulated as,

$$\mathbf{u}_z = \mathbf{d}_z M_z, \tag{16}$$

where $\mathbf{d}_z$ is a realization of $(\mathbf{b}_z^\top)^\dagger_{W_z}$. It also defines the distribution of the required moment to each of the thruster. By constructing $\mathbf{d}_z$ as

$$\mathbf{d}_z = \begin{bmatrix} d_{z1}\sin\alpha_1 & d_{z1}\cos\alpha_1 & \dots & d_{zn}\sin\alpha_n & d_{zn}\cos\alpha_n \end{bmatrix}^\top \tag{17}$$

where α_n is the azimuth angle for which the thrust vector is normal to the moment arm, the saturation level can be incorporated. This is done through the distribution coefficient, defined as

$$d_{zi} = \frac{u_{BPi}}{\sum_1^n l_j u_{BPj}}, \tag{18}$$

where u_{BPi}, is the i-th thruster saturation level, and $\sum_1^n l_j u_{BPj}$ constitutes the total moment capability of the thruster configuration. By utilizing this formulation, the distribution vector $\mathbf{d}_z$ can be shown to be a realization of the inverse of $\mathbf{b}_z^\top$,

$$\mathbf{b}_z^\top \mathbf{d}_z = 1 \tag{19}$$

$$\sum_1^n l_{yi} \frac{u_{BPi}\sin\alpha_i}{\sum_1^n l_j u_{BPj}} + l_{xi}\frac{u_{BPi}\cos\alpha_i}{\sum_1^n l_j u_{BPj}} = 1 \tag{20}$$

$$\sum_1^n l_i \sin\alpha_i \frac{u_{BPi}\sin\alpha_i}{l_j \sum_1^n u_{BPj}} + l_i\cos\alpha_i \frac{u_{BPi}\cos\alpha_i}{\sum_1^n l_j u_{BPj}} = 1 \tag{21}$$

$$\sum_1^n l_i \frac{u_{BPi}}{\sum_1^n l_j u_{BPj}} = 1 \tag{22}$$

$$\frac{1}{\sum_1^n l_j u_{BPj}} \sum_1^n l_i u_{BPi} = 1. \tag{23}$$

and thus,

$$\mathbf{b}_z^\top \mathbf{u}_z = \mathbf{b}_z^\top \mathbf{d}_z M_z \tag{24}$$

$$\mathbf{b}_z^\top \mathbf{u}_z = M_z. \tag{25}$$

It is worth noticing that if one thruster saturates during $\mathbf{u}_z$ allocation, all thrusters saturate. This is utilized to constrain $\mathbf{u}_z$ within the capability of each of the thrusters as,

$$\mathbf{u}_z = \begin{cases} \mathbf{d}_z M_z & \text{if } \ M_z \le M_{z,max} \\ \mathbf{d}_z M_{z,max} & \text{else} \end{cases} \tag{26}$$

where $M_{z,max}$ is the largest possible moment given a thruster configuration.

If there is remaining capacity after the allocation of $\mathbf{u}_z$, this must be distributed amongst $\mathbf{u}_x$ and $\mathbf{u}_y$. To do this, and obtain a nullspace realizations of $\mathbf{u}_x$ and $\mathbf{u}_y$, the following relation is utilized,

$$k\mathbf{v} \in \{\mathcal{N}(\mathbf{b}) | \mathbf{v} \in \mathcal{N}(\mathbf{b}) \ \forall \ k \in [0 \ 1]\}. \tag{27}$$

This basically means that the magnitude of the nullspace vector is irrelevant for it to be in the nullspace. Hence, the full expression of the total output $\mathbf{u}$ can be written as

$$\mathbf{u} = \mathbf{u}_z + k_x\mathbf{u}_x + k_y\mathbf{u}_y, \tag{28}$$

where $k_x, k_y \in \mathbb{R}$ are scaling factors which enforce the saturation limits of the thusters. The lower bound is determined by the fact that it is unfeasible to change sign of the nullspace vectors, and the upper bound by the infeasibility to increase the magnitude, as $k_x = 1$ or $k_y = 1$ is sufficient to enforce the thrust level required by the control system.

In order to obtain a feasible $\mathbf{u}_x$ and $\mathbf{u}_y$ allocation with respect to the remaining available thruster power, a similar distribution strategy as seen in (16) - (26) is necessary. Thus, (13) and (14) can be re-defined as,

$$\mathbf{c}_x = \mathbf{N}_z^\dagger \mathbf{d}_x \left(F_x - \mathbf{b}_x^\top \mathbf{u}_{zy}\right) \tag{29}$$
$$\mathbf{c}_y = \mathbf{N}_z^\dagger \mathbf{d}_y \left(F_y - \mathbf{b}_y^\top \mathbf{u}_{zx}\right), \tag{30}$$

where

$$\mathbf{d}_x = \begin{bmatrix} d_{x1} & 0 & \dots & d_{xn} & 0 \end{bmatrix}^\top diag(\mathbf{b}_x) \tag{31}$$
$$\mathbf{d}_y = \begin{bmatrix} 0 & d_{y1} & \dots & 0 & d_{yn} \end{bmatrix}^\top diag(\mathbf{b}_y), \tag{32}$$

and

$$d_{xi} = \frac{\sqrt{u_{BPi}^2 - u_{zy,2i-1}^2} - u_{zy,2i}}{\sum_1^n \left(\sqrt{u_{BPj}^2 - u_{zy,2j-1}^2} - u_{zy,2i}\right)} \tag{33}$$

$$d_{yi} = \frac{\sqrt{u_{BPi}^2 - u_{zx,2i}^2} - u_{zx,2i-1}}{\sum_1^n \left(\sqrt{u_{BPj}^2 - u_{zx,2j}^2} - u_{zx,2i}\right)}. \tag{34}$$

The scaling factors k_x and k_y are found as,

$$k_x = \min\{k_{x_1}, k_{x_2}, \dots, k_{x_n}\} \tag{35}$$
$$k_y = \min\{k_{y_1}, k_{y_2}, \dots, k_{y_n}\} \tag{36}$$

where k_{x_i} and k_{y_i} are found by solving

$$\left(\mathbf{u}_{zy_i} + k_{x_i}\mathbf{u}_{x_i}\right)^\top \left(\mathbf{u}_{zy_i} + k_x\mathbf{u}_{x_i}\right) = u_{BP_i} \tag{37}$$
$$\left(\mathbf{u}_{zx_i} + k_{y_i}\mathbf{u}_{y_i}\right)^\top \left(\mathbf{u}_{zx_i} + k_y\mathbf{u}_{y_i}\right) = u_{BP_i} \tag{38}$$

for each individual thruster $i = [1 \dots n]$, where $\mathbf{u}_{zy_i}, \mathbf{u}_{zx_i} \in \mathbb{R}^2$ follow the prioritization of (15), and $\mathbf{u}_{x_i}, \mathbf{u}_{y_i} \in \mathbb{R}^2$ contain the individual x and y contribution of each individual thurster.

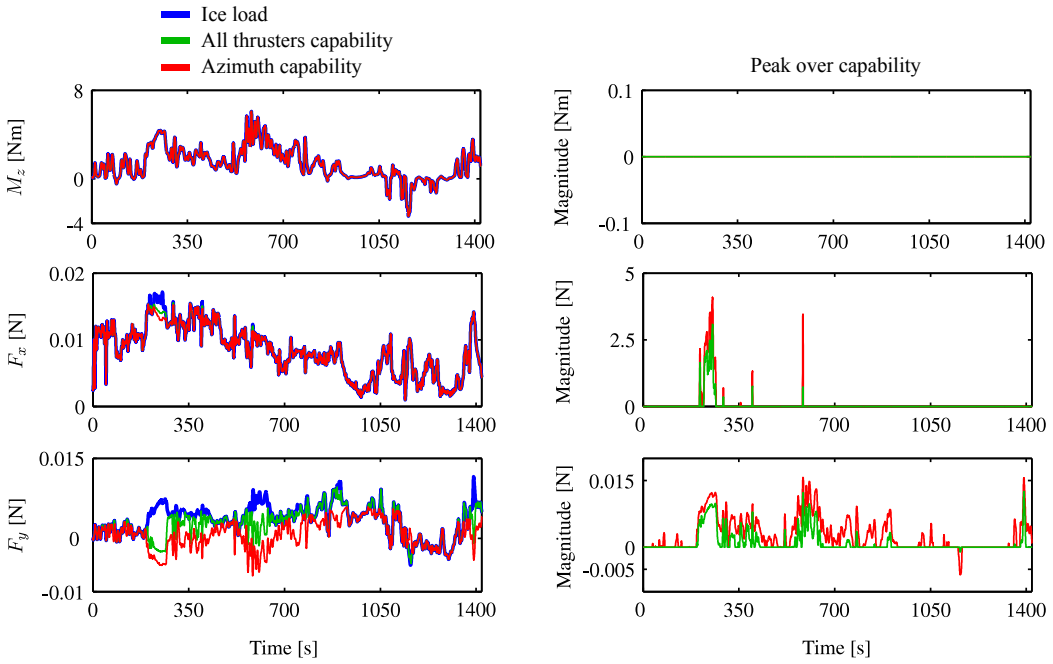

Figure 1: Allocation verification on a ice load time-series with the two cases; all actuators and just azimuths. The time-series are normalized.

CASE STUDY

In order to analyze and verify the functionality of the prioritizing allocation algorithm and discuss the concept of capability, a set of DP load time-series was investigated. The vessel subject to investigation was the CIVArctic vessel which mainly is designed for open-water operation, but with ice going capabilities, both for transit, through a double acting design, and bow first DP. Table 1 features the characteristics of the thruster configuration used in the algorithm where the thruster forces are approximated by their rated power as defined in (Zahalka, 2008).

The applied dataset features towing DP force tests set in managed ice, which originates from the May 2011 test campaign at Aker Arctic. The setup was reported to comply with the AARC methodology, where a rigid 6-component balance was used (Valtonen, 2011). The model was towed through the stationary ice sheet with a constant velocity using only the tank carriage for propulsion. The relative heading between the vessel and the ice was fixed throughout each experiment. While surge, sway and yaw was restricted to capture the loads, the vessel was free to move in heave, pitch and roll. The experiments were carried out in high ice concentration with low velocity for different ice thicknesses and relative ice drift headings. See Table 2 for further elaboration.

Table 1: The CIVArctiv vessel thruster configuration characteristics.

	No.	Propulsor type	Hull position [m]	Power [MW]	Max. force [kN]
Stern	1	Azimuth	[-49.9 6.0]	5	720
	2	Azimuth	[-49.9 -6.0]	5	720
Bow	3	Azimuth	[44.6 0]	1.5	216
	4	Azimuth	[43.5 0]	1.5	216
	5	Tunnel	[49,1 0]	1.5	200
	6	Tunnel	[31.9 0]	1.5	200

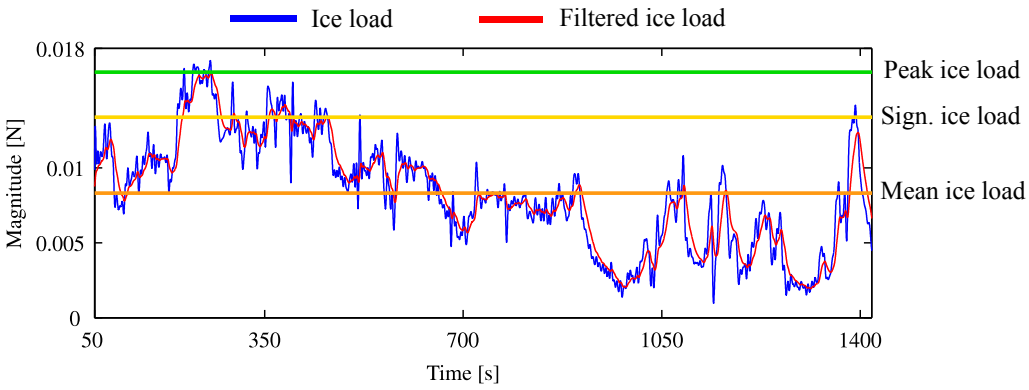

Figure 2: Comparison between a filtered and raw ice load time-series along with the applied ice load definitions. The time-series are normalized.

Based on the above table, the following thruster $\mathbf{B}$ matrix was utilized in the allocation algorithm;

$$\mathbf{B} = \begin{bmatrix} 1 & 0 & 1 & 0 & 1 & 0 & 1 & 0 & 0 & 0 & 0 & 0 \\ 0 & 1 & 0 & 1 & 0 & 1 & 0 & 1 & 0 & 1 & 0 & 1 \\ l_{y1} & l_{x1} & l_{y2} & l_{x2} & l_{y3} & l_{x3} & l_{y4} & l_{x4} & l_{y5} & l_{x5} & l_{y6} & l_{x6} \end{bmatrix} \tag{39}$$

Notice that the tunnel thrusters (no. 5 and 6) do not have any longitudinal capability as they are purely transversal actuators. Thus, they are not able to contribute in surge. Another challenge is the potential for clogging of ice in the hull tunnel, which degrades the actuator performance. Hence, the implications of tunnel thruster loss will be investigated with respect to the capability of the CIVArctic vessel.

Time-series allocation

In order to verify the performance of the allocation algorithm itself, an ice load time-series from the above mentioned dataset was applied as the generalized forces $\boldsymbol{\tau}$. This provides the loads that the vessel must withstand to maintain the exact position. Figure 1 features both the ice load and vessel capability with and without tunnel thrusters. Here it can be seen that the yam moment allocation is prioritized as it does not contain loss of capability. Surge and sway are prioritized such that sway is the least emphasized degree of freedom. The functionality of this can be verified by the peak over capability curve. This effect is further enforced when the transversal tunnel thrusters are omitted. Overall, the results indicate that the functionality of the allocation algorithm is as intended.

As seen in the peak over capability plots in Figure 1, both actuation cases feature time-periods of inability to generate the required surge and sway loads. When occurring, the ice will push the vessel off position in the respective degree of freedom. The severity of the loss of capability is determined mainly by three factors;

1. The energy content of the unattended ice load
2. The frequency of loss of capability
3. The positioning correcting actuation capacity when the vessel is capable

In essence, to cater for positioning the vessel must be able to attenuate the acquired position loss between the losses of capability. However, it is challenging is to calculate this based on the peak over capability curve as the dynamics and characteristics of the load changes when the vessel

would start to move. Likewise, it is challenging to compute the energy needed to attenuate the position loss as both of these phenomena heavily depend on spatial and temporal conditions in the environment.

Ice load definitions

In order to evaluate and quantify the performance of the thruster configuration, a reasonable qualification and quantification of the loss of capability must be applied. This is solved by calculating descriptive numbers of the ice load and evaluate these. The following definitions are applied to quantify the load levels associated with a ice condition;

1. **The maximum peak load** is defined as the maximum recorded ice load value during a experiment in a given ice condition.

$$\tau_{max} = \sup_{0 \leq k \leq N} F(k) \tag{40}$$

   where $F(t) \in \mathbb{R}$ is the load time series, and N is the number of samples in the measurement.

2. **The significant ice load** is defined as the mean of the one-third-highest recorded ice load values during an experiment in a given ice condition,

$$\tau_{sig} = \sup\{\tau_h, \tau_l\} \tag{41}$$

   where τ_h and τ_l are the upper and lower significant load level of the recorded values,

$$\tau_h = \frac{1}{N - j_s} \sum_{k=j_s}^{N} Q(k), \tag{42}$$

$$\tau_l = \frac{1}{j_l} \sum_{k=0}^{j_l} Q(k), \tag{43}$$

   $Q(k)$ is the absolute values of the ascending magnitude content of the recorded values, and j_s and j_l are found by solving

$$\sum_{k=j_s}^{N} Q(k) = \frac{1}{3} \sum_{k=0}^{N} Q(k) \tag{44}$$

$$\sum_{k=0}^{j_l} Q(k) = \frac{1}{3} \sum_{k=0}^{N} Q(k) \tag{45}$$

3. **The mean ice load** is defined as the mean of all recorded ice load values during a experiment in a given ice condition,

$$\tau_{mean} = \frac{\sum_{k=0}^{k=N} F(k)}{N}. \tag{46}$$

Although the definitions do not incorporate the temporal aspect of the ice load, they provides a reasonable measure of the stationkeeping potential of the ice condition when evaluated against the thruster configuration. Figure 2 feature the definitions applied to a filtered ice load time-series.

It is also worth mentioning that $|\tau_{max}| \geq |\tau_{sig}| \geq |\tau_{mean}|$, and that all of the load definitions are independent of the statistical distribution of the ice load.

Table 2: Capability mapping of the processed towing tank ice-load data.

Ice condition				Capability all thr.			Capability azimuth		
h_i [m]	c [%]	$\boldsymbol{\nu}_r$ [m/s]	ψ_r [deg]	Yaw	Surge	Sway	Yaw	Surge	Sway
0.5	90	0.2	0						
			5						
			10						
			20						
	100	0.2	0						
			5						
			10						
			20						
0.8	90	0.1	0						
			5						
			20						
	90	0.2	0						
			5						
			20						
	100	0.2	0						
			5						
			20						
1.2	90	0.2	0						
			5						
			10						
			20						
	100	0.2	0						
			5						
			10						
			20						

Capability: Peak load Significant load Mean load Uncapable

CIVArctic vessel broken ice load allocation analysis

By investigation of Figure 1 and 2 it can be seen that the ice load contains substantial high frequency components. These are believed to be intensified through the lack of vessel dynamics during towing. In a free-floating scenario, the vessel inertia and damping will attenuate such loads passively, and their contribution to the dynamics of the vessel is low. To approximate this, the dataset is lowpass-filtered based on the linearized vessel model to isolate the frequency range which is the major contributor to the dynamics. The result of one such filtering is seen in Figure 2. This attenuations of high frequent components is further underlined by investigation of the DP ice loads presented in (Metrikin et al., 2012), which can be seen to be smoother.

Table 2 features the allocation capability of the CIVArctic vessel with respect to the ice load quantification definitions applied to the filtered broken managed ice load time-series. The table includes the two mentioned actuation cases, with and without the tunnel thrusters. The results show both the functionality of the allocation prioritization through degrading sway first, and the potential for stationkeeping in the different ice conditions. As expected, the capability of the vessel degrades with tougher ice conditions. Also, as indicated by the above time-series allocation, the case without tunnel thrusters severely impacts the sway capability.

Summarized, the results indicate that the vessel is capable of maintaining the peak load for yaw and surge in broken ice conditions up to 100% ice concentration, ice thicknesses ranging up to 0.8 m, relative velocity 0.2 m/s, and for relative headings up to 20°, regardless of the state of the tunnel thrusters. The sway capabiltiy is heavily affected by the state of the tunnel thrusters. In the case of 1.2 m ice thickness, the capability is heavily affected by the ice concentration. Although the table gives an indication of the ice conditions feasible for operation, a DP-ice capability plot as seen in (Su et al., 2013) features a more compact and comprehensible display of the capability of the vessel. Such plots should be developed for the relevant operational ice conditions to verify both the vessel design and the operation.

CONCLUSIONS

This paper presents a novel constrained thrust allocation algorithm which prioritizes the allocation of the yaw moment over surge and sway. The method was found to be computationally light and feature feasible performance. The algorithm served as an evaluation tool to investigate the capability of a vessels thruster configuration subjected to various ice conditions. To enable this, a set of ice load definitions was proposed to quantify the load levels of a recorded ice load time-series. The capability of the construction and intervention vessel (CIVArctic) was investigated based on a set of towing time-series in broken managed ice. A consistent relationship between the capability, ice condition, and thruster configuration was found.

ACKNOWLEDGEMENTS

The authors acknowledge the support from the partners in the KMB project “Construction and Intervention Vessels for Arctic Oil and Gas” (CIVARCTIC). The research is funded through the Research Council of Norway, project 199567 “Arctic DP”.

REFERENCES

Fossen, T. I., 2011. Handbook of Marine Craft Hydrodynamics and Motion Control. Wiley.

International Maritime Organization, 1994. Guidelines for Vessels with Dynamic Positioning Systems. MSC/circ.645.

Johansen, T. A. & Fossen, T. I., 2013. Control Allocation - A Survey. Automatica.

Metrikin, I., Løset, S., Jenssen, N. A., & Kerkeni, S., 2012. Numerical simulation of dynamic positioning in ice. In Dynamic Positioning Conference, Houston, USA, October 9-10.

Moran, K., Backman, J., & Farrell, J. W., 2006. Deepwater drilling in the Arctic Ocean's permanent sea ice. In Proceedings of the Integrated Ocean Drilling Program, volume 302.

Sørensen, A. J., 2005. Lecture Notes Marine Cybernetics: Modeling and Control. Faculty of Engineering Science and Technology, NTNU, Trondheim, Norway.

Su, B., Kjerstad, Ø. K., Skjetne, R., & Berg, T. E., 2013. Ice-going capability assessment and DP-ice capability plot for a double acting intervention vessel in level ice. In Proceedings of the 22th International Conference on Port and Ocean Engineering under Arctic Conditions, Helsinki, Finland.

Valtonen, V., 2011. Analysis of ice loads affecting on vessel in DP, based on ice model test measurements. AARC Report K-151. Technical report, Aker Arctic.

Zahalka, C. P., 2008. Bollard pull. Technical report, Association of Hanseatic Marine Underwriters.

Observer Design With Disturbance Rejection by Acceleration Feedforward

Observer design with disturbance rejection by acceleration feedforward ⋆

Øivind Kåre Kjerstad * **Roger Skjetne** *

* *Department of Marine Technology, Norwegian University of Science and Technology, Otto Nielsens vei 10, NO-7491 Trondheim, Norway.*
E-mails: oivind.k.kjerstad@ntnu.no and skjetne@ieee.org

Abstract: This paper addresses observer design of mechanical systems subject to unknown external disturbances and unmodeled dynamics. For fast-acting disturbance forces, realistic and accurate physical models do not always exist, such as for dynamic positioning of marine vessels in ice-infested waters. To accommodate such forces and provide disturbance rejection, a delayed acceleration measurement is used to form an acceleration feedforward which captures the perturbations and enhances the observer phase margins. Through the acceleration measurement, an inherent sensor bias is introduced, creating a pseudo-force in the system. This is tracked and compensates by a bias estimate. The theoretical foundation is exemplified by the derivation of a DP observer and a simulation study featuring an inverted pendulum.

Keywords: Disturbance rejection, Dynamic positioning, Feedforward compensation, Acceleration feedforward, Disturbance estimation

1. INTRODUCTION

In motion control the main objective is to control the position and velocity of an object to a desired state by measurements of the position and velocity states only. Although these systems are proved stable and robust it is not given that the control laws and observers handle unmodeled dynamics and provide adequate environmental compensation. Any inertial system controlled by state feedback influenced by a step in the disturbance force will have to perform unnecessary work as momentum has been gained before the control law begins compensation. Similarly, the observer must track such errors through the measured state vector. By introducing an acceleration signal, a measurement of the net force acting on the system is obtained. This provides a powerful tool for developing robust control systems which rejects disturbances and model uncertainties sensed directly, and not through time integrals of the force.

This paper will deal with the development of an observer augmented by a slightly delayed acceleration measurement. This is introduced to enhance performance when the target system is subject to forces that cannot be accurately mathematically described for control purposes. Dynamic positioning of marine vessels in broken sea ice is an example which fits the description. Ice forces are highly nonlinear and chaotic, and dependent on a high number of parameters such as relative velocity, temperature, salinity, mass, floe geometry, floe size distribution, interaction geometry, etc. Hence, a simplified control model providing a sufficient estimate is challenging to obtain. Due to the inherent richness and availability of the acceleration measurement, which is proportional to the resulting force, it can be utilized to provide a measure of the external forces acting on the vessel. By including this in the observer, it enables for increased tracking performance which results in an enhanced phase margin, which is highly beneficial for accurate control purposes, both with regards to precision and efficiency.

The acceleration measurement is assumed to be slightly delayed due to signal processing and communication, where it is assumed that noise and the gravity error component of the sensor output can be mitigated with other means. This must be done as the overall system performance will deteriorate if a raw unfiltered measurement is allowed directly into the closed-loop system.

Acceleration signals are seldom applied directly in motion control applications. Among the exceptions is the work by de Jager (1994), where the goal is to increase performance and robustness of mechanical systems by applying acceleration measurements, and Kempf and Kobayashi (1999) and Chen et al. (2000), where disturbance observers are developed to attenuate the effect of the disturbances on the system. In Lindegaard (2003) an observer and a proportional acceleration feedback control law is derived. Here the acceleration term is used to virtually modify a marine vessel‘s mass as seen from the disturbance to obtain a favorable closed-loop dynamic response. Also for marine vessels, Fossen et al. (2002) incorporated acceleration feedback in a design technique to virtually shape the kinetic energy. In aerospace applications acceleration measurements have been used to some extent; see for instance Blakelock (1991).

The paper is organized as follows. First, the modeling of a perturbed mechanical system is reviewed, which is the foundation for the development of the observer. Then, an acceleration feedforward augmented observer is derived

⋆ Supported by the Research Council of Norway under grant 199567/I40 : "Arctic DP".

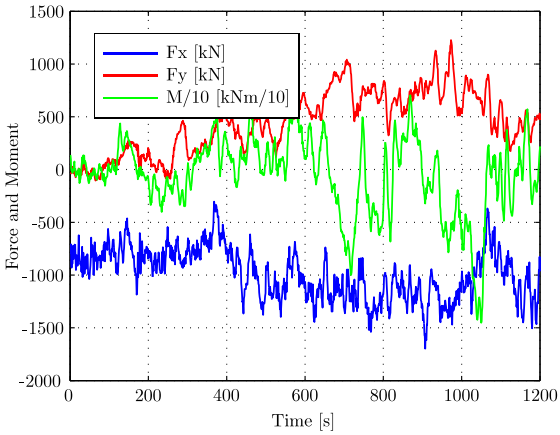

Figure 1. Recorded ice forces and moment on a vessel performing dynamic positioning. Courtesy Jenssen et al. (2009).

and proved to enhance the system performance given an unbiased acceleration signal. This motivates the enhanced observer incorporating bias estimation. The theoretical results are followed up in sections 4 and 5 featuring a simulation study and a DP observer example incorporating discussion on the practical implications. The paper ends with the conclusions and future work.

Notations: GES stands for Globally Exponentially Stable, and ISS for Input to State Stable. Total time derivatives of $\mathbf{x}(t)$ is denoted $\dot{\mathbf{x}}$, $\ddot{\mathbf{x}}$, $\mathbf{x}^{(3)}$,.., $\mathbf{x}^{(n)}$. The Euclidean vector norm is $|\mathbf{x}| := (\mathbf{x}^\top \mathbf{x})^{1/2}$, a general p-norm is $|.|_p$, the distance to a set $\mathcal{M}$ is $|\mathbf{x}|_{\mathcal{M}} := \inf\{|\mathbf{x}-\mathbf{y}| : \mathbf{y} \in \mathcal{M}\}$, and the supremum signal norm is $||\mathbf{x}|| := \operatorname{ess\,sup}\{|\mathbf{x}(t)| : t \geq 0\}$. A diagonal matrix is denoted $\operatorname{diag}\{a_1,..,a_n\} \in \mathbb{R}^{n\times n}$. Stacking several vectors into one is denoted $\operatorname{col}(\mathbf{x},\mathbf{y},\mathbf{z}) := [\mathbf{x}^\top,\mathbf{y}^\top,\mathbf{z}^\top]^\top$, and whenever convenient, $|(\mathbf{x},\mathbf{y},\mathbf{z})| = |\operatorname{col}(\mathbf{x},\mathbf{y},\mathbf{z})|$. Time delayed signals are denoted $\mathbf{x}_\delta(t) = \mathbf{x}(t-\delta)$, and cancellations based on time delayed signals are denoted $\tilde{\mathbf{x}}_\delta(t) = \mathbf{x}(t) - \mathbf{x}(t-\delta)$.

2. PERTURBED MECHANICAL SYSTEMS

Typically, mechanical systems such as marine vessels are perturbed by external forces which are predominantly slowly varying and can be compensated well by integral action. However, in this paper we are motivated by mechanical systems perturbed by fast-acting disturbance forces for which realistic and accurate physical models do not exist. This is, for instance, the case for dynamic positioning of marine vessels in arctic ice-infested regions (Jenssen et al., 2009), where the ice-hull interaction forces are very large, random, and rapidly fluctuating as seen in Figure 3. The aim in this work is the design of state observers for mechanical systems with built-in robustness to such fast-acting disturbances, and the tool is Acceleration Feedforward (AFF) compensation (Kjerstad et al., 2011).

To motivate the design method, we consider first a mechanical system modeled according to Newton's 2nd law

$$\begin{aligned} \mathbf{M}\ddot{\boldsymbol{\xi}} &= \sum \mathbf{f}_i = \mathbf{g}_0(\boldsymbol{\xi},t) + \mathbf{g}_1(\dot{\boldsymbol{\xi}},\boldsymbol{\xi},t) + \mathbf{u}(t) + \mathbf{d}(t) \\ \mathbf{y} &= \boldsymbol{\xi}, \end{aligned} \tag{1}$$

where $\boldsymbol{\xi} \in \mathbb{R}^n$ is the measured positional state, $\mathbf{M} = \mathbf{M}^\top > 0$ is the inertia matrix, $\mathbf{u} : \mathbb{R}_{\geq 0} \to \mathbb{R}^n$ is the control force input, and $\mathbf{d} : \mathbb{R}_{\geq 0} \to \mathbb{R}^n$ is an unknown force disturbance. The functions $\mathbf{g}_0 : \mathbb{R}^n \times \mathbb{R}_{\geq 0} \to \mathbb{R}^n$ and $\mathbf{g}_1 : \mathbb{R}^n \times \mathbb{R}^n \times \mathbb{R}_{\geq 0} \to \mathbb{R}^n$ are known in structure, but $\mathbf{g}_1$ depends on the unmeasured velocity $\dot{\boldsymbol{\xi}}$ and becomes uncertain.

Let $\mathbf{x} := \operatorname{col}(\mathbf{x}_1,\mathbf{x}_2) := \operatorname{col}(\boldsymbol{\xi},\dot{\boldsymbol{\xi}})$ such that the system can be rewritten in the state space form (with a slight abuse of notation)

$$\begin{aligned} \dot{\mathbf{x}}_1 &= \mathbf{x}_2 \\ \mathbf{M}\dot{\mathbf{x}}_2 &= \mathbf{g}_0(\mathbf{x}_1,t) + \mathbf{g}_1(\mathbf{x},t) + \mathbf{u}(t) + \mathbf{d}(t) \\ \mathbf{y} &= \mathbf{x}_1, \end{aligned} \tag{2}$$

We make the following assumptions:

- The control force $\mathbf{u}$ is bounded, that is, $\exists u_M > 0$ such that $\|\mathbf{u}\| \leq u_M$.
- For the disturbance force, the function $t \mapsto \mathbf{d}(t)$ is absolutely continuous, and $\exists d_M > 0$ such that $\max\{\|\mathbf{d}\|, \|\dot{\mathbf{d}}\|\} \leq d_M$.
- The mechanical system (2) is stable in the sense that, for bounded $\mathbf{u}(t) + \mathbf{d}(t)$, then the velocities and accelerations are also bounded, that is, $\|\dot{\mathbf{x}}\| < \infty$.
- The function $\mathbf{g}_1(\mathbf{x},t)$ is globally Lipschitz in $\mathbf{x}$, uniformly in t.

Define $\mathbf{r}(t) := \mathbf{M}^{-1}(\mathbf{d}(t) + \mathbf{g}_1(\mathbf{x}(t),t))$ and rewrite the system as

$$\begin{aligned} \dot{\mathbf{x}}_1 &= \mathbf{x}_2 \\ \dot{\mathbf{x}}_2 &= \mathbf{M}^{-1}\mathbf{g}_0(y,t) + \mathbf{M}^{-1}\mathbf{u}(t) + \mathbf{r}(t). \end{aligned} \tag{3}$$

Lemma 1. The function $t \mapsto \mathbf{r}(t)$ is globally Lipschitz, that is, $\exists L_r > 0$ such that

$$|\mathbf{r}(t) - \mathbf{r}(\tau)| \leq L_r |t-\tau|, \quad \forall t,\tau \in \mathbb{R}_{\geq 0}. \tag{4}$$

◇

The proof follows from the global Lipschitz assumption on $\mathbf{g}_1$ together with necessary absolute continuity and boundedness properties. Details are omitted.

2.1 AFF observer design

An observer for the nominal system, with $\mathbf{r}(t) = 0$, is given by copying the plant dynamics and adding injection terms, that is,

$$\begin{aligned} \dot{\hat{\mathbf{x}}}_1 &= \hat{\mathbf{x}}_2 + \mathbf{L}_1\tilde{\mathbf{y}} \\ \dot{\hat{\mathbf{x}}}_2 &= \mathbf{M}^{-1}\mathbf{g}_0(\mathbf{y},t) + \mathbf{M}^{-1}\mathbf{u}(t) + \mathbf{L}_2\tilde{\mathbf{y}} + \boldsymbol{\alpha} \\ \hat{\mathbf{y}} &= \hat{\mathbf{x}}_1. \end{aligned} \tag{5}$$

where $\tilde{\mathbf{y}} := \mathbf{y} - \hat{\mathbf{y}}$, and $\boldsymbol{\alpha}$ is yet to be designed. In the error coordinates $\tilde{\mathbf{x}}_1 := \mathbf{x}_1 - \hat{\mathbf{x}}_1$ and $\tilde{\mathbf{x}}_2 := \mathbf{x}_2 - \hat{\mathbf{x}}_2$, the closed loop becomes

$$\begin{aligned} \dot{\tilde{\mathbf{x}}}_1 &= \tilde{\mathbf{x}}_2 - \mathbf{L}_1\tilde{\mathbf{x}}_1 \\ \dot{\tilde{\mathbf{x}}}_2 &= -\mathbf{L}_2\tilde{\mathbf{x}}_1 + \mathbf{r}(t) - \boldsymbol{\alpha}. \end{aligned} \tag{6}$$

We then have the result:

Proposition 2. The nominal error dynamics (6), with $\mathbf{r}(t) - \boldsymbol{\alpha} = 0$, is GES for $\mathbf{L}_1 = \mathbf{L}_1^\top > 0$ and $\mathbf{L}_2 = \mathbf{L}_2^\top > 0$. $\diamond$

The proof of this follows from the closed-loop matrix

$$\mathbf{A}_1 = \begin{bmatrix} -\mathbf{L}_1 & -\mathbf{I} \\ -\mathbf{L}_2 & \mathbf{0} \end{bmatrix},$$

which is always Hurwitz for positive definite $\mathbf{L}_1$ and $\mathbf{L}_2$.

To handle the fast-acting disturbance $\mathbf{r}(t)$, we incorporate AFF (Kjerstad et al., 2011). Ideally, we assume the availability of an acceleration measurement $\mathbf{a}(t) = \ddot{\boldsymbol{\xi}}(t - \delta) = \dot{\mathbf{x}}_2(t - \delta)$ where $\delta > 0$ is a short time delay due to measurement processing and signal communication. By letting $\boldsymbol{\alpha}$ in (5) be designed as an acceleration injection term,

$$\boldsymbol{\alpha}(t) = \mathbf{a}(t) - \mathbf{M}^{-1}\left(\mathbf{g}_0(\mathbf{y}(t-\delta), t-\delta) + \mathbf{u}(t-\delta)\right), \quad (7)$$

we get

$$\begin{aligned} \dot{\tilde{\mathbf{x}}}_1 &= \tilde{\mathbf{x}}_2 - \mathbf{L}_1\tilde{\mathbf{x}}_1 \\ \dot{\tilde{\mathbf{x}}}_2 &= -\mathbf{L}_2\tilde{\mathbf{x}}_1 + \tilde{\mathbf{r}}_\delta(t), \end{aligned} \quad (8)$$

where $\tilde{\mathbf{r}}_\delta(t) := \mathbf{r}(t) - \mathbf{r}(t-\delta)$.

Theorem 3. The observer (5) with acceleration feedforward (7) renders the error dynamics (8) ISS with respect to the bounded perturbation $\tilde{\mathbf{r}}_\delta(t)$, and the solutions converge to the set

$$\mathcal{B}_1 = \left\{ \tilde{x} \in \mathbb{R}^{2n} : |\tilde{x}| \le 4\sqrt{\frac{p_{1M}}{p_{1m}}}\frac{p_{1M}}{q_{1m}} L_r \delta \right\} \quad (9)$$

Proof. Let the error dynamics (8) be written as $\dot{\tilde{\mathbf{x}}} = \mathbf{A}_1\tilde{\mathbf{x}} + \mathbf{B}_1\tilde{\mathbf{r}}_\delta$, and apply the Lyapunov function $V_1(\tilde{\mathbf{x}}) = \tilde{\mathbf{x}}^\top\mathbf{P}_1\tilde{\mathbf{x}}$. Let $\mathbf{P}_1 = \mathbf{P}_1^\top > 0$ satisfy the Lyapunov equation $\mathbf{P}_1\mathbf{A}_1 + \mathbf{A}_1^\top\mathbf{P}_1 = -\mathbf{Q}_1$ for a chosen $\mathbf{Q}_1 = \mathbf{Q}_1^\top > 0$, and let $p_{1M} := \lambda_{max}(\mathbf{P}_1)$, $p_{1m} := \lambda_{min}(\mathbf{P}_1)$, and $q_{1m} := \lambda_{min}(\mathbf{Q}_1)$ be the respective maximum and minimum eigenvalues. Taking the time derivative gives

$$\begin{aligned} \dot{V}_1 &\le -q_{1m}|\tilde{\mathbf{x}}|^2 + 2p_{1M}|\tilde{\mathbf{x}}||\tilde{\mathbf{r}}_\delta| \\ &\le -\frac{q_{1m}}{2}|\tilde{\mathbf{x}}|^2, \quad \forall |\tilde{\mathbf{x}}| \ge 4\frac{p_{1M}}{q_{1m}}|\tilde{\mathbf{r}}_\delta|, \end{aligned}$$

which shows ISS from $\tilde{\mathbf{r}}_\delta$. From Lemma 1 we get that $\|\tilde{\mathbf{r}}_\delta\| \le L_r\delta$. This implies

$$\dot{V}_1 \le -\frac{q_{1m}}{2p_{1M}}V_1(\tilde{\mathbf{x}}), \quad \forall V_1(\tilde{\mathbf{x}}) \ge 16\frac{p_{1M}^3}{q_{1m}^2}L_r^2\delta^2.$$

It follows that the solutions must then converge to the set

$$\left\{ \tilde{\mathbf{x}} \in \mathbb{R}^{2n} : V_1(\tilde{\mathbf{x}}) \le 16\frac{p_{1M}^3}{q_{1m}^2}L_r^2\delta^2 \right\}$$

which is contained in $\mathcal{B}_1$. $\diamond$

It is seen from Theorem 3 that the ultimate bound for the observer error state is made smaller, either by making $\frac{p_{1M}}{q_{1m}}$ smaller, by tuning of $\mathbf{L}_1$ and $\mathbf{L}_2$, or by a shorter communication delay δ. In the limit as $\delta \to 0$ the set $\mathcal{B}_1$ is reduced to the origin, and the error state will converge exponentially to zero.

It should be noted that the error dynamics in (8) are linear, which enables linear tuning techniques, where the relative damping ratio and the cut-off frequency can be set up by the adjustment of $\mathbf{L}_1$ and $\mathbf{L}_2$.

3. ACCELERATION MEASUREMENTS

Unfortunately, obtaining the actual acceleration of the system is challenging. Accelerometers are influenced by the physical environment through temperature, mounting and gravity, where this creates a pseudo-force reading added to the actual acceleration. By considering that the sensor also contains noise, a model of the sensor output in the body frame is given in (Fossen, 2011),

$$\mathbf{a}(t) = \mathbf{R}(\boldsymbol{\Theta})\left(\ddot{\boldsymbol{\xi}}(t) + \mathbf{g}\right) + \mathbf{b}(t) + \mathbf{n}(t), \quad (10)$$

where $\Theta = [\phi\ \theta\ \psi]^\top$ is the attitude vector of the mechanical system, $\ddot{\boldsymbol{\xi}}(t)$ is the actual acceleration, $\mathbf{g}$ is the constant gravitational component, $\mathbf{n}(t)$ is noise, and $\mathbf{b}(t)$ is a slowly varying bounded bias which is independent of the system acceleration. It is usually assumed that this is driven by the mechanical arrangement and the operating temperature of the sensor itself.

In this paper we assume that the body frame of the system is perpendicular to the gravity vector, and that noise and the gravity component can be accounted for by other means. Hence, the model reduces to

$$\mathbf{a}(t) = \ddot{\boldsymbol{\xi}}_\delta(t) + \mathbf{b}(t), \quad (11)$$

where $\ddot{\boldsymbol{\xi}}_\delta(t)$ is the δ delayed acceleration of the system due to the signal processing.

3.1 AFF observer design with bias compensation

We return to the observer design in Section 2.1 and consider the effect of a slowly drifting bias on the acceleration measurement $a(t)$ and how this can be compensated. In (6) it is seen that the nominal observer error dynamics is perturbed by the fast-acting disturbance $\mathbf{r}(t)$. Without further measures, this would significantly deteriorate the observer accuracy. However, using feedforward compensation by the ideal acceleration measurement in (7), this disturbance becomes effectively rejected. If, on the other hand, the acceleration measurement contains an unknown slowly drifting bias $\mathbf{b}(t)$, as discussed above, the desired disturbance rejection becomes less effective. In this case, the bias $\mathbf{b}(t)$ will show up in the acceleration injection term (7), such that the closed loop system (8) becomes

$$\dot{\tilde{\mathbf{x}}} = \mathbf{A}_1\tilde{\mathbf{x}} + \mathbf{B}_1(\tilde{\mathbf{r}}_\delta(t) - \mathbf{b}(t)).$$

If we compare this system to the nominal error dynamics in (6), we see that for $\tilde{\mathbf{r}}_\delta(t) = 0$the disturbance $\mathbf{r}(t)$ is replaced by the much nicer "virtual" disturbance $\mathbf{b}(t)$ which is slowly varying and easier to compensate.

To this end, we assume as in (Fossen, 2011) that the accelerometer bias can be modeled as a Wiener process and augment the plant (3) correspondingly,

$$\begin{aligned}\dot{\mathbf{x}}_1 &= \mathbf{x}_2\\ \dot{\mathbf{x}}_2 &= \mathbf{M}^{-1}\mathbf{g}_0(\mathbf{y},t) + \mathbf{M}^{-1}\mathbf{u}(t) + \mathbf{r}(t)\\ \dot{\mathbf{b}} &= \mathbf{w}_b,\end{aligned} \tag{12}$$

where $\mathbf{w}_b$ is a zero-mean Gaussian driving noise. We then propose the observer

$$\begin{aligned}\dot{\hat{\mathbf{x}}}_1 &= \hat{\mathbf{x}}_2 + \mathbf{L}_1\tilde{\mathbf{y}}\\ \dot{\hat{\mathbf{x}}}_2 &= \mathbf{M}^{-1}\mathbf{g}_0(\mathbf{y},t) + \mathbf{M}^{-1}\mathbf{u}(t) - \hat{\mathbf{b}} + \mathbf{L}_2\tilde{\mathbf{y}} + \boldsymbol{\alpha}\\ \dot{\hat{\mathbf{b}}} &= \mathbf{L}_3\tilde{\mathbf{y}}\\ \hat{\mathbf{y}} &= \hat{\mathbf{x}}_1,\end{aligned} \tag{13}$$

where the acceleration injection law (7) now becomes perturbed by the bias, that is,

$$\begin{aligned}\boldsymbol{\alpha}(t) &= \mathbf{a}(t) - \mathbf{M}^{-1}\mathbf{g}_0(\mathbf{y}_\delta(t), t-\delta) - \mathbf{M}^{-1}\mathbf{u}_\delta(t)\\ &= \mathbf{b}(t) + \mathbf{r}_\delta(t).\end{aligned} \tag{14}$$

With this acceleration injection law inserted into (13), and letting $\hat{\mathbf{X}} := \mathrm{col}(\hat{\mathbf{x}}_1, \hat{\mathbf{x}}_2, \hat{\mathbf{b}})$, the augmented observer can be written

$$\begin{aligned}\dot{\hat{\mathbf{X}}} &= \mathbf{A}\hat{\mathbf{X}} + \mathbf{L}\tilde{\mathbf{y}} + \boldsymbol{\phi}(\mathbf{y},t) + \mathbf{B}(\mathbf{b}(t) + \mathbf{r}_\delta)\\ \hat{\mathbf{y}} &= \mathbf{C}\hat{\mathbf{X}},\end{aligned} \tag{15}$$

where

$$\mathbf{A} = \begin{bmatrix}\mathbf{0} & \mathbf{I} & \mathbf{0}\\ \mathbf{0} & \mathbf{0} & -\mathbf{I}\\ \mathbf{0} & \mathbf{0} & \mathbf{0}\end{bmatrix}, \quad \mathbf{L} = \begin{bmatrix}\mathbf{L}_1\\ \mathbf{L}_2\\ \mathbf{L}_3\end{bmatrix}, \quad \mathbf{C} = [\mathbf{I}\ \mathbf{0}\ \mathbf{0}]$$

$$\mathbf{B} = \begin{bmatrix}\mathbf{0}\\ \mathbf{I}\\ \mathbf{0}\end{bmatrix}, \quad \boldsymbol{\phi}(\mathbf{y},t) = \begin{bmatrix}\mathbf{0}\\ \mathbf{M}^{-1}(\mathbf{g}_0(\mathbf{y},t) + \mathbf{u}(t))\\ \mathbf{0}\end{bmatrix}.$$

It can be shown that the pair $(\mathbf{C}, \mathbf{A})$ is observable, and it follows that an injection gain matrix $\mathbf{L}$ can be designed so that $\mathbf{A}_2 := \mathbf{A} - \mathbf{LC}$ is Hurwitz. Letting $\tilde{\mathbf{X}} := col(\tilde{\mathbf{x}}_1, \tilde{\mathbf{x}}_2, \tilde{\mathbf{b}}) = col(\mathbf{x}_1 - \hat{\mathbf{x}}_1, \mathbf{x}_2 - \hat{\mathbf{x}}_2, \mathbf{b} - \hat{\mathbf{b}})$, the closed-loop error dynamics become

$$\dot{\tilde{\mathbf{X}}} = \mathbf{A}_2\tilde{\mathbf{X}} + \mathbf{B}\tilde{\mathbf{r}}_\delta + \mathbf{E}\mathbf{w}_b, \tag{16}$$

where $\mathbf{E} = \mathrm{col}(\mathbf{0}, \mathbf{0}, \mathbf{I})$. Let $\mathbf{P}_2 = \mathbf{P}_2^\top > 0$ satisfy the Lyapunov equation $\mathbf{P}_2\mathbf{A}_2 + \mathbf{A}_2^\top\mathbf{P}_2 = -\mathbf{Q}_2$ where $\mathbf{Q}_2 = \mathbf{Q}_2^\top > 0$ is chosen by design. Then the time derivative of the Lyapunov function $V_2(\tilde{\mathbf{X}}) = \tilde{\mathbf{X}}^\top\mathbf{P}_2\tilde{\mathbf{X}}$ becomes

$$\dot{V}_2 \leq -\frac{q_{2m}}{2}|\tilde{\mathbf{X}}|^2, \quad \forall |\tilde{\mathbf{X}}| \geq 4\frac{p_{2M}}{q_{2m}}L_r\delta, \tag{17}$$

where $p_{2M} := \lambda_{max}(\mathbf{P}_2)$, $p_{2m} := \lambda_{min}(\mathbf{P}_2)$, and $q_{2m} := \lambda_{min}(\mathbf{Q}_2)$. This gives the result:

Theorem 4. Assume the noise $\mathbf{w}_b = 0$. Then the observer (13) with acceleration feedforward (14) renders the error dynamics (16) ISS with respect to the bounded perturbation $\tilde{\mathbf{r}}_\delta(t)$, and the solutions converge to the set

$$\mathcal{B}_2 = \left\{\tilde{\mathbf{X}} \in \mathbb{R}^{3n} : |\tilde{\mathbf{X}}| \leq 4\sqrt{\frac{p_{2M}}{p_{2m}}}\frac{p_{2M}}{q_{2m}}L_r\delta\right\}. \tag{18}$$

◇

Once again we see that the set $\mathcal{B}_2$ reduces to the origin as $\delta \to 0$, in which case perfect state estimation, including bias estimation, is achieved.

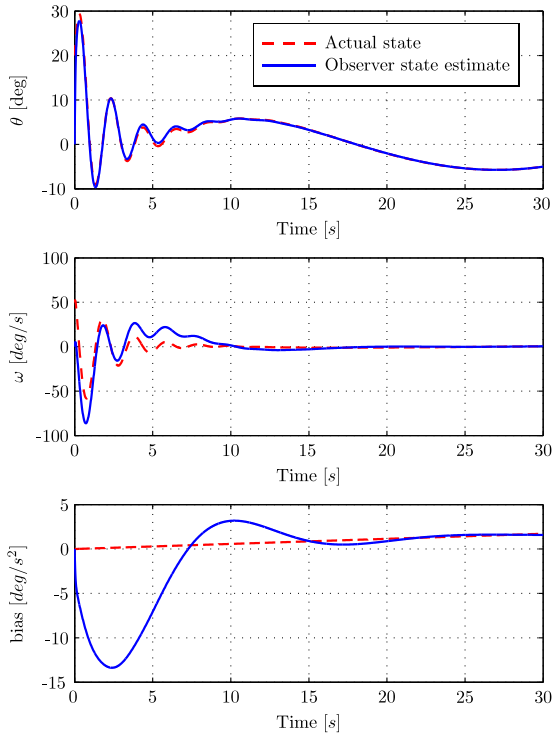

Figure 2. Plot of scalar inverted pendulum subject to an unmodeled sinusoidal disturbance and drifting accelerometer bias.

3.2 Simulation example

A simulation study was conducted to evaluate and verify the derived observer. The investigated system is a scalar inverted pendulum model,

$$\dot{\theta} = \omega \tag{19}$$

$$mL\dot{\omega} = mLg\sin\theta + d(t) + u(t) \tag{20}$$

which fits (1) with $g_0 = 0$ and $g_1(\dot{\xi}, \xi, t) = mL\sin\theta$, where θ is the angle of the pendulum relative the upright position, ω is the angular velocity, L is the pendulum length, and m is the mass of the pendulum bulb, located at the end of the pendulum. The disturbance $d(t)$ was modeled as

$$d(t) = A_d\sin(\omega_d t). \tag{21}$$

where $\omega_d = 2\pi f_d$ is the frequency of the disturbance, and A_d its amplitude. The bias accelerometer was modeled as

$$a(t) = \dot{\omega}_\delta + b(t) \tag{22}$$

$$b(t) = A_b t \tag{23}$$

where the bias drift rate A_d is set in accordance with a low cost accelerometer. The control input was simply generated by a nonlinear PD controller defined as,

$$u(t) = -k_p\hat{x_1} - k_d\hat{x_2} - mLg\sin\theta. \tag{24}$$

where k_p and k_d are control gains.

Figure 2 features the simulation output where the observer, targeting the scalar inverted pendulum system subject to both the environmental forces and accelerometer bias, was set up as in (13)-(14). The simulation featured the following parametric setup

m	L	δ	L_1	L_2	L_3	k_p	k_d
1	1	0.01	25	10	−5	10	1

From the figure it can be seen that the observer features feasible and robust performance as it converges to and tracks the system output, both with respect to the measured angular position, in addition to the unmeasured angular velocity and bias. Hence, the theoretical foundation is verified, and it can be concluded that the observer successfully handles both the disturbance and uncertain dynamics.

4. DP OBSERVER WITH AFF

As mentioned, DP is an application subject to a variety of unmodeled forces, especially when subject to ice. In this paper it is assumed that the vessel operates in a pre-broken moving ice regime where the sea ice covers a high percentage of the surface. Such an environmental force is challenging to model for control purposes due to its highly nonlinear and chaotic nature. As significant amounts of ice is assumed to surround the vessel, the 1st order wave forces can be omitted from the model. Some recent results on DP can be found in (Nguyen et al., 2011) and (Jenssen et al., 2009). From (Fossen, 2011), a marine vessel can be modeled as

$$\begin{aligned} \dot{\boldsymbol{\eta}} &= \mathbf{R}(\psi)\boldsymbol{\nu} \\ \mathbf{M}\dot{\boldsymbol{\nu}} + \mathbf{C}(\boldsymbol{\nu})\boldsymbol{\nu} + \mathbf{D}(\boldsymbol{\nu})\boldsymbol{\nu} &= \mathbf{u}(t) + \mathbf{d}(t) \\ \mathbf{y} &= \boldsymbol{\eta}, \end{aligned} \tag{25}$$

where

$$\mathbf{R}(\psi) = \begin{bmatrix} \cos\psi & -\sin\psi & 0 \\ \sin\psi & \cos\psi & 0 \\ 0 & 0 & 1 \end{bmatrix} \tag{26}$$

is the kinematic rotation matrix relating the position and heading vector $\boldsymbol{\eta} = [x\ y\ \psi]^\top$ to the velocity vector $\boldsymbol{\nu} = [u\ v\ r]^\top$, $\mathbf{M} \in \mathbb{R}^{3\times3}$ is the vessel mass matrix, $\mathbf{D}(\boldsymbol{\nu}) \in \mathbb{R}^{3\times3}$ is the hydrodynamic damping matrix, $\mathbf{C}(\boldsymbol{\nu}) \in \mathbb{R}^{3\times3}$ is the Coriolis and centripetal force matrix, $\mathbf{u}(t) \in \mathbb{R}^{3\times1}$ is the control input vector, and $\mathbf{d}(t) \in \mathbb{R}^{3\times1}$ is an environmental disturbance force vector which is assumed to encompass ice loads, current forces, 2nd order wave drift forces, and other unmodeled dynamics.

It is assumed that the DP vessel sensor suite contains a motion reference unit (MRU) measuring accelerations, and a position and heading measurement system. Velocity is normally not directly available, which underline the need for an observer, in addition to filtering and merging measurements to achieve a feasible state vector estimate. As in (Fossen, 2011) it is assumed that the precision of the heading measurement is sufficient for direct application in the observer. This enables direct calculations of the kinematic relations.

By utilizing the framework in Section 2, $\mathbf{g}_0$ and $\mathbf{g}_1$ are selected as,

$$\begin{aligned} \mathbf{g}_0(\boldsymbol{\eta}_p, t) &= 0 \\ \mathbf{g}_1(\boldsymbol{\nu}, t) &= \mathbf{d}(t) - \mathbf{C}(\boldsymbol{\nu})\boldsymbol{\nu} - \mathbf{D}(\boldsymbol{\nu})\boldsymbol{\nu}. \end{aligned} \tag{27}$$

It should be noted that all forces that are a function of the unmeasured vessel velocity $\boldsymbol{\nu}$ is enclosed in $\mathbf{g}_1$ due to their uncertainty. Hence, we have the following simplified model,

$$\begin{aligned} \dot{\boldsymbol{\eta}} &= \mathbf{R}(\psi)\boldsymbol{\nu} \\ \dot{\boldsymbol{\nu}} &= \mathbf{M}^{-1}\mathbf{u}(t) + \mathbf{M}^{-1}\mathbf{r}(t) \\ \mathbf{y} &= \boldsymbol{\eta}. \end{aligned} \tag{28}$$

For the nominal model of (28), setting $\mathbf{r}(t) = \mathbf{0}$, we assume there exists an observer, such that the error dynamics

$$\dot{\tilde{\boldsymbol{\eta}}} = \mathbf{f}_\eta(\tilde{\boldsymbol{\eta}}, \tilde{\boldsymbol{\nu}}, t) \tag{29}$$

$$\dot{\tilde{\boldsymbol{\nu}}} = \mathbf{f}_\nu(\tilde{\boldsymbol{\eta}}, \tilde{\boldsymbol{\nu}}, t) \tag{30}$$

is UGES, and that there exists a corresponding Lyapunov function satisfying the bounds

$$c_1 \left|(\tilde{\boldsymbol{\eta}}, \tilde{\boldsymbol{\nu}})\right|^2 \leq V(\tilde{\boldsymbol{\eta}}, \tilde{\boldsymbol{\nu}}) \leq c_2 \left|(\tilde{\boldsymbol{\eta}}, \tilde{\boldsymbol{\nu}})\right|^2 \tag{31}$$

$$\frac{\partial V}{\partial \tilde{\boldsymbol{\eta}}}\mathbf{f}_\eta(\tilde{\boldsymbol{\eta}}, \tilde{\boldsymbol{\nu}}, t) + \frac{\partial V}{\partial \tilde{\boldsymbol{\nu}}}\mathbf{f}_\nu(\tilde{\boldsymbol{\eta}}, \tilde{\boldsymbol{\nu}}, t) \leq -c_3 \left|(\tilde{\boldsymbol{\eta}}, \tilde{\boldsymbol{\nu}})\right|^2. \tag{32}$$

According to the results of (Loria and Panteley, 1999), (Aamo et al., 2000), and (Skjetne and Shim, 2001), such observers do exist for the DP model with $\mathbf{D} = \mathbf{0}$.

For the actual case, with $\mathbf{r}(t) \neq \mathbf{0}$, we can again augment this observer with the AFF term

$$\boldsymbol{\alpha} = \mathbf{a}(t) - \mathbf{M}^{-1}\mathbf{u}_\delta(t), \tag{33}$$

in which case (30) becomes

$$\dot{\tilde{\boldsymbol{\nu}}} = \mathbf{f}_\nu(\tilde{\boldsymbol{\eta}}, \tilde{\boldsymbol{\nu}}, t) + \mathbf{M}^{-1}\tilde{\mathbf{r}}_\delta(t) \tag{34}$$

where $\tilde{\mathbf{r}}_\delta(t) := \mathbf{r}(t) - \mathbf{r}_\delta(t)$. Since the nominal error dynamics is UGES, it is also ISS for bounded disturbances. Hence, assuming that global Lipschitzness can be shown for $\mathbf{r}(t)$ such that $|\tilde{\mathbf{r}}_\delta(t)| \leq L_r\delta$, $\forall t$, there exists $c_4 > 0$ such that (32) becomes

$$\frac{\partial V}{\partial \tilde{\boldsymbol{\eta}}}\mathbf{f}_\eta(\tilde{\boldsymbol{\eta}}, \tilde{\boldsymbol{\nu}}, t) + \frac{\partial V}{\partial \tilde{\boldsymbol{\nu}}}\mathbf{f}_\nu(\tilde{\boldsymbol{\eta}}, \tilde{\boldsymbol{\nu}}, t) \leq -c_3 \left|(\tilde{\boldsymbol{\eta}}, \tilde{\boldsymbol{\nu}})\right|^2 + c_4\delta. \tag{35}$$

From standard ISS results it follows that the error states $(\tilde{\boldsymbol{\eta}}, \tilde{\boldsymbol{\nu}})$ will converge to a limit set containing the origin, with size parameterized by δ.

An example of an observer for (28) with the desired properties is

$$\begin{aligned} \dot{\hat{\boldsymbol{\eta}}} &= \mathbf{R}(\psi)\hat{\boldsymbol{\nu}} + \mathbf{L}_1\tilde{\mathbf{y}} \\ \dot{\hat{\boldsymbol{\nu}}} &= \mathbf{M}^{-1}\mathbf{u}(t) + \boldsymbol{\alpha} + \mathbf{R}(\psi)^\top\mathbf{L}_2\tilde{\mathbf{y}} \\ \hat{\mathbf{y}} &= \hat{\boldsymbol{\eta}}, \end{aligned} \tag{36}$$

where $\tilde{\mathbf{y}} = \mathbf{y} - \hat{\mathbf{y}} = \tilde{\boldsymbol{\eta}}$.

UGES of the nominal error dynamics, with $\mathbf{r}(t) - \boldsymbol{\alpha}(t) = \mathbf{0}$, is shown by using the global diffeomorphism $\mathbf{z}_1 := \mathbf{R}(\psi)\tilde{\boldsymbol{\nu}}$, $\mathbf{z}_2 := \mathbf{L}_2\tilde{\boldsymbol{\eta}} - c\mathbf{R}(\psi)\tilde{\boldsymbol{\nu}}$, $c > 0$, and the quadratic Lyapunov function $V := 0.5\mathbf{z}_1^\top\mathbf{z}_1 + 0.5\mathbf{z}_2^\top\mathbf{z}_2$.

As has here been shown, augmenting an observer for a mechanical system, such as a DP system, with AFF provides a powerful and robust tool for handling uncertain forces (that is, forces that are velocity dependent, parametrically uncertain, or unmodeled).

Another aspect is that AFF as a design methodology can also be applied to mechanical systems that require more sophisticated observers. For instance, for the DP

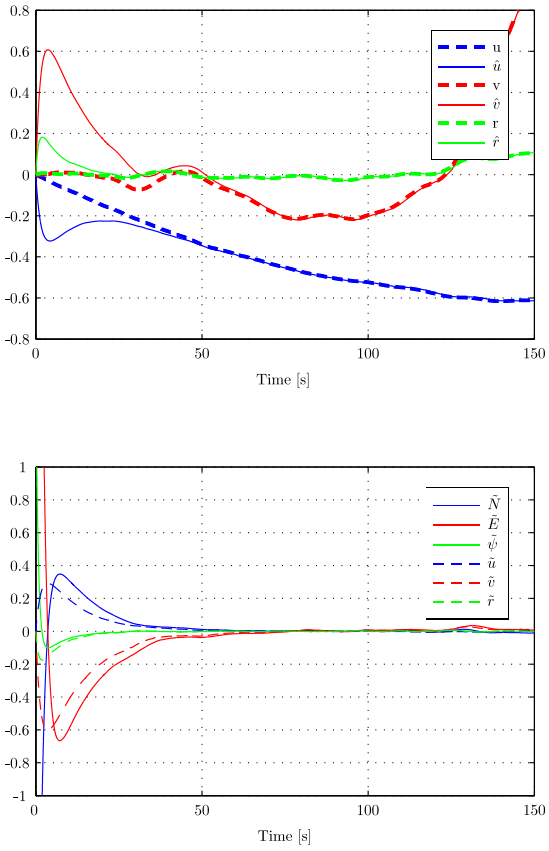

Figure 3. Top: Actual and estimated velocities of the AFF DP observer with $\delta = 1$ subject to unmodeled disturbances and deviant initial conditions. Bottom: Error variables.

application the first order wave forces will, if not handled, create oscillations in the position and velocity estimates that in turn may induce unnecessary wear-and-tear in the machinery systems. Extending the AFF methodology with a first-order wave filter, as seen in (Fossen, 2011), will in this case constitute a more practical and robust observer.

As an illustrative example of a system with an unmodeled disturbance force, Figure 3 features the estimated velocities and error variables of the AFF DP observer subject to ice forces similar to those depicted in Figure 1. It is seen that the unmodeled ice forces are handled in an efficient manner by the observer. Note that the phase lag often encountered with unmodeled disturbances in conventional observers is here significantly enhanced by use of AFF. This example, along with the theoretical foundation established in this paper underlines the potential of AFF in observer design.

5. CONCLUSIONS

In this paper a general AFF observer for a mechanical system has been developed which robustly handles unmodeled disturbances and unmodeled internal dynamics. This is done by incorporating an acceleration measurement which is utilized to form an acceleration feedforward capable of handling such disturbances. An estimator handles the bias force originating from the mis-reading of the accelerometer. Thus, the observer is made to provide feasible robust performance.

REFERENCES

Aamo, O.M., Arcak, M., Fossen, T.I., and Kokotovic, P.V. (2000). Global output tracking control of a class of euler-lagrange systems. *Internat. J. Control*, 74, 649–658.

Blakelock, J.H. (1991). *Automatic Control of Aircraft and Missiles*. Wiley-Interscience.

Chen, W., Ballance, D., Gawthrop, P., and O'Reilly, J. (2000). A nonlinear disturbance observer for robotic manipulators. *Industrial Electronics, IEEE Transactions on*, 47(4), 932–938.

de Jager, B. (1994). Acceleration assisted tracking control. *IEEE Control Systems Magazine*, 14, 20–27.

Fossen, T.I., Lindegaard, K.P., and Skjetne, R. (2002). Inertia shaping techniques for marine vessels using acceleration feedback. In *Proc IFAC World Congress*.

Fossen, T.I. (2011). *Handbook of Marine Craft Hydrodynamics and Motion Control*. Wiley.

Jenssen, N.A., Muddesitti, S., Phillips, D., and Backstrom, K. (2009). Dp in ice conditions. In *Dynamic Positioning Conference, Huston, Texas, USA*.

Kempf, C. and Kobayashi, S. (1999). Disturbance observer and feedforward design for a high-speed direct-drive positioning table. *IEEE Transactions on Control Systems Technology*, 7(5), 513–526.

Kjerstad, Ø., Skjetne, R., and Jenssen, N.A. (2011). Disturbance rejection by acceleration feedforward: Application to dynamic positioning. In *Proceedings of IFAC World Congress, Milan, Italy*.

Lindegaard, K.P.W. (2003). *Acceleration Feedback in Dynamic Positioning*. Ph.D. thesis, Norwegian University of Science and Technology.

Loria, A. and Panteley, E. (1999). A separation principle for a class of euler-lagrange systems.

Nguyen, D.H., Nguyen, D.T., Quek, S.T., and Sørensen, A.J. (2011). Position-moored drilling vessel in level ice by control of riser end angles. *Cold Regions Science and Technology*, 66(2–3), 65 – 74.

Skjetne, R. and Shim, H. (2001). A systematic nonlinear observer design for a class of euler-lagrange systems. In *Proceedings of 9th Mediterranean Conf. Control and Automation (Med'01), Dubrovnik, Croatia, June 2001*.

Feedforward Linearization and Disturbance Rejection of Mechanical Systems Using Acceleration Measurements

Feedforward linearization and disturbance rejection of mechanical systems using acceleration measurements ⋆

Øivind Kåre Kjerstad * **Roger Skjetne** *

* *Department of Marine Technology, Norwegian University of Science and Technology, Otto Nielsens vei 10, NO-7491 Trondheim, Norway. E-mails: oivind.k.kjerstad@ntnu.no and skjetne@ieee.org*

Abstract: In this paper a time-delayed acceleration measurement is used to linearize a second order nonlinear system. A theoretical foundation is developed, and a control strategy is presented which handles the challenges related to classical linearization. Utilizing the acceleration measurement to directly cancel the nonlinearities constitute a feedforward approach which increases robustness with respect to unmodeled dynamics and model uncertainties. Due to the time-delay, one or more perturbation terms dependent on a previous state of the system appears. This work outlines a stability criterion which these terms must satisfy in order for the linearization to be valid, where it is shown that the performance of the scheme is dependent on the measurement time-delay. The proposed method proves feasible when compared to two other nonlinear control strategies, including a conventional linearization control law and a sliding mode control law. In comparison, the feedforward linearization features robust performance without aggressive control input.

Keywords: Feedforward, Linearization, Nonlinear systems, Delayed systems, Sliding mode

1. INTRODUCTION

Dealing with nonlinear systems is a challenge with a truly wide scope, and in many cases the most practical way to approach the stabilization problem is to appeal to the strong results available for linear systems. Hence, to enable this, a linearization of the nonlinear system in scope must be performed. For the class of systems that can be modeled with Newton's second law, the main objective is often to control the position and velocity of an object to a desired state by measurements. During design of the control system compensation of the nonlinear dynamics is done by applying the same position and state measurements. Acceleration measurements are typically not used. Although these systems are proved stable and robust it is not guaranteed that the control laws provide adequate compensation of unstable dynamics when subject to parametric uncertainty, or when influenced by unmodeled dynamics. An acceleration measurement of the system will encompass the full right hand side of the state equation, and thus, will be ideal for linearization as it does not rely on reconstruction of the governing dynamics based on parameter estimates and modeling assumptions in order to replicate the system dynamics.

Regardless of control approach, the general problem when canceling nonlinearities of a system is that it requires perfect knowledge of the state equation. In any practical matter, exact mathematical cancellation is challenging, both as a time-delay will be present when measuring a state and using it as feedback, and in addition to this, the parametric and model uncertainty. For linearization based on state measurements, these effects will almost always result in a closed-loop system, which is a perturbation of the exponentially stable nominal linear system we seek to obtain. Another aspect of linearization is that it only handles modeled nonlinearities. In this paper the goal is to investigate how some of these challenges can be overcome if a time-delayed acceleration measurement is available. The motivation and basic idea is to utilize the fact that this measurement contains all dynamics of the system, and use this to effectively linearize the system, and obtain a linear system. As the acceleration measurement is assumed to be time-delayed due to signal processing and communication, a perturbation of the nominal linear system will occur as the cancellation is imperfect. Thus, a theoretical foundation must be established, providing proofs of its feasibility and usability. The aim of this paper is to establish this, and provide a comparison with conventional linearization, and other nonlinear control methods.

Using acceleration measurements in control is not a new idea, both when it comes to increase robustness and handle disturbances. Some relevant applications can be seen in [de Jager, 1994] and [Jinzenji et al., 2001] where acceleration measurements are utilized to increase robustness and performance. They can also be utilized as in [Kempf and Kobayashi, 1999] and [Chen et al., 2000], where disturbance observers are developed to attenuate the effect of the disturbances on the system. It is also a known fact that linearization is extensively used in robotic systems

⋆ Supported by the Research Council of Norway under grant 199567/I40 : "Arctic DP".

[Spong et al., 2005, Siciliano et al., 2011]. This work is also a continuation of [Kjerstad et al., 2011] where a similar approach was used to compensate an external force acting on a marine vessel. Also, a related approach can be seen in [Fossen et al., 2002].

In this paper it is assumed that the position and velocity states are available for feedback without any time-delay, which is a well established approach in the control community. The paper is structured as follows, in Section 2 the linearizing method is presented and theoretically investigated, in order to propose stability criterion for using the approach. In Section 3 a simulation study investigates the effect of the time delay and compares the approach with a classical linearization control law and a sliding mode approach. Concluding remarks are made in Section 4.

Notations: In GS, LAS, LES, UGAS, UGES, etc., stands G for Global, L for Local, S for Stable, U for Uniform, A for Asymptotic, and E for Exponential. Total time derivatives of $x(t)$ is denoted $\dot{x}$, $\ddot{x}$, $x^{(3)}$,.., $x^{(n)}$. The Euclidean vector norm is $|\mathbf{x}| := (\mathbf{x}^\top \mathbf{x})^{1/2}$. A diagonal matrix is denoted $diag\{a_1, .., a_n\} \in \mathbb{R}^{n\times n}$. Stacking several vectors into one is denoted $\text{col}(x, y, z) := [x^\top, y^\top, z^\top]^\top$, and whenever convenient, $|(x, y, z)| = |\text{col}(x, y, z)|$. Time delayed signals are denoted $x_\delta = x(t-\delta)$, and cancellations based on time delayed signals are denoted $\tilde{x}_\delta = x(t) - x(t-\delta)$.

2. FEEDFORWARD LINEARIZATION

2.1 Method introduction

Suppose we have a second order mechanical system modeled by Newtons 2. law as

$$m\ddot{\xi} = \sum F, \tag{1}$$

where $\xi \in \mathbb{R}$, which for convenience can be written as

$$m\ddot{\xi} = \rho(\xi) + d(t) + u, \tag{2}$$

where the internal dynamics of the system $\rho(\xi)$ is continuous and locally Lipschitz on $\mathbb{R}^n$, in addition to $\rho(\xi) \to 0$ as $\xi \to 0$. The external forces $d(t)$ are assumed to be globally Lipschitz. u is the control input which will be used to linearize the system. For simplicity we can write the system as

$$\dot{x}_1 = x_2 \tag{3}$$
$$m\dot{x}_2 = \rho(x) + d(t) + u, \tag{4}$$

where $x = col(x_1, x_2) = col(\dot{\xi}, \ddot{\xi})$.

The concept of feedforward linearization utilizes an acceleration measurement to cancel the nonlinear dynamics and external forces of the system through the following proposed control input

$$u = \alpha(x) - (m\dot{x}_{2\delta} - u_\delta), \tag{5}$$

where the subscript δ denotes that the measurement is delayed by δ time, such as $\dot{x}_{2\delta} = \dot{x}_2(t-\delta)$. $\alpha(x)$ is a nominal control law to be designed. From (5) it can be seen how $m\dot{x}_{2\delta} - u_\delta$ constitute a delayed measurement of the right hand side of (4),

$$m\dot{x}_{2\delta} - u_\delta = \rho(x_\delta) + d_\delta. \tag{6}$$

Thus, this feedforward term can be used to linearize both the internal and external components of (4) directly. By closing the loop with the proposed control input (5) the system becomes

$$\dot{x}_1 = x_2 \tag{7}$$
$$m\dot{x}_2 = \alpha(x) + \tilde{\rho}_\delta + \tilde{d}_\delta \tag{8}$$

where

$$\tilde{\rho}_\delta = \rho(x) - \rho(x_\delta) \tag{9}$$
$$\tilde{d}_\delta = d - d_\delta. \tag{10}$$

Due to the introduction of the time-delay, the model of the system is transformed from an Ordinary Differential Equation (ODE), to a Delayed Differential Equation (DDE). Hence, the system development is no longer just dependent on present time, but also an earlier state of the system [Gu et al., 2003]. This gives rise to some challenges, which is illustrated in the following example.

2.2 Example: Delayed internal dynamics

To evaluate the stability challenges that might arise due to the δ time-delay, the following unstable system is chosen,

$$\dot{z} = z^2 + u, \quad z(0) = z_0 \tag{11}$$

which fits (4) with $d(t) = 0$, and $m = 1$. In the uncontrolled case this is a finite escape time system, provided that $z(0) \neq 0$. Suppose that the feedforward linearization is applied, using the following linearizing control input

$$u = -kz - (\dot{z}_\delta - u_\delta) \tag{12}$$
$$= -kz - z_\delta^2, \tag{13}$$

where $k > 0$ is a feedback gain. The closed-loop system then becomes

$$\dot{z} = -kz + z^2 - z_\delta^2, \quad z(0) = z_0. \tag{14}$$

In order for this to be well defined, the initial conditions of z_δ on the interval $t \in [0 \;\; \delta)$ must be defined. By assuming that

$$z_\delta = 0, \quad 0 \leq t < \delta, \tag{15}$$

the closed-loop dynamics for the initialization interval becomes

$$\dot{z} = -kz + z^2 \quad 0 \leq t < \delta, \tag{16}$$

which solution is

$$z(t) = \frac{k}{(\frac{k}{z_0} - 1)e^{kt} + 1}, \tag{17}$$

where it can be seen that if $k < z_0 < \infty$, $z(t)$ will escape in finite time, given by

$$t_\infty = \frac{1}{k} ln\left(\frac{1}{1 - \frac{k}{z_0}}\right). \tag{18}$$

In order for the feedforward linearization to work, the cancellation of the destabilizing term z^2 must begin before the system escapes to infinity. Hence,

$$\delta < t_\infty. \tag{19}$$

In addition, the stabilizing term $-kz$ must hereafter suppress the fraction $z^2 - z_\delta^2$. We investigate this using the following Lyapunov function candidate

$$V(z) = \frac{1}{2}z^2, \tag{20}$$

for which time derivative becomes

$$\dot{V}(z) = z\dot{z} \tag{21}$$
$$= z(-kz + z^2 - z_\delta^2) \tag{22}$$
$$= -kz^2 + z(z^2 - z_\delta^2) \tag{23}$$

In order to have a guaranteed negative definite Lyapunov function, the linear feedback must dominate the nonlinear error term. Hence,

$$\dot{V}(z) = -\frac{1}{2}kz^2 - \frac{1}{2}kz^2 + z(z^2 - z_\delta^2) \tag{24}$$

$$\leq -\frac{1}{2}kz^2 \quad \forall \frac{1}{2}k|z| > |z^2 - z_\delta^2| \tag{25}$$

Based on this we can conclude that there is a bounded open set,

$$\mathcal{D}_0(z) := \left\{ z \in \mathbb{R} \ : \ \frac{1}{2}k|z| > |z^2 - z_\delta^2| \right\} \tag{26}$$

in the neighborhood of $z = 0$ where the linearization works. Outside of $\mathcal{D}_0$ it fails as the cancellation error of the nonlinearity becomes dominant. In order to evaluate effect of the time delay the solution of (14) at time $t = \delta$ must be evaluated. The reason for this is the fact that if the solution resides inside $\mathcal{D}_0$ at time $t = \delta$, we have that,

$$z(t) \leq z(\delta)e^{-\gamma(t-\delta)} \quad \forall t \in [\delta \ \infty), \tag{27}$$

for $\gamma > 0$, due to the negative definiteness of the Lyapunov function, and the fact that $z^2 < |z| < 1$. However, if outside $\mathcal{D}_0$ at $t = \delta$ the solution will grow indefinitely. Hence, the stability of the system applying feedforward linearization relies on

$$|kz(\delta)| > |z(\delta)^2 - z(0)^2|, \tag{28}$$

as this is the point in time where the trajectory of the solution will have propagated furthest away from the equilibrium $z = 0$ as no cancellation of the destabilizing term is active. However, it will be the value of z_0 that is ultimately deciding if the system is able to propagate out of $\mathcal{D}_0$ or not, as there will be a subset $\Omega_0 \subset \mathcal{D}_0$ which ensures that $z \in \mathcal{D}_0 \ \forall \ t$. If $z_0 \notin \Omega_0$ the solution will propagate out of $\mathcal{D}_0$, and approach infinity. It should also be noted that if $z_0 < k$ the time-delay challenge is eased due to the guaranteed domination of the linear term in (25). In any case, the size of $\mathcal{D}_0$, and inherently Ω_0 can be increased by increasing k, and also the stability margin could be enhanced by choosing $z_\delta = z_0 \ \forall t \in [0 \ \ \delta]$.

2.3 Delayed external disturbance cancellation

As with the internal dynamics, external forces will also be suppressed by the linearization as seen in (7)-(10). Similarly, the level of suppression will be δ-dependent. Due to the global Lipschitz assumption the following inequality holds

$$|d - d_\delta| \leq L\delta, \tag{29}$$

where $L > 0$.

Although a strict requirement, it is not necessarily unfeasible as environmental forces such as wind or ocean current tend to be bounded and continuous. Also, unmodeled dynamics will be encompassed by this term. Hence, sufficient knowledge in order to verify the Lipschitz condition is required.

In any case, the unknown independent external force fraction will always be present. Hence, it will not disappear when the trajectory of the solution approaches the origin.

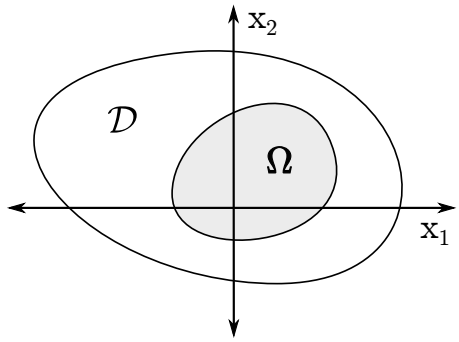

Fig. 1. Illustration of the sets $\mathcal{D}$ and Ω.

Generally, this means that the solution will converge to a ball around the equilibrium rather the point itself.

2.4 Stability analysis

Based on the above discussion, the closed-loop system (7) - (8) can be viewed as linear system with two perturbation terms, where the one from the internal dynamics is vanishing, and the other, from the external disturbance is non-vanishing. Hence, the system can be written as

$$\dot{x} = \begin{bmatrix} 0 & 1 \\ -k_1 & -k_2 \end{bmatrix} x + \begin{bmatrix} 0 \\ \tilde{\rho} \end{bmatrix} + \begin{bmatrix} 0 \\ \tilde{d} \end{bmatrix} \tag{30}$$

$$= Ax + g(t, x) \tag{31}$$

provided that

$$\alpha(x) = -k_1 x_1 - k_2 x_2. \tag{32}$$

By investigation we see that the nominal system $\dot{x} = Ax$ and its first partial derivatives with respect to x are continuous, bounded, and Lipschitz in x, uniformly in t, for all $(t, x) \in \mathbb{R}^2$. If $k_1, k_2 > 0$ the matrix A is Hurwitz, and thus there exist a solution $P = P^\top > 0$ of the Lyapunov equation such that

$$V(x) = x^\top P x \tag{33}$$

has a negative definite time derivative

$$\dot{V}(x) = -\|kx\|^2 \leq -W_3(x), \tag{34}$$

where $W_3(x)$ is a continuous positive definite function on $\mathbb{R}^2$. From this we can conclude that the nominal system is GES.

Although, the nominal system is stable, the perturbation terms must be investigated in order to establish the stability properties of the overall system. Provided that δ can be chosen sufficiently small such that

$$x(\delta) \in \mathcal{D} \tag{35}$$

where

$$\mathcal{D} := \left\{ x \in \mathbb{R}^2 \mid \|kx(\delta)\| > \|\rho(x(\delta)) - \rho(x(0))\| + L\delta \right\}, \tag{36}$$

there will exist a set $\Omega \subset \mathcal{D}$, as depicted in 1, which for all

$$\mathbf{x}_0 \in \Omega \tag{37}$$

we have that the

$$\|g(t, x)\| \leq \mu, \quad \forall (t, x) \in [0, \infty] \times \mathcal{D} \tag{38}$$

where $\mu > 0$. It should be pointed out that if there are no destabilizing terms in ρ, then $\mathcal{D} = \mathbb{R}^2$.

The prerequisites for Theorem 9.1 in [Khalil, 2001] has now been met, and thus we can conclude that

$$\|z(t) - y(t)\| \leq k_e e^{-\gamma(t-t_0)} \|z(t_0) - y(t_0)\| + \beta\mu \quad (39)$$

where $y(t)$ and $z(t)$ denote the solutions of the nominal system and the perturbed system, respectively. This means that the solution converges to a ball around the equilibrium, spanned by $\beta\mu$. It should be noted that the size of this ball is determined by δ, as $\delta \to 0$ is the unperturbed system. The results from above are summarized in the following Theorem.

Theorem 1. Given a system on the form (2), where the internal dynamics ρ are locally Lipschitz, and the disturbance d is globally Lipschitz. Then a linearization using a δ time-delayed acceleration measurement is possible provided that δ can be chosen sufficiently small, such that $x(\delta) \in \mathcal{D}$, where

$$\mathcal{D} := \left\{ x \in \mathbb{R}^2 \mid \|kx(\delta)\| > \|\rho(x(\delta)) - \rho(x(0))\| + L\delta \right\}, \quad (40)$$

and $k > 0$ is the feedback linearization gain. Then, the solution $y(t)$ of the linear nominal system, and $z(t)$ of the perturbed system will converge to a ball around the equilibrium as

$$\|z(t) - y(t)\| \leq k_e e^{-\gamma(t-t_0)} \|z(t_0) - y(t_0)\| + \beta\mu, \quad (41)$$

where $\beta > 0$ and $\|g(t,x)\| \leq \mu$ where $g(t,x)$ is the sum of the perturbation terms.

2.5 Usability considerations

From a practical point of view there are several aspects of the presented approach that are interesting. As the full right hand side of the equation is measured, and through cancellation forcing the dynamics to behave linearly, parameter uncertainty and unmodeled dynamics can be handled directly. The use of the acceleration measurement also effectively enhances the phase margin, enabling for reactive control. Although, any inertial system controlled by state feedback, influenced by an external disturbance, will have to perform unnecessary work as momentum has been gained before the control law begins compensation, the deviations can be caught at an earlier stage as the force disturbance is sensed directly and not through time integrals of the force. This makes the method applicable not only when the system contains unstable dynamics, but also in order to reject or attenuate unmodeled disturbances. However, some knowledge of the system is required in order to evaluate the stability, especially if the internal dynamics contains destabilizing terms.

For all applications, δ should be chosen as small as possible, as this will improve cancellation. $\delta = 0$ is impossible in practice, as there will be a delay originating from signal processing and communication of the accelerometer measurements. Also, mathematically, δ must be present in order to avoid breaking causality. Due to the time delay the method is only local, and not global. However, in practical applications the operating points will always be a local subset of $\mathbb{R}$.

In order to implement the scheme, an accurate acceleration measurement is required. Unfortunately, this is challenging as accelerometers, produce biased and noisy signals where the output is the sum of the acceleration induced by the dynamic system, a bias term, and a gravity component dependent on the sensor orientation. Allowing such measurements directly into a closed-loop feedback system is destined to deteriorate the overall performance. Hence, signal processing removing noise and the gravity contribution is required. This has been investigated in [Lindegaard, 2003].

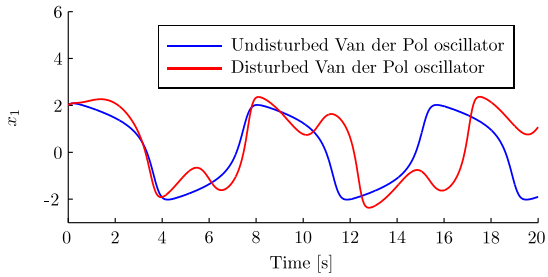

Fig. 2. Time development of the undisturbed and unforced Van der Pol oscillator with initial conditions $x_{1,0} = 2$ and $x_{2,0} = 1$, and parameters $m = 1$, $\epsilon = 2$

3. SIMULATION STUDY

3.1 Feasibility evaluation

In order to evaluate the performance of the feedforward linearization scheme, a simulation study was performed. During which, the Van der Pol equation was the system of evaluation,

$$\dot{x}_1 = x_2 \quad (42)$$

$$m\dot{x}_2 = -x_1 + \epsilon(1 - x_1^2)x_2 + d(t) + u \quad (43)$$

where, u is the control input, m is a scaling parameter, and $d(t)$ is an external unmodeled disturbance effect that will make the system behave chaotic. The Van der Pol equation is well established and has been used in both physical and biological sciences to describe systems which contain a stable limit cycle around the origin [Khalil, 2001]. Fig.2 features the time development of both the disturbed and undisturbed system provided $x_{1,0} = 2$ and $x_{2,0} = 1$ as initial conditions. These will remain the same for the rest of the simulation study.

As the system contains a stable limit cycle it can be guaranteed that the solution will not escape to infinity before the cancellation begins. This means that $x(\delta)$ is uniformly bounded, and thus, it is possible to apply the feedforward linearization scheme. The perturbation terms appearing from the cancellation are not bringing the solution out of the set $\mathcal{D}$ where the linear feedback dominates. Hence, the inequality

$$\|kx(\delta)\| \geq \|\tilde{\rho}_\delta\| + L\delta \quad (44)$$

is achieved, and hence $\mathcal{D} = \mathbb{R}^2$ for all x_0 provided that k is chosen sufficiently large. If the linearizing feedback gains are chosen such that the nominal unperturbed linear system is exponentially stable and, and δ is sufficiently

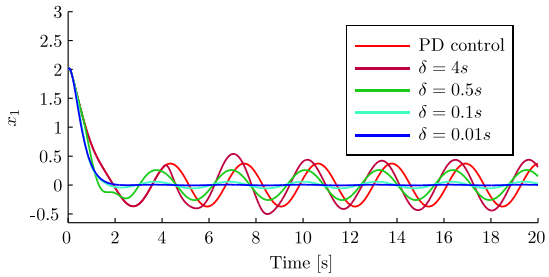

Fig. 3. Linearizing performance of the Van der Pol system subject to a disturbance, using different δ values, compared to a PD control law.

small, then Theorem 1 can be applied. Although there is no upper δ limit in terms of stability for this system, the performance will depend on it as the perturbation terms approach zero, as $\delta \to 0$.

Fig.3 shows the linearizing performance using different δ time delay values. The results are compared to a PD controller, using the same feedback gains as in the feedforward linearization scheme, in order to verify the performance increase as $\delta \to 0$. It should be mentioned that the performance can deteriorate if δ is too high. This can be seen when $\delta = 4$, as the attenuation to the oscillations decreases significantly. It should be noted that this delay is probably the worst case, due to the fact that this is approximately the half the system oscillations period of the Van der Pol system, as seen in Fig.2. Another point of importance is the phase performance, also seen in the figure, where the PD control law, as an example of ordinary control using position and velocity feedback, is lagging significantly behind the feedforward linearization scheme.

As predicted, the performance of the linearization is significantly improved when δ is decreased, and the trajectory retains linear characteristics. Thus, verification of the theoretical investigation is obtained. In the following $\delta = 0.1s$ is used.

3.2 Control strategy comparison

For the feedforward linearization to be viable, it must offer increased performance when compared to similar control strategies. Hence, a linearizing controller was developed as follows,

$$u_{lin} = -k_1 x_1 - k_2 x_2 - \hat{\epsilon}(1 - x_1^2)x_2, \tag{45}$$

Where $\hat{\epsilon}$ is a off-line parametric estimate of ϵ. As mentioned previously, it can be seen that the performance of the approach is dependent on $\epsilon - \hat{\epsilon} \approx 0$. Also there is no structure accounting for the fact that unmodeled disturbances will be unattended. In addition to the conventional linearizing control law, a sliding mode control law is developed as reference, as

$$u_{sm} = \frac{s}{|s|} k_s \left(-x_1 + \hat{\epsilon}(1 - x_1^2)x_2 + a x_2 + \beta_0\right) \tag{46}$$

$$s = a x_1 + x_2, \tag{47}$$

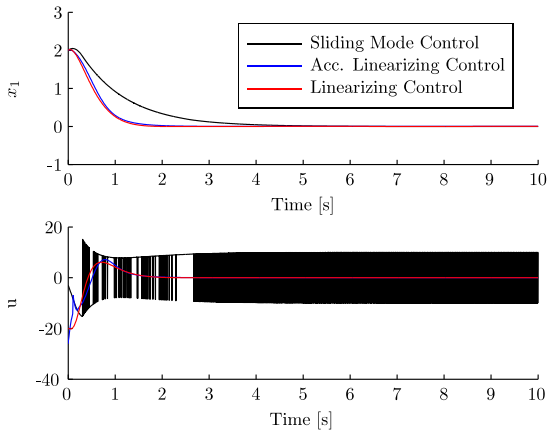

Fig. 4. Top: Time development of the disturbed Van der Pol oscillator controlled by the different control strategies. Bottom: Control input for each of the three controllers.

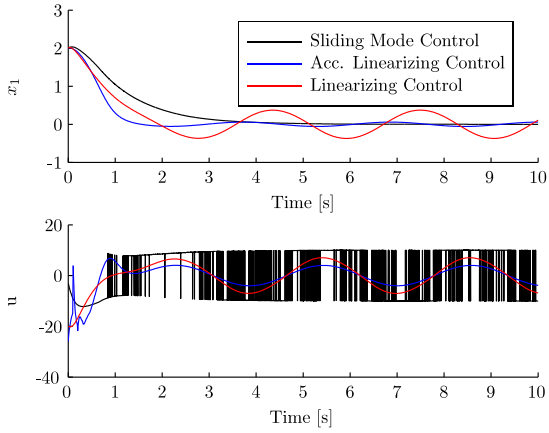

Fig. 5. Top: Time development of the disturbed Van der Pol oscillator controlled by the different control strategies subject to parametric uncertainties. Bottom: Control input for each of the three controllers.

where s is the sliding surface. The stability of the control laws used in this study can be proved by conventional methods described in [Khalil, 2001]. Fig.4 features a comparison of the stabilization problem, where the objective is $x_1 = 0$, and no disturbance or parametric uncertainty is present.

From the figure it can be seen that the performance of the three control strategies are somewhat similar. All obtain the control objective, displaying feasible performance. This was expected as all control laws are able to attenuated the nonlinear dynamics. It should be noted that the control input of the sliding mode control law features the known shattering problem associated with this scheme. Unattended it will be unfeasible in a practical implementation.

Fig.5 features the control law performances when subject to a parametric uncertainty in addition to a unmodeled disturbance force, implemented as a sinusoidal disturbance. This case is more relevant as it encompasses two of the major challenges when designing control laws for nonlinear systems. The first thing to notice is the significant oscillations experienced by the conventional linearization scheme. This was expected as the approach heavily depends on a correct estimate of the system parameters, and a complete model of the system dynamics. Although the sliding mode control law features high performance, it will be unfeasible as the performance is obtained through a high frequency control scheme. This will most likely not be applicable in a real implementation. The feedforward linearization control law on the other hand, feature robust performance, although it is slightly affected by the disturbance and parametric uncertainty. A notable observation is that the control input of the feedforward linearization control law is significantly less aggressive than the other two, which originates from the enhanced phase margin.

Based on the theoretical findings and the results of the simulation study, the concept of feedforward linearization seems promising. However, it strongly depends on obtaining a feasible acceleration measurement where the time delay of signal processing does not exceed the critical value for the system in scope, and the noise is reduced within acceptable limits. Although obtaining and filtering an acceleration signal can be done in within a very short time frame, the gravity influence, noise and bias of the accelerometer sensor must be compensated in order to enable usage of the control law. An alternative can be to develop an observer determining the acceleration. However, the bandwidth and delay of this must be determined.

4. CONCLUSIONS

In this paper it has been shown how to utilize a time-delayed acceleration signal in order to linearize a second order system. A theoretical foundation has been presented which proposes a control strategy which is robust against unmodeled dynamics, model and parametric uncertainties.

The performance was found to be dependent on the delay time of the measurement applied for linearization. However, the proposed method proved feasible performance when compared to other nonlinear control approaches.

4.1 Future work

The next step is to conduct experimental testing, building a deterministic test rig in order to investigate if the theoretical and simulated results reflect reality.

REFERENCES

W.H. Chen, D.J. Ballance, P.J. Gawthrop, and J. O'Reilly. A nonlinear disturbance observer for robotic manipulators. *Industrial Electronics, IEEE Transactions on*, 47 (4):932–938, 2000.

B de Jager. Acceleration assisted tracking control. *IEEE Control Systems Magazine*, 14:20–27, 1994.

T. I. Fossen, K. P. Lindegaard, and Roger Skjetne. Inertia shaping techniques for marine vessels using acceleration feedback. In *Proc IFAC World Congress*, 2002.

Keqin Gu, Vladimir L. Kharitonov, and Jie Chen. *Stability of Time-Delay Systems (Control Engineering)*. Birkhuser Boston, 2003. ISBN 0817642129.

Akihide Jinzenji, Tatsuro Sasamoto, Koichi Aikawa, Susumu Yoshida, and Keiji Aruga. Acceleration feedforward control against rotational disturbance in hard disk drives. In *IEEE Transactions on Magnetics*, pages 888 – 893, 2001.

C.J. Kempf and S. Kobayashi. Disturbance observer and feedforward design for a high-speed direct-drive positioning table. *IEEE Transactions on Control Systems Technology*, 7(5):513–526, 1999.

Hassan K. Khalil. *Nonlinear Systems (3rd Edition)*. Prentice Hall, 2001. ISBN 0130673897.

Ø. Kjerstad, R. Skjetne, and N. A. Jenssen. Disturbance rejection by acceleration feedforward: Application to dynamic positioning. In *Proceedings of IFAC World Congress, Milan, Italy*, 2011.

Karl-Petter W. Lindegaard. *Acceleration Feedback in Dynamic Positioning*. PhD thesis, Norwegian University of Science and Technology, 2003.

Bruno Siciliano, Lorenzo Sciavicco, Luigi Villani, and Giuseppe Oriolo. *Robotics: Modelling, Planning and Control (Advanced Textbooks in Control and Signal Processing)*. Springer, 2011. ISBN 1846286417.

Mark W. Spong, Seth Hutchinson, and M. Vidyasagar. *Robot Modeling and Control*. Wiley, 2005. ISBN 0471649902.

Disturbance Rejection by Acceleration Feedforward: Application to Dynamic Positioning

Disturbance rejection by acceleration feedforward: Application to dynamic positioning ⋆

Øivind Kåre Kjerstad * **Roger Skjetne** * **Nils Albert Jenssen** **

* *Department of Marine Technology, Norwegian University of Science and Technology, Otto Nielsens vei 10, NO-7491 Trondheim, Norway. E-mails: oivind.k.kjerstad@ntnu.no and skjetne@ieee.org*
** *Kongsberg Maritime AS, Kirkegaardsveien 45, NO-3601 Kongsberg, Norway. E-mail: nils.albert.jenssen@kongsberg.com*

Abstract: This paper addresses environmental disturbance rejection in dynamic systems by means of acceleration feedforward. A feedforward structure calculates the environmental force and magnitude by comparing the filtered acceleration measurement with the acceleration due to actuation and known forces. Direct compensation of the environment by feedforward will alleviate the position and velocity feedback terms. The presented scheme compensates environmental disturbances affecting the system in addition to model uncertainties. First, the design is used for a mechanical system and illustrated for an inverted pendulum. Then, the main application, being a dynamic positioning system affected by ice forces in an Arctic operation, is controlled by acceleration feedforward to give enhanced performance.

Keywords: Disturbance rejection, Dynamic positioning, Feedforward compensation, Acceleration feedforward, Disturbance estimation, Arctic marine operations

1. INTRODUCTION

In motion control the main objective is to control the position and velocity of an object to a desired state by measurements of the position and velocity states only. Acceleration measurements are typically not used. Although these systems are proved stable and robust it is not given that the control laws provide adequate environmental compensation. Any inertial system controlled by state feedback influenced by a step in the disturbance force will have to perform unnecessary work as momentum has been gained before the control law begins compensation. By introducing an acceleration feedback, such effects can be caught at an earlier stage since the force disturbance is sensed directly and not through time integrals of the force.

Acceleration signals are seldom applied directly in marine motion control applications. Among the exceptions is the work by Lindegaard (2003), where an observer and a proportional acceleration feedback control law is derived. Here the acceleration term is used to virtually modify the vessel's mass as seen from the disturbance to obtain a favorable closed-loop dynamic response of the vessel. Also, Fossen et al. (2002) incorporated acceleration feedback in a design technique to virtually shape the kinetic energy of the vessel. For aerospace applications, on the other hand, acceleration measurements have been used to some extent; see for instance (Blakelock, 1991). Other relevant references are (de Jager, 1994), where the goal is to increase performance and robustness of mechanical systems by applying acceleration measurements, and (Kempf and Kobayashi, 1999) and (Chen et al., 2000), where disturbance observers are developed to attenuate the effect of the disturbances on the system.

As the acceleration is a proportional measure of the resulting force acting on an object, this can be utilized to derive the environmental contribution through a simple relationship, decomposing the absolute acceleration $\mathbf{a}$ into $\mathbf{a} = \mathbf{a}_a + \mathbf{a}_e$, where $\mathbf{a}_e$ represents the unknown environmental contribution and $\mathbf{a}_a$ represents the acceleration due to actuation and other known forces. As a result, a feedforward term can be applied in the control structure for direct compensation of the unknown environmental forces.

To obtain a feasible acceleration measurement, several challenges have to be overcome. First of all, the gravitational component must be removed as this will affect the linear accelerations during roll and pitch motion. For an inertial measurement unit (IMU) this can either be done by horizontal stabilization of the sensor platform or, by a dynamic compensation scheme. Second, the noise, bias, and nonlinearities of the accelerometers must be handled. Using an observer to produce a filtered acceleration signal based on the acceleration, velocity, and position measurements, significantly aids that problem, and this strategy is used in this paper in addition to assuming that the gravitational effect is removed (Lindegaard, 2003).

Notations: In GS, LAS, LES, UGAS, UGES, etc., stands G for Global, L for Local, S for Stable, U for Uniform, A for Asymptotic, and E for Exponential. Total time derivatives of $x(t)$ is denoted $\dot{x}$, $\ddot{x}$, $x^{(3)}$,.., $x^{(n)}$. The Euclidean vector norm is $|\mathbf{x}| := (\mathbf{x}^\top \mathbf{x})^{1/2}$, a general p-norm is $|.|_p$, and the distance to a set $\mathcal{M}$ is $|x|_{\mathcal{M}} := \inf\{|x - y| : y \in \mathcal{M}\}$. A diagonal matrix is de-

⋆ Supported by the Research Council of Norway under grant 199567/I40 : "Arctic DP".

noted $diag\{a_1, .., a_n\} \in \mathcal{R}^{n\times n}$. Stacking several vectors into one is denoted $\text{col}(x, y, z) := [x^\top, y^\top, z^\top]^\top$, and whenever convenient, $|(x, y, z)| = |\text{col}(x, y, z)|$.

2. ILLUSTRATIVE STUDY: A SCALAR MECHANICAL SYSTEM

Consider the mechanical system modeled according to Newton's 2nd law

$$m\ddot{\xi} = \sum f_i = \rho(\xi, \dot{\xi}) + u + d(t), \tag{1}$$

where $\xi \in \mathbb{R}$ is the positional state, $\rho(\cdot, \cdot)$ is a known force function, $u \in \mathbb{R}$ is the control force input, and $d(t) : \mathbb{R}_{\geq 0} \to \mathbb{R}$ is an exogenous force disturbance. We assume the disturbance $d(\cdot)$ is globally Lipschitz, that is, $\exists L > 0$ such that

$$|d(t) - d(\tau)| \leq L\,|t - \tau|\,, \forall t, \tau \in \mathbb{R}_{\geq 0}. \tag{2}$$

Let $\mathbf{x}_d(t) := \text{col}(\xi_d(t), \dot{\xi}_d(t))$ be a desired position and velocity for the system in (1), and assume by construction that $\mathbf{x}_d(t)$ is bounded and absolutely continuous, and $\exists M > 0$ such that $|\dot{\mathbf{x}}_d(t)| \leq M$, a.a. $t \geq 0$.

The tracking control objective is to render the set

$$\mathcal{A} := \left\{(\mathbf{x}, t) \in \mathbb{R}^2 \times \mathbb{R}_{\geq 0} :\ \mathbf{x} - \mathbf{x}_d(t) = 0\right\} \tag{3}$$

UGAS, where $\mathbf{x} := \text{col}\,(x_1, x_2) := \text{col}(\xi, \dot{\xi})$.

2.1 Nominal disturbance-free case

In the disturbance-free case, $d(t) \equiv 0$, a PD-type control law that solves the control objective is

$$\begin{aligned} u &= \alpha(x, t) \\ &= -mk_1(x_1 - \xi_d) - mk_2(x_2 - \dot{\xi}_d) + m\ddot{\xi}_d - \rho\,(x_1, x_2)\,, \end{aligned} \tag{4}$$

resulting in the 'nominal' closed-loop system

$$\dot{\mathbf{x}} = \mathbf{A}\,(\mathbf{x} - \mathbf{x}_d(t)) + \dot{\mathbf{x}}_d(t) \tag{5}$$

where $\mathbf{A} \in \mathbb{R}^{2\times 2}$ is a Hurwitz matrix.

Proposition 1. The closed, forward invariant set $\mathcal{A}$ is UGES with respect to the closed-loop system (5).

Proof. Clearly, the linear system (5) is forward complete under the stated assumptions. Let $\mathbf{P} = \mathbf{P}^\top > 0$ be the solution to $\mathbf{PA} + \mathbf{A}^\top\mathbf{P} = -\mathbf{I}$. We will then show that

$$V(\mathbf{x}, t) = (\mathbf{x} - \mathbf{x}_d(t))^\top\mathbf{P}(\mathbf{x} - \mathbf{x}_d(t)) \tag{6}$$

is a smooth Lyapunov function for (5) with respect to the set $\mathcal{A}$. From the absolute continuity of $\mathbf{x}_d(t)$ and boundedness of $\dot{\mathbf{x}}_d(t)$, which implies that $\mathbf{x}_d(t)$ is globally Lipschitz, the following equivalence relation holds

$$c\,|\mathbf{x} - \mathbf{x}_d(t)| \leq |(\mathbf{x}, t)|_{\mathcal{A}} \leq |\mathbf{x} - \mathbf{x}_d(t)| \tag{7}$$

where $c = 1/(\sqrt{2}\max(1, M))$. This gives

$$p_m\,|(\mathbf{x}, t)|^2_{\mathcal{A}} \leq V(\mathbf{x}, t) \leq \frac{p_M}{c^2}\,|(\mathbf{x}, t)|^2_{\mathcal{A}} \tag{8}$$

where p_m and p_M are the minimum and maximum eigenvalues of $\mathbf{P}$, respectively. Differentiating (6) along the solutions of (5) gives

$$\dot{V} = \frac{\partial V}{\partial \mathbf{x}}\dot{\mathbf{x}} + \frac{\partial V}{\partial t} = -\,|\mathbf{x} - \mathbf{x}_d|^2 \leq -\,|(\mathbf{x}, t)|^2_{\mathcal{A}} \tag{9}$$

and the conclusion of the proposition thereby follows from Lyapunov theorems for set stability; for instance, Theorem A.10 in (Skjetne, 2005).

2.2 Handling the disturbance by robust control

With the disturbance present, the goal is to recover the closed-loop behavior of (5) as close as possible. In this case, (5) is augmented with the additive term $\mathbf{g}d(t)$ where $\mathbf{g} := \text{col}\left(0, \frac{1}{m}\right)$, to give the perturbed closed-loop system

$$\dot{\mathbf{x}} = \mathbf{A}\,(\mathbf{x} - \mathbf{x}_d(t)) + \dot{\mathbf{x}}_d(t) + \mathbf{g}d(t) \tag{10}$$

in accordance with (1). Assuming that the disturbance $d(t)$ is bounded, the time derivative of (6) becomes

$$\begin{aligned} \dot{V} \leq -\,|(\mathbf{x}, t)|^2_{\mathcal{A}} + \frac{\delta V}{\delta \mathbf{x}}\mathbf{g}d(t) \leq -\frac{1}{2}\,|(\mathbf{x}, t)|^2_{\mathcal{A}} + k\,|d(t)|^2 \\ k := 2\left(\frac{p_M}{mc}\right)^2 \end{aligned} \tag{11}$$

which shows that the closed-loop system is ISS with respect to the 0-invariant set $\mathcal{A}$ (Lin, 1992).

However, since the force disturbance in practice can change rapidly it may be difficult for the control law to dominate the disturbance by feedback fast enough. This motivates a feedforward term in the control law that instead can compensate the disturbance directly.

A first attempt towards this goal is to use adaptive control under the assumption that the disturbance is constant or at least slowly varying. An adaptive control law that accomplishes this is

$$\begin{aligned} \dot{\hat{d}} &= 2\gamma\mathbf{g}^\top\mathbf{P}\,(\mathbf{x} - \mathbf{x}_d)\,, \quad \gamma > 0 \\ u &= \alpha(x, t) - \hat{\delta}. \end{aligned} \tag{12}$$

UGS and convergence $|\mathbf{x}(t) - \mathbf{x}_d(t)| \to 0$ can be shown by differentiating the adaptive CLF $W(\mathbf{x}, \hat{d}, t) := V(\mathbf{x}, t) + \frac{1}{2\gamma}\tilde{d}^2$ where $\tilde{d} := d - \hat{d}$ (Krstic et al., 1995). In fact, an investigation of the closed-loop adaptive system will also reveal that the disturbance estimate $\hat{d}(t)$ must converge to the true value d if this is constant. This is convenient for accurate cancellation of the disturbance. However, as the disturbance becomes time-varying, exact cancellation is no longer possible, and the resulting estimation error must once again be attenuated by the feedback terms. As the disturbance gets more severe it will rapidly deteriorate the closed-loop performance. Another attempt could then be to use integral action, but that also has best effect when the disturbance is constant.

2.3 Acceleration feedforward

As an alternative to robust control measures, we propose to employ an acceleration measurement for direct feedforward compensation of $d(t)$. This is motivated by the fact that accelerometers today are available off-the-shelf as small, light, and inexpensive sensor devices. Furthermore, in many motion control applications, for instance dynamic positioning of ships, these measurements are already available in the installed equipment. However, accelerometers are known to be problematic as they produce noisy, biased, and scaled measurements. They are also affected by gravity, but this effect is as stated above assumed to be removed by a compensation scheme.

$$a_m = \epsilon(a_r + b) + w_1, \tag{13}$$

where a_r is the acceleration found using the system model. ϵ is the scale factor, and b is the bias. These are modeled as in (Vik, 2000),

$$\dot{\epsilon} = T_\epsilon^{-1}\epsilon + w_2 \tag{14}$$

$$\dot{b} = T_b^{-1}b + w_3 \tag{15}$$

where T_ϵ^{-1} and T_b^{-1} are the time constants of the scale factor and bias drift, and w_1, w_2, and w_3 are white noise.

The acceleration signal produced by (13) is not directly applicable in a closed-loop control system as it may inject noise into the system. This will increase the wear-and-tear on the actuator in addition to give deteriorated system performance. To employ disturbance rejection by acceleration feedforward, an observer must be developed to produce a filtered acceleration measurement. In the following, for the sake of the example, we assume that the actual acceleration in (1), can be estimated with a short time delay, to produce the measurement

$$a(t) = \ddot{\xi}(t-\delta) \tag{16}$$

where $\delta > 0$ is the time-delay from the instant of the actual acceleration to the filtered signal is available. An estimate of the disturbance force is then

$$\hat{d}(t) = ma(t) - u(t-\delta) - \rho(\xi(t-\delta), \dot{\xi}(t-\delta)) = d(t-\delta). \tag{17}$$

Based on this measurement we propose the control law

$$u = \alpha(x,t) - \hat{d}(t), \tag{18}$$

resulting in the closed-loop system

$$\dot{\mathbf{x}} = \mathbf{A}\left(\mathbf{x} - \mathbf{x}_d(t)\right) + \dot{\mathbf{x}}_d(t) + \mathbf{g}\tilde{d}(t), \tag{19}$$

where $\tilde{d}(t) := d(t) - \hat{d}(t) = d(t) - d(t-\delta)$. As seen, the faster the measurement and communication is done, the smaller the delay δ is, and consequently the more accurate the estimate of $d(t)$ becomes. Ideally, the limit as $\delta \to 0$ the estimation error $\tilde{d}(t)$ vanishes and the system becomes the unperturbed nominal system in (5). However, $\delta = 0$ cannot be possible as this would violate causality.

Theorem 2. The closed-loop system (19) with $\tilde{d}(t)$ as input, is globally input-to-state stable (ISS) with respect to the closed 0-invariant set $\mathcal{A}$ in (3), and the solution $\mathbf{x}(t)$ of (19) converges to the set

$$\mathcal{B} := \left\{ (\mathbf{x},t) : |(\mathbf{x},t)|_{\mathcal{A}} \leq \sqrt{\frac{3kp_M}{c^2 p_m}} L\delta \right\}. \tag{20}$$

Proof. We check that (6) is an ISS-Lyapunov function for (19). Differentiating it along the solutions of (19) gives in accordance with (11) the bound

$$\dot{V} \leq -\frac{1}{2}\left|(\mathbf{x},t)\right|_{\mathcal{A}}^2 + k|\tilde{d}(t)|^2 \tag{21}$$

From the boundedness of $\mathbf{x}_d(t)$, the system is finite escape-time detectable through $|\cdot|_{\mathcal{A}}$ (Teel, 2002; Skjetne, 2005). Forward completeness follows then from (7), (8), and (21), and this proves the ISS part. To show convergence to $\mathcal{B}$ we use (8) and the global Lipschitz property of $d(\cdot)$ to get

$$\begin{aligned}\dot{V} &\leq -\frac{c^2}{2p_M}V + k\left(L\delta\right)^2 \\ &\leq -\frac{c^2}{6p_M}V, \qquad \forall V \geq \frac{3kp_M(L\delta)^2}{c^2}\end{aligned} \tag{22}$$

This last inequality shows that the trajectory $(\mathbf{x}(t),t)$ must converge to the set

$$\mathcal{B}' = \left\{ (\mathbf{x},t) : V(\mathbf{x},t) \leq \frac{3kp_M(L\delta)^2}{c^2} \right\} \tag{23}$$

which is contained in $\mathcal{B}$.

2.4 Example: Inverted pendulum

To illustrate the use of acceleration feedforward, we consider as an example a fixed suspension point inverted pendulum, modeled by the scalar differential equation

$$mL^2\ddot{\theta} = mLg\sin\theta + u + d(t) \tag{24}$$

where θ, m, L, g, u, and $d(t)$ is the angle deviation from the upright position, the mass located at the end of the pendulum, the length of the pendulum, the gravity constant, the control input, and a disturbance force, respectively. For convenience the mass and pendulum length is set to $m = 1$ and $L = 1$ such that

$$\ddot{\theta} = g\sin\theta + u + d(t). \tag{25}$$

This system clearly match (1) by making the appropriate substitutions.

By assuming we have an acceleration signal produced by (13) available, a simple observer is

$$\dot{\hat{\omega}} = g\sin\hat{\theta} + u + k_1 a_f + k_2\tilde{\omega} + k_3\tilde{\theta} \tag{26}$$

$$\dot{\hat{\theta}} = \hat{\omega} + k_4\tilde{\theta}, \tag{27}$$

where $\tilde{\omega} = \omega - \hat{\omega}$ and $\tilde{\theta} = \theta - \hat{\theta}$. The filtered acceleration term a_f is modeled by

$$\dot{a}_f = k_a(-a_f + a_m - g\sin\hat{\theta} - u), \tag{28}$$

where a_m is the output of the accelerometer. This is the same strategy for incorporating acceleration measurements into an observer as in (Lindegaard, 2003).

To extract the disturbance estimate from the acceleration signal, the contributions of the state-dependent terms and the control law are subtracted as

$$\hat{d}(t) = \dot{\hat{\omega}}(t) - (g\sin\hat{\theta}(t) + u(t)). \tag{29}$$

The behavior of the control law incorporating the acceleration feedforward (18) is in the following simulation compared to the nominal control law (4), which was shown to ensure an ISS property with respect to the disturbance, and the adaptive control law (12), which ensures disturbance compensation by an adaptive feedforward term.

According to (4), the nominal control law is chosen as

$$u = \alpha(\theta,\dot{\theta}) = -k_1\theta - k_2\omega - g\sin\theta \tag{30}$$

where the feedback gains are set to $k_1 = 25$ and $k_2 = 15$. In the adaptive control law, the adaptation gain is set to $\gamma = 8$, while the gains of the observer was set to $k_a = 0.1$, $k_1 = 1$, $k_2 = 10$, $k_3 = 40$, and $k_3 = 75$. The accelerometer was set up with

$$\dot{\epsilon} = -0.1\epsilon + w_2 \tag{31}$$

$$\dot{b} = -b + w_3, \tag{32}$$

where w_1 was set to have noise power 0.005, w_2 set to 10, and w_3 set to 0.01.

Figure 1 shows a comparison of performance in four cases, the first case without disturbances as the nominal response, the second with a constant disturbance, the third with a sine wave disturbance, and in the final case a random walk disturbance. For the constant disturbance, the acceleration and the adaptive schemes have similar performance by exact cancellation of the disturbance when the adaptive variable has converged. In the case with the sine wave disturbance, on the other hand, it is seen in

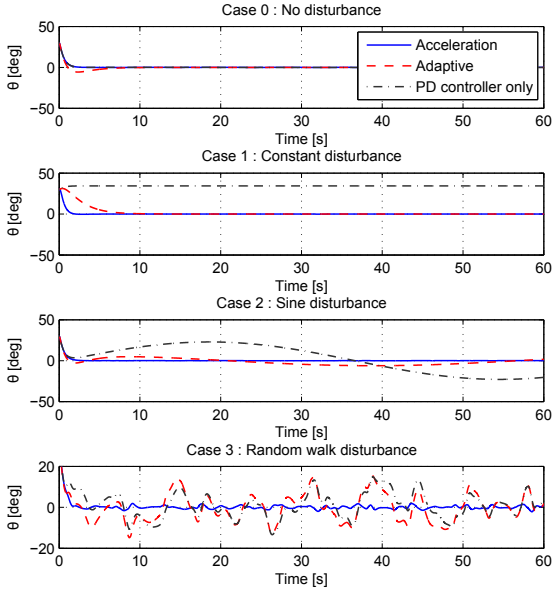

Figure 1. Angular responses to different disturbances affecting the inverted pendulum.

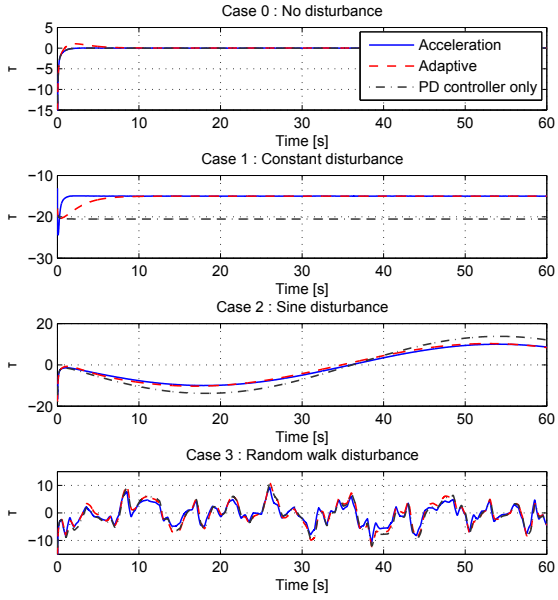

Figure 2. Input vector of the inverted pendulum subject to different disturbances.

Figure 1 that the performance of the adaptive system has deteriorated significantly. Finally, in the last case with a random walk disturbance the performance of the adaptive scheme is as bad as the PD control law without disturbance rejection. The acceleration feedforward control law, on the other hand, shows good performance in all cases, even for unknown disturbances with random characteristics. This statement is also justified by the plots of the control effort in Figure 2. Here it is seen that the acceleration feedforward control law is not more aggressive than needed, nor does it apply an increased average control effort.

It should also be emphasized that even though the feedforward control law is subject to a noisy acceleration measurement, it still outperforms the other two. Figure 3 features the measured and estimated acceleration subject to a constant disturbance.

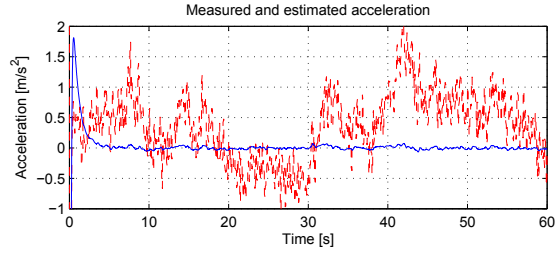

Figure 3. Measured and estimated acceleration subject to a constant disturbance.

3. CASE STUDY: DYNAMIC POSITIONING SYSTEM

Dynamic positioning of marine surface vessels is subject to severe, time-varying disturbances due to wind, waves, and currents. In addition, DP operations have recently turned towards Arctic offshore fields where ice is the governing environmental force. Ice floes acting on a vessel performing stationkeeping, is a major disturbance characterized by a rapid force build-up and release process governed by the geometry and composition of the ice floes. In such an environment, the use of integral action can be inadequate. The problem becomes even more difficult due to insufficient models of the ice-hull interaction forces. In this context, acceleration feedforward is proposed to complement integral action for environmental disturbance rejection.

Another aspect justifying disturbance rejection by feedforward is the need to instantly counteract the large momentum of the vessel if set in motion by the environment. If only compensated by feedback, this will imply excessive work and higher fuel consumption as the motion must be stopped and reversed to correct the deviation.

Consider the standard DP vessel model (Fossen, 2002)

$$\dot{\boldsymbol{\eta}} = \mathbf{R}(\psi)\boldsymbol{\nu} \tag{33}$$

$$\mathbf{M}\dot{\boldsymbol{\nu}} + \mathbf{D}\boldsymbol{\nu} = \boldsymbol{\tau} + \boldsymbol{\tau}_e, \tag{34}$$

where $\boldsymbol{\tau}_e$ is a disturbance force acting on the vessel. As explained above, an observer has to be constructed (Lindegaard, 2003) with the structure proposed as:

$$\mathbf{M}\dot{\hat{\boldsymbol{\nu}}} = \boldsymbol{\tau} - \mathbf{D}\hat{\boldsymbol{\nu}} + \mathbf{k}_1\mathbf{a}_f + \mathbf{k}_2\tilde{\boldsymbol{\nu}} + \mathbf{k}_3\mathbf{R}(\psi)^\top\tilde{\boldsymbol{\eta}} \tag{35}$$

$$\dot{\hat{\boldsymbol{\eta}}} = \mathbf{R}(\psi)\hat{\boldsymbol{\nu}} + \mathbf{k}_4\tilde{\boldsymbol{\eta}} \tag{36}$$

$$\dot{\mathbf{a}}_f = \mathbf{k}_a\left(-\mathbf{a}_f + \dot{\boldsymbol{\nu}} - \left(\mathbf{M}^{-1}\left(\boldsymbol{\tau} - \mathbf{D}\hat{\boldsymbol{\nu}}\right)\right)\right). \tag{37}$$

This outputs the filtered position, velocity, and acceleration as used in the control law, proposed as

$$\boldsymbol{\tau} = \boldsymbol{\alpha}(\hat{\boldsymbol{\eta}}, \hat{\boldsymbol{\nu}}, t) - \boldsymbol{\tau}_{ff}(t) \tag{38}$$

where $\boldsymbol{\alpha}(\hat{\boldsymbol{\eta}}, \hat{\boldsymbol{\nu}}, t)$ is a conventional PID control law defined as

$$\boldsymbol{\alpha}(\hat{\boldsymbol{\eta}}, \hat{\boldsymbol{\nu}}, t) = \mathbf{K}_p \left(\hat{\boldsymbol{\eta}} - \boldsymbol{\eta}_d(t)\right) + \mathbf{K}_d \left(\hat{\boldsymbol{\nu}} - \boldsymbol{\nu}_d(t)\right) + \mathbf{K}_i \int_0^t \left(\hat{\boldsymbol{\eta}} - \boldsymbol{\eta}_d(\tau)\right) d\tau \tag{39}$$

which is proven to be LAS and GAS if $\mathbf{K}_i = 0$ by Fossen (2002). The acceleration feedforward term is assigned as

$$\boldsymbol{\tau}_{ff}(t) = \mathbf{M}\dot{\hat{\boldsymbol{\nu}}}(t-\delta) + \mathbf{D}\hat{\boldsymbol{\nu}}(t-\delta) - \boldsymbol{\tau}(t-\delta) \tag{40}$$

such that $\boldsymbol{\tau}_{ff}$ becomes an estimate of the environmental forces and moments acting on the vessel. A causality problem is avoided since historic values of $\dot{\hat{\boldsymbol{\nu}}}$ and $\boldsymbol{\tau}$ are used. Note that this estimate will also encapsulate contributions from model uncertainties.

Inserting (38) and (40) into (34) gives

$$\mathbf{M}\dot{\boldsymbol{\nu}} + \mathbf{D}\boldsymbol{\nu} = \boldsymbol{\alpha}(\hat{\boldsymbol{\eta}}, \hat{\boldsymbol{\nu}}, t) + \boldsymbol{\tau}_e(t) - \boldsymbol{\tau}_e(t-\delta), \tag{41}$$

where the damping $\mathbf{D}\boldsymbol{\nu}$ helps stabilize the system. As the disturbance is canceled by the feedforward, the need for integral effect is reduced compared to a conventional PID approach. However, as the disturbance cancellation is imperfect some integral effect is appropriate.

3.1 Example: DP of a supply vessel

A simulator of a DP supply vessel, with (38) as the control law, is created by the Marine Systems Simulator (2010) toolbox for Matlab/Simulink. The respective mass and damping matrices are

$$\mathbf{M} = \begin{bmatrix} 5.3122 \cdot 10^6 & 0 & 0 \\ 0 & 8.2831 \cdot 10^6 & 0 \\ 0 & 0 & 3.7454 \cdot 10^9 \end{bmatrix} \tag{42}$$

$$\mathbf{D} = \begin{bmatrix} 5.0242 \cdot 10^4 & 0 & 0 \\ 0 & 2.7229 \cdot 10^5 & -4.3933 \cdot 10^6 \\ 0 & -4.3933 \cdot 10^6 & 4.1894 \cdot 10^8 \end{bmatrix}. \tag{43}$$

The ice force disturbances used in the simulation, which is seen in Figure 4, is a pre-recorded time series obtained by model scale experiments; see (Jenssen et al., 2009). These experimental data are recorded for a model of a larger vessel than the one used in this example, and have been scaled accordingly. Using these ice forces open-loop in the simulation does not correspond exactly to the expected ice-hull interaction forces. However, it verifies the performance of the acceleration feedforward scheme and its ability to handle real acceleration measurements.

The control law is set up to obtain and maintain the position [5 5] with 45° heading starting at [0 0] with 0°. The PID control law was set up using the following gains

$$\mathbf{K}_p = 10^4 \cdot diag\{20, 17, 5, 2500\} \tag{44}$$

$$\mathbf{K}_d = 10^5 \cdot diag\{35, 25, 5000\} \tag{45}$$

$$\mathbf{K}_i = 10^3 \cdot diag\{15, 15, 300\}. \tag{46}$$

Since this amount of integral effect is not necessary when using the feedforward, it was set to $\mathbf{K}_i = 0$ when the feedforward was enabled.

The acceleration feedforward term τ_{ff} is given by (40) where $\dot{\hat{\nu}}(t-\delta)$ is obtained from the observer, and the measurement delay is $\delta = 0.1$.

The observer gains in (35)-(37) were set to:

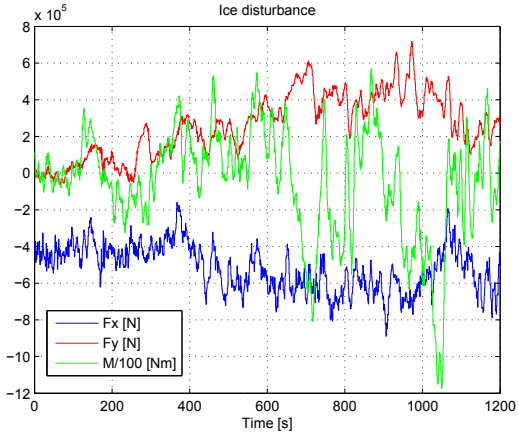

Figure 4. Ice interaction forces and moment affecting the vessel during DP. Courtesy to Jenssen et al. (2009).

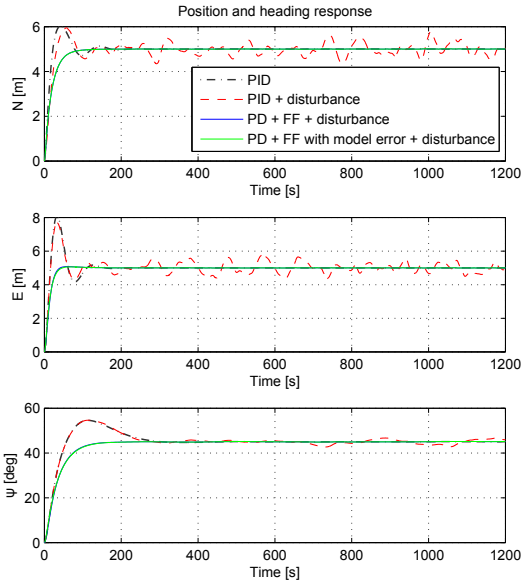

Figure 5. Position and heading response of the supply vessel subject to a gusty disturbance.

$$\mathbf{k}_a = diag\{0.5, 0.5, 0.5\} \tag{47}$$

$$\mathbf{k}_1 = diag\{1, 1, 1\} \tag{48}$$

$$\mathbf{k}_2 = diag\{25, 25, 25\} \tag{49}$$

$$\mathbf{k}_3 = diag\{25, 25, 25\} \tag{50}$$

$$\mathbf{k}_4 = diag\{20, 10, 10\}. \tag{51}$$

The accelerometers producing the acceleration measurement used in the observer were modeled as in (13). The bias and scale factors were set up for all DOFs as

$$\dot{\epsilon} = -0.001\epsilon + w_2 \tag{52}$$

$$\dot{b} = -0.001b + w_3, \tag{53}$$

where w_1, w_2, and w_3 are white noise with power 10^{-10}, 1.0, and 0.02, respectively.

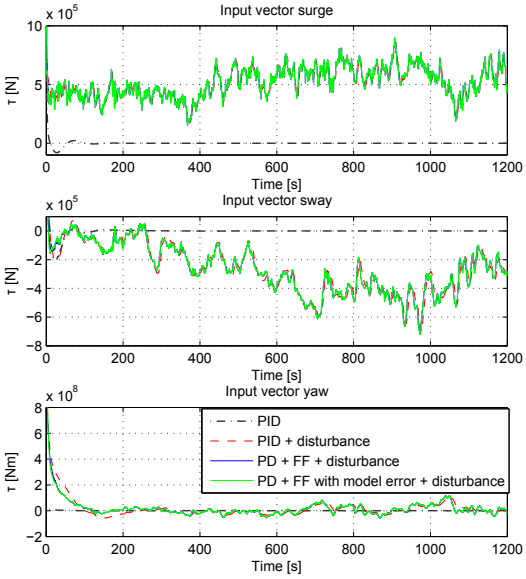

Figure 6. Input vector of the supply vessel subject to a gusty disturbance.

Four different scenarios were simulated. First, the acceleration feedforward was disabled for the disturbance-free case. Second, the disturbances were enabled to illustrate the PID performance alone. The third case illustrates the performance improvement with the acceleration feedforward enabled. In the last case, the system matrices are made uncertain, by setting them to $\hat{\mathbf{M}} = 0.75\mathbf{M}$ and $\hat{\mathbf{D}} = 0.9\mathbf{D}$, showing that the acceleration feedforward is effective also for unmodeled dynamics. This is a realistic scenario as the vessel weight will vary with its loading condition.

Figure 5 features the position and heading response of the vessel where it is seen that the use of the feedforward term improves performance by its rapid cancellation of disturbances and unmodeled dynamics. Due to the ideal actuation system, the acceleration feedforward control law produces an almost perfect response. This is not realistic when the thruster system is included in the loop, with its rate limitations and maximum bollard pull. In Figure 6 it is seen though that the control input is not more aggressive by the use of acceleration feedforward, but rather responds more quickly to the emerging disturbances.

It should be noted that an improved response with the PID could have been achieved with better tuning. However, as the disturbances and unmodeled dynamics are canceled by the acceleration feedforward, this caters for an easier tuning of the PID terms in the control law as it virtually experiences only a calm sea state. The performance, though, is limited by the actuation device's ability to change thrust magnitude and direction fast enough.

Note, also that in conventional DP systems, the wind influence is regarded an issue due to problems of obtaining a correct measurement of the wind force, and then to calculate the correct feedforward compensation. By using the proposed approach, this is a lesser problem.

4. CONCLUSIONS

In this paper we have presented a design scheme augmenting conventional control design by a disturbance rejection based on acceleration feedforward. The approach is applicable for a wide range of applications where disturbances and unwanted effects can be suppressed to give a resulting linear system characteristics. As an acceleration measurement captures the resulting force acting on the system, the disturbance rejection will offer compensation for environmental forces and model uncertainties. In turn this will enable for easier tuning of the feedback control terms.

REFERENCES

Blakelock, J.H. (1991). *Automatic Control of Aircraft and Missiles*. Wiley-Interscience.

Chen, W., Ballance, D., Gawthrop, P., and O'Reilly, J. (2000). A nonlinear disturbance observer for robotic manipulators. *Industrial Electronics, IEEE Transactions on*, 47(4), 932–938.

de Jager, B. (1994). Acceleration assisted tracking control. *IEEE Control Systems Magazine*, 14, 20–27.

Fossen, T.I. (2002). *Marine Control Systems: Guidance, Navigation and Control of Ships, Rigs, and Underwater Vehicles*. Marine Cybernetics.

Fossen, T.I., Lindegaard, K.P., and Skjetne, R. (2002). Inertia shaping techniques for marine vessels using acceleration feedback. In *Proc IFAC World Congress*.

Jenssen, N.A., Muddesitti, S., Phillips, D., and Backstrom, K. (2009). DP in ice conditions. In *Dynamic Positioing Conference*.

Kempf, C. and Kobayashi, S. (1999). Disturbance observer and feedforward design for a high-speed direct-drive positioning table. *IEEE Transactions on Control Systems Technology*, 7(5), 513–526.

Krstic, M., Kanellakopoulos, I., and Kokotovic, P.V. (1995). *Nonlinear and Adaptive Control Design (Adaptive and Learning Systems for Signal Processing, Communications and Control Series)*. Wiley-Interscience.

Lin, Y. (1992). *Lyapunov Function Techniques for Stabilization*. PhD thesis, New Brunswick Rutgers, State Univ. New Jersey, New Brunswick, NJ, USA.

Lindegaard, K.P.W. (2003). *Acceleration Feedback in Dynamic Positioning*. Ph.D. thesis, Norwegian University of Science and Technology.

Marine Systems Simulator (2010). URL `http://www.marinecontrol.org/download.html`.

Skjetne, R. (2005). *The Maneuvering Problem*. PhD thesis, NTNU, Dept. Eng. Cybernetics, Trondheim, Norway.

Teel, A.R. (2002). Notes on nonlinear control and analysis. Lecture Notes: Courses ECE 236, 237, and 594D.

Vik, B. (2000). *Nonlinear Design and Analysis of Integrated GPS and Inertial Navigation Systems*. PhD thesis, NTNU, Dept. Eng. Cybernetics, Trondheim, Norway.

Part III

Closing Remarks

Chapter 7

Summary and Conclusions

This thesis has focused on DP of marine vessels in ice where most emphasis is put on the dynamic broken, or managed, sea-ice environment. Three research questions, rooted in the argued limited foundation for development of a capable DP control system, have governed the work:

1. What is the load governing physics of the low velocity ship-managed ice interactions, and how does it relate to the ice condition and how does it affect the vessel motion dynamics?

2. How can the ship-ice interactions be modeled, and how can different approaches to increased reactivity be implemented in the DP control system?

3. What are feasible operation strategies, and how can proactive actions be implemented in the control system?

The starting point for answering the first question was an analysis of model scale experiment datasets to study the ship-managed ice interactions. The results of this indicate that the mean ice load level is strongly dependent on the oblique heading angle but independent of the relative velocity between the vessel and the ice (in the low velocity range). It is also found that the managed ice cover characteristics (namely, the ice concentration, ice thickness, and floe size distribution) impact both the mean ice load level and the signal variation, leading to significant and rapid transients in the global ice load signal. From a phenomenological perspective ice floe contact networks and accumulated ice mass concepts are introduced and considered important for interpreting the observed signal dynamics. These provide a

framework for understanding the major trends of the load signal. The findings are argued to have several implications on DP control systems design, but foremost the following:

- Modelling the ice using the conventional model based design methodology is challenging.
- The control design should have increased reactivity and operate the vessel compliantly with the ice dynamics.

To investigate new control designs a closed-loop development framework using a state-of-the-art high fidelity numerical model was established. Its main advantage is that it captures two of the fundamental vessel-ice and ice-ice processes found in the model scale experiment datasets analysis. This ability enables realistic simulation of the coupled vessel-ice dynamics, considered key for testing motion control systems. It also enabled rapid design iterations in a variety of operational scenarios with varying ice drift.

To answer the second research question three approached was considered:

- By extending conventional model based designs to capture the ice dynamics.
- By introducing hybrid dynamical systems theory to allow for instantaneous change of estimated variables.
- By incorporation of inertial measurements to capture and handle all unmodelled dynamics acting on the vessel.

Extending conventional model based control designs requires a deterministic ice load model coupling the ice load to measurable variables (and/or system states). Creating such a model is challenging as the phenomenological processes governing the load consist of multiple and complex ice-ice and ship-ice interactions. Control design with specific ice load model was not established since no applicable relationship between the time-varying ice load variations and measurable variables (and/or system states) was found. Nevertheless, the state-of-the-art open water control model is shown capable for control design in light to moderate managed ice conditions if the wave model is removed and the system tuned appropriately.

Although modifying the conventional design methodology may give increased reactivity in some scenarios there is still a challenge with rapid unmodelled and umeasuresd external disturbances. The key challenge is to detect and act as early as possible. This motivated the application of hybrid dynamical

systems theory to create a resetting control design for DP of marine vessels. It combines continuous-time and discrete-time state descriptions and allows the state estimates to jump when the measured estimation error is sufficiently large (providing overall reduction of the estimation error). The performance of the control design was investigated with simulations and model scale experiments, both showing significant increase in performance when compared to a conventional system only differing in the use of resets. The presented design is particularly interesting as it improves state estimation without gain adjustments, new measurements, or new dynamic models.

The acceleration signals from inertial sensors are seldom used in motion control for marine vessels, despite their powerful disturbance rejection potential. The reason for this is that measuring, decoupling, and utilizing the dynamic acceleration from the inertial measurements is not trivial. This thesis presents a solution for marine vessels building on conventional methods together with a novel control law design where the dynamic acceleration signals are used to form a dynamic disturbance compensation (similar to the approach of wind feedforward), named acceleration feedforward. A key enabler of improved performance is that the kinetic model used in conventional control design can be reformulated to use kinematic and sensor models for describing the velocity dynamics. This implies significant less model uncertainty as all significant physical processes acting on the vessel are captured through the input of the inertial measurements. In the proposed design the acceleration feedforward replaces conventional integral action and enables unmeasured external loads and unmodel dynamics to be counteracted with low time lag. The proposed design was investigated with both experimental data and numerical simulations, both showing feasibility and effectiveness of the proposed design methodology.

While control reactivity is key to DP in ice its also considered important to minimize the loads on the vessel through it's operational strategy. This was the target of the third research question which was approached by investigated tracking of the ice drift direction with the vessel's bow (or stern). A potential consequence of not achieving ice drift tracking is loss of position as severe loading scenarios beyond the capability of the propulsion system may arise as ice will accumulate on the hull at oblique headings. The WOPC method is adapted and investigated because it incorporates the drift tracking directly without the need for additional measurements. Furthermore, it pro-actively exploits the environment for actuation. A case study using the developed simulation framework indicated that the concept

works as intended for severe ice drift reversals in high ice concentrations.

Further compliant ice-vessel motion behavior beyond tracking the ice drift direction may be achieved if the operational area is sufficiently large, and the vessel has freedom to maneuver. Then, two additional proactive measures may be incorporated in the control design:

- Seek the weakest path through the ice cover within the allowed operational area.
- Utilize the vessel momentum and inertia to address challenging ice features.

In summary, this thesis highlights some of the key challenges for effective stationkeeping in ice using a DP control system and proposes countermeasures. The enhancements are based on the characteristics of the ice environment, but do not employ any specific ice measurements or models. Thus, from the promising theoretically as well as numerical and experimental results the control designs have applicability and potential in other high disturbance environments. Additionally, the thesis showcases the importance of using high fidelity numerical tools as a DP control system development and assessment framework.

Proposals for further research and evaluation may include:

- Extension of the high-fidelity numerical ice model to include more complex ice features and scenarios.
- Further experimental validation of the high-fidelity numerical ice model.
- Experimental validation of the proposed control designs in full-scale.
- Research the use of spare thruster capacity to manipulate the ice cover adjacent to the vessel for increased maneuverability and IM.
- Research the incorporation of proactive measures in the control design.
- Research on a unified motion control system through hybrid dynamical systems theory and application of inertial sensors complementing the conventional sensor suite.
- Sensor integration for increased the level of autonomy allowing the operators to focus on strategic proactive choices and risk evaluation rather than data collection and interpretation.

References

Aksnes, V. Ø. (2011). *Experimental and Numerical Studies of Moored Ships in Level Ice*. PhD thesis, Norwegian University of Science and Technology, Trondheim, Norway.

Balchen, J. G., Jenssen, N. A., Mathisen, E., and Sælid, S. (1980). Dynamic Positioning System Based on Kalman Filtering and Optimal Control. *Modeling, Identification and Control*, 1(3):135–163.

Bray, D. (2011). *The DP Operator's Handbook*. The Nautical Institute.

Breivik, M. (2010). *Topics in Guided Motion Control of Marine Vehicles*. PhD thesis, Norwegian University of Science and Technology, Trondheim, Norway.

Breivik, M., Kvaal, S., and Østby, P. (2015). From Eureka to K-Pos: Dynamic Positioning as a Highly Successful and Important Marine Control Technology.

Broström, G. and Christensen, K. (2008). Waves in sea ice. Technical report, Norwegian Meteorological Institute.

Campbell, M., Egerstedt, M., How, J. P., and Murray, R. M. (2010). Autonomous driving in urban environments: approaches, lessons and challenges. *Philosophical Transactions of the Royal Society of London A: Mathematical, Physical and Engineering Sciences*, 368(1928):4649–4672.

Comfort, G., Singh, S., and Spencer, D. (1999). Evaluation of Ice Model Test Data for Moored Structures. Technical Report PERD/CHC Report 26-195.

Croasdale, K., Bruce, J., and Liferov, P. (2009). Sea ice loads due to managed ice. In *Proceedings of the 20th International Conference on Port and Ocean Engineering under Arctic Conditions*.

Det Norske Veritas (2011). Dynamic Positioning Systems. Rules for classification of ships.

Det Norske Veritas (2013). Winterization for Cold Climate Operations (Tentative). Offshore Standard DNV-OS-A201.

Eik, K. J. (2010). *Ice Management in Arctic Offshore Operations and Field Developments*. PhD thesis, Norwegian University of Science and Technology, Trondheim, Norway.

Ettema, R. and Nixon, W. A. (2005). Ice Tank Tests on Ice Rubble Loads Against a Cable-Moored Conical Platform. *Journal of Cold Regions Engineering*, 19(4):103–116.

Fay, H. (1989). *Dynamic Positioning Systems: Principles, Design and Applications*. Editions Technip.

Fossen, T. I. (2011). *Handbook of Marine Craft Hydrodynamics and Motion Control*. Wiley.

Frankenstein, S., Løset, S., and Shen, H. (2001). Wave-ice interactions in barents sea marginal ice zone. *Journal of Cold Regions Engineering*, 15(2):91–102.

Gash, R. and Millan, J. (2012). Managed ice loads on a dynamically positioned vessel. In *Proceedings of OTC Arctic Technology Conference*.

Gautier, D. L., Bird, K. J., Charpentier, R. R., Grantz, A., Houseknecht, D. W., Klett, T. R., Moore, T. E., Pitman, J. K., Schenk, C. J., Schuenemeyer, J. H., Sørensen, K., Tennyson, M. E., Valin, Z. C., and Wandrey, C. J. (2009). Assessment of Undiscovered Oil and Gas in the Arctic. *Science*, 324(5931):1175–1179.

Goebel, R., Sanfelice, R. G., and Teel, A. R. (2012). *Hybrid Dynamical Systems: Modeling, Stability, and Robustness*. Princeton University Press.

Hals, T. and Efraimsson, F. (2011). DP Ice Model Test of Arctic Drillship . In *Proceedings of the Dynamic Positioning Conference*.

Hals, T. and Jenssen, N. A. (2012). DP ice model tests of Arctic drillship and polar research vessel. In *Proceedings of the 31st International Conference on Ocean, Offshore and Arctic Engineering*.

Hamilton, J. M., Holub, C. J., Blunt, J., Mitchell, D., and Kokkinis, T. (2011). Ice Management for Support of Arctic Floating Operations. In *Proceedings of the Arctic Technology Conference*.

Hamilton, J. M., Holub, C. J., Shafrova, S., Blunt, J., Foltz, R., and Ritch, R. (2014). A Case Study of Ice Management for Exploration Floating Drilling. In *Proceedings of the International Conference and Exhibition on Ships and Structures in Ice*.

Haugen, J. (2014). *Autonomous Aerial Ice Observation*. PhD thesis, Norwegian University of Science and Technology, Trondheim, Norway.

Haugen, J., Imsland, L., Løset, S., and Skjetne, R. (2011). Ice Observer System for Ice Management Operations. In *Proceedings of the Twenty-first International Offshore and Polar Engineering Conference*.

International Maritime Organization (1994). Guidelines for vessels with dynamic positioning systems. Technical Report MSC/circ.645.

Jenssen, N. A., Muddesitti, S., Phillips, D., and Backstrom, K. (2009). DP In Ice Conditions. In *Proceedings of the Dynamic Positioning Conference*.

Keinonen, A. and Martin, E. H. (2012). Modern day pioneering and its safety in the floating ice offshore. In *Proceedings of the International Conference and Exhibition on Ships and Structures in Ice*.

Keinonen, A., Shirley, M., Liljeström, G., and Pilkington, R. (2006). Transit and Stationary Coring Operations in the Central Polar Pack. In *Proceedings of the International Conference and Exhibition on Performance of Ships and Structures in Ice*.

Keinonen, A., Wells, H., Dunderdale, P., Pilkington, R., Miller, G., and Brovin, A. (2000). Dynamic positioning operation in ice, offshore Sakhalin, May–June 1999. In *Proceedings of the Tenth International Offshore and Polar Engineering Conference*, volume 1, pages 683–690.

Kerkeni, S., Dal Santo, X., and Metrikin, I. (2013). Dynamic Positioning in Ice - Comparison of Control Laws in Open Water and Ice. In *Proceedings of the 32st International Conference on Ocean, Offshore and Arctic Engineering*.

Kjerstad, N. (2011). *Ice Navigation*. Tapir Academic Press.

Kongsberg Maritime (2015). KSIM Offshore, simulator system maximizing performance. Brochure.

Leppäranta, M. (2011). *The Drift of Sea Ice (Springer Praxis Books)*. Springer.

Lindegaard, K.-P. W. (2003). *Acceleration Feedback in Dynamic Positioning*. PhD thesis, Norwegian University of Science and Technology.

Lubbad, R., Løset, S., and Skjetne, R. (2015). Numerical Simulations Verifying Arctic Offshore Field Activities. In *Proceedings of POAC*.

Maimone, M., Biesiadecki, J., Tunstel, E., Cheng, Y., and Leger, C. (2006). Surface navigation and mobility intelligence on the mars exploration rovers. *Intelligence for Space Robotics*, pages 45–69.

Marine Cybernetics (2014). Third-party testing of software, product guide 2014. Brochure.

Marintek (2014). SIMA Fact Sheet. Brochure.

Metrikin, I. (2014). A Software Framework for Simulating Stationkeeping of a Vessel in Discontinuous Ice. *Modeling, Identification and Control*.

Metrikin, I. (2015). *Experimental and Numerical Investigations of Dynamic Positioning in Discontinuous Ice*. PhD thesis, NTNU.

Metrikin, I., Gürtner, A., Bonnemaire, B., Tan, X., Fredriksen, A., and Sapelnikov, D. (2015). SIBIS: A Numerical Environment For Simulating Offshore Operations In Discontinuous Ice. In *Proceedings of POAC*.

Moran, K., Backman, J., and Farrell, J. W. (2006). Deepwater drilling in the Arctic Ocean's permanent sea ice. In *Proceedings of the Integrated Ocean Drilling Program*, volume 302.

Navis Engineering (2014). NavDP 4000 Series Dynamic Positioning System. Brochure.

Nguyen, D. H., Nguyen, D. T., Quek, S. T., and Sørensen, A. J. (2011). Position-moored drilling vessel in level ice by control of riser end angles. *Cold Regions Science and Technology*, 66(2–3):65 – 74.

Nguyen, D. T., Sørbø, A. H., and Sørensen, A. J. (2009). Modelling and control for dynamic positioned vessels in level ice. In *Proceedings of Conference on Manoeuvring and Control of Marine Craft*, pages 229 – 236.

Nguyen, T. D. (2006). *Design of Hybrid Marine Control Systems for Dynamic Positioning*. PhD thesis, National University of Singapore.

Nguyen, T. D., Sørensen, A. J., and Quek, S. T. (2007). Design of Hybrid Controller for Dynamic Positioning from Calm to Extreme Sea Conditions. *IFAC Journal Automatica*, 43(5):768–785.

Østby, P. and Kvaal, S. (2015). *The Jewel in the Crown - Kongsberg Dynamic Positioning Systems 1975 - 2015*. Pax Forlag.

Rohlén, Å. (2009). Relationship Between Ice-Management and Station Keeping in Ice. Presentation at the Dynamics Positioning Conference.

Ruth, E. (2008). *Propulsion control and thrust allocation on marine vessels*. PhD thesis, Norwegian University of Science and Technology, Trondheim, Norway.

Sayed, M., Kubat, I., Watson, D., Wright, B., Gash, R., and Millan, J. (2015). Simulations of the StationKeeping of Drillships Under Changing Direction of Ice Movement. In *Proceedings of the Offshore Technology Conference*.

Septseault, C., Beal, P. A., Yaouanq, S. L., Dudal, A., and Roberts, B. (2015). Update on a New Ice Simulation Tool using a Multi-Model Program. In *Proceedings of the Offshore Technology Conference*.

Shell Offshore Inc. (2011). Ice Management Plan - Beaufort Sea. Technical report.

Skjetne, R. (2005). *The Maneuvering Problem*. PhD thesis, NTNU, Dept. Eng. Cybernetics, Trondheim, Norway.

Skjetne, R., Imsland, L., and Løset, S. (2014). The Arctic DP Research Project: Effective Stationkeeping in Ice. *Modeling, Identification and Control*, 35(4):191–210.

Smogeli, Ø. N. (2006). *Control of Marine Propellers*. PhD thesis, Norwegian University of Science and Technology, Trondheim, Norway.

Snyder, J. (2007). Tourism in the Polar Regions - The Sustainability Challenge.

Sørensen, A. J. (2005). Structural issues in the design and operation of marine control systems. *Annual Reviews in Control*, 29(1):125 – 149.

Sørensen, A. J. (2011). A survey of dynamic positioning control systems. *Annual Reviews in Control*, 35(1):123 – 136.

Sørensen, A. J. (2012). *Marine Control Systems: Propulsion and Motion Control of Ships and Ocean Structures*. Department of Marine Technology, NTNU, Norway.

Sørensen, A. J., Sagatun, S. I., and Fossen, T. I. (1996). The design of a dynamic positioning system using model-based control. *IFAC Journal of Control Engineering in Practice*, 4(3):359–368.

Strand, J. P. (1999). *Nonlinear Position Control Systems Design for Marine Vessels*. PhD thesis, NTNU, Dept. Eng. Cybernetics, Trondheim, Norway.

The Society of Naval Architects Marine Engineers (1950). Nomenclature for treating the motion of a submerged body through a fluid. Technical report. Technical and Research Bulletin, 1-5.

Urmson, C., Anhalt, J., Bagnell, D., Baker, C., Bittner, R., Clark, M., Dolan, J., Duggins, D., Galatali, T., Geyer, C., et al. (2008). Autonomous driving in urban environments: Boss and the urban challenge. *Journal of Field Robotics*, 25(8):425–466.

Valanto, P. (2001). The Resistance of Ships in Level Ice. *Transactions of Society of Naval Architects and Marine Engineers*, 109:53–83.

Volvo Penta (2014). Volvo Penta IPS - A new era in yacht power. Brochure.

Wang, B., Daley, C., Sayed, M., and Liu, J. (2010). Global Ice Loads on Arctic Drillships. In *Proceedings International Conference and Exhibition on Performance of Ships and Structures in Ice*.

Wold, H. E. (2013). *Thrust allocation for DP in ice*. Master thesis, NTNU.

World Meteorological Organization (2014). Sea Ice Nomenclature. Technical report.

Wright, B. D. (2001). Ice loads on the Kulluk in managed ice conditions. In *Proceedings of the 16th International Conference on Port and Ocean Engineering under Arctic Conditions*.

Younan, A. H., Hamilton, J. M., Garas-Yanni, V. Y., Blunt, J., Holub, C. J., and Kokkinis, T. (2012). An Integrated Ice Management Alert System. In *Proceedings of the International Offshore and Polar Engineering Conference*.

Zahedi, B. and Norum, L. E. (2013). Modeling and simulation of all-electric ships with low-voltage dc hybrid power systems. *IEEE Transactions on Power Electronics*, 28(10):4525–4537.

Previous PhD theses published at the Departement of Marine Technology
(earlier: Faculty of Marine Technology)
NORWEGIAN UNIVERSITY OF SCIENCE AND TECHNOLOGY

Report No.	Author	Title
	Kavlie, Dag	Optimization of Plane Elastic Grillages, 1967
	Hansen, Hans R.	Man-Machine Communication and Data-Storage Methods in Ship Structural Design, 1971
	Gisvold, Kaare M.	A Method for non-linear mixed -integer programming and its Application to Design Problems, 1971
	Lund, Sverre	Tanker Frame Optimalization by means of SUMT-Transformation and Behaviour Models, 1971
	Vinje, Tor	On Vibration of Spherical Shells Interacting with Fluid, 1972
	Lorentz, Jan D.	Tank Arrangement for Crude Oil Carriers in Accordance with the new Anti-Pollution Regulations, 1975
	Carlsen, Carl A.	Computer-Aided Design of Tanker Structures, 1975
	Larsen, Carl M.	Static and Dynamic Analysis of Offshore Pipelines during Installation, 1976
UR-79-01	Brigt Hatlestad, MK	The finite element method used in a fatigue evaluation of fixed offshore platforms. (Dr.Ing. Thesis)
UR-79-02	Erik Pettersen, MK	Analysis and design of cellular structures. (Dr.Ing. Thesis)
UR-79-03	Sverre Valsgård, MK	Finite difference and finite element methods applied to nonlinear analysis of plated structures. (Dr.Ing. Thesis)
UR-79-04	Nils T. Nordsve, MK	Finite element collapse analysis of structural members considering imperfections and stresses due to fabrication. (Dr.Ing. Thesis)
UR-79-05	Ivar J. Fylling, MK	Analysis of towline forces in ocean towing systems. (Dr.Ing. Thesis)
UR-80-06	Nils Sandsmark, MM	Analysis of Stationary and Transient Heat Conduction by the Use of the Finite Element Method. (Dr.Ing. Thesis)
UR-80-09	Sverre Haver, MK	Analysis of uncertainties related to the stochastic modeling of ocean waves. (Dr.Ing. Thesis)
UR-81-15	Odland, Jonas	On the Strength of welded Ring stiffened cylindrical Shells primarily subjected to axial Compression
UR-82-17	Engesvik, Knut	Analysis of Uncertainties in the fatigue Capacity of

		Welded Joints
UR-82-18	Rye, Henrik	Ocean wave groups
UR-83-30	Eide, Oddvar Inge	On Cumulative Fatigue Damage in Steel Welded Joints
UR-83-33	Mo, Olav	Stochastic Time Domain Analysis of Slender Offshore Structures
UR-83-34	Amdahl, Jørgen	Energy absorption in Ship-platform impacts
UR-84-37	Mørch, Morten	Motions and mooring forces of semi submersibles as determined by full-scale measurements and theoretical analysis
UR-84-38	Soares, C. Guedes	Probabilistic models for load effects in ship structures
UR-84-39	Aarsnes, Jan V.	Current forces on ships
UR-84-40	Czujko, Jerzy	Collapse Analysis of Plates subjected to Biaxial Compression and Lateral Load
UR-85-46	Alf G. Engseth, MK	Finite element collapse analysis of tubular steel offshore structures. (Dr.Ing. Thesis)
UR-86-47	Dengody Sheshappa, MP	A Computer Design Model for Optimizing Fishing Vessel Designs Based on Techno-Economic Analysis. (Dr.Ing. Thesis)
UR-86-48	Vidar Aanesland, MH	A Theoretical and Numerical Study of Ship Wave Resistance. (Dr.Ing. Thesis)
UR-86-49	Heinz-Joachim Wessel, MK	Fracture Mechanics Analysis of Crack Growth in Plate Girders. (Dr.Ing. Thesis)
UR-86-50	Jon Taby, MK	Ultimate and Post-ultimate Strength of Dented Tubular Members. (Dr.Ing. Thesis)
UR-86-51	Walter Lian, MH	A Numerical Study of Two-Dimensional Separated Flow Past Bluff Bodies at Moderate KC-Numbers. (Dr.Ing. Thesis)
UR-86-52	Bjørn Sortland, MH	Force Measurements in Oscillating Flow on Ship Sections and Circular Cylinders in a U-Tube Water Tank. (Dr.Ing. Thesis)
UR-86-53	Kurt Strand, MM	A System Dynamic Approach to One-dimensional Fluid Flow. (Dr.Ing. Thesis)
UR-86-54	Arne Edvin Løken, MH	Three Dimensional Second Order Hydrodynamic Effects on Ocean Structures in Waves. (Dr.Ing. Thesis)
UR-86-55	Sigurd Falch, MH	A Numerical Study of Slamming of Two-Dimensional Bodies. (Dr.Ing. Thesis)
UR-87-56	Arne Braathen, MH	Application of a Vortex Tracking Method to the Prediction of Roll Damping of a Two-Dimension Floating Body. (Dr.Ing. Thesis)

UR-87-57	Bernt Leira, MK	Gaussian Vector Processes for Reliability Analysis involving Wave-Induced Load Effects. (Dr.Ing. Thesis)
UR-87-58	Magnus Småvik, MM	Thermal Load and Process Characteristics in a Two-Stroke Diesel Engine with Thermal Barriers (in Norwegian). (Dr.Ing. Thesis)
MTA-88-59	Bernt Arild Bremdal, MP	An Investigation of Marine Installation Processes – A Knowledge - Based Planning Approach. (Dr.Ing. Thesis)
MTA-88-60	Xu Jun, MK	Non-linear Dynamic Analysis of Space-framed Offshore Structures. (Dr.Ing. Thesis)
MTA-89-61	Gang Miao, MH	Hydrodynamic Forces and Dynamic Responses of Circular Cylinders in Wave Zones. (Dr.Ing. Thesis)
MTA-89-62	Martin Greenhow, MH	Linear and Non-Linear Studies of Waves and Floating Bodies. Part I and Part II. (Dr.Techn. Thesis)
MTA-89-63	Chang Li, MH	Force Coefficients of Spheres and Cubes in Oscillatory Flow with and without Current. (Dr.Ing. Thesis
MTA-89-64	Hu Ying, MP	A Study of Marketing and Design in Development of Marine Transport Systems. (Dr.Ing. Thesis)
MTA-89-65	Arild Jæger, MH	Seakeeping, Dynamic Stability and Performance of a Wedge Shaped Planing Hull. (Dr.Ing. Thesis)
MTA-89-66	Chan Siu Hung, MM	The dynamic characteristics of tilting-pad bearings
MTA-89-67	Kim Wikstrøm, MP	Analysis av projekteringen for ett offshore projekt. (Licenciat-avhandling)
MTA-89-68	Jiao Guoyang, MK	Reliability Analysis of Crack Growth under Random Loading, considering Model Updating. (Dr.Ing. Thesis)
MTA-89-69	Arnt Olufsen, MK	Uncertainty and Reliability Analysis of Fixed Offshore Structures. (Dr.Ing. Thesis)
MTA-89-70	Wu Yu-Lin, MR	System Reliability Analyses of Offshore Structures using improved Truss and Beam Models. (Dr.Ing. Thesis)
MTA-90-71	Jan Roger Hoff, MH	Three-dimensional Green function of a vessel with forward speed in waves. (Dr.Ing. Thesis)
MTA-90-72	Rong Zhao, MH	Slow-Drift Motions of a Moored Two-Dimensional Body in Irregular Waves. (Dr.Ing. Thesis)
MTA-90-73	Atle Minsaas, MP	Economical Risk Analysis. (Dr.Ing. Thesis)
MTA-90-74	Knut-Aril Farnes, MK	Long-term Statistics of Response in Non-linear Marine Structures. (Dr.Ing. Thesis)
MTA-90-75	Torbjørn Sotberg, MK	Application of Reliability Methods for Safety Assessment of Submarine Pipelines. (Dr.Ing.

		Thesis)
MTA-90-76	Zeuthen, Steffen, MP	SEAMAID. A computational model of the design process in a constraint-based logic programming environment. An example from the offshore domain. (Dr.Ing. Thesis)
MTA-91-77	Haagensen, Sven, MM	Fuel Dependant Cyclic Variability in a Spark Ignition Engine - An Optical Approach. (Dr.Ing. Thesis)
MTA-91-78	Løland, Geir, MH	Current forces on and flow through fish farms. (Dr.Ing. Thesis)
MTA-91-79	Hoen, Christopher, MK	System Identification of Structures Excited by Stochastic Load Processes. (Dr.Ing. Thesis)
MTA-91-80	Haugen, Stein, MK	Probabilistic Evaluation of Frequency of Collision between Ships and Offshore Platforms. (Dr.Ing. Thesis)
MTA-91-81	Sødahl, Nils, MK	Methods for Design and Analysis of Flexible Risers. (Dr.Ing. Thesis)
MTA-91-82	Ormberg, Harald, MK	Non-linear Response Analysis of Floating Fish Farm Systems. (Dr.Ing. Thesis)
MTA-91-83	Marley, Mark J., MK	Time Variant Reliability under Fatigue Degradation. (Dr.Ing. Thesis)
MTA-91-84	Krokstad, Jørgen R., MH	Second-order Loads in Multidirectional Seas. (Dr.Ing. Thesis)
MTA-91-85	Molteberg, Gunnar A., MM	The Application of System Identification Techniques to Performance Monitoring of Four Stroke Turbocharged Diesel Engines. (Dr.Ing. Thesis)
MTA-92-86	Mørch, Hans Jørgen Bjelke, MH	Aspects of Hydrofoil Design: with Emphasis on Hydrofoil Interaction in Calm Water. (Dr.Ing. Thesis)
MTA-92-87	Chan Siu Hung, MM	Nonlinear Analysis of Rotordynamic Instabilities in Highspeed Turbomachinery. (Dr.Ing. Thesis)
MTA-92-88	Bessason, Bjarni, MK	Assessment of Earthquake Loading and Response of Seismically Isolated Bridges. (Dr.Ing. Thesis)
MTA-92-89	Langli, Geir, MP	Improving Operational Safety through exploitation of Design Knowledge - an investigation of offshore platform safety. (Dr.Ing. Thesis)
MTA-92-90	Sævik, Svein, MK	On Stresses and Fatigue in Flexible Pipes. (Dr.Ing. Thesis)
MTA-92-91	Ask, Tor Ø., MM	Ignition and Flame Growth in Lean Gas-Air Mixtures. An Experimental Study with a Schlieren System. (Dr.Ing. Thesis)
MTA-86-92	Hessen, Gunnar, MK	Fracture Mechanics Analysis of Stiffened Tubular Members. (Dr.Ing. Thesis)

MTA-93-93	Steinebach, Christian, MM	Knowledge Based Systems for Diagnosis of Rotating Machinery. (Dr.Ing. Thesis)
MTA-93-94	Dalane, Jan Inge, MK	System Reliability in Design and Maintenance of Fixed Offshore Structures. (Dr.Ing. Thesis)
MTA-93-95	Steen, Sverre, MH	Cobblestone Effect on SES. (Dr.Ing. Thesis)
MTA-93-96	Karunakaran, Daniel, MK	Nonlinear Dynamic Response and Reliability Analysis of Drag-dominated Offshore Platforms. (Dr.Ing. Thesis)
MTA-93-97	Hagen, Arnulf, MP	The Framework of a Design Process Language. (Dr.Ing. Thesis)
MTA-93-98	Nordrik, Rune, MM	Investigation of Spark Ignition and Autoignition in Methane and Air Using Computational Fluid Dynamics and Chemical Reaction Kinetics. A Numerical Study of Ignition Processes in Internal Combustion Engines. (Dr.Ing. Thesis)
MTA-94-99	Passano, Elizabeth, MK	Efficient Analysis of Nonlinear Slender Marine Structures. (Dr.Ing. Thesis)
MTA-94-100	Kvålsvold, Jan, MH	Hydroelastic Modelling of Wetdeck Slamming on Multihull Vessels. (Dr.Ing. Thesis)
MTA-94-102	Bech, Sidsel M., MK	Experimental and Numerical Determination of Stiffness and Strength of GRP/PVC Sandwich Structures. (Dr.Ing. Thesis)
MTA-95-103	Paulsen, Hallvard, MM	A Study of Transient Jet and Spray using a Schlieren Method and Digital Image Processing. (Dr.Ing. Thesis)
MTA-95-104	Hovde, Geir Olav, MK	Fatigue and Overload Reliability of Offshore Structural Systems, Considering the Effect of Inspection and Repair. (Dr.Ing. Thesis)
MTA-95-105	Wang, Xiaozhi, MK	Reliability Analysis of Production Ships with Emphasis on Load Combination and Ultimate Strength. (Dr.Ing. Thesis)
MTA-95-106	Ulstein, Tore, MH	Nonlinear Effects of a Flexible Stern Seal Bag on Cobblestone Oscillations of an SES. (Dr.Ing. Thesis)
MTA-95-107	Solaas, Frøydis, MH	Analytical and Numerical Studies of Sloshing in Tanks. (Dr.Ing. Thesis)
MTA-95-108	Hellan, Øyvind, MK	Nonlinear Pushover and Cyclic Analyses in Ultimate Limit State Design and Reassessment of Tubular Steel Offshore Structures. (Dr.Ing. Thesis)
MTA-95-109	Hermundstad, Ole A., MK	Theoretical and Experimental Hydroelastic Analysis of High Speed Vessels. (Dr.Ing. Thesis)
MTA-96-110	Bratland, Anne K., MH	Wave-Current Interaction Effects on Large-Volume Bodies in Water of Finite Depth. (Dr.Ing. Thesis)
MTA-96-111	Herfjord, Kjell, MH	A Study of Two-dimensional Separated Flow by a Combination of the Finite Element Method and

		Navier-Stokes Equations. (Dr.Ing. Thesis)
MTA-96-112	Æsøy, Vilmar, MM	Hot Surface Assisted Compression Ignition in a Direct Injection Natural Gas Engine. (Dr.Ing. Thesis)
MTA-96-113	Eknes, Monika L., MK	Escalation Scenarios Initiated by Gas Explosions on Offshore Installations. (Dr.Ing. Thesis)
MTA-96-114	Erikstad, Stein O., MP	A Decision Support Model for Preliminary Ship Design. (Dr.Ing. Thesis)
MTA-96-115	Pedersen, Egil, MH	A Nautical Study of Towed Marine Seismic Streamer Cable Configurations. (Dr.Ing. Thesis)
MTA-97-116	Moksnes, Paul O., MM	Modelling Two-Phase Thermo-Fluid Systems Using Bond Graphs. (Dr.Ing. Thesis)
MTA-97-117	Halse, Karl H., MK	On Vortex Shedding and Prediction of Vortex-Induced Vibrations of Circular Cylinders. (Dr.Ing. Thesis)
MTA-97-118	Igland, Ragnar T., MK	Reliability Analysis of Pipelines during Laying, considering Ultimate Strength under Combined Loads. (Dr.Ing. Thesis)
MTA-97-119	Pedersen, Hans-P., MP	Levendefiskteknologi for fiskefartøy. (Dr.Ing. Thesis)
MTA-98-120	Vikestad, Kyrre, MK	Multi-Frequency Response of a Cylinder Subjected to Vortex Shedding and Support Motions. (Dr.Ing. Thesis)
MTA-98-121	Azadi, Mohammad R. E., MK	Analysis of Static and Dynamic Pile-Soil-Jacket Behaviour. (Dr.Ing. Thesis)
MTA-98-122	Ulltang, Terje, MP	A Communication Model for Product Information. (Dr.Ing. Thesis)
MTA-98-123	Torbergsen, Erik, MM	Impeller/Diffuser Interaction Forces in Centrifugal Pumps. (Dr.Ing. Thesis)
MTA-98-124	Hansen, Edmond, MH	A Discrete Element Model to Study Marginal Ice Zone Dynamics and the Behaviour of Vessels Moored in Broken Ice. (Dr.Ing. Thesis)
MTA-98-125	Videiro, Paulo M., MK	Reliability Based Design of Marine Structures. (Dr.Ing. Thesis)
MTA-99-126	Mainçon, Philippe, MK	Fatigue Reliability of Long Welds Application to Titanium Risers. (Dr.Ing. Thesis)
MTA-99-127	Haugen, Elin M., MH	Hydroelastic Analysis of Slamming on Stiffened Plates with Application to Catamaran Wetdecks. (Dr.Ing. Thesis)
MTA-99-128	Langhelle, Nina K., MK	Experimental Validation and Calibration of Nonlinear Finite Element Models for Use in Design of Aluminium Structures Exposed to Fire. (Dr.Ing. Thesis)
MTA-99-	Berstad, Are J., MK	Calculation of Fatigue Damage in Ship Structures.

129		(Dr.Ing. Thesis)
MTA-99-130	Andersen, Trond M., MM	Short Term Maintenance Planning. (Dr.Ing. Thesis)
MTA-99-131	Tveiten, Bård Wathne, MK	Fatigue Assessment of Welded Aluminium Ship Details. (Dr.Ing. Thesis)
MTA-99-132	Søreide, Fredrik, MP	Applications of underwater technology in deep water archaeology. Principles and practice. (Dr.Ing. Thesis)
MTA-99-133	Tønnessen, Rune, MH	A Finite Element Method Applied to Unsteady Viscous Flow Around 2D Blunt Bodies With Sharp Corners. (Dr.Ing. Thesis)
MTA-99-134	Elvekrok, Dag R., MP	Engineering Integration in Field Development Projects in the Norwegian Oil and Gas Industry. The Supplier Management of Norne. (Dr.Ing. Thesis)
MTA-99-135	Fagerholt, Kjetil, MP	Optimeringsbaserte Metoder for Ruteplanlegging innen skipsfart. (Dr.Ing. Thesis)
MTA-99-136	Bysveen, Marie, MM	Visualization in Two Directions on a Dynamic Combustion Rig for Studies of Fuel Quality. (Dr.Ing. Thesis)
MTA-2000-137	Storteig, Eskild, MM	Dynamic characteristics and leakage performance of liquid annular seals in centrifugal pumps. (Dr.Ing. Thesis)
MTA-2000-138	Sagli, Gro, MK	Model uncertainty and simplified estimates of long term extremes of hull girder loads in ships. (Dr.Ing. Thesis)
MTA-2000-139	Tronstad, Harald, MK	Nonlinear analysis and design of cable net structures like fishing gear based on the finite element method. (Dr.Ing. Thesis)
MTA-2000-140	Kroneberg, André, MP	Innovation in shipping by using scenarios. (Dr.Ing. Thesis)
MTA-2000-141	Haslum, Herbjørn Alf, MH	Simplified methods applied to nonlinear motion of spar platforms. (Dr.Ing. Thesis)
MTA-2001-142	Samdal, Ole Johan, MM	Modelling of Degradation Mechanisms and Stressor Interaction on Static Mechanical Equipment Residual Lifetime. (Dr.Ing. Thesis)
MTA-2001-143	Baarholm, Rolf Jarle, MH	Theoretical and experimental studies of wave impact underneath decks of offshore platforms. (Dr.Ing. Thesis)
MTA-2001-144	Wang, Lihua, MK	Probabilistic Analysis of Nonlinear Wave-induced Loads on Ships. (Dr.Ing. Thesis)
MTA-2001-145	Kristensen, Odd H. Holt, MK	Ultimate Capacity of Aluminium Plates under Multiple Loads, Considering HAZ Properties. (Dr.Ing. Thesis)
MTA-2001-146	Greco, Marilena, MH	A Two-Dimensional Study of Green-Water

		Loading. (Dr.Ing. Thesis)
MTA-2001-147	Heggelund, Svein E., MK	Calculation of Global Design Loads and Load Effects in Large High Speed Catamarans. (Dr.Ing. Thesis)
MTA-2001-148	Babalola, Olusegun T., MK	Fatigue Strength of Titanium Risers – Defect Sensitivity. (Dr.Ing. Thesis)
MTA-2001-149	Mohammed, Abuu K., MK	Nonlinear Shell Finite Elements for Ultimate Strength and Collapse Analysis of Ship Structures. (Dr.Ing. Thesis)
MTA-2002-150	Holmedal, Lars E., MH	Wave-current interactions in the vicinity of the sea bed. (Dr.Ing. Thesis)
MTA-2002-151	Rognebakke, Olav F., MH	Sloshing in rectangular tanks and interaction with ship motions. (Dr.Ing. Thesis)
MTA-2002-152	Lader, Pål Furset, MH	Geometry and Kinematics of Breaking Waves. (Dr.Ing. Thesis)
MTA-2002-153	Yang, Qinzheng, MH	Wash and wave resistance of ships in finite water depth. (Dr.Ing. Thesis)
MTA-2002-154	Melhus, Øyvin, MM	Utilization of VOC in Diesel Engines. Ignition and combustion of VOC released by crude oil tankers. (Dr.Ing. Thesis)
MTA-2002-155	Ronæss, Marit, MH	Wave Induced Motions of Two Ships Advancing on Parallel Course. (Dr.Ing. Thesis)
MTA-2002-156	Økland, Ole D., MK	Numerical and experimental investigation of whipping in twin hull vessels exposed to severe wet deck slamming. (Dr.Ing. Thesis)
MTA-2002-157	Ge, Chunhua, MK	Global Hydroelastic Response of Catamarans due to Wet Deck Slamming. (Dr.Ing. Thesis)
MTA-2002-158	Byklum, Eirik, MK	Nonlinear Shell Finite Elements for Ultimate Strength and Collapse Analysis of Ship Structures. (Dr.Ing. Thesis)
IMT-2003-1	Chen, Haibo, MK	Probabilistic Evaluation of FPSO-Tanker Collision in Tandem Offloading Operation. (Dr.Ing. Thesis)
IMT-2003-2	Skaugset, Kjetil Bjørn, MK	On the Suppression of Vortex Induced Vibrations of Circular Cylinders by Radial Water Jets. (Dr.Ing. Thesis)
IMT-2003-3	Chezhian, Muthu	Three-Dimensional Analysis of Slamming. (Dr.Ing. Thesis)
IMT-2003-4	Buhaug, Øyvind	Deposit Formation on Cylinder Liner Surfaces in Medium Speed Engines. (Dr.Ing. Thesis)
IMT-2003-5	Tregde, Vidar	Aspects of Ship Design: Optimization of Aft Hull with Inverse Geometry Design. (Dr.Ing. Thesis)
IMT-	Wist, Hanne Therese	Statistical Properties of Successive Ocean Wave

2003-6		Parameters. (Dr.Ing. Thesis)
IMT-2004-7	Ransau, Samuel	Numerical Methods for Flows with Evolving Interfaces. (Dr.Ing. Thesis)
IMT-2004-8	Soma, Torkel	Blue-Chip or Sub-Standard. A data interrogation approach of identity safety characteristics of shipping organization. (Dr.Ing. Thesis)
IMT-2004-9	Ersdal, Svein	An experimental study of hydrodynamic forces on cylinders and cables in near axial flow. (Dr.Ing. Thesis)
IMT-2005-10	Brodtkorb, Per Andreas	The Probability of Occurrence of Dangerous Wave Situations at Sea. (Dr.Ing. Thesis)
IMT-2005-11	Yttervik, Rune	Ocean current variability in relation to offshore engineering. (Dr.Ing. Thesis)
IMT-2005-12	Fredheim, Arne	Current Forces on Net-Structures. (Dr.Ing. Thesis)
IMT-2005-13	Heggernes, Kjetil	Flow around marine structures. (Dr.Ing. Thesis
IMT-2005-14	Fouques, Sebastien	Lagrangian Modelling of Ocean Surface Waves and Synthetic Aperture Radar Wave Measurements. (Dr.Ing. Thesis)
IMT-2006-15	Holm, Håvard	Numerical calculation of viscous free surface flow around marine structures. (Dr.Ing. Thesis)
IMT-2006-16	Bjørheim, Lars G.	Failure Assessment of Long Through Thickness Fatigue Cracks in Ship Hulls. (Dr.Ing. Thesis)
IMT-2006-17	Hansson, Lisbeth	Safety Management for Prevention of Occupational Accidents. (Dr.Ing. Thesis)
IMT-2006-18	Zhu, Xinying	Application of the CIP Method to Strongly Nonlinear Wave-Body Interaction Problems. (Dr.Ing. Thesis)
IMT-2006-19	Reite, Karl Johan	Modelling and Control of Trawl Systems. (Dr.Ing. Thesis)
IMT-2006-20	Smogeli, Øyvind Notland	Control of Marine Propellers. From Normal to Extreme Conditions. (Dr.Ing. Thesis)
IMT-2007-21	Storhaug, Gaute	Experimental Investigation of Wave Induced Vibrations and Their Effect on the Fatigue Loading of Ships. (Dr.Ing. Thesis)
IMT-2007-22	Sun, Hui	A Boundary Element Method Applied to Strongly Nonlinear Wave-Body Interaction Problems. (PhD Thesis, CeSOS)
IMT-2007-23	Rustad, Anne Marthine	Modelling and Control of Top Tensioned Risers. (PhD Thesis, CeSOS)
IMT-2007-24	Johansen, Vegar	Modelling flexible slender system for real-time simulations and control applications
IMT-2007-25	Wroldsen, Anders Sunde	Modelling and control of tensegrity structures.

		(PhD Thesis, CeSOS)
IMT-2007-26	Aronsen, Kristoffer Høye	An experimental investigation of in-line and combined inline and cross flow vortex induced vibrations. (Dr. avhandling, IMT)
IMT-2007-27	Gao, Zhen	Stochastic Response Analysis of Mooring Systems with Emphasis on Frequency-domain Analysis of Fatigue due to Wide-band Response Processes (PhD Thesis, CeSOS)
IMT-2007-28	Thorstensen, Tom Anders	Lifetime Profit Modelling of Ageing Systems Utilizing Information about Technical Condition. (Dr.ing. thesis, IMT)
IMT-2008-29	Refsnes, Jon Erling Gorset	Nonlinear Model-Based Control of Slender Body AUVs (PhD Thesis, IMT)
IMT-2008-30	Berntsen, Per Ivar B.	Structural Reliability Based Position Mooring. (PhD-Thesis, IMT)
IMT-2008-31	Ye, Naiquan	Fatigue Assessment of Aluminium Welded Box-stiffener Joints in Ships (Dr.ing. thesis, IMT)
IMT-2008-32	Radan, Damir	Integrated Control of Marine Electrical Power Systems. (PhD-Thesis, IMT)
IMT-2008-33	Thomassen, Paul	Methods for Dynamic Response Analysis and Fatigue Life Estimation of Floating Fish Cages. (Dr.ing. thesis, IMT)
IMT-2008-34	Pákozdi, Csaba	A Smoothed Particle Hydrodynamics Study of Two-dimensional Nonlinear Sloshing in Rectangular Tanks. (Dr.ing.thesis, IMT/ CeSOS)
IMT-2007-35	Grytøyr, Guttorm	A Higher-Order Boundary Element Method and Applications to Marine Hydrodynamics. (Dr.ing.thesis, IMT)
IMT-2008-36	Drummen, Ingo	Experimental and Numerical Investigation of Nonlinear Wave-Induced Load Effects in Containerships considering Hydroelasticity. (PhD thesis, CeSOS)
IMT-2008-37	Skejic, Renato	Maneuvering and Seakeeping of a Singel Ship and of Two Ships in Interaction. (PhD-Thesis, CeSOS)
IMT-2008-38	Harlem, Alf	An Age-Based Replacement Model for Repairable Systems with Attention to High-Speed Marine Diesel Engines. (PhD-Thesis, IMT)
IMT-2008-39	Alsos, Hagbart S.	Ship Grounding. Analysis of Ductile Fracture, Bottom Damage and Hull Girder Response. (PhD-thesis, IMT)
IMT-2008-40	Graczyk, Mateusz	Experimental Investigation of Sloshing Loading and Load Effects in Membrane LNG Tanks Subjected to Random Excitation. (PhD-thesis, CeSOS)
IMT-2008-41	Taghipour, Reza	Efficient Prediction of Dynamic Response for Flexible amd Multi-body Marine Structures. (PhD-

		thesis, CeSOS)
IMT-2008-42	Ruth, Eivind	Propulsion control and thrust allocation on marine vessels. (PhD thesis, CeSOS)
IMT-2008-43	Nystad, Bent Helge	Technical Condition Indexes and Remaining Useful Life of Aggregated Systems. PhD thesis, IMT
IMT-2008-44	Soni, Prashant Kumar	Hydrodynamic Coefficients for Vortex Induced Vibrations of Flexible Beams, PhD thesis, CeSOS
IMT-2009-45	Amlashi, Hadi K.K.	Ultimate Strength and Reliability-based Design of Ship Hulls with Emphasis on Combined Global and Local Loads. PhD Thesis, IMT
IMT-2009-46	Pedersen, Tom Arne	Bond Graph Modelling of Marine Power Systems. PhD Thesis, IMT
IMT-2009-47	Kristiansen, Trygve	Two-Dimensional Numerical and Experimental Studies of Piston-Mode Resonance. PhD-Thesis, CeSOS
IMT-2009-48	Ong, Muk Chen	Applications of a Standard High Reynolds Number Model and a Stochastic Scour Prediction Model for Marine Structures. PhD-thesis, IMT
IMT-2009-49	Hong, Lin	Simplified Analysis and Design of Ships subjected to Collision and Grounding. PhD-thesis, IMT
IMT-2009-50	Koushan, Kamran	Vortex Induced Vibrations of Free Span Pipelines, PhD thesis, IMT
IMT-2009-51	Korsvik, Jarl Eirik	Heuristic Methods for Ship Routing and Scheduling. PhD-thesis, IMT
IMT-2009-52	Lee, Jihoon	Experimental Investigation and Numerical in Analyzing the Ocean Current Displacement of Longlines. Ph.d.-Thesis, IMT.
IMT-2009-53	Vestbøstad, Tone Gran	A Numerical Study of Wave-in-Deck Impact usin a Two-Dimensional Constrained Interpolation Profile Method, Ph.d.thesis, CeSOS.
IMT-2009-54	Bruun, Kristine	Bond Graph Modelling of Fuel Cells for Marine Power Plants. Ph.d.-thesis, IMT
IMT 2009-55	Holstad, Anders	Numerical Investigation of Turbulence in a Sekwed Three-Dimensional Channel Flow, Ph.d.-thesis, IMT.
IMT 2009-56	Ayala-Uraga, Efren	Reliability-Based Assessment of Deteriorating Ship-shaped Offshore Structures, Ph.d.-thesis, IMT
IMT 2009-57	Kong, Xiangjun	A Numerical Study of a Damaged Ship in Beam Sea Waves. Ph.d.-thesis, IMT/CeSOS.
IMT 2010-58	Kristiansen, David	Wave Induced Effects on Floaters of Aquaculture Plants, Ph.d.-thesis, CeSOS.

IMT 2010-59	Ludvigsen, Martin	An ROV-Toolbox for Optical and Acoustic Scientific Seabed Investigation. Ph.d.-thesis IMT.
IMT 2010-60	Hals, Jørgen	Modelling and Phase Control of Wave-Energy Converters. Ph.d.thesis, CeSOS.
IMT 2010- 61	Shu, Zhi	Uncertainty Assessment of Wave Loads and Ultimate Strength of Tankers and Bulk Carriers in a Reliability Framework. Ph.d. Thesis, IMT/ CeSOS
IMT 2010-62	Shao, Yanlin	Numerical Potential-Flow Studies on Weakly-Nonlinear Wave-Body Interactions with/without Small Forward Speed, Ph.d.thesis,CeSOS.
IMT 2010-63	Califano, Andrea	Dynamic Loads on Marine Propellers due to Intermittent Ventilation. Ph.d.thesis, IMT.
IMT 2010-64	El Khoury, George	Numerical Simulations of Massively Separated Turbulent Flows, Ph.d.-thesis, IMT
IMT 2010-65	Seim, Knut Sponheim	Mixing Process in Dense Overflows with Emphasis on the Faroe Bank Channel Overflow. Ph.d.thesis, IMT
IMT 2010-66	Jia, Huirong	Structural Analysis of Intect and Damaged Ships in a Collission Risk Analysis Perspective. Ph.d.thesis CeSoS.
IMT 2010-67	Jiao, Linlin	Wave-Induced Effects on a Pontoon-type Very Large Floating Structures (VLFS). Ph.D.-thesis, CeSOS.
IMT 2010-68	Abrahamsen, Bjørn Christian	Sloshing Induced Tank Roof with Entrapped Air Pocket. Ph.d.thesis, CeSOS.
IMT 2011-69	Karimirad, Madjid	Stochastic Dynamic Response Analysis of Spar-Type Wind Turbines with Catenary or Taut Mooring Systems. Ph.d.-thesis, CeSOS.
IMT - 2011-70	Erlend Meland	Condition Monitoring of Safety Critical Valves. Ph.d.-thesis, IMT.
IMT – 2011-71	Yang, Limin	Stochastic Dynamic System Analysis of Wave Energy Converter with Hydraulic Power Take-Off, with Particular Reference to Wear Damage Analysis, Ph.d. Thesis, CeSOS.
IMT – 2011-72	Visscher, Jan	Application of Particla Image Velocimetry on Turbulent Marine Flows, Ph.d.Thesis, IMT.
IMT – 2011-73	Su, Biao	Numerical Predictions of Global and Local Ice Loads on Ships. Ph.d.Thesis, CeSOS.
IMT – 2011-74	Liu, Zhenhui	Analytical and Numerical Analysis of Iceberg Collision with Ship Structures. Ph.d.Thesis, IMT.
IMT – 2011-75	Aarsæther, Karl Gunnar	Modeling and Analysis of Ship Traffic by Observation and Numerical Simulation. Ph.d.Thesis, IMT.

Imt – 2011-76	Wu, Jie	Hydrodynamic Force Identification from Stochastic Vortex Induced Vibration Experiments with Slender Beams. Ph.d.Thesis, IMT.
Imt – 2011-77	Amini, Hamid	Azimuth Propulsors in Off-design Conditions. Ph.d.Thesis, IMT.
IMT – 2011-78	Nguyen, Tan-Hoi	Toward a System of Real-Time Prediction and Monitoring of Bottom Damage Conditions During Ship Grounding. Ph.d.thesis, IMT.
IMT- 2011-79	Tavakoli, Mohammad T.	Assessment of Oil Spill in Ship Collision and Grounding, Ph.d.thesis, IMT.
IMT- 2011-80	Guo, Bingjie	Numerical and Experimental Investigation of Added Resistance in Waves. Ph.d.Thesis, IMT.
IMT- 2011-81	Chen, Qiaofeng	Ultimate Strength of Aluminium Panels, considering HAZ Effects, IMT
IMT- 2012-82	Kota, Ravikiran S.	Wave Loads on Decks of Offshore Structures in Random Seas, CeSOS.
IMT- 2012-83	Sten, Ronny	Dynamic Simulation of Deep Water Drilling Risers with Heave Compensating System, IMT.
IMT- 2012-84	Berle, Øyvind	Risk and resilience in global maritime supply chains, IMT.
IMT- 2012-85	Fang, Shaoji	Fault Tolerant Position Mooring Control Based on Structural Reliability, CeSOS.
IMT- 2012-86	You, Jikun	Numerical studies on wave forces and moored ship motions in intermediate and shallow water, CeSOS.
IMT- 2012-87	Xiang ,Xu	Maneuvering of two interacting ships in waves, CeSOS
IMT- 2012-88	Dong, Wenbin	Time-domain fatigue response and reliability analysis of offshore wind turbines with emphasis on welded tubular joints and gear components, CeSOS
IMT- 2012-89	Zhu, Suji	Investigation of Wave-Induced Nonlinear Load Effects in Open Ships considering Hull Girder Vibrations in Bending and Torsion, CeSOS
IMT- 2012-90	Zhou, Li	Numerical and Experimental Investigation of Station-keeping in Level Ice, CeSOS
IMT- 2012-91	Ushakov, Sergey	Particulate matter emission characteristics from diesel enignes operating on conventional and alternative marine fuels, IMT
IMT- 2013-1	Yin, Decao	Experimental and Numerical Analysis of Combined In-line and Cross-flow Vortex Induced Vibrations, CeSOS

IMT-2013-2	Kurniawan, Adi	Modelling and geometry optimisation of wave energy converters, CeSOS
IMT-2013-3	Al Ryati, Nabil	Technical condition indexes doe auxiliary marine diesel engines, IMT
IMT-2013-4	Firoozkoohi, Reza	Experimental, numerical and analytical investigation of the effect of screens on sloshing, CeSOS
IMT-2013-5	Ommani, Babak	Potential-Flow Predictions of a Semi-Displacement Vessel Including Applications to Calm Water Broaching, CeSOS
IMT-2013-6	Xing, Yihan	Modelling and analysis of the gearbox in a floating spar-type wind turbine, CeSOS
IMT-7-2013	Balland, Océane	Optimization models for reducing air emissions from ships, IMT
IMT-8-2013	Yang, Dan	Transitional wake flow behind an inclined flat plate-----Computation and analysis, IMT
IMT-9-2013	Abdillah, Suyuthi	Prediction of Extreme Loads and Fatigue Damage for a Ship Hull due to Ice Action, IMT
IMT-10-2013	Ramìrez, Pedro Agustìn Pèrez	Ageing management and life extension of technical systems- Concepts and methods applied to oil and gas facilities, IMT
IMT-11-2013	Chuang, Zhenju	Experimental and Numerical Investigation of Speed Loss due to Seakeeping and Maneuvering. IMT
IMT-12-2013	Etemaddar, Mahmoud	Load and Response Analysis of Wind Turbines under Atmospheric Icing and Controller System Faults with Emphasis on Spar Type Floating Wind Turbines, IMT
IMT-13-2013	Lindstad, Haakon	Strategies and measures for reducing maritime CO2 emissons, IMT
IMT-14-2013	Haris, Sabril	Damage interaction analysis of ship collisions, IMT
IMT-15-2013	Shainee, Mohamed	Conceptual Design, Numerical and Experimental Investigation of a SPM Cage Concept for Offshore Mariculture, IMT
IMT-16-2013	Gansel, Lars	Flow past porous cylinders and effects of biofouling and fish behavior on the flow in and around Atlantic salmon net cages, IMT
IMT-17-2013	Gaspar, Henrique	Handling Aspects of Complexity in Conceptual Ship Design, IMT
IMT-18-2013	Thys, Maxime	Theoretical and Experimental Investigation of a Free Running Fishing Vessel at Small Frequency of Encounter, CeSOS
IMT-19-2013	Aglen, Ida	VIV in Free Spanning Pipelines, CeSOS

IMT-1-2014	Song, An	Theoretical and experimental studies of wave diffraction and radiation loads on a horizontally submerged perforated plate, CeSOS
IMT-2-2014	Rogne, Øyvind Ygre	Numerical and Experimental Investigation of a Hinged 5-body Wave Energy Converter, CeSOS
IMT-3-2014	Dai, Lijuan	Safe and efficient operation and maintenance of offshore wind farms ,IMT
IMT-4-2014	Bachynski, Erin Elizabeth	Design and Dynamic Analysis of Tension Leg Platform Wind Turbines, CeSOS
IMT-5-2014	Wang, Jingbo	Water Entry of Freefall Wedged – Wedge motions and Cavity Dynamics, CeSOS
IMT-6-2014	Kim, Ekaterina	Experimental and numerical studies related to the coupled behavior of ice mass and steel structures during accidental collisions, IMT
IMT-7-2014	Tan, Xiang	Numerical investigation of ship's continuous- mode icebreaking in leverl ice, CeSOS
IMT-8-2014	Muliawan, Made Jaya	Design and Analysis of Combined Floating Wave and Wind Power Facilities, with Emphasis on Extreme Load Effects of the Mooring System, CeSOS
IMT-9-2014	Jiang, Zhiyu	Long-term response analysis of wind turbines with an emphasis on fault and shutdown conditions, IMT
IMT-10-2014	Dukan, Fredrik	ROV Motion Control Systems, IMT
IMT-11-2014	Grimsmo, Nils I.	Dynamic simulations of hydraulic cylinder for heave compensation of deep water drilling risers, IMT
IMT-12-2014	Kvittem, Marit I.	Modelling and response analysis for fatigue design of a semisubmersible wind turbine, CeSOS
IMT-13-2014	Akhtar, Juned	The Effects of Human Fatigue on Risk at Sea, IMT
IMT-14-2014	Syahroni, Nur	Fatigue Assessment of Welded Joints Taking into Account Effects of Residual Stress, IMT
IMT-1-2015	Bøckmann, Eirik	Wave Propulsion of ships, IMT
IMT-2-2015	Wang, Kai	Modelling and dynamic analysis of a semi-submersible floating vertical axis wind turbine, CeSOS
IMT-3-2015	Fredriksen, Arnt Gunvald	A numerical and experimental study of a two-dimensional body with moonpool in waves and current, CeSOS
IMT-4-2015	Jose Patricio Gallardo Canabes	Numerical studies of viscous flow around bluff bodies, IMT

IMT-5-2015	Vegard Longva	Formulation and application of finite element techniques for slender marine structures subjected to contact interactions, IMT
IMT-6-2015	Jacobus De Vaal	Aerodynamic modelling of floating wind turbines, CeSOS
IMT-7-2015	Fachri Nasution	Fatigue Performance of Copper Power Conductors, IMT
IMT-8-2015	Oleh I Karpa	Development of bivariate extreme value distributions for applications in marine technology,CeSOS
IMT-9-2015	Daniel de Almeida Fernandes	An output feedback motion control system for ROVs, AMOS
IMT-10-2015	Bo Zhao	Particle Filter for Fault Diagnosis: Application to Dynamic Positioning Vessel and Underwater Robotics, CeSOS
IMT-11-2015	Wenting Zhu	Impact of emission allocation in maritime transportation, IMT
IMT-12-2015	Amir Rasekhi Nejad	Dynamic Analysis and Design of Gearboxes in Offshore Wind Turbines in a Structural Reliability Perspective, CeSOS
IMT-13-2015	Arturo Jesùs Ortega Malca	Dynamic Response of Flexibles Risers due to Unsteady Slug Flow, CeSOS
IMT-14-2015	Dagfinn Husjord	Guidance and decision-support system for safe navigation of ships operating in close proximity, IMT
IMT-15-2015	Anirban Bhattacharyya	Ducted Propellers: Behaviour in Waves and Scale Effects, IMT
IMT-16-2015	Qin Zhang	Image Processing for Ice Parameter Identification in Ice Management, IMT
IMT-1-2016	Vincentius Rumawas	Human Factors in Ship Design and Operation: An Experiential Learning, IMT
IMT-2-2016	Martin Storheim	Structural response in ship-platform and ship-ice collisions, IMT
IMT-3-2016	Mia Abrahamsen Prsic	Numerical Simulations of the Flow around single and Tandem Circular Cylinders Close to a Plane Wall, IMT
IMT-4-2016	Tufan Arslan	Large-eddy simulations of cross-flow around ship sections, IMT

IMT-5-2016	Pierre Yves-Henry	Parametrisation of aquatic vegetation in hydraulic and coastal research,IMT
IMT-6-2016	Lin Li	Dynamic Analysis of the Instalation of Monopiles for Offshore Wind Turbines, CeSOS
IMT-7-2016	Øivind Kåre Kjerstad	Dynamic Positioning of Marine Vessels in Ice, IMT